RADC-TR-76-101, Vol VIII (of eight)
Phase Report
August 1980

LEVEL

12

APPLICATIONS OF MULTICONDUCTOR TRANSMISSION LINE THEORY TO THE PREDICTION OF CABLE COUPLING
Prediction of Crosstalk Involving Braided-Shield Cables

University of Kentucky

Clayton R. Paul

ROME AIR DEVELOPMENT CENTER
Air Force Systems Command
Griffiss Air Force Base, New York 13441

This report has been reviewed by the RADC Public Affairs Office (PA) and is releasable to the National Technical Information Service (NTIS). At NTIS it will be releasable to the general public, including foreign nations.

RADC-TR-76-101, Vol VIII (of eight) has been reviewed and is approved for publication.

APPROVED: Roy F. Stratton

ROY F. STRATTON
Project Engineer

APPROVED: Quentin J. Porter

QUENTIN J. PORTER
Acting Chief
Reliability and Compatibility Division

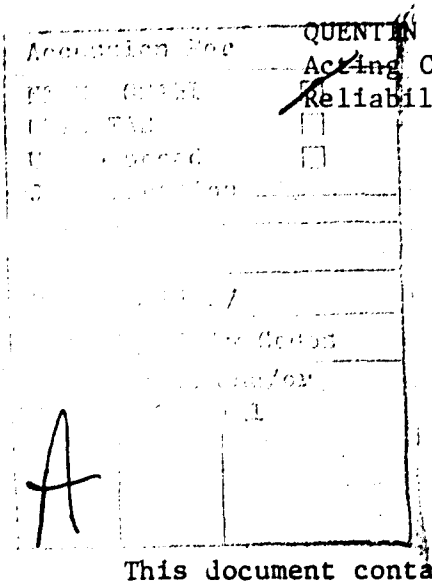

FOR THE COMMANDER: John P. Huss

JOHN P. HUSS
Acting Chief, Plans Office

SUBJECT TO EXPORT CONTROL LAWS

This document contains information for manufacturing or using munitions of war. Export of the information contained herein, or release to foreign nationals within the United States, without first obtaining an export license, is a violation of the International Traffic in Arms Regulations. Such violation is subject to a penalty of up to 2 years imprisonment and a fine of $100,000 under 22 U.S.C 2778.

Include this notice with any reproduced portion of this document.

If your address has changed or if you wish to be removed from the RADC mailing list, or if the addressee is no longer employed by your organization, please notify RADC (RBCT) Griffiss AFB NY 13441. This will assist us in maintaining a current mailing list.

Do not return this copy. Retain or destroy.

(19) 74-76-101-Vol-8

UNCLASSIFIED (Volume VIII)

SECURITY CLASSIFICATION OF THIS PAGE (When Data Entered)

REPORT DOCUMENTATION PAGE

READ INSTRUCTIONS BEFORE COMPLETING FORM

(18) 1. REPORT NUMBER: RADC-TR-76-101, Vol VIII (of eight)

2. GOVT ACCESSION NO.: AD-A091751

3. RECIPIENT'S CATALOG NUMBER:

(6) 4. TITLE (and Subtitle): APPLICATIONS OF MULTICONDUCTOR TRANSMISSION LINE THEORY TO THE PREDICTION OF CABLE COUPLING • Prediction of Crosstalk Involving Braided-Shield Cables

5. TYPE OF REPORT & PERIOD COVERED: (9) Phase Report.

6. PERFORMING ORG. REPORT NUMBER: N/A

(10) 7. AUTHOR(s): Clayton R. Paul

(15) 8. CONTRACT OR GRANT NUMBER(s): F30602-79-C-0011, F30602-78-C-0120

9. PERFORMING ORGANIZATION NAME AND ADDRESS: University of Kentucky, Department of Electrical Engineering, Lexington KY 40506

10. PROGRAM ELEMENT, PROJECT, TASK AREA & WORK UNIT NUMBERS: 62702F; (16) 23380317; (17) 03

11. CONTROLLING OFFICE NAME AND ADDRESS: Rome Air Development Center (RBCT), Griffiss AFB NY 13441

(11) 12. REPORT DATE: August 1980

13. NUMBER OF PAGES: 250

14. MONITORING AGENCY NAME & ADDRESS (if different from Controlling Office): Same (12) 256

15. SECURITY CLASS. (of this report): UNCLASSIFIED

15a. DECLASSIFICATION DOWNGRADING SCHEDULE: N/A

16. DISTRIBUTION STATEMENT (of this Report)

Approved for public release; distribution unlimited.

17. DISTRIBUTION STATEMENT (of the abstract entered in Block 20, if different from Report)

Same

18. SUPPLEMENTARY NOTES

RADC Project Engineer: Roy F. Stratton (RBCT)

19. KEY WORDS (Continue on reverse side if necessary and identify by block number)

Electromagnetic Compatibility	Braided-shield Cables
Cable Coupling	Coaxial Lines
Transmission Lines	Surface Transfer Impedance
Multiconductor Transmission Lines	Shielded Wires
Wire-to-Wire Coupling	Shielded Cables

20. ABSTRACT (Continue on reverse side if necessary and identify by block number)

The contents of this report are concerned with the electromagnetic coupling (crosstalk) between braided-shield cables. The effect of pigtails (exposed sections of braided-shield cables in which the shield is stripped back exposing the interior wire) on crosstalk was investigated. It was found that even though the length of these exposed sections constitutes only a very small fraction of the total line length the dominant coupling to the shielded cable can occur via these pigtail

DD FORM 1 JAN 73 1473 EDITION OF 1 NOV 65 IS OBSOLETE

UNCLASSIFIED

SECURITY CLASSIFICATION OF THIS PAGE (When Data Entered)

400 722

sections. If the pigtail sections are eliminated, an additional reduction in crosstalk of as much as 30dB may be realized. The modeling and prediction of this crosstalk was also investigated. A low-frequency model provided accurate predictions for electrically short lines. The multiconductor transmission line (MTL) model was also formulated. The MTL model provided predictions within 1-3dB for electrically short lines and within 6-10dB when the line was electrically long. Extensive experimental data are reported.

This volume completes the eight volume series of technical reports:

"Applications of Multiconductor Transmission Line Theory to the Prediction of Cable Coupling," RADC-TR-76-101, Technical Reports, Rome Air Development Center, Griffiss AFB NY 13441.

The individual volumes (each bearing the RADC-TR-76-101 number) are:

Vol I (C.R. Paul) "Multiconductor Transmission Line Theory," April 1976, (A025028)

Vol II (A.E. Feather and C. R. Paul) "Computation of the Capacitance Matrices for Ribbon Cables," April 1976, (A025029)

Vol III (C. R. Paul) "Prediction of Crosstalk in Random Cable Bundles," February 1977, (A038316)

Vol IV (C. R. Paul) "Prediction of Crosstalk in Ribbon Cables," February 1978, (A053548)

Vol V (J. A. McKnight and C. R. Paul) "Prediction of Crosstalk Involving Twisted Wire Pairs," February 1978, (A053559)

Vol VI (C. R. Paul) "A Digital Computer Program for Determining Terminal Currents Induced in a Multiconductor Transmission Line by an Incident Electromagnetic Field," February 1978, (A053560)

Vol VII (C. R. Paul) "Digital Computer Programs for the Analysis of Multiconductor Transmission Lines," July 1977, (A046662)

Vol VIII (C. R. Paul) "Prediction of Crosstalk Involving Braided-Shield Cables," August 1980.

TABLE OF CONTENTS

LIST OF ILLUSTRATIONS

For page numbers of figures in each of the Appendices (A, B, C, D, E) see the listing at the beginning of each Appendix.

I. Introduction

Shielded cables have been used extensively on aircraft, ground and space-missile systems to reduce the electromagnetic coupling (crosstalk) between electrical equipments which are interconnected by wires. The wires which interconnect these electrical and electronic devices are generally routed in densely-packed, cable bundles. The unintentional electromagnetic coupling or crosstalk between these wires may be of sufficient magnitude to degrade the performance of the equipments which the wires interconnect. In order to reduce this level of crosstalk, shielded cables and twisted pairs of wires have been employed.

In order to assess the effectiveness of these prevention measures, it is desirable to have prediction models which characterize this coupling. The objective of this report is to investigate such prediction models for shielded cables. Also we wish to show that a common practice - use of pigtails - can seriously degrade the effectiveness of braided-shield cables. Experimental as well as computed results will be presented to show the effect of these pigtails.

Shielded cables are predominantly of the braided-shield variety as shown in Fig. 1. The braided-shield cable consists of a circular, cylindrical shield which is composed of belts of wires, interwoven to provide flexibility and an interior wire (the shielded wire) located on the axis of the shield as shown in Fig. 1. The interior wire or shielded wire is of radius r_w and the shield has interior radius r_s. The shield thickness, t_s, is approximately equal to the diameter of the wires making up the braid which have radius r_b, i.e., $t_s \cong 2r_b$. The shielded cable usually has an overall, insulating jacket of thickness t_j, and the shield is woven in B belts of wires with a weave angle of θ_w as shown in Fig. 1. Each belt contains W wires. If the length of the shield is denoted by ℓ_s, then each braid wire is of length $\ell_s/\cos\theta_w$. The medium internal to the shield and surrounding the interior, shielded wire is a dielectric with permittivity $\epsilon = \epsilon_r\epsilon_v$ and permeability $\mu = \mu_v$ where the permittivity and permeability of free space are denoted by ϵ_v and μ_v, respectively.

There exist other, less frequently used, types of shield constructions such as solid, conduit types and tape-wound shields. These are discussed in [1].

In terminating a braided-shield cable, for example, at a connector, the

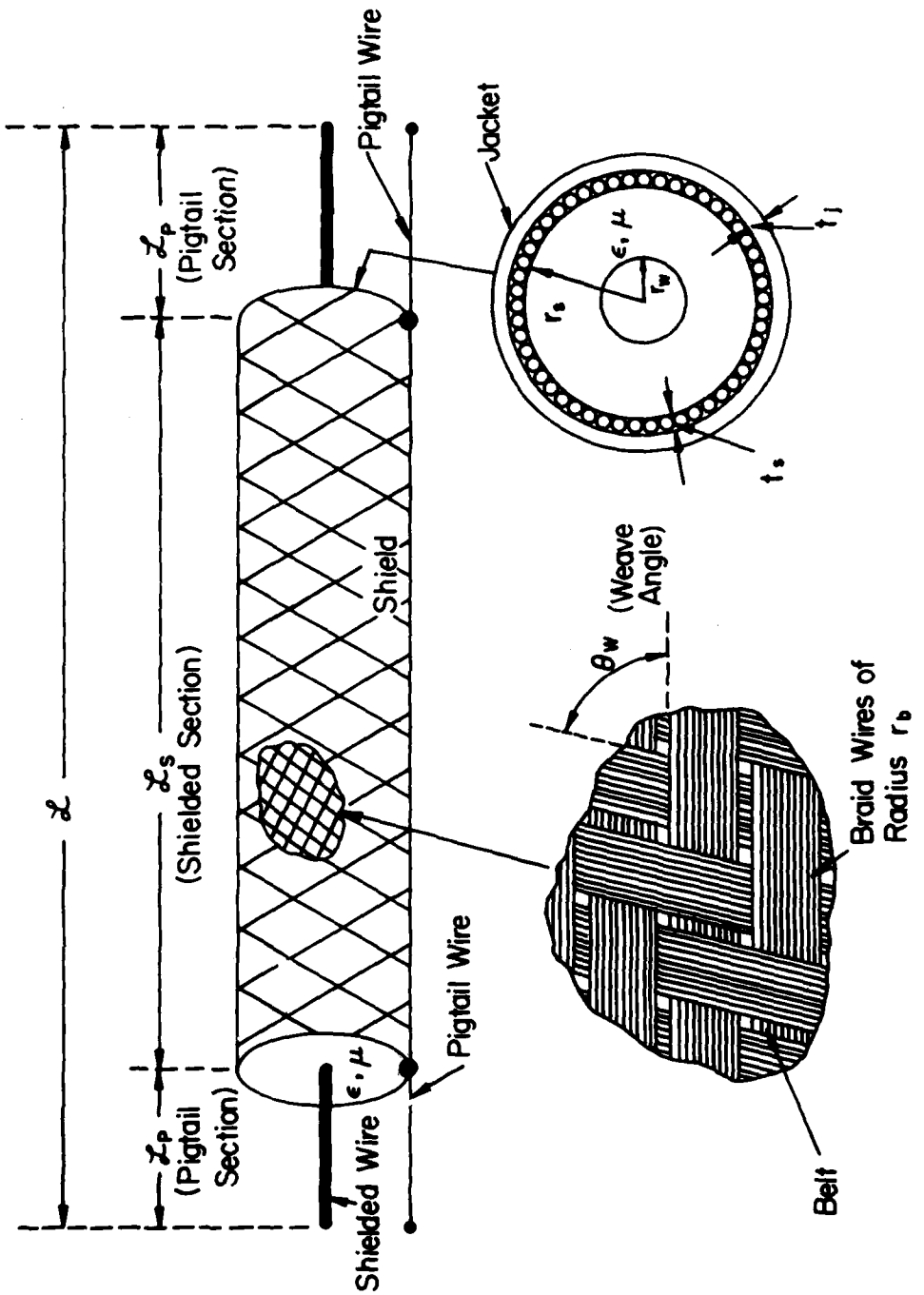

Fig. 1. Braided-shield construction.

braid is often stripped back exposing the interior wire (the shielded wire) as shown in Fig. 1. The braid is terminated (usually to a ground plane such as an aircraft structural skin) via another wire which will be referred to as the pigtail wire. These exposed terminal sections will be referred to as pigtails throughout this report although this use of the term is not standard. The term pigtail is sometimes used elsewhere to denote the pigtail wire. The lengths of the pigtail sections are denoted by ℓ_p and the length of the shielded section of the cable is denoted by ℓ_s. The total length of the cable is denoted by $\ell = \ell_s + 2\ell_p$ as shown in Fig. 1.

When braided-shield cables are terminated in connectors in this fashion, the shielded wire is directly exposed over the pigtail sections to other wires in the cable bundle which are also terminated at the connector as shown in Fig. 2. If it is required to carry a shield connection through the connector, a separate wire, the pigtail wire, connects the shield braid to an additional connector pin. The various design handbooks [2,3,4] seem to recommend against this procedure, however, it appears to be common nevertheless [5,6]. In fact, the author has observed pigtail sections in excess of 6 inches. (The connector pins may also be considered to add an additional length to the pigtail section.) In these installation configurations, the interior, shielded wire is directly exposed to crosstalk from any adjacent wire in the cable bundle; no intervening shield is present to restrict the crosstalk contribution over the pigtail sections.

One of the purposes of this report will be to demonstrate that the coupling over the pigtail sections may constitute the dominant coupling mechanism to the shielded cable. Even though the lengths of the pigtail sections, $2\ell_p$, may constitute only a minor fraction of the total cable length, ℓ, we will show that, depending on the values of the cable termination impedances, the contribution to the received voltages at either end of the cable due to the pigtail sections can be larger than the contribution over the (much longer) shielded section. In this situation, the shield simply serves to reduce the exposed length of the interior wire ($2\ell_p$) from what it would be (ℓ) if no shield were present. Thus the shield still provides a reduction in crosstalk. However it will be shown that if the pigtail sections were eliminated, one could realize an additional reduction in crosstalk of as much as 30 dB (over certain frequency ranges). Thus the effectiveness of the shield in reducing crosstalk has been

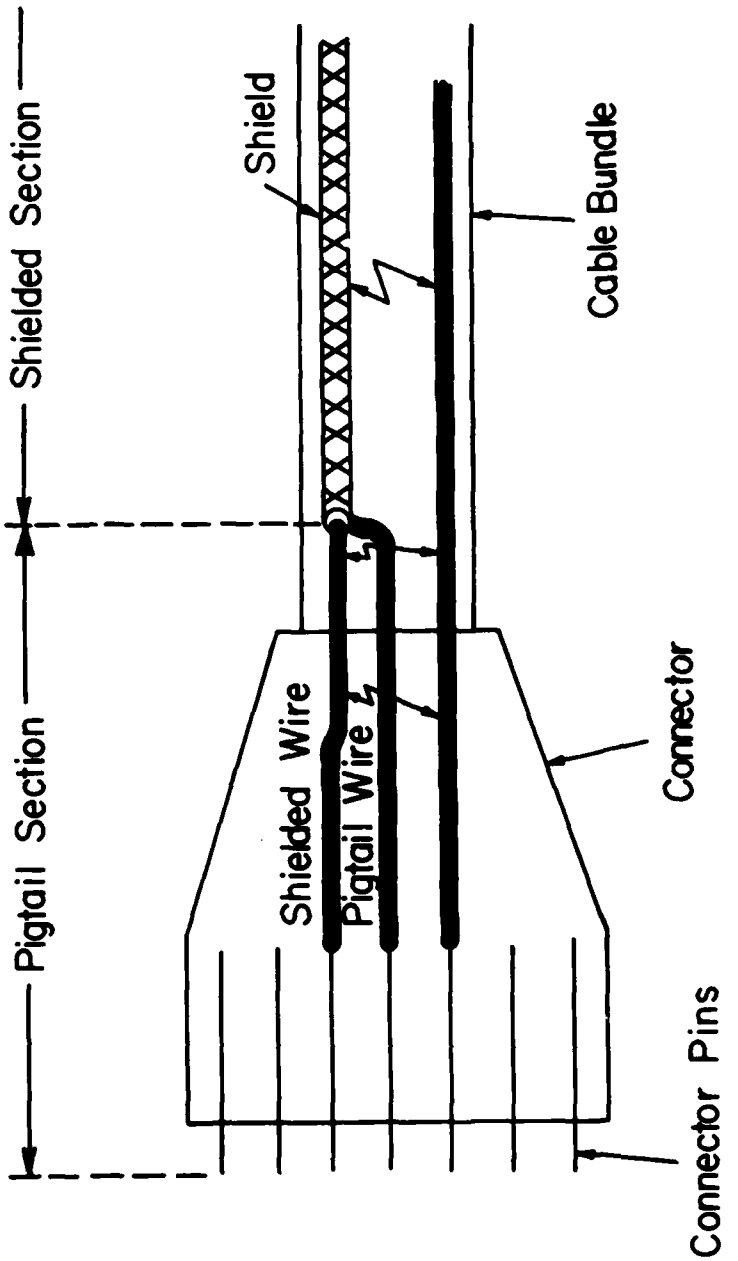

Fig. 2. Termination of braid-shield cables in connectors.

substantially reduced by the pigtail sections.

The second objective of this report is to investigate the feasibility of developing a prediction model to accurately simulate the crosstalk to or from a braided-shield cable. A transmission line model will be employed, and the requisite, general background for this model is given in [7]. The earlier work on predicting crosstalk to or from shielded cables has generally been applicable to low-frequency models [8-10]. The term low-frequency is used here to mean frequencies for which the cable is sufficiently short, electrically, so that lumped circuit models provide adequate characterization. It will be shown that this frequency limit is also a function of the cable terminal impedances.

Some of the very early work of significance in characterizing shielded cables was by Schelkunoff [11,12]. A surface transfer impedance relating the shield current to the per-unit-length voltage drop (electric field) on the interior and exterior shield surfaces was developed for solid shields. This work has been extended to braided-shield cables in [14-19]. However, these works concentrate on the vulnerability of braided-shield cables to external, incident fields as opposed to coupling from other adjacent wire circuits in cable bundles above a ground plane. A discussion and rather thorough bibliography is given in [18].

There has been an attempt to characterize the crosstalk from adjacent wire circuits via the transmission line model in [13]. However, the analysis assumes weak coupling between the two circuits; that is, the back interaction of the shield (pickup) circuit on the generating wire can be ignored. This weak coupling assumption was also employed in a lumped circuit model in [10]. In a later section we investigate the use of the distributed parameter, transmission line model to characterize this coupling without invoking the weak coupling assumption.

In this report, we will concentrate on the prediction of crosstalk to or from braided-shield cables which are suspended above an infinite ground plane. The three basic configurations are shown in Fig. 3. The first configuration shown in Fig. 3(a) is referred to as the unshielded to unshielded configuration (UU). This case, although not involving a shielded cable, is included for completeness for the primary reason of having a structure to compare the other structures in Fig. 3 to so that the effectiveness of the shield in

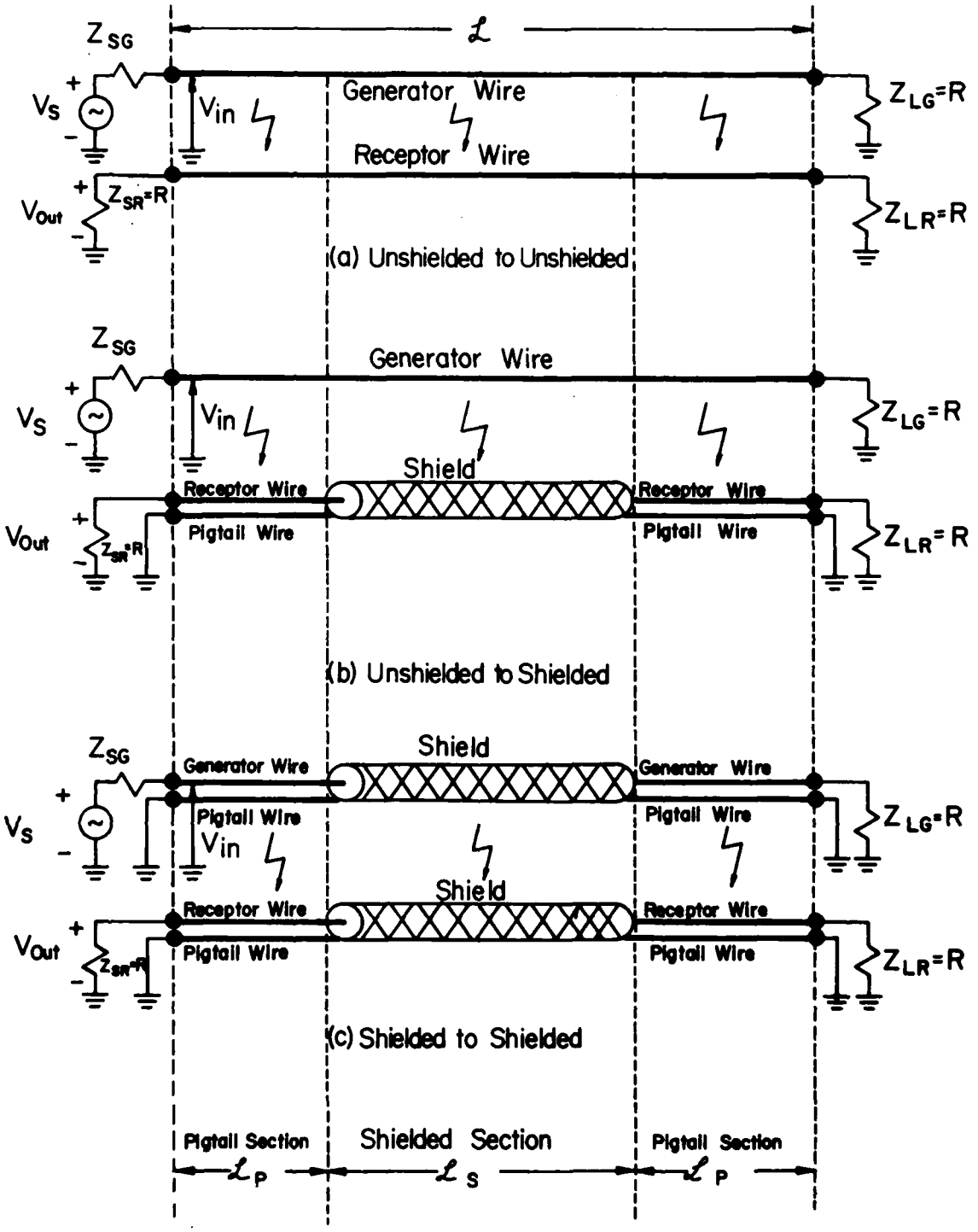

Fig. 3. The three configurations investigated.

reducing crosstalk can be assessed, quantitatively. The second configuration is shown in Fig. 3(b) and is referred to as the unshielded to shielded configuration (US). The third configuration shown in Fig. 3(c) is referred to as the shielded to shielded configuration (SS). A fourth configuration not shown in Fig. 3 will also be investigated. This configuration is referred to as the shielded to unshielded configuration (SU) and differs from the unshielded to shielded configuration in Fig. 3(b) only in that the shield surrounds the generator wire instead of the receptor wire.

For the cases in Fig. 3(b) and 3(c) involving shielded cables, the total line length ℓ will be divided into two pigtail sections each of identical length ℓ_p and a shielded section of length ℓ_s. Although the unshielded to unshielded case in Fig. 3(a) contains no shields, we will, nevertheless, divide the line length into the same corresponding lengths as for shielded cables for later, illustrative purposes.

One wire with the ground plane will be referred to as the generator circuit and will be driven by a sinusoidal voltage source, V_S, having source impedance Z_{SG}. This wire will be referred to as the generator wire. Another wire with the ground plane will constitute the receptor circuit, and the wire of this circuit will be referred to as the receptor wire. The generator wire is terminated to ground in an impedance Z_{LG}, and the ends of the receptor wire are terminated to ground in impedances Z_{SR} and Z_{LR}. The first subscript on these quantities refers to the appropriate end of the line, Source end or Load end. The left end of each line will be referred to as the source end although no actual source is present in the receptor line at this end. Similarly, the right end of each line will be referred to as the load end. The second subscript refers to the appropriate circuit, Generator or Receptor. In the experiment to be described, Z_{SG} will be zero and all other termination impedances will be purely resistive and equal, i.e., $Z_{LG} = Z_{SR} = Z_{LR} = R$, as is indicated in Fig. 3. The voltages V_{in} and V_{out} across the resistance at the source end of the receptor circuit will be measured at discrete frequencies, and we will be interested in the voltage transfer ratio V_{out}/V_{in} as a measure of the crosstalk between the two circuits, i.e.,

$$\text{Voltage Transfer Ratio} = \frac{V_{out}}{V_{in}} .$$

In each case involving braided shields, there are four possibilities for shield grounding. The shield may be ungrounded at both ends (ungrounded), grounded at the source end and ungrounded at the load end (single-end grounded, source end), ungrounded at the source end and grounded at the load end (single-end grounded, load end), and grounded at both ends (double-end grounded). We will observe that, depending on the circuit terminal impedances, there are some interesting and very significant differences in crosstalk resulting from these various grounding configurations.

The report will be organized as follows. The experimental test configuration will be described in Section II. Section III will investigate the effect of pigtails on crosstalk. It will be shown that even though the pigtail sections constitute only a small fraction of the total cable length (no more than 4% in the results to be shown), they may constitute the dominant coupling mechanism to the braided-shield cable. It will be shown rather dramatically that one can obtain as much as 30 dB additional reduction in crosstalk if these seemingly insignificant pigtail sections are eliminated. Section IV will discuss a low-frequency, approximate model. This model, although limited in applicability to a sufficiently small frequency, will effectively serve to illustrate why pigtails have this rather dramatic effect and will provide detailed insight into the coupling mechanism. Section V will discuss the effect of the shield grounding configuration. Section VI will discuss the distributed parameter, transmission line model, and the predictions of this model will be given in Section VII. Up to this point, the pigtail wire lies parallel to the shielded wire over the pigtail sections. The separation between these two wires is 0.5 cm. In Section VIII, we will investigate the effect of varying the loop area between the pigtail wire and the shielded wire. In some installations, the pigtail wire is not terminated in a connector but is connected directly to the system structure. The effect of this pigtail configuration will also be investigated in Section VIII.

II. The Experiment

The experimental investigation of all three configurations shown in Fig. 3 (as well as the shielded to unshielded configuration) was conducted. The total line length, ℓ, was 12 feet (3.6576 m) in all cases. The generator and receptor wires were supported at a height of 1.5 cm above an aluminum ground plane which was 1/8 inch in thickness. The generator wire circuit was driven by a sinusoidal source, V_S, and terminated in a resistance R. Both ends of the receptor circuit were also terminated in a resistance R and two values of R will be investigated, R = 50Ω and R = 1kΩ.

These two values of R were chosen for the following reason. For the unshielded to unshielded case in Fig. 3(a), one can show [21] that for a sufficiently small frequency, the received voltages across R at each end of the receptor circuit can be separated into an inductive coupling component due to mutual inductance between the two circuits and a capacitive coupling component due to mutual capacitance between the two circuits. For the unshielded to unshielded configuration investigated here, one can show that inductive coupling dominates capacitive coupling for "low impedance loads" such as R = 50Ω and vice-versa for "high impedance loads" such as R = 1kΩ. Previous experience has shown that the response of coupled lines can be quite different for these two coupling mechanisms. We will find this to be true for configurations involving shielded cables although this concept has not been explicitly shown for shielded cables as was done for unshielded cables in [21].

The measured voltages will be V_{in} at the input to the generator line and V_{out} across the resistance R at the source end of the receptor circuit. We will be interested in the voltage transfer ratio

$$\text{Voltage Transfer Ratio} = \frac{V_{out}}{V_{in}}$$

between the two circuits. The voltages V_{out} and V_{in} will be measured in steps of 1, 1.5, 2, 2.5, 3, 4, 5, 6, 7, 8, 9 in each decade from 100 Hz to 100 MHz, and the voltage transfer ratio will be plotted on the graphs at these discrete frequencies. The measurement and excitation equipment are

			Frequency Range
(1)	HP 8405A	Vector Voltmeter	1 MHz → 100 MHz
(2)	HP 3400A	RMS Voltmeter	100 Hz → 1 MHz

		Frequency Range
(3)	HP 205AG Audio Signal Generator	100 Hz → 15k Hz
(4)	HP 8601A Generator/sweeper	1 MHz → 100 MHz
(5)	Wavetek 134 Sweep Generator	15k Hz → 1 MHz
(6)	Tektronix DC502 Counter	100 Hz → 100 MHz

Photographs of the experimental setup are shown in Fig. 4.

Several configurations of shield grounding will be investigated in Section V. In Section III, the shields will be grounded at both ends via the pigtail wires as shown in Fig. 3(b) and 3(c). The pigtail wires are #20 gauge, solid, copper (bare) wires which are placed parallel to the shielded wires at a distance of 0.5 cm from these wires. The pigtail wires are also maintained at a height of 1.5 cm above the ground plane. Three lengths of pigtail sections were investigated: ℓ_p = 0.5 cm (~1/4 inch), ℓ_p = 3 cm (~1 1/4 inches) and ℓ_p = 8 cm (~3 1/4 inches).

In the unshielded to unshielded case shown in Fig. 3(a), the two wires were #22 gauge, stranded, copper wires with teflon insulation. In the unshielded to shielded case in Fig. 3(b) and the shielded to unshielded case, the unshielded wire was a #20 gauge, solid, copper wire with PVC insulation 17 mils in thickness. The characteristics of the braided-shield cables are (see Fig. 1):

Interior wire #22 gauge stranded	r_w = 12.65 mils
Interior insulation (Teflon)	ϵ_r = 2.1
Interior shield radius	r_s = 35 mils
Braid wires #36 gauge	r_b = 2.5 mils
Weave angle	$\theta_w \cong$ 30 degrees
Number of belts	B = 16
Number of wires per belt	W = 4
Overall, nylon jacket of thickness	t_j = 5 mils

The cross-sectional dimensions of the individual configurations are shown in Fig. 5. In the unshielded to unshielded configuration, two separations will be investigated. (See Fig. 5(a).) The SEPARATION: TOUCHING configuration has a separation of .23 cm corresponding to the shielded to shielded case, and the SEPARATION: WIDE configuration has a separation of 1.5 cm.

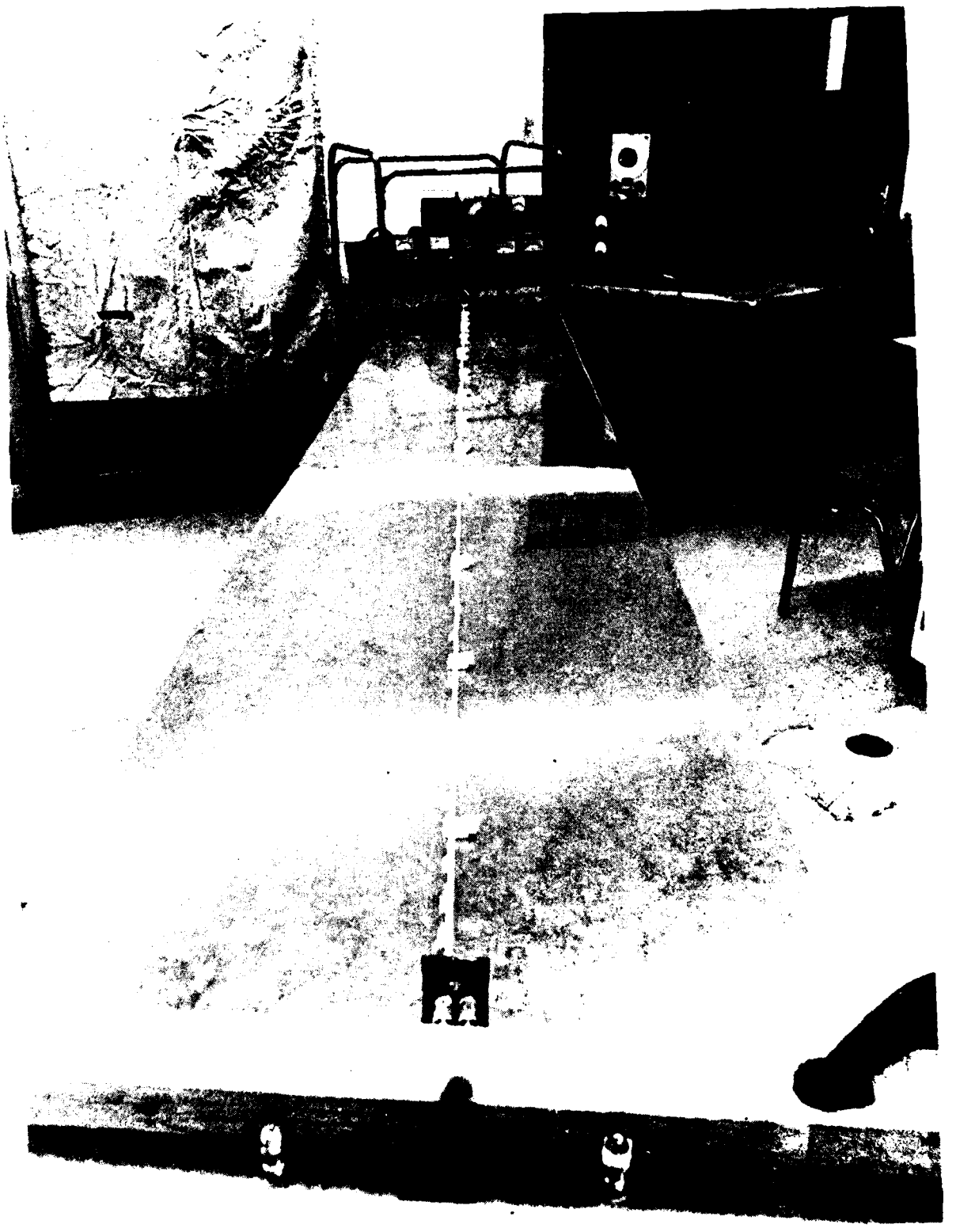

Fig. 4. The experimental configuration (continued).

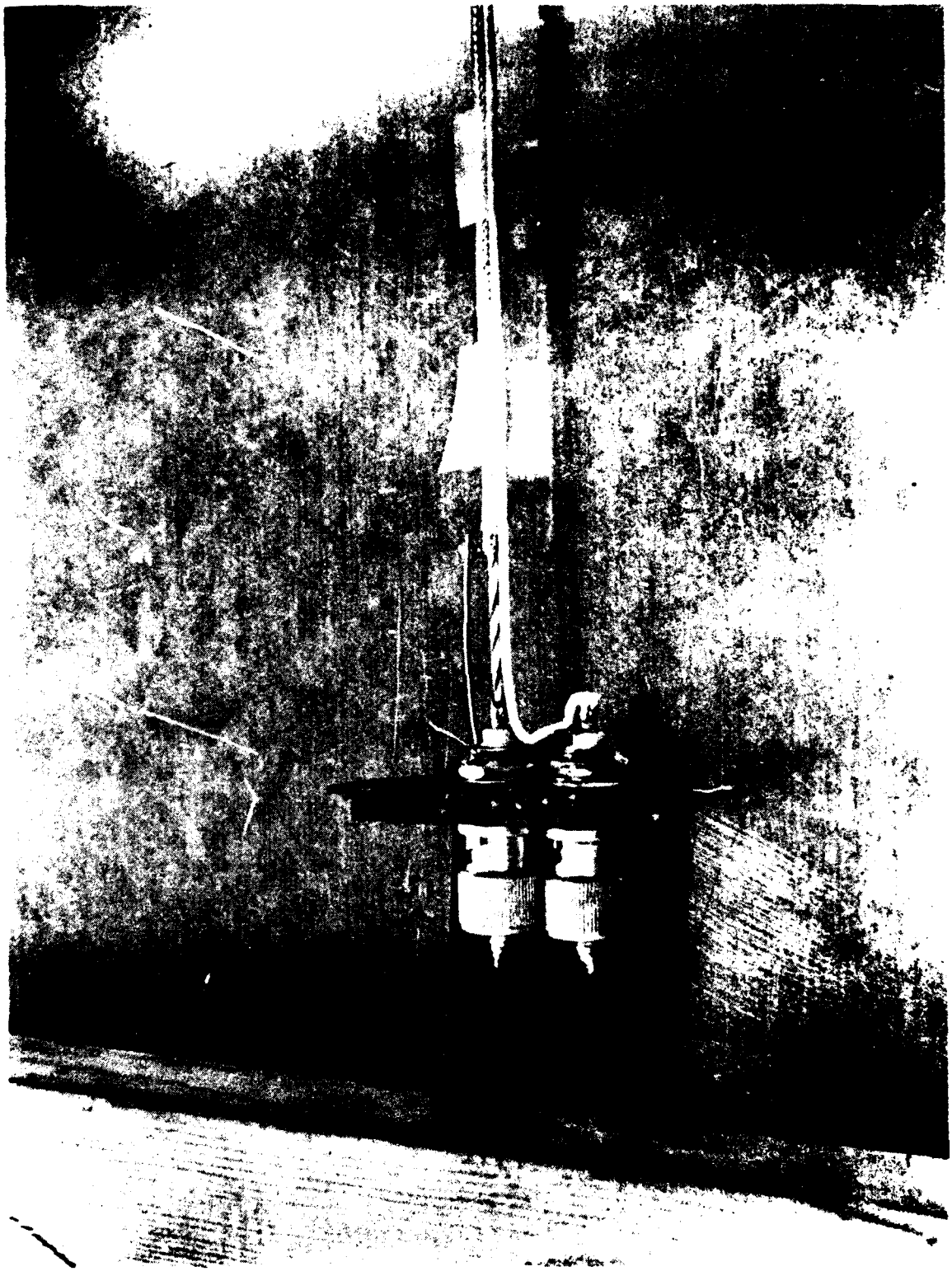

Fig. 4. The experimental configuration.

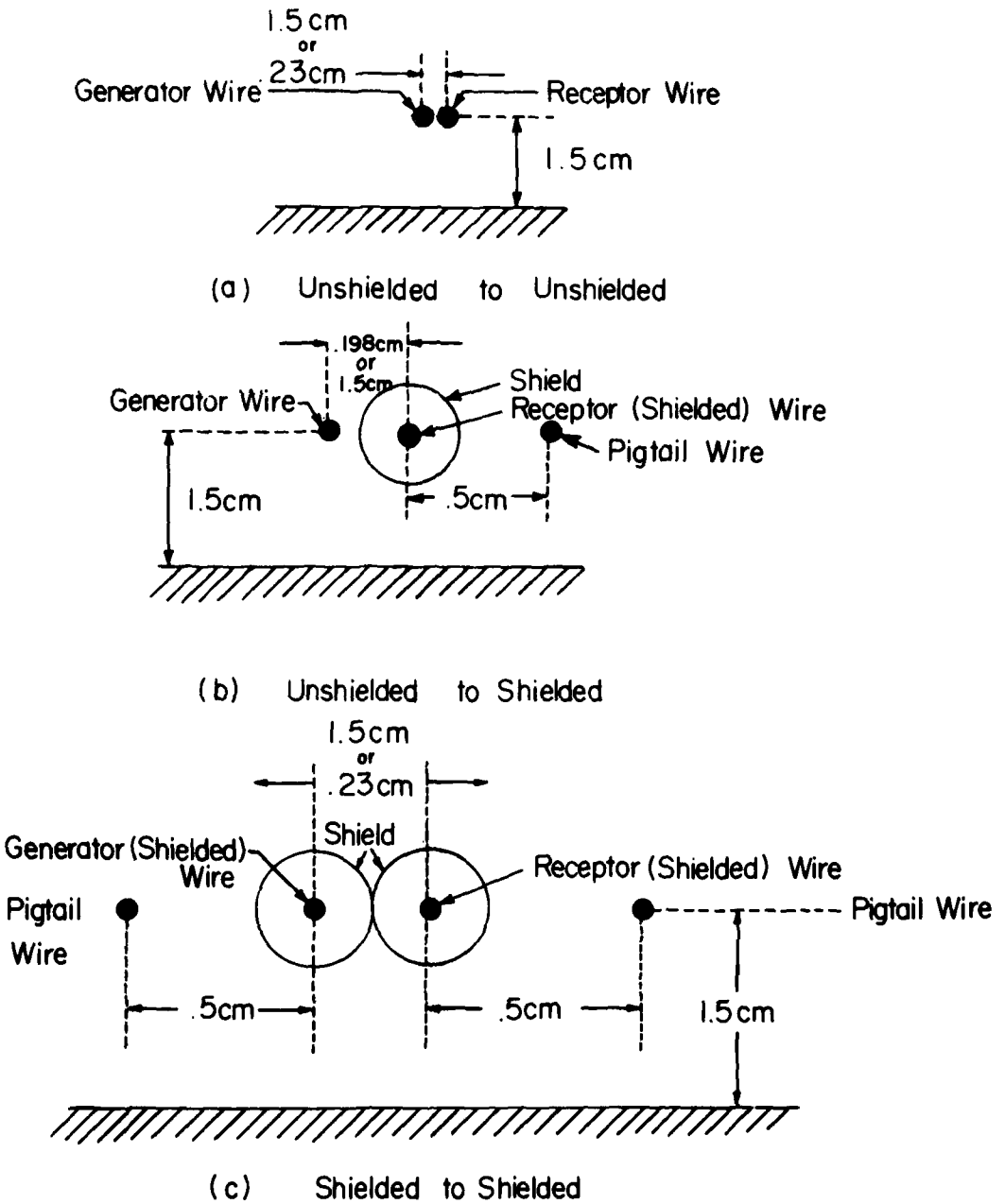

Fig. 5. The cross-sectional dimensions of the line configurations.

In the unshielded to shielded and shielded to unshielded configurations two wire separations were investigated as shown in Fig. 5(b): .198 cm and 1.5 cm. The .198 cm separation occurs when the wires are taped together and is denoted on the graphs by SEPARATION : TOUCHING. The 1.5 cm separation is denoted on the graphs by SEPARATION : WIDE.

In the shielded to shielded configuration, two separations are also investigated. In the SEPARATION: TOUCHING case, the two shields are taped together resulting in a separation of .23 cm. In the SEPARATION: WIDE case, the shields are separated by 1.5 cm. For the WIDE separation only the 8.0 cm pigtail section lengths were investigated. The sensitivity of the measurement equipment was such that the crosstalk could not be measured for the 0.5 cm pigtail section lengths for the shielded to shielded case and WIDE separation.

III. Effect of Pigtails

For the unshielded to shielded case in Fig. 3(b) (and the shielded to unshielded case), the experimental and computed data indicate that, for a sufficiently small frequency, it is possible to superimpose the pigtail coupling and the coupling over the shielded section as shown in Fig. 6 and described in Section IV, i.e.,

$$V_{out} \cong V_{\text{left pigtail}} + V_{\text{shielded section}} + V_{\text{right pigtail}} \qquad (3\text{-}1)$$

Based on the observation that the lengths of the pigtail sections usually constitute only a very small portion of the total line length (0.3% - 4% in the results to be shown), one might suspect that the pigtail coupling is insignificant. Cases will be shown which illustrate that, depending on the load impedances,

$$V_{\text{left pigtail}} > V_{\text{shielded section}}$$

$$V_{\text{right pigtail}} > V_{\text{shielded section}}$$

Therefore for these situations, the portion of the coupled voltage, V_{out}, over the shielded section, $V_{\text{shielded section}}$, is obscured by the pigtail coupling.

This does not imply that the effectiveness of the shield is totally destroyed. On the contrary, when the dominant coupling occurs via the pigtail sections, the shield simply serves to reduce the exposed section of the interior shielded wire from what it would be if no shield were present. Thus the shield provides an "optical" coverage of the interior wire for these situations. Nevertheless, we will show experimental results which point out that when pigtail sections constitute only a "small" portion of the total cable length, ℓ, for example, 4% of ℓ, the total coupling can be some 30 dB over the coupling which would result if the pigtail section lengths were minimized such as 0.3% of ℓ. Thus the effectiveness of the shield is substantially reduced by these pigtails. These concepts also appear to apply to the shielded to shielded case in Fig. 3(c) in a similar fashion.

The experimental results are contained in Appendix A. In these results, three values of pigtail section lengths are investigated: 0.5 cm (~1/4 inch), 3.0 cm (~1 1/4 inches) and 8.0 cm (~3 1/4 inches). The results for R = 50Ω and TOUCHING separation are shown for the unshielded to shielded case and all

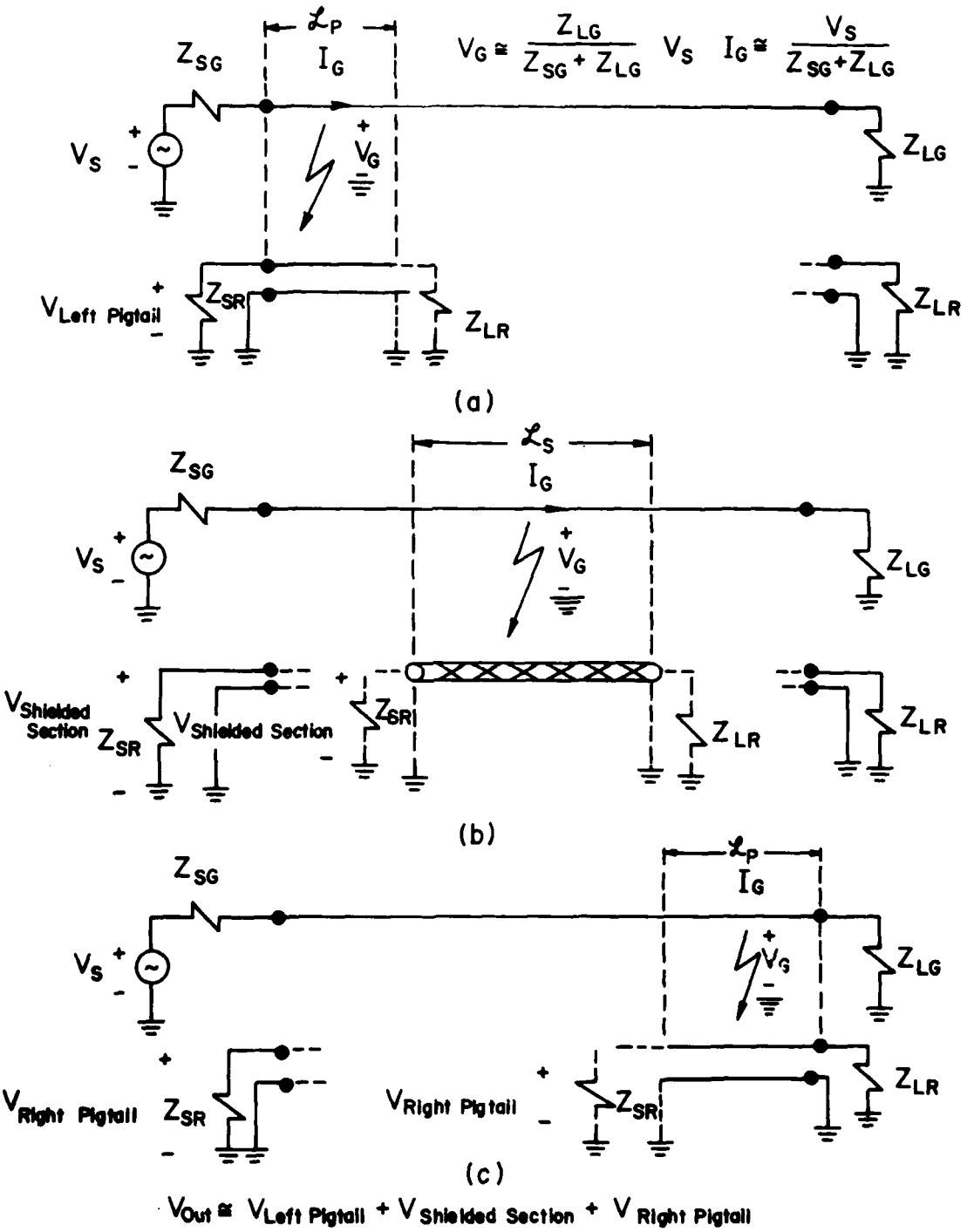

Fig. 6. Superposition of the coupling contributions.

shield grounding configurations in Fig. A-1 through A-4. Note in Fig. A-1 for both ends of the shield grounded, a change in pigtail length from 0.5 cm (0.3% of λ) to 8.0 cm (4% of λ) results in a maximum increase of some 30 dB (at 1 MHz). For the other shield grounding configurations shown in Fig. A-2 through A-4, there is virtually no difference in coupling for the different pigtail lengths. The low frequency model discussed in the following section seems to explain this phenomenon.

The corresponding results for R = 50Ω and the WIDE separation are shown in Fig. A-5 through A-8. There are essentially no differences in the conclusions to be drawn for this separation and the TOUCHING separation.

The results for R = 1kΩ and the TOUCHING separation are shown in Fig. A-9 through A-12. There are some significant differences between these results and the corresponding results for R = 50Ω. Note in Fig. A-9 for both ends of the shield grounded, that there is a maximum difference in crosstalk for the three pigtail lengths on the order of 25 dB, and the pigtail effect extends to well below 1k Hz although not to the same degree as at the higher frequencies. Note also in Fig. A-10 and A-11 for the single-end grounded case that there is a difference in crosstalk for the different pigtail lengths as opposed to the R = 50Ω case. The low-frequency model discussed in the following section also seems to explain these phenomena.

The corresponding results for R = 1kΩ and the WIDE separation are shown in Fig. A-13 through Fig. A-16. Again there are no major differences in the conclusions to be drawn for this separation and the corresponding results for the TOUCHING separation.

A similar effect is observed for coupling from a shielded cable to another shielded cable (SS). These results are shown for the TOUCHING separation in Fig. A-17 (R = 50Ω) and Fig. A-18 (R = 1kΩ). Note in Fig. A-17 for R = 50Ω a change in pigtail length from 0.5 cm (both ends of both cables) to 8 cm (both ends of both cables) results in an increase of <u>at least</u> 30 dB. Measurements of the coupling at 250 kHz and 300 kHz could not be obtained since the coupling levels were below the sensitivity of the measurement equipment. The results for R = 1kΩ given in Fig. A-18 show a similar, dramatic effect of pigtail length, and there is a more widespread increase in coupling of some 25 dB from 30 kHz to 10 MHz with an increase in pigtail lengths from 0.5 cm to 8 cm.

To further illustrate the effects of pigtails, we will compare the previous results for unshielded to shielded coupling and shielded to shielded coupling to the crosstalk between two unshielded wires. These results for R = 50Ω, 0.5 cm pigtails on the shielded cables and both ends of each shield grounded are shown in Fig. A-19. The corresponding results for R = 50Ω and 8 cm pigtails are shown in Fig. A-20. The results for R = 1kΩ and for 0.5 cm pigtails and 8 cm pigtails are shown in Fig. A-21 and A-22, respectively. Comparing Fig. A-19 and Fig. A-20, we observe that the difference in crosstalk between the case of two unshielded wires and two shielded wires decreases from approximately 60 dB to 35 dB from 300 kHz to 1 MHz when the pigtails are increased from 0.5 cm to 8 cm. The corresponding results for the WIDE separation are shown for R = 50Ω in Fig. A-23 and for R = 1kΩ in Fig. A-24.

It is interesting to note that for the R = 50Ω cases in Fig. A-19, Fig. A-20 and Fig. A-23 that when pigtail coupling is dominant, the unshielded to shielded and the shielded to shielded results are not identical. For example, we will show in the next section that for R = 50Ω, pigtail coupling is dominant above approximately 1 MHz in Fig. A-19, above approximately 100 kHz in Fig. A-20 and above approximately 100 kHz in Fig. A-23. (See also Fig. A-17.) However, when pigtail coupling is dominant, it may appear that the corresponding unshielded to shielded and shielded to shielded results should be identical since the pigtail sections are of the same length. However, there is an important difference; there is an additional pigtail wire on the generator circuit in the shielded to shielded case which is not present in the unshielded to shielded case. In Section VI, the multiconductor transmission line model predictions for all these cases are within 1.5 dB of the appropriate experimental results. The multiconductor transmission line model includes the presence of and interactions between all adjacent conductors (all pigtail wires and the generator and receptor wires). Thus the pigtail wires in the shielded to shielded case appear to have a substantial effect.

Note also that for 8 cm pigtails and R = 1kΩ in Fig. A-22 and Fig. A-24 that there is virtually no difference between the unshielded to shielded coupling and the shielded to shielded coupling. This again occurs because pigtail coupling is dominant. The pigtail wires seem to have much less of an effect than for R = 50Ω as discussed above, and the multiconductor transmission line model predicts these results quite well.

Also for the 0.5 cm pigtails in Fig. A-21, pigtail coupling is dominant above approximately 30 kHz.

These results indicate that a worthwhile objective in the installation of braided shield cables would be to eliminate, or at least minimize, the pigtail sections. In this experiment, the 8 cm pigtails constituted only 4% of the total line length, and the 0.5 cm pigtails constituted only 0.3% of the total line length. Thus it is clear that pigtail section lengths which constitute only a small fraction of the total cable length are not insignificant from the standpoint of affecting crosstalk to or from a braided-shield cable.

It is also of related interest to examine the difference between crosstalk for the unshielded to shielded configuration (US) shown in Fig. 3(b) and the shielded to unshielded configuration (SU). These results are compared in Fig. B-1 through Fig. B-16. It is clear from these results that the US and SU configurations are reciprocal when the line is electrically short. When the line is not electrically short, for example above 800 kHz ($\ell = \frac{1}{100}\lambda$) some results show differences between the US and SU configurations (for example, see Fig. B-10).

IV. A Low-Frequency Model

The results of the previous section indicate that pigtails can result in a significant degradation in the effectiveness of a shielded cable in the reduction of crosstalk. The purpose of this section is to develop an approximate prediction model which seems to explain this pigtail effect. The model to be developed relies on the frequency being sufficiently small and is therefore referred to as a low-frequency model. The line must be sufficiently short in electrical length so that a lumped circuit model of the line is valid. However, an electrically short line is necessary but not sufficient to insure the validity of the model. The computed results will show that the range of frequencies for which the model is valid also depends on the values of the line termination impedances. Thus it is not possible to state a frequency range in terms of line length, e.g., $\ell \leq \frac{1}{100}\lambda$, for which the model will be valid in all cases. Nevertheless, the model will be useful in indicating qualitative effects of the pigtails, and the valid frequency range will be clear when the model predictions are compared to the appropriate experimental results. The results of this section rely on the results in [8], [21] and [32].

For the unshielded to unshielded configuration in Fig. 3(a) and a sufficiently small frequency, it was shown in [21] that we may separate the portions of the received voltage, V_{out}, across Z_{SR} into inductive and capacitive coupling contributions. The inductive coupling contribution is given by [21]

$$V_{out}^{IND} = \left(\frac{Z_{SR}}{Z_{SR} + Z_{LR}}\right) (j\omega \ell_{GR} \ell) I_G \tag{4-1a}$$

and the capacitive coupling contribution is given by [21]

$$V_{out}^{CAP} = \left(\frac{Z_{SR}\, Z_{LR}}{Z_{SR} + Z_{LR}}\right) (j\omega c_{GR} \ell) V_G \tag{4-1b}$$

where ℓ_{GR} is the per-unit-length mutual inductance and c_{GR} is the per-unit-length mutual capacitance between the generator and receptor wires. The corresponding result for the received voltage across Z_{LR} is obtained by replacing Z_{SR} (Z_{LR}) in (4-1) by Z_{LR} (Z_{SR}) and the sign of the inductive coupling term becomes negative [21]. The items I_G and V_G are the low-frequency current and voltage, respectively, of the generator line and are given by

$$I_G = \frac{V_S}{Z_{SG} + Z_{LG}} \tag{4-2a}$$

$$V_G = \frac{Z_{LG}}{Z_{SG} + Z_{LG}} V_S \qquad (4\text{-}2b)$$

The input voltage to the line is approximately $V_{in} = V_G$.

The per-unit-length mutual inductance is given by [7]

$$\ell_{GR} = \frac{\mu_v}{4\pi} \ell n \left[1 + \frac{4h_G h_R}{d_{GR}^2}\right] \text{ H/m} \qquad (4\text{-}3)$$

The quantities h_G and h_R are the heights of the generator and receptor wires, respectively, above the ground plane. For the experiment, $h_G = h_R = 1.5$ cm. The quantity d_{GR} is the separation between the generator and receptor wires. For the experiment, $d_{GR} = 0.23$ cm or $d_{GR} = 1.5$ cm.

The mutual capacitance, c_{GR}, is computed in a similar fashion [7]. We form the 2 x 2 per-unit-length inductance matrix

$$\underset{\sim}{L} = \begin{bmatrix} \ell_{GG} & \ell_{GR} \\ \ell_{GR} & \ell_{RR} \end{bmatrix} \text{ H/m} \qquad (4\text{-}4)$$

where ℓ_{GG} and ℓ_{RR} are the per-unit-length self inductances of the generator and receptor circuits, respectively, which are given by [7]

$$\ell_{GG} = \frac{\mu_v}{2\pi} \ell n \left(\frac{2h_G}{r_{wG}}\right) \qquad (4\text{-}5a)$$

$$\ell_{RR} = \frac{\mu_v}{2\pi} \ell n \left(\frac{2h_R}{r_{wR}}\right) \qquad (4\text{-}5b)$$

The quantities r_{wG} and r_{wR} are the radii of the generator and receptor wires, respectively. For the experiment, $r_{wG} = r_{wR} = 12.65$ mils. The per-unit-length capacitance matrix of this configuration is written as [7]

$$\underset{\sim}{C} = \begin{bmatrix} (c_{GG} + c_{GR}) & -c_{GR} \\ -c_{GR} & (c_{RR} + c_{GR}) \end{bmatrix} \text{ F/m} \qquad (4\text{-}6)$$

where c_{GG} and c_{RR} are the appropriate, per-unit-length self capacitances of the circuits. If we ignore the dielectric insulations of the wires, then [7]

$$\underset{\sim}{C} = \mu_v \varepsilon_v \underset{\sim}{L}^{-1} \tag{4-7}$$

where $\underset{\sim}{L}^{-1}$ is the inverse of $\underset{\sim}{L}$. From this result we obtain

$$c_{GR} = \frac{\ell_{GR}}{|\underset{\sim}{L}|} \tag{4-8}$$

where $|\underset{\sim}{L}|$ is the determinant of $\underset{\sim}{L}$. From the results of [21] we may write, in terms of the above quantities,

$$V_{out} = V_{out}^{IND} + V_{out}^{CAP} \tag{4-9}$$

which is valid for a sufficiently small frequency.

Although there are no pigtail or shielded sections in the unshielded to unshielded configuration in Fig. 3(a), we will find it helpful to separate the total line length $\mathcal{L}$ into three sections corresponding to the pigtail and shielded sections of Fig. 3(b) and Fig. 3(c). Thus $\mathcal{L} = 2\mathcal{L}_p + \mathcal{L}_s$, and (4-1a) and (4-1b) may be separated as (for comparison with the shielded cable configurations in Fig. 3(b) and Fig. 3(c))

$$V_{out}^{IND} = \left(\frac{Z_{SR}}{Z_{SR} + Z_{LR}}\right) j\omega \ell_{GR} I_G (\mathcal{L}_p + \mathcal{L}_s + \mathcal{L}_p) \tag{4-10a}$$

$$V_{out}^{CAP} = \left(\frac{Z_{SR} Z_{LR}}{Z_{SR} + Z_{LR}}\right) j\omega c_{GR} V_G (\mathcal{L}_p + \mathcal{L}_s + \mathcal{L}_p) \tag{4-10b}$$

Since the line length factors out of the inductive and capacitive coupling expressions as in (4-10), it is clear from (4-10) that the total coupling may be considered to be the superposition of the inductive and capacitive coupling contributions over the individual sections of the line for a sufficiently small frequency such that (4-1) holds.

Although the corresponding results for the unshielded to shielded configuration in Fig. 3(b) have not been rigorously derived as for the unshielded to unshielded configuration above, we will suppose that the same principle of superposition of the coupling over the individual, coupled sections holds

for a sufficiently small frequency in a similar fashion as shown in Fig. 6 for the following reasons. If the frequency is sufficiently small so that the line and any section are electrically short, the impedance seen at the end of each section is approximately the impedance at the appropriate end of the line as indicated in Fig. 6. Thus the coupling over each section can be calculated by moving the load impedances to the appropriate ends of the section and considering three individual coupling problems as shown in Fig. 6. The voltages induced at the left end of each section, for example, $V_{\text{shielded section}}$ and $V_{\text{right pigtail}}$, due to coupling over these sections individually may then be transferred to the point of measurement of V_{out} since the section of the receptor line between V_{out} and the left end of a section is also electrically short as indicated in Fig. 6.

Consequently, we need to consider three separate coupling calculations shown in Fig. 6. The coupling over the pigtail sections is computed in a fashion similar to the unshielded to unshielded configuration with the exception that the per-unit-length mutual capacitance c_{GR} is computed in the presence of the pigtail wires. The coupling over the shielded section relies on the result of Mohr [8] which will be explained in detail. (See also [32].)

With regard to the superposition of the coupling contributions over the individual sections of the unshielded to shielded configuration in Fig. 3(b) as discussed above, we obtain the following relations. The pigtail coupling contributions are divided into inductive contributions:

$$V^{IND}_{\text{left pigtail}} = \left(\frac{Z_{SR}}{Z_{SR} + Z_{LR}}\right) (j\omega \ell_{GR} \ell_p) \, I_G \tag{4-11a}$$

$$V^{IND}_{\text{right pigtail}} = V^{IND}_{\text{left pigtail}} \tag{4-11b}$$

and capacitive contributions:

$$V^{CAP}_{\text{left pigtail}} = \left(\frac{Z_{SR} Z_{LR}}{Z_{SR} + Z_{LR}}\right) (j\omega c_{GR} \ell_p) \, V_G \tag{4-12a}$$

$$V^{CAP}_{\text{right pigtail}} = V^{CAP}_{\text{left pigtail}} \tag{4-12b}$$

in a fashion similar to the unshielded to unshielded case. I_G and V_G are again given by (4-2a) and (4-2b).

The per-unit-length mutual inductance, ℓ_{GR}, and mutual capacitance, c_{GR}, between the generator and receptor wires are computed, for this case, in the presence of the pigtail wires as opposed to the unshielded to unshielded case. The per-unit-length mutual inductance is essentially the same as the unshielded to unshielded case and is given in (4-3). The per-unit-length capacitance, c_{GR}, however is different from (4-8). We form the 3 x 3 per-unit-length inductance matrix of the generator, receptor and pigtail wires as

$$\underset{\sim}{L} = \begin{bmatrix} \ell_{GG} & \ell_{GR} & \ell_{GP} \\ \ell_{GR} & \ell_{RR} & \ell_{RP} \\ \ell_{GP} & \ell_{RP} & \ell_{PP} \end{bmatrix} \quad \text{H/m} \tag{4-13a}$$

where ℓ_{GG}, ℓ_{RR}, ℓ_{PP} are the per-unit-length self-inductances of the generator, receptor and pigtail wires, respectively, and ℓ_{GR}, ℓ_{GP}, ℓ_{RP} are the corresponding mutual inductances. If we ignore the dielectric insulations of the generator and receptor wires (the pigtail wire is bare in the experiment), we may compute the 3 x 3 per-unit-length capacitance matrix as

$$\underset{\sim}{C} = \mu_v \varepsilon_v \underset{\sim}{L}^{-1}$$

$$= \begin{bmatrix} (c_{GG} + c_{GR} + c_{GP}) & -c_{GR} & -c_{GP} \\ -c_{GR} & (c_{RR} + c_{GR} + c_{RP}) & -c_{RP} \\ -c_{GP} & -c_{RP} & (c_{PP} + c_{GP} + c_{RP}) \end{bmatrix} \text{F/m} \tag{4-13b}$$

where c_{GG}, c_{RR}, c_{PP} are the per-unit-length self-capacitances of the appropriate circuits and c_{GR}, c_{GP}, c_{RP} are the appropriate per-unit-length mutual capacitances. From this result we obtain

$$c_{GR} = \mu_v \varepsilon_v \frac{(\ell_{GP}\ell_{RP} - \ell_{GR}\ell_{PP})}{|\underset{\sim}{L}|} \quad \text{F/m} \tag{4-14}$$

A similar principle is applied to the shielded section and is based on the results of Mohr [8]. We will presume that grounding at least one end of the shield reduces the capacitive coupling over the shielded section to essentially zero, i.e.,

$$V^{CAP}_{\text{shielded section}} \cong 0 \tag{4-15}$$

The inductive coupling is not zero due to the finite impedance of the shield as pointed out by Mohr [8]. (See also the discussion in [32].) The results of [8] provide

$$V^{IND}_{\text{shielded section}} = \left(\frac{Z_{SR}}{Z_{SR} + Z_{LR}}\right) (j\omega \ell_{GS} \mathcal{L}_s)\ I_G \left(\frac{Z_{SH}}{Z_{SH} + j\omega \ell_{SS} \mathcal{L}_s}\right) \tag{4-16}$$

where ℓ_{GS} is the per-unit-length mutual inductance between the generator wire and the shield [7] and

$$\ell_{GS} = \ell_{GR} = \frac{\mu_v}{4\pi} \ell n \left[1 + \frac{4h_G h_S}{d_{GS}^2}\right] \text{ H/m} \tag{4-17}$$

where $h_S = h_R$ and $d_{GS} = d_{GR}$. I_G is given by (4-2a). The term ℓ_{SS} is the per-unit-length self-inductance of the shield above ground given by [7]

$$\ell_{SS} = \frac{\mu_v}{2\pi} \ell n \left[\frac{2h_S}{(r_s + t_s)}\right] \text{ H/m} \tag{4-18}$$

and Z_{SH} is the total impedance of the shield braid.

The result in (4-16) can be derived in the following manner. As a preliminary requirement we will assume that the frequency is sufficiently small so that each current is uniformly distributed over the appropriate conductor cross-section, i.e., skin effect may be neglected. Clearly, if the shield were a solid, cylindrical conductor instead of being composed of wire braids, the currents carried by the shield would concentrate towards the shield surfaces as the frequency is increased. If the shield wall thickness is less than, say, one skin depth, then it is probably reasonable to assume a uniform distribution of current over its cross section. The skin depth, δ, is given by

$$\delta = \frac{1}{\sqrt{\pi f \mu_v \sigma}} \tag{4-19}$$

where $\sigma = 5.8 \times 10^7$ is the conductivity of copper. If we approximate the shield as being a cylinder with wall thickness equal to the diameter of the strands of the braid, $t_s = 2r_b = 5.0$ mils, then the wall thickness would be one skin depth at a frequency of 270.8 kHz. From the standpoint of this low-frequency, approximate model we will therefore presume the current to be distributed uniformly over the shield cross section.

Consider a cross section of the line shown in Fig. 7 in which the currents are uniformly distributed over the conductor cross sections. The mutual inductance ℓ_{GR} relates the generator wire current, I_G, to the magnetic flux passing between the receptor wire and the ground plane. The mutual inductance ℓ_{GS} relates the generator wire current, I_G, to the magnetic flux passing between the shield and the ground plane. Each of these fluxes induce a voltage in the appropriate circuit as shown in Fig. 8. Each of these induced voltage sources also produces a current circulating in the appropriate circuit as shown in Fig. 8. In addition, the induced shield current, I_S, induces, via a second-order effect, an additional voltage source in the receptor circuit via the mutual inductance ℓ_{RS} between the receptor circuit and the shield as shown in Fig. 8. In Fig. 8, we have shown the total impedance of the shield braid, Z_{SH}, and the self inductance of the shield with the ground plane, $\ell_{SS}\mathcal{L}_s$. The self impedances of the generator and receptor wires are neglected. The current induced in the shield-ground plane circuit due to the generator current is

$$I_S = - \frac{j\omega\ell_{GS}\mathcal{L}_s I_G}{Z_{SH} + j\omega\ell_{SS}\mathcal{L}_s} \tag{4-20}$$

The receptor wire induced current due to the generator wire current and the shield current is

$$I_R = \frac{-j\omega\ell_{GR}\mathcal{L}_s I_G - j\omega\ell_{RS}\mathcal{L}_s I_S}{Z_{SR} + Z_{LR}} \tag{4-21}$$

The resultant voltage across Z_{SR} becomes

$$V_{\text{shielded section}} = -Z_{SR} I_R \tag{4-22}$$

Combining (4-20), (4-21) and (4-22) we obtain

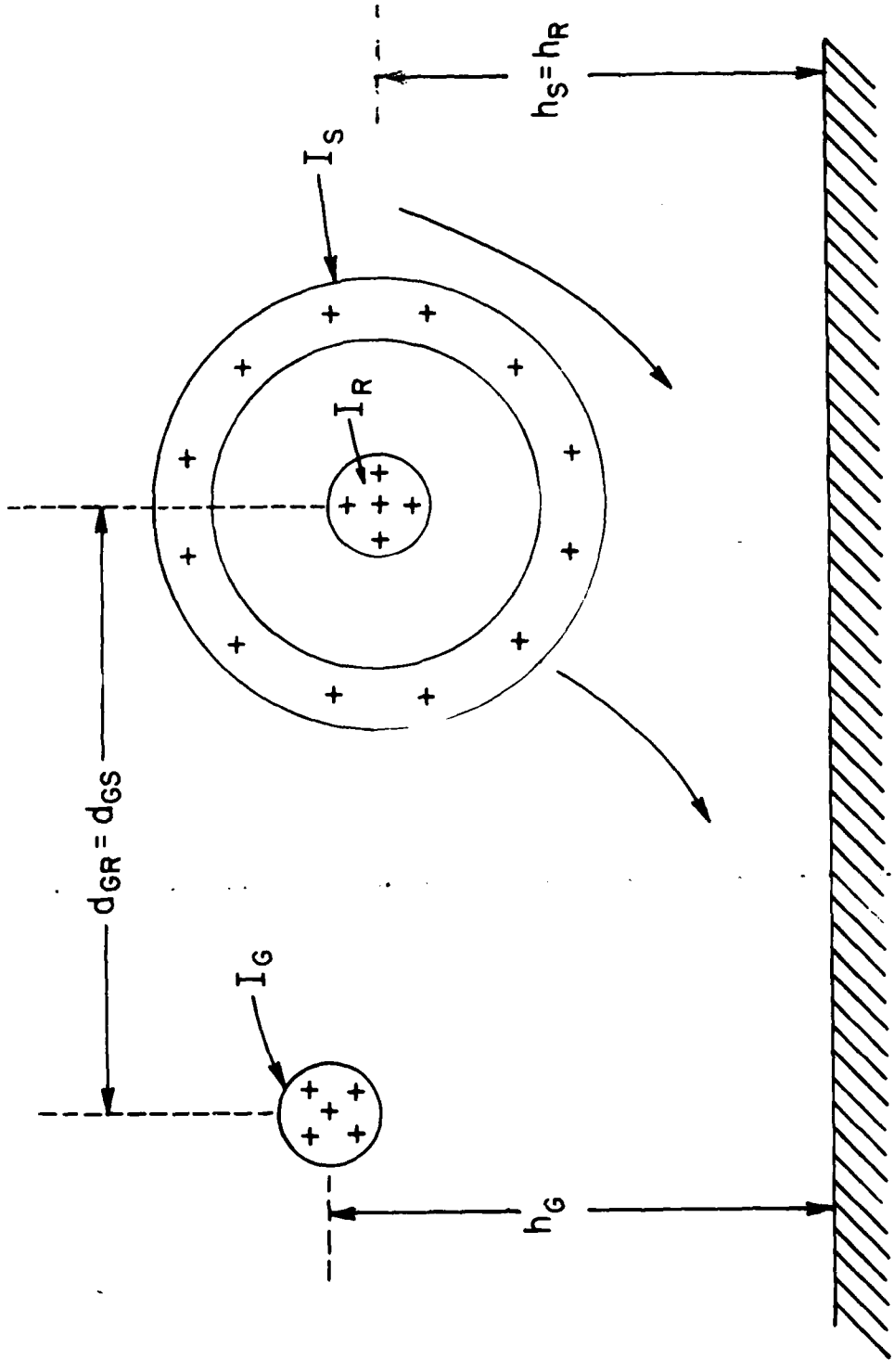

Fig. 7. A cross section of the unshielded to shielded configuration illustrating the uniform current distribution assumption.

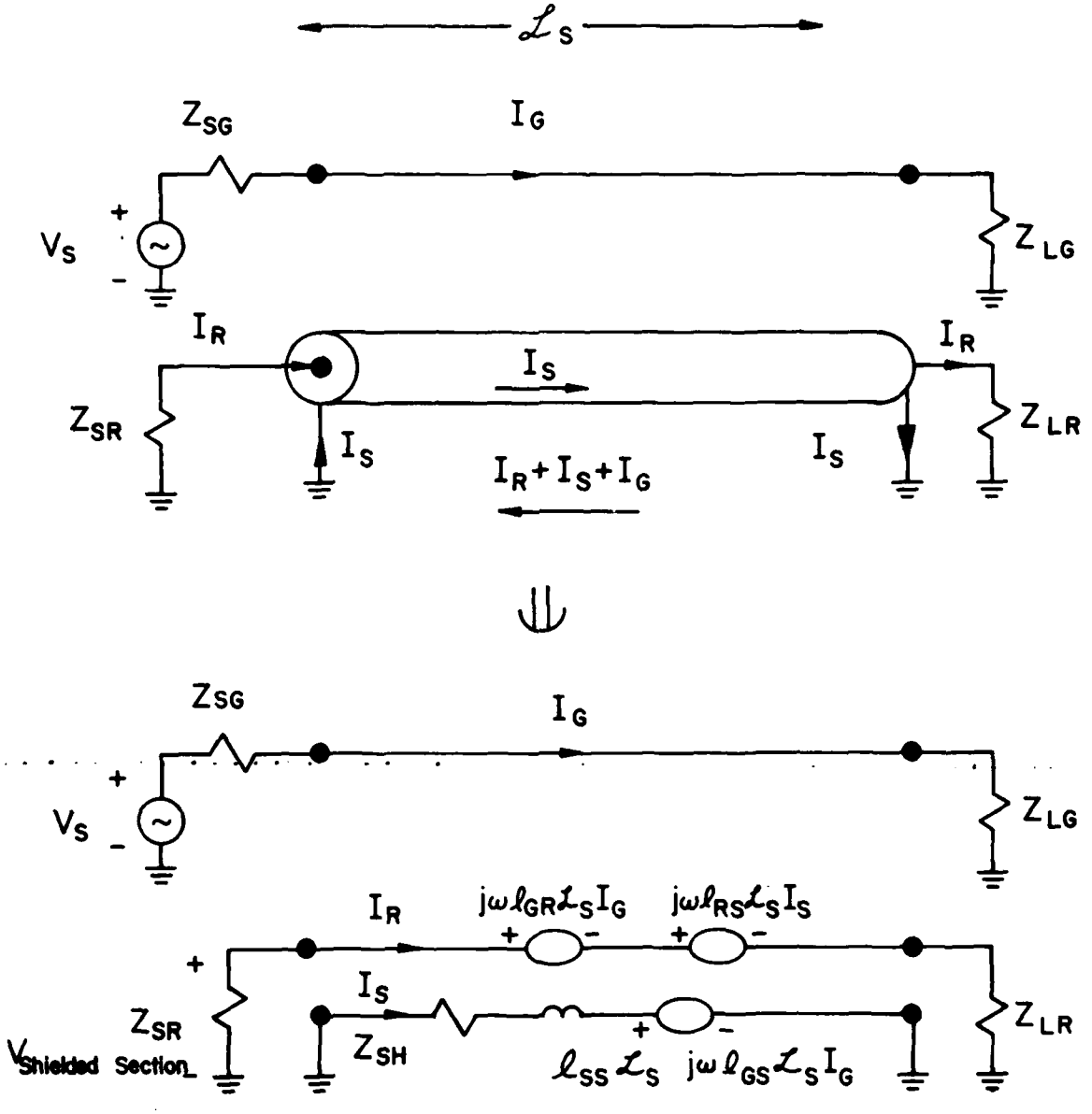

Fig. 8. The low-frequency equivalent circuit for the unshielded to shielded configuration.

$$V_{\text{shielded section}} = \frac{Z_{SR}}{Z_{SR}+Z_{LR}}\left[j\omega\ell_{GR}\mathcal{I}_s - j\omega\ell_{RS}\mathcal{I}_s\left(\frac{j\omega\ell_{GS}\mathcal{I}_s}{Z_{SH}+j\omega\ell_{SS}\mathcal{I}_s}\right)\right]I_G \tag{4-23}$$

$$= \frac{Z_{SR}}{Z_{SR}+Z_{LR}}\left[\frac{j\omega\ell_{GR}\mathcal{I}_s Z_{SH} - \omega^2\ell_{GR}\mathcal{I}_s\ell_{SS}\mathcal{I}_s + \omega^2\ell_{RS}\mathcal{I}_s\ell_{GS}\mathcal{I}_s}{Z_{SH}+j\omega\ell_{SS}\mathcal{I}_s}\right]$$

Here we have only considered first-order effects from the generator current to the receptor wire and to the shield and a second-order effect from the shield to the receptor wire.

Note that the self inductance of the shield with the ground plane, ℓ_{SS}, is approximately the same as the mutual inductance between the receptor wire and the shield ℓ_{RS}, i.e.,

$$\ell_{RS} \cong \ell_{SS} \tag{4-24}$$

Similarly, the mutual inductance between the generator and receptor wires, ℓ_{GR}, and the mutual inductance between the generator wire and the shield, ℓ_{GS}, are approximately the same, i.e.,

$$\ell_{GR} \cong \ell_{GS} \tag{4-25}$$

These results follow from the definitions of self and mutual inductance. For example, to show (4-24), we observe that ℓ_{RS} is the ratio of the flux passing between the shield and the ground plane to the receptor wire current. Similarly, ℓ_{SS} is the ratio of the flux passing between the shield and the ground plane to the shield current. Assuming that the receptor and shield currents are uniformly distributed over the cross sections of these conductors then it would make little difference in the computation of ℓ_{RS} and ℓ_{SS} whether the shield current is in the shield wall or concentrated at the center of the shield (the position of the receptor wire). Thus it is clear that $\ell_{RS} \cong \ell_{SS}$. Substituting (4-24) and (4-25) into (4-23) results in

$$V_{\text{shielded section}} = \frac{Z_{SR}}{Z_{SR}+Z_{LR}}\, j\omega\ell_{GS}\mathcal{I}_s\left[\frac{Z_{SH}}{Z_{SH}+j\omega\ell_{SS}\mathcal{I}_s}\right] \tag{4-26}$$

where we have replaced ℓ_{GR} with ℓ_{GS} via (4-25).

The term Z_{SH} in (4-16) is the total impedance of the shield braid and is computed in the following approximate manner. First we compute the per-unit-length impedance of an isolated strand of the braid

$$z_{ST} = r_{ST} + j\omega\ell_{ST} \ \Omega/m \tag{4-27}$$

This calculation is standard and is described in [22]. An approximation to the exact result for this isolated strand is given by the following. We first compute the per-unit-length D-C resistance

$$r_0 = \frac{1}{\pi\sigma r_b^2} \ \Omega/m \tag{4-28}$$

and per-unit-length D-C internal inductance

$$\ell_0 = \frac{\mu_v}{8\pi} \quad H/m$$
$$= .5 \times 10^{-7} \tag{4-29}$$

of each strand where r_b is the strand radius. In terms of these parameters, the resistance, r_{ST}, and internal inductance, ℓ_{ST}, of the strand are approximated by [22]

(I) $r_b \leq \delta$

$$r_{ST} = r_0 \tag{4-30a}$$
$$\ell_{ST} = \ell_0$$

(II) $\delta < r_b < 3\delta$

$$r_{ST} = \frac{1}{4}\left(\frac{r_b}{\delta} + 3\right) r_0 \tag{4-30b}$$

$$\ell_{ST} = \left[1.15 - .15\left(\frac{r_b}{\delta}\right)\right]\ell_0$$

(III) $r_b \geq 3\delta$

$$r_{ST} = \frac{r_b}{2\delta} r_0 \qquad (4\text{-}30c)$$

$$\ell_{ST} = \frac{2\delta}{r_b} \ell_0$$

We will further assume that the shield consists of a total of all wire strands connected electrically in parallel. If the braid consists of B belts with W wires per belt then a total of BW wires are connected in parallel. The weave angle of the belts, Θ_w, causes the actual length of the braid wires to be longer than the shield length, $\mathcal{L}_s$, by a factor of $\cos\Theta_w$. Thus the shield impedance is taken to be

$$Z_{SH} \cong \frac{Z_{ST} \mathcal{L}_s}{BW \cos\Theta_w} \quad \Omega \qquad (4\text{-}31)$$

The equations for the individual braid wire impedances given in (4-30) include skin effect but presume a current distribution over the cross section of the braid wire which is symmetric about the wire axis. The close proximity of the wires in the braid obviously invalidates this symmetric current assumption to some degree. We choose to ignore this practicality since, the calculation of the exact value of shield impedance appears to be a formidable problem and the model predictions based on the symmetric current assumption in the braid wires prove to be adequate as is shown later in this section.

It should be noted that Mohr, in a publication [9] subsequent to [8], and Shenfeld in [10] pointed out that, theoretically, equation (4-16) is not correct. The shield effectiveness term in (4-16)

$$\frac{Z_{SH}}{Z_{SH} + j\omega \ell_{SS} \mathcal{L}_s}$$

is amended by Mohr in [9] to be

$$\frac{Z_T}{Z_T + j\omega \ell_{SS} \mathcal{L}_s}$$

and by Shenfeld in [10] to be

$$\frac{Z_T}{Z_{SH} + j\omega\ell_{SS}\mathcal{L}_s}$$

The quantity Z_T is the shield surface transfer impedance and an equation for braided shields such as were used in this investigation is given by Vance [16]. Although Vance's result was derived for an isolated, braided-shield cable with no ground plane present, we will nevertheless, use his result for our configurations.

The surface transfer impedance relates the axial, induced electric field (V/m) on one surface of the shield to the current on the other surface and was originally developed by Schelkunoff for solid, cylindrical shields [11,18]. For a solid, cylindrical shield and a frequency which is sufficiently small so that the current is uniformly distributed (or approximately so) over the shield cross section, it becomes clear that Z_T and Z_{SH} are equivalent. Using Vance's expression for Z_T, we will show in Section VI that Z_T and Z_{SH} are virtually identical for the braided shield which was used in the investigation below 1 MHz. In fact, both expressions are approximately equal to the D-C resistance of the shield braid below 1 MHz so that we could have simply used the D-C resistance of the shield braid up to 1 MHz in (4-16) instead of Z_{SH}. Thus, for the purposes of the low-frequency model it is irrelevant which term is used in (4-16). We chose to use Z_{SH}. A more complete discussion of the concept of surface transfer impedance will be given in Section VI.

For frequencies such that the shield-ground plane self-inductance, $\omega\ell_{SS}\mathcal{L}_s$, is less than the shield self-impedance, Z_{SH}, (4-16) becomes

$$V^{IND}_{\text{shielded section}} = \frac{Z_{SR}}{Z_{SR} + Z_{LR}} j\omega\ell_{GR}\mathcal{L}_s' I_G \qquad (4\text{-}32)$$

$$\omega\ell_{SS}\mathcal{L}_s << Z_{SH}$$

where $\ell_{GR} = \ell_{GS}$. Note that (4-32) is identical to the inductive coupling to the shieldedwire over the shielded section if no shield were present. (See (4-1a) with $\mathcal{L}_s$ substituted for $\mathcal{L}$.) It is also the result if the shield were not grounded at both ends since for this situation, we may substitute $Z_{SH} = \infty$ in (4-16).

For higher frequencies, (4-16) becomes

$$V^{IND}_{\text{shielded section}} = \frac{Z_{SR}}{Z_{SR} + Z_{LR}} Z_{SH} \frac{\ell_{GR}}{\ell_{SS}} I_G \qquad (4\text{-}33)$$

$$\omega \ell_{SS} \mathcal{L}_s \gg Z_{SH}$$

so that the inductive coupling over the shielded section is independent of frequency. (Frequency dependence of the termination impedances, Z_{SR} and Z_{LR}, as well as Z_{SH}, however result in a frequency dependence of (4-33). For our results, Z_{SR} and Z_{LR} are purely resistive and Z_{SH} shows only a minor frequency dependence over the frequency range for which this model will be used.) As discussed by Ott [32], this seems to occur because for frequencies such that $\omega \ell_{SS} \mathcal{L}_s \gg Z_{SH}$, the majority of the shielded (receptor) wire current returns via the shield instead of the ground plane thus reducing the loop area for coupling.

Thus, according to (4-16), for the shield to reduce the inductive coupling to the shielded wire over the shielded section, it should be grounded at both ends and the frequency must be such that $\omega \ell_{SS} \mathcal{L}_s \gg Z_{SH}$. As for capacitive coupling to the shielded wire over the shielded section, the shield need be grounded at only one end to achieve a substantial reduction in this component of the total coupling.

Therefore, the superposition of these various coupling factors takes the form

$$\begin{aligned} V_{out} = {} & V^{IND}_{\text{left pigtail}} + V^{CAP}_{\text{left pigtail}} \\ & + V^{IND}_{\text{shielded section}} + \cancel{V^{CAP}_{\text{shielded section}}}\ 0 \\ & + V^{IND}_{\text{right pigtail}} + V^{CAP}_{\text{right pigtail}} \end{aligned} \qquad (4\text{-}34)$$

The capacitve coupling over the shielded section, $V^{CAP}_{\text{shielded section}}$, is not taken to be zero unless at least one end of the shield is grounded. Each of these factors will be plotted separately against the experimental results.†

†See Appendix C.

The left and right pigtail factors will be combined as

$$V^{IND}_{pigtail} = V^{IND}_{left\ pigtail} + V^{IND}_{right\ pigtail} \tag{4-35a}$$

$$V^{CAP}_{pigtail} = V^{CAP}_{left\ pigtail} + V^{CAP}_{right\ pigtail} \tag{4-35b}$$

For the shielded to shielded case shown in Fig. 3(c), we apply a similar principle of superimposing the coupling over the individual segments. The pigtail coupling contributions are identical in form to the unshielded to shielded case given in (4-11) and (4-12). The per-unit-length mutual inductance ℓ_{GR} is given by (4-3). However the per-unit-length capacitance, c_{GR}, is different from the unshielded to shielded case since one should include the effect of the pigtail wire of the generator circuit shield. This may be accommodated by using the 4 x 4 per-unit-length inductance and capacitance matrices similar to (4-13) and again using the relation $\underset{\sim}{C} = \mu_v \varepsilon_v \underset{\sim}{L}^{-1}$ to compute c_{GR}. The inductive coupling contribution over the shielded section is changed to account for an additional shield on the generator circuit and we obtain in a similar fashion to the unshielded to shielded case [8]

$$V^{IND}_{shielded\ section} = \left(\frac{Z_{SR}}{Z_{SR}+Z_{LR}}\right)(j\omega\ell_{GR}\mathcal{L}_s)I_G \left(\frac{Z^G_{SH}}{Z^G_{SH}+j\omega\ell^G_{SS}\mathcal{L}_s}\right)\left(\frac{Z^R_{SH}}{Z^R_{SH}+j\omega\ell^R_{SS}\mathcal{L}_s}\right) \tag{4-36}$$

where $Z^G_{SH}(Z^R_{SH})$ and $\ell^G_{SS}(\ell^R_{SS})$ are the shield impedance and self inductance with the ground plane, respectively, of the generator (receptor) circuit shield. We will again presume that the capacitive coupling contribution over the shielded section is zero when at least one end of the shield is grounded. The received voltage across Z_{LR} can be obtained by substituting $Z_{SR}(Z_{LR})$ for $Z_{LR}(Z_{SR})$ in the above equations and changing the sign of (4-36) and (4-16).

The calculation of the per-unit-length mutual inductance, ℓ_{GR}, over the pigtail sections is essentially the same for all of the three cases (unshielded to unshielded, unshielded to shielded, and shielded to shielded) and is given by (4-3). However, the calculation of the per-unit-length mutual capacitance, c_{GR}, over the pigtail sections is, theoretically, affected by the pigtail wires as indicated above. Practically, however, it appears that the pigtail wires have little effect on c_{GR} (at least for this configuration

and these dimensions). For example, c_{GR} for unshielded to unshielded, unshielded to shielded and shielded to shielded were computed to be 10.3 pF/m, 11.8 pF/m, and 9.05 pF/m, respectively. Thus the per-unit-length mutual capacitance c_{GR} over the pigtail sections may be reasonably calculated for these dimensions by ignoring the pigtail wires. For other dimensions and pigtail configurations, however, this may not be true.

These low-frequency models do not take into account the pigtail wires over the pigtail sections except in the computation of c_{GR}. The interaction between the pigtail wires and the generator and receptor wires is not taken into account. In Section VI, the multiconductor transmission line model will be formulated. This model takes into account the presence of and interaction between all adjacent conductors (e.g., the pigtail wires and the generator and receptor wires). We will find that in the shielded to shielded case, the pigtail wires have a substantial effect on the coupling

for R = 50Ω (on the order of 10 dB - 20 dB) which is predicted by the multiconductor transmission line model within 1.5 dB. Thus these low-frequency models may be used for obtaining only first-order, conservative estimates of the crosstalk, although the principle of superimposing the coupling contributions over the pigtail and shielded sections seems to be valid.

Now we compare the predictions of the above low-frequency models to the experimental results. These graphs are contained in Appendix C.

The results for the unshielded to unshielded configuration illustrated in Fig. 3(a) are shown for the TOUCHING separation for R = 50Ω in Fig. C-1 and for R = 1kΩ in Fig. C-2. Note that for R = 50Ω, the coupling is predominantly inductive and the low-frequency model provides prediction accuracies within 1 dB for frequencies less than 2 MHz. (The line is approximately 1/30 λ in length at 3 MHz.) For R = 1kΩ, the coupling is predominantly capacitive. However the prediction accuracy of the low-frequency model is not as good as for R = 50Ω but is typically within 6 dB. This relatively poor prediction when capacitive coupling is dominant is attributable to the close proximity of the wires (.23 cm) and the fact that the calculation of the mutual capacitance c_{GR} ignored the presence of the wire insulation dielectric. In Appendix G it is shown that the dielectric insulation may increase the mutual capacitance, c_{GR}, by factors of as much as 1.96 (5.85 dB) for the TOUCHING separation and 1.2 (1.6 dB) for the WIDE separation. Thus the ca-

pactive coupling contributions in Appendix C should be increased by approximately these amounts. Thus the predictions for R = 1kΩ in Fig. C-2 are truly in error by only about 2 dB. Due to the dominance of inductive coupling for R = 50Ω, the result in Fig. C-1 is virtually unaffected by the dielectric insulation. The corresponding results for the WIDE separation are shown in Fig. C-3 and Fig. C-4. Note that for R = 1kΩ and the WIDE separation in Fig. C-4 that the predictions of the low frequency model are quite good even though capacitive coupling is dominant and the wire insulation dielectric was neglected in computing c_{GR}. This result also indicates that the poor predictions for R = 1kΩ and the TOUCHING separation in Fig. C-2 are due to neglecting the insulation dielectric in computing c_{GR}.

The predictions of the low-frequency model for the unshielded to shielded configuration illustrated in Fig. 3(b) are given in Fic. C-5 through Fig. C-12. The results for R = 50Ω are given in Fig. C-5 through Fig. C-8. Note in Fig. C-5 for the TOUCHING separation and .5 cm pigtails that the low-frequency model provides good predictions (within 1 dB) up to 800 kHz ($\ell \doteq \frac{1}{100}\lambda$). Also observe that the coupling is due predominantly to the shielded section below 1 MHz. The corresponding results for the 8 cm pigtails are shown in Fig. C-6. Again, we obtain good predictions with the low-frequency model up to 3 MHz. However, note that above 100 kHz, the predominant coupling is via the pigtails and is inductive. The pigtail coupling, although "small", is larger than the coupling over the shielded section above 100 kHz and thus becomes the dominant coupling factor. The corresponding results for R = 50Ω, and WIDE separation (1.5 cm) are given in Fig. C-7 and Fig. C-8 and result in the same observations. The dielectric insulation has virtually no effect on the results in Fig. C-5 through Fig. C-8 since inductive coupling is predominant.

The results for unshielded to shielded and R = 1kΩ are shown in Fig. C-9 through Fig. C-12. Note in Fig. C-9 for the TOUCHING separation and .5 cm pigtails that the low-frequency model provides good predictions up to 1 MHz. Below 100 kHz, the coupling over the shielded section is dominant. Above 100 kHz the pigtail coupling becomes dominant and is capacitive. The results for the TOUCHING separation and 8 cm pigtails are shown in Fig. C-10. In Fig. C-10, we observe that the shield (inductive) coupling and pigtail (capacitive) coupling are equal below 2 kHz above which the pigtail (capacitive) coupling dominates. The capacitive coupling should be increased by approxi-

mately 5 dB to account for the dielectric. The predictions then show a modest error of approximately 1 dB. The corresponding results for R = 1kΩ and the WIDE separation (1.5 cm) are shown in Fig. C-11 and Fig. C-12 and result in the same observations. For these WIDE separations, the dielectric insulations increase c_{GR} by only about 1.5 dB so only a minor increase in the capacitive coupling predictions result.

The corresponding results for the shielded to shielded configuration and the TOUCHING separations are shown in Fig. C-13 through Fig. C-16. The dielectric insulations of the wires once again increase the mutual capacitance, c_{GR}, of the pigtails by approximately 5 dB for these TOUCHING separations. Thus the pigtail capacitive coupling predictions should be increased by approximately this amount and the resulting total predictions are in error by only about 1.5 dB. The "overpredictions" of the low-frequency model for R = 50Ω when pigtail coupling is dominant are again apparently due to the presence of the pigtail wires as discussed previously. The results for the WIDE separation and 8 cm pigtails are shown for R = 50Ω in Fig. C-17 and for R = 1kΩ in Fig. C-18. Again the predictions for R = 50Ω are above the experimental results when pigtail coupling is dominant which is apparently due to the pigtail wires. For R = 1kΩ the predictions are quite good for this WIDE separation which again tends to confirm the effect of neglecting the dielectric insulation in the computation of c_{GR}.

Again the low-frequency model provides reasonably accurate predictions. These results tend to support the previous conclusions for the unshielded to shielded case in a similar manner. In these figures, one can observe the magnitude and frequency range of the degradation in the effectiveness of the shield due to the pigtails since we would presume that for no pigtails, the coupling would follow the predictions of shield (inductive). These results, therefore, seem to indicate that the approximate, low-frequency model is reasonably accurate for a sufficiently small frequency. They also seem to support the idea that one may superimpose the individual coupling contributions over the pigtail and shielded sections as described above. It thus becomes clear that pigtail sections which constitute only a minor fraction of the total cable length may play a significant role in the degradation of the effectiveness of the shield in the reduction of crosstalk.

V. Effect of Shield Grounding Configurations

In this section, we will investigate the effects of the shield grounding configuration on the crosstalk to a braided-shield cable. In all previous results, both ends of a shield were grounded via the pigtail wires as illustrated in Fig. 3. In this section, we will investigate the effect of grounding only one end or neither end of the shield. The coupling from an unshielded wire to a shielded wire illustrated in Fig. 3(b) will be shown for these shield grounding configurations. The results are shown in Appendix D.

The results for R = 50Ω, 0.5 cm pigtails and TOUCHING separation are given in Fig. D-1. Note that the crosstalk when the shield is ungrounded or grounded at only one end is virtually the same. In fact, by comparing these results to the results for coupling between two unshielded wires given in Fig. A-19 we find that the shield has virtually no effect for R = 50Ω unless both ends are grounded. Intuitively, this is reasonable since for these "low impedance" loads, one can show that inductive coupling predominates in the unshielded to unshielded case. (See, for example, Fig. C-1.) As pointed out by Ott [32], the shield should have a closed path with the ground plane to allow a shield current to flow in order to counteract this inductive coupling. (See also the derivation of the low-frequency model in the previous chapter.) However, note that even if both ends of the shield are grounded, the effectiveness of the shield in reducing crosstalk (over that for the coupling between two unshielded wires illustrated in Fig. 3(a)) comes into play for R = 50Ω only above a certain frequency (in this case, approximately 6 kHz).

The low-frequency models discussed in the previous section seem to explain these two phenomena. In the unshielded to unshielded case and R = 50Ω, one can show that the coupling is predominantly inductive and given by (4-10a). (See Fig. C-1 and Fig. C-3.) Placing a shield around the receptor wire has virtually no effect on this (dominant) inductive coupling over the shielded section unless both ends of the shield are grounded and the self-impedance of the shield-ground plane circuit, $\omega \ell_{SS} \mathcal{L}_s$, exceeds the braid self-impedance, Z_{SH}. (See (4-32) and (4-33) and the accompanying discussion. A simple calculation will show that $\omega \ell_{SS} \mathcal{L}_s = Z_{SH}$ at 5.5 kHz.) Although grounding the shield at at least one end substantially reduces the capacitive coupling to the shielded wire over the shielded section, this effect is not seen since inductive coupling is predominant when the shield is removed (the unshielded

to unshielded case).

It should be pointed out that grounding both ends of the shield may have its disadvantages with respect to ground-loop problems. A noise voltage induced in the shield-ground plane loop will induce current in the loop which may be coupled to the receptor circuit [32]. However, it is clear that in this case (R = 50Ω) that if the shield is not grounded at both ends, the presence of the shield affords no advantage over an unshielded wire.

The results for R = 50Ω, TOUCHING separation and 3 cm pigtails are shown in Fig. D-2 and for 8 cm pigtails in Fig. D-3. We reach the same conclusions as for the 0.5 cm pigtails concerning the effect of the shield grounding. However, the pigtails have substantially reduced the effectiveness of the shield.

The corresponding results for R = 50Ω and the WIDE separation are given in Fig. D-4 through Fig. D-6. These results yield the same conclusions as for the TOUCHING separation.

The results for R = 1kΩ and the TOUCHING separation are shown in Fig. D-7 through Fig. D-9. For this value of load resistance, a single-end grounded shield and an ungrounded shield show a difference in reduction of crosstalk as opposed to the R = 50Ω case. We also observed, for R = 50Ω, that even though the shield was grounded at both ends, the effectiveness of the shield came into play above approximately 6 kHz; below 6 kHz there was virtually no difference between the unshielded to unshielded case and the unshielded to shielded case for all grounding configurations. For R = 1kΩ in Fig. D-7 through Fig. D-9, the single-end grounded and double-end grounded cases are again virtually identical below 6 kHz.

The corresponding results for R = 1kΩ and the WIDE separation are given in Fig. D-10 through Fig. D-12. These results yield the same conclusions as for the TOUCHING separation.

These differences between the R = 1kΩ and R = 50Ω cases also seem to be explainable in terms of the low-frequency models. For the unshielded to unshielded case and R = 1kΩ, one can show that the coupling is predominantly capacitive. (See Fig. C-2 and Fig. C-4.) For the unshielded to shielded case, one can show that when the shield is ungrounded, the results are virtually identical to the unshielded to unshielded case (capacitive). (For example, compare Fig. D-7 and Fig. A-21. There is a maximum difference of less

than 1.5 dB for frequencies less than 10 MHz.) Placing a shield around the receptor wire and grounding it at at least one end substantially reduces this capacitive coupling to the shielded wire over the shielded section. Thus for a single-end grounded shield and R = 1kΩ, the contribution to the total coupling over the shielded section reverts to a lower value which is essentially the inductive coupling to the shielded wire for the unshielded to unshielded case over this shielded section given by (4-1a) with $\mathcal{L}_s$ substituted for $\mathcal{L}$. When both ends of the shield are grounded, the coupling over the shielded section falls to an even lower value of inductive coupling given by (4-1b). For frequencies such that $\omega \ell_{SS} \mathcal{L}_s < Z_{SH}$, this inductive coupling over the shielded section becomes the same for the double-end grounded case and the single-end grounded cases as discussed above for the R = 50Ω termination. Thus the results merge at approximately 6 kHz. These differences in the coupling behavior for R = 50Ω and R = 1kΩ thus seem to be clearly explainable, and the low-frequency model plays an important role in the clarity of these explanations.

Thus the low-frequency model is helpful in explaining these differences in the effect of the shield grounding configuration and the effect of the terminal impedances. The above observations can be summarized by the following. (We only consider the contribution to the coupling over the shielded section in the following since the shield grounding configuration does not affect the pigtail coupling contribution.) For the shield ungrounded, the capacitive and inductive coupling are virtually unaffected by the presence of the shield and are essentially the same as if the shield were removed. Depending on the terminal impedances, either capacitive or inductive coupling predominates. Now consider a single-end grounded shield. Grounding only one end of the shield removes the above capacitive coupling (over the shielded section) but has no effect on the inductive coupling. Thus when at least one end of the shield is grounded, the total coupling to the shielded wire over the shielded section is inductive. If inductive coupling was predominant in the ungrounded case, grounding only one end of the shield will result in no reduction in this coupling over the shielded section. If the capacitive coupling was predominant in the ungrounded case, grounding only one end of the shield <u>will</u> result in a reduction in this coupling over the shielded section. If we further ground both ends of the shield, the inductive coupling of the above single-end grounded

case (which was the total coupling over the shielded section) will be reduced via (4-16) so long as the shield is effective; that is, so long as the self-inductive reactance of the shield, $\omega \ell_{SS} \angle_s$, is greater than the shield impedance, Z_{SH}. Otherwise, grounding both ends of the shield will show no reduction in coupling over the single-end grounded case. These points should be kept in mind when assessing the effectiveness of a shield grounding configuration.

Note in Fig. D-7 through Fig. D-12 that, above approximately 200 kHz, there is a difference in crosstalk depending on which end of the shield is grounded. This is also quite reasonable if one imagines the measured voltage, V_{out}, as being the sum of the voltage between the shielded wire and the shield and the voltage between the shield and the ground plane. If the shield is grounded at the source end, the voltage between the shield and ground is eliminated from V_{out} resulting in a different voltage than would result if the shield were grounded at the load end (and ungrounded at the source end). Obviously the line must be somewhat significant in length, electrically, in order that the shield to ground voltage at the ungrounded end be different from zero (at the grounded end). The data in Fig. D-7 through D-12 reflect this, and at 200 kHz the line is $\frac{1}{410}$ λ in electrical length.

The corresponding results for the shielded to unshielded configuration are shown in Fig. D-13 through Fig. D-16 and result in similar conclusions.

VI. The Multiconductor Transmission Line Model

The low-frequency models discussed in the previous section relied on the frequency being sufficiently small so that lumped-circuit models provide an adequate characterization of the line. In addition, these models utilized only the primary inductance and capacitance parameters - the mutual elements ℓ_{GR} and c_{GR} - between the generator and receptor circuits. The self inductances and capacitances of the line were not employed directly in the model. (The self inductances, however, were employed in the calculation of c_{GR}.) Thus not only must the line be electrically short in order that lumped models suffice, but the frequency must be sufficiently small so that the omission of these self elements does not significantly affect the model predictions. In addition, to consider the effect of pigtails, we simply superimposed the coupling contributions over the pigtail sections and the shielded section. This also is an approximate technique which clearly relies on the frequency being sufficiently small.

In this section, we wish to formulate the distributed parameter, multiconductor transmission line (MTL) model of the coupled line [7]. In this model, the distributed effects prevalent at the higher frequencies are taken into account, and many of the other approximations inherent in the low-frequency model, such as the assumption of weak coupling and the neglect of the self inductances and capacitances, are not employed in this model. The model, however, requires considerably more computational effort than the low-frequency model, but the predictions of both models should converge at the lower frequencies.

Some of the interesting phenomena arising in the experimental data are predictable with the MTL model. For example, the case of a single-end grounded shield showed different coupling above approximately 200 kHz for $R = 1k\Omega$ depending on which end of the shield was grounded. The MTL model predicts this within 1 dB whereas the low-frequency model made no distinction between which end of the shield was grounded. In addition, when the line is electrically long, say $\ell > \frac{1}{10}\lambda$, we observed rather severe variations in the voltage transfer ratio with a change in frequency. The low-frequency model is, of course, not expected to provide predictions in this frequency range. These variations are, of course, expected and the frequency range for which

$\ell > \frac{1}{10}\lambda$ will be referred to as the "standing wave region." In the standing wave region, we will find that the predictions of the MTL model tend to follow the experimental results but are somewhat poorer than when the line is electrically short.

As indicated in Section I, there has been considerable interest in modeling shielded cables dating back to the earlier work of Schelkunoff [11,12]. Low-frequency models similar to those in Section III (but without pigtail considerations) were developed by Mohr [8,9]. More recently, work has been concentrated on modeling a single, braided-shield cable which is illuminated by an incident field [13-19]. These works stem from the interest in the vulnerability of the shielded cable (or, more importantly, the equipments at its terminals) to a nuclear electromagnetic pulse (NEMP), a lightning induced electromagnetic pulse (LEMP) or a high-power radar. The coupling considered in these works is therefore appropriately characterized as field-to-wire. The coupling considered in this report is appropriately characterized as wire-to-wire since we are interested in the coupling to a braided-shield cable from other, adjacent wires and not an incident field, although the wire-to-wire coupling is via field quantities also.

In the above field-to-wire problems, the coupling through a braided-shield cable to the interior, shielded wire from the incident field is related to the surface transfer impedance and transfer admittance of the braid. These quantities can be illustrated as follows. First we consider the shield transfer impedance [11,14-18]. As a preliminary, we consider an infinitely long, solid conducting cylinder. Suppose the cylinder carries a total current I directed in the axial (x) direction where $I = I_{in} + I_{out}$. The return path for I_{in} is within the cylindrical surface while the return path for I_{out} is outside the surface. The conducting cylinder has finite conductivity σ and therefore the current I flowing along the cylinder will induce electric fields on the inner and outer surfaces of the cylinder, E_{in} and E_{out}, respectively, which are directed in the axial direction of the cylinder. The currents and induced electric fields may be related as [11,18]

$$\begin{bmatrix} E_{in} \\ E_{out} \end{bmatrix} = \begin{bmatrix} z_{ii} & z_{io} \\ z_{oi} & z_{oo} \end{bmatrix} \begin{bmatrix} I_{in} \\ I_{out} \end{bmatrix} \quad \text{V/m} \qquad (6\text{-}1)$$

The terms z_{ii} and z_{oo} may be thought of as per-unit-length self impedances of the surfaces:

$$z_{ii} = \frac{E_{in}}{I_{in}}\bigg|_{I_{out} = 0} \quad \Omega/m \tag{6-2a}$$

$$z_{oo} = \frac{E_{out}}{I_{out}}\bigg|_{I_{in} = 0} \quad \Omega/m \tag{6-2b}$$

whereas the terms z_{io} and z_{oi} are called surface transfer impedances (per-unit-length):

$$z_{io} = \frac{E_{in}}{I_{out}}\bigg|_{I_{in} = 0} \quad \Omega/m \tag{6-3a}$$

$$z_{oi} = \frac{E_{out}}{I_{in}}\bigg|_{I_{out} = 0} \quad \Omega/m \tag{6-3b}$$

These surface transfer impedances relate the current on one surface of the cylinder to the induced field on the other surface.

The two surface transfer impedances z_{io} and z_{oi} will be assumed to be equal and will be designated as z_T, i.e.,

$$z_T = z_{io} = z_{oi} \tag{6-4a}$$

The self-impedances of the shield, z_{ii} and z_{oo} will also be taken to be the same and designated as z_{SH}, i.e.,

$$z_{SH} \cong z_{ii} \cong z_{oo} \tag{6-4b}$$

Certainly for cylinders with wall thicknesses which are sufficiently small, these will be reasonable approximations. Thus (6-1) becomes

$$\begin{bmatrix} E_{in} \\ E_{out} \end{bmatrix} = \begin{bmatrix} z_{SH} & z_T \\ z_T & z_{SH} \end{bmatrix} \begin{bmatrix} I_{in} \\ I_{out} \end{bmatrix} \tag{6-5}$$

The surface transfer impedance accounts for skin effect - the tendency for a current to concentrate on a conductor surface nearest its source. At D-C, any current flowing in the shield will tend to be uniformly distributed over the shield cross section. As the frequency is increased the current tends to concentrate towards the shield surfaces. Thus for increasing frequencies less current diffuses through the wall to induce an electric field on the opposite surface. In the limit as the frequency is increased without bound there is perfect isolation between the inner and outer walls of the shield. As was pointed out in Section IV, if the frequency is sufficiently small so that the shield thickness is less than a few skin depths, the surface transfer impedance is approximately equal to the impedance of the shield. In fact, the two should converge as the frequency is reduced to zero.

The surface transfer impedance represents the coupling of some field external to the cylinder to the field internal to the cylinder and occurs via diffusion through the finitely conducting shield. This surface impedance is employed to predict the coupling from some field incident on a coaxial cable to the loads connected to the end points of the coaxial cable in the following manner [18]. As an example, consider the coaxial cable above a ground plane shown in Fig. 9(a). The coaxial cable consists of a conducting cylinder and a concentrically-located, conducting wire. An incident field, such as a uniform plane wave, illuminates the cable and induces a current, I_{out}, flowing along the shield and returning through the ground plane. For the purposes of computing this induced current, I_{out}, it is universally assumed that the interior of the shield and, in particular, I_{in} have no effect on the external circuit [18]. In other words, I_{out} is traditionally calculated as simply the current induced on an isolated cylinder above ground. Thus we assume a unilateral effect - outside to inside - to simplify the calculations. Then the effect of this induced current, I_{out}, and consequently the incident field, on the internal structure is manifested as a per-unit-length voltage source in the cable interior equal to $z_T I_{out}$ (V/m). The equivalent circuit representing a small, Δx section of the shield and interior, shielded wire is shown in Fig. 9(b).

The per-unit-length impedance of the interior wire is represented by z_w and the per-unit-length inductance and capacitance of this Δx section of the line are represented by ℓ and c, respectively. The current I_{in} produces

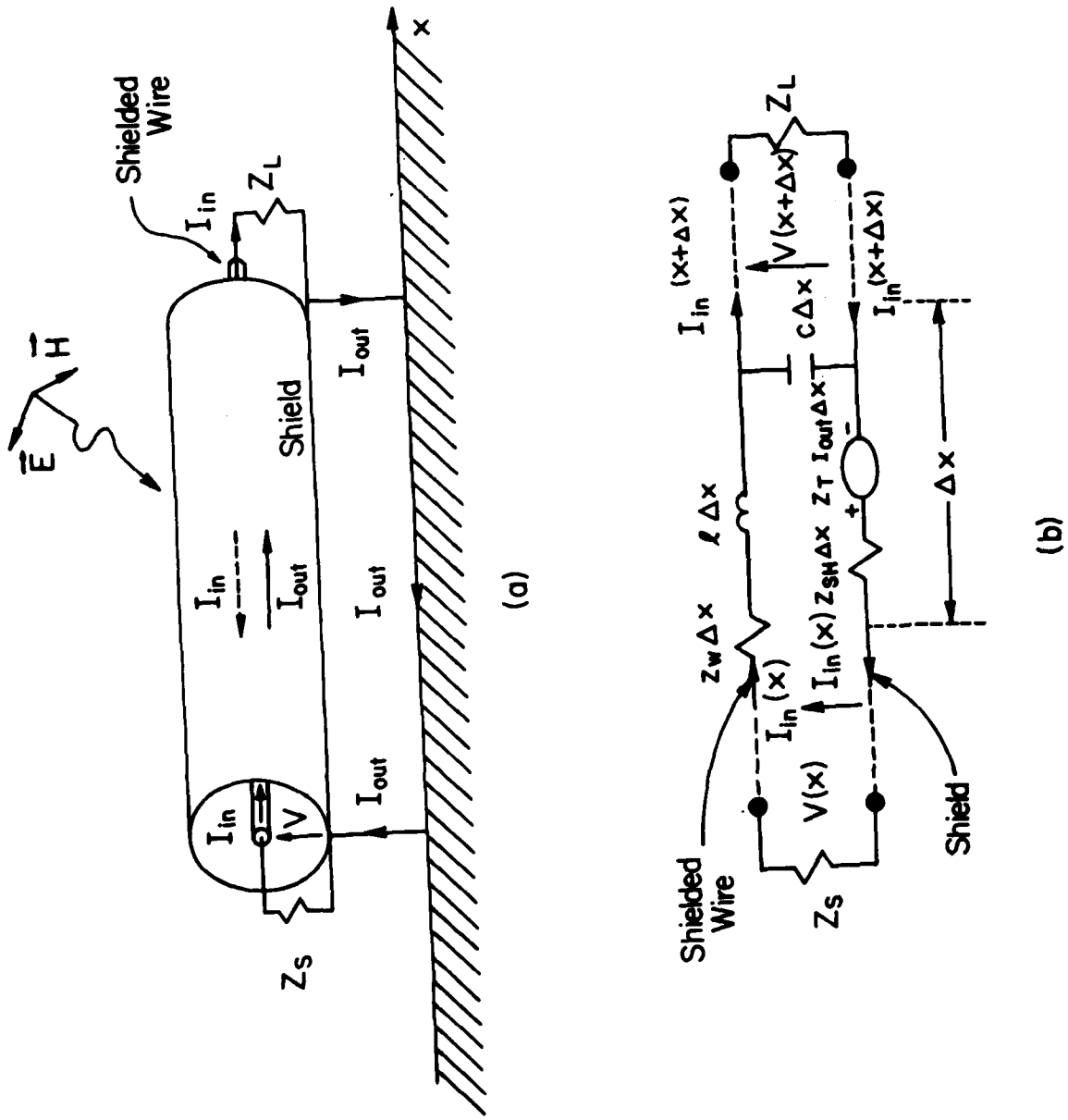

Fig. 9. Field-to-wire coupling involving shielded cables.

a voltage drop $z_{SH}\Delta x\, I_{in}$ along the interior surface of the shield as indicated by (6-1) and (6-2a), and the effect of the external shield current, I_{out}, induced by the incident field is represented by a voltage source $z_T I_{out}\Delta x$ as indicated by (6-1) and (6-3a).

From the equivalent circuit in Fig. 9(b), we may derive the line equations as [7]

$$\frac{dV(x)}{dx} = -(z_w + z_{SH} + j\omega\ell)I_{in}(x) + z_T I_{out}(x) \qquad (6\text{-}6a)$$

$$\frac{dI_{in}(x)}{dx} = -j\omega\, c\, V(x) \qquad (6\text{-}6b)$$

Note that the effect of the incident field appears in these transmission line equations as a driving term, $z_T I_{out}$.

This is an example of the use of the surface transfer impedance for solid, cylindrical shields. However, the main interest in this work is on braided-shield, coaxial cables. As was indicated previously, the braided-shield cable consists of a cylindrical surface composed of belts of wires interwoven to provide flexibility as shown in Fig. 1. This construction of the shield braid introduces small, diamond-shaped holes between the belts of wires. These holes allow other coupling mechanisms to occur between the outside environment and the interior, shielded wire which were not present for a solid shield. For the solid shield the coupling from the exterior to the interior occurred only by diffusion through the metal. For the braided shield, additional inductive and capacitive coupling occur via the holes in the shield as discussed by Vance [16]. Vance has calculated the mutual inductance and mutual capacitance between the interior and exterior of the shield [16] and the transmission-line equations for the field-to-wire example in Fig. 9 are modified by Latham [14] to

$$\frac{dV(x)}{dx} = -(z_w + z_{SH} + j\omega\ell)I_{in}(x) + z_T I_{out}(x) \qquad (6\text{-}7a)$$

$$\frac{dI_{in}(x)}{dx} = -j\omega c\, V(x) - j\omega c_T\, V_{out}(x) \qquad (6\text{-}7b)$$

where V_{out} is the voltage between the interior, shielded wire and the external, shield return path (ground in Fig. 9).

Vance [16] modified the surface transfer impedance for solid shields, z_T, to include the magnetic coupling through the holes in the shield where

$$z_T = \hat{z}_T + j\omega m_T \tag{6-8}$$

the term m_T is the mutual inductance between the center conductor-shield circuit and the shield-shield return (ground) circuit. This parameter is a function of the hole shape (assumed by Vance to be elliptical), the coverage (density of holes) and the shield radius. This mutual inductance is independent of frequency. The term $\hat{z}_T$ represents the diffusion through the metal braid and is approximated by Vance in the following manner. Vance assumed that all strands of the braid were connected (electrically) in parallel as we have done in Section IV. For example, if there are B belts of wires, W wires per belt and the braid is woven with a weave angle Θ_w, then the per-unit-length D-C resistance of the braid is given by

$$r_{DC} = \frac{1}{\pi r_b^2 \sigma \, BW \cos\Theta_w} \ \Omega/m \tag{6-9}$$

where r_b is the radius of each strand and σ is the strand conductivity. Vance presumes that this braid impedance is modified with increasing frequency in exactly the same manner as the solid cylinder. Thus $\hat{z}_T$ is taken by Vance to be

$$\hat{z}_T \cong r_{DC} \frac{\gamma d}{\sinh \gamma d} \ \Omega/m \tag{6-10}$$

where d is the diameter of the braid wires, $d = 2r_b$, and $\gamma = (1 + j)/\delta$ where $\delta = (\pi f \mu_v \sigma)^{-1/2}$ is the skin depth. It should therefore be noted that if r_{DC} were the per-unit-length D-C resistance of a solid cylinder of wall thickness d, then (6-10) would be its total surface transfer impedance, i.e., in (6-8), m_T would be zero.

The term c_T in (6-7b) is the per-unit-length mutual capacitance between the interior, shielded wire and the exterior circuit produced by electric flux lines penetrating the shield holes. The quantity $j\omega c_T$ is the transfer admittance of the braided shield. This term is related to the per-unit-length

capacitances between the shielded wire and the shield and between the shield and its return path (ground), the hole shape and shield coverage [16]. For the shield which was used in this investigation, we may calculate from the results of [16]

$$z_T = (2.46 \times 10^{-2}) \frac{2r_b\gamma}{\sinh(2r_b\gamma)} + j\omega(7.47 \times 10^{-10}) \ \Omega/m \qquad (6\text{-}11a)$$

and

$$c_T = 2.35 \times 10^{-14} \ F/m \qquad (6\text{-}11b)$$

Strictly speaking, Vance's derivation of z_T was obtained for an isolated shield (no ground plane present) and thus does not apply here. However, we will use his result for our purposes where a ground plane is present on the assumption that the current and charge are uniformly distributed around the shield periphery.

The per-unit-length self impedance of the shield braid, z_{SH}, was calculated in (4-31) in Section IV as the impedance of an isolated strand of the braid (including skin effect) and assuming that all of the braid wires are connected (electrically) in parallel. A comparison of the total shield transfer impedance $Z_T = z_T \ell_s$ and the total braid impedance $Z_{SH} = z_{SH} \ell_s$ is given in Fig. 10. Note in Fig. 10 that for frequencies less than approximately 1 MHz, the two quantities are equal and both converge to the total D-C resistance of the shield braid, R_{DC}. Again, this is an expected result since for frequencies such that the current is distributed essentially uniformly over the shield cross section, (6-2) and (6-3) yield equivalent results. It should be observed in Fig. 10 that at the higher frequencies, Z_T increases directly with frequency as should be clear from (6-8) yet Z_{SH} increases as the square root of frequency as is clear from (4-30c) since the impedance of an isolated wire approaches $\sqrt{f}$ dependence. However, it is clear from the experimental evidence cited for braided shields in [16] that Z_T does, in fact, increase as f and not $\sqrt{f}$ so that Z_{SH} cannot be correct for an approximation to Z_T at these higher frequencies.

6.1 The MTL Equations

We now turn our attention to developing the multiconductor transmission line model for the unshielded to shielded configuration shown in Fig. 3(b). Consider Fig. 11(a). In order to employ the concept of surface transfer impedance, we will define the currents of the generator wire, receptor wire and shield as shown in Fig. 11(a). The line is directed in the x direction as

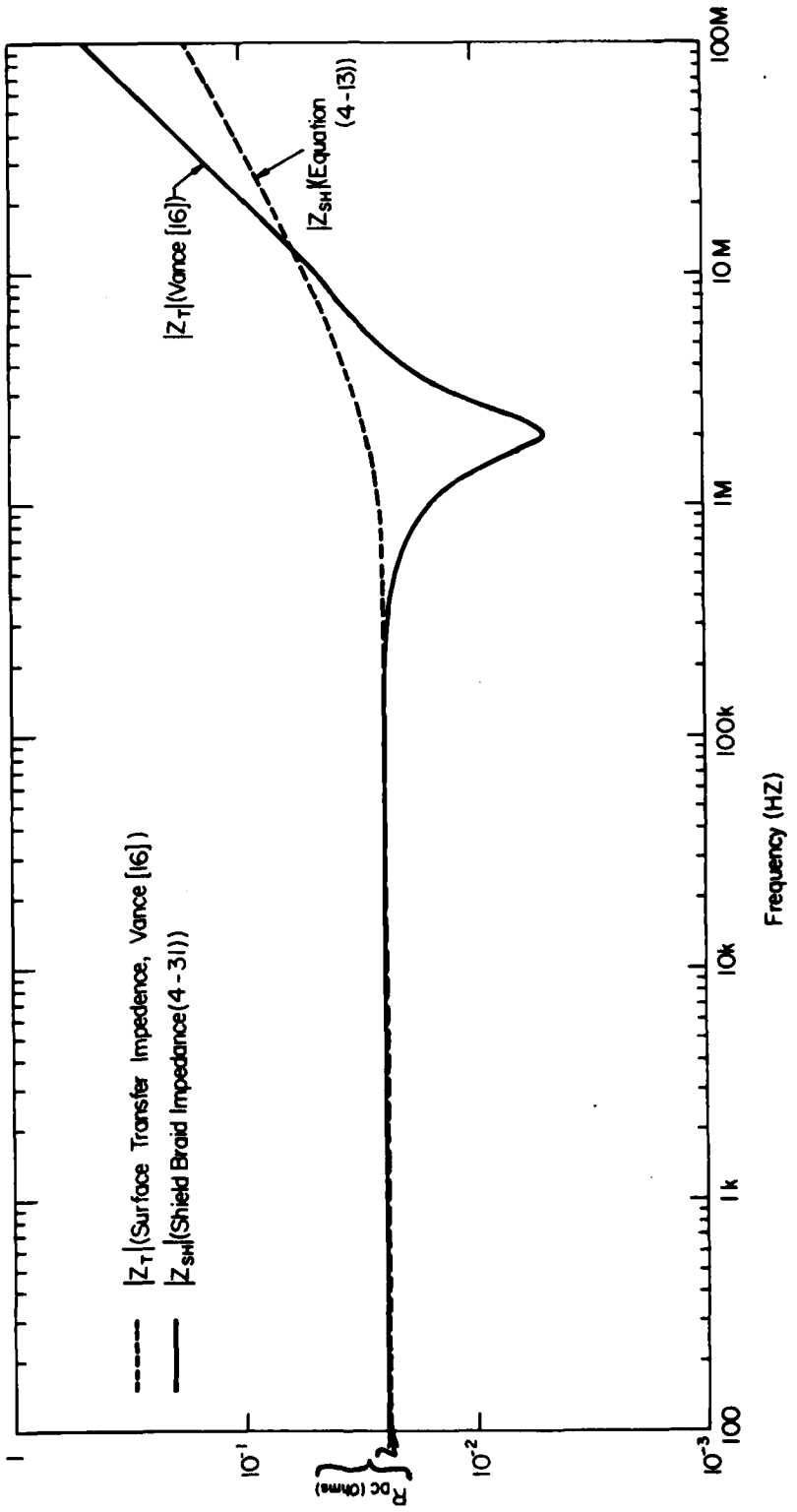

Fig. 10. A comparison of the shield braid impedance Z_{SH} and the surface transfer impedance Z_T.

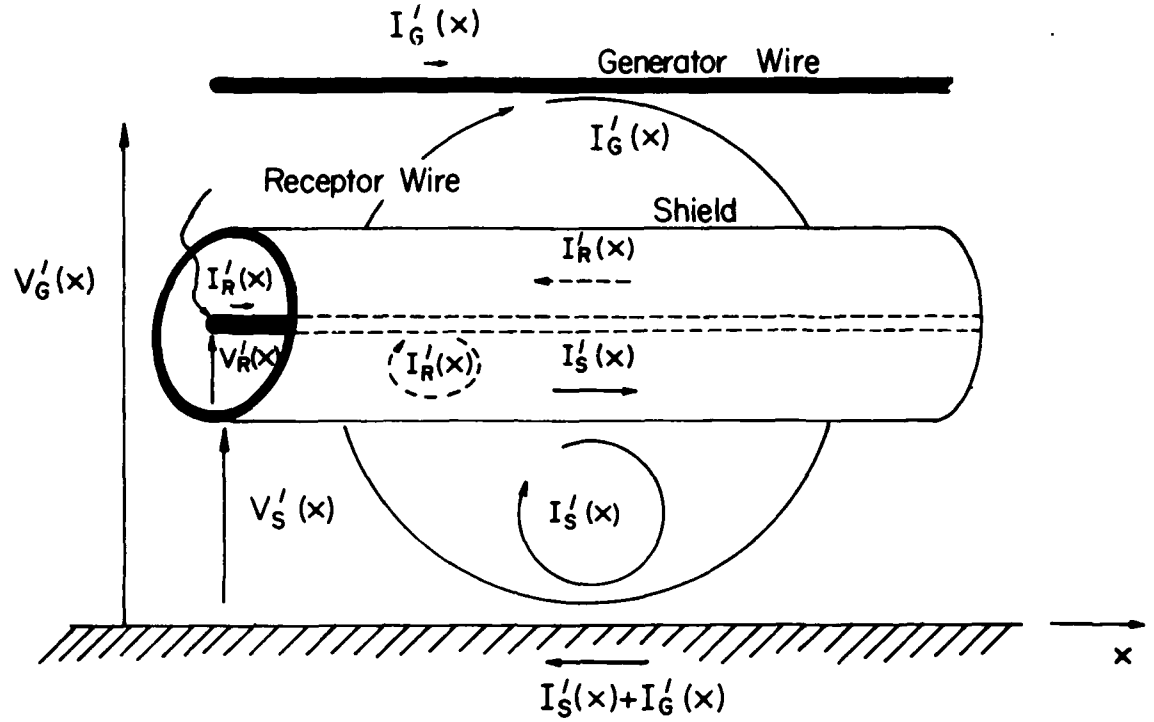

(a)

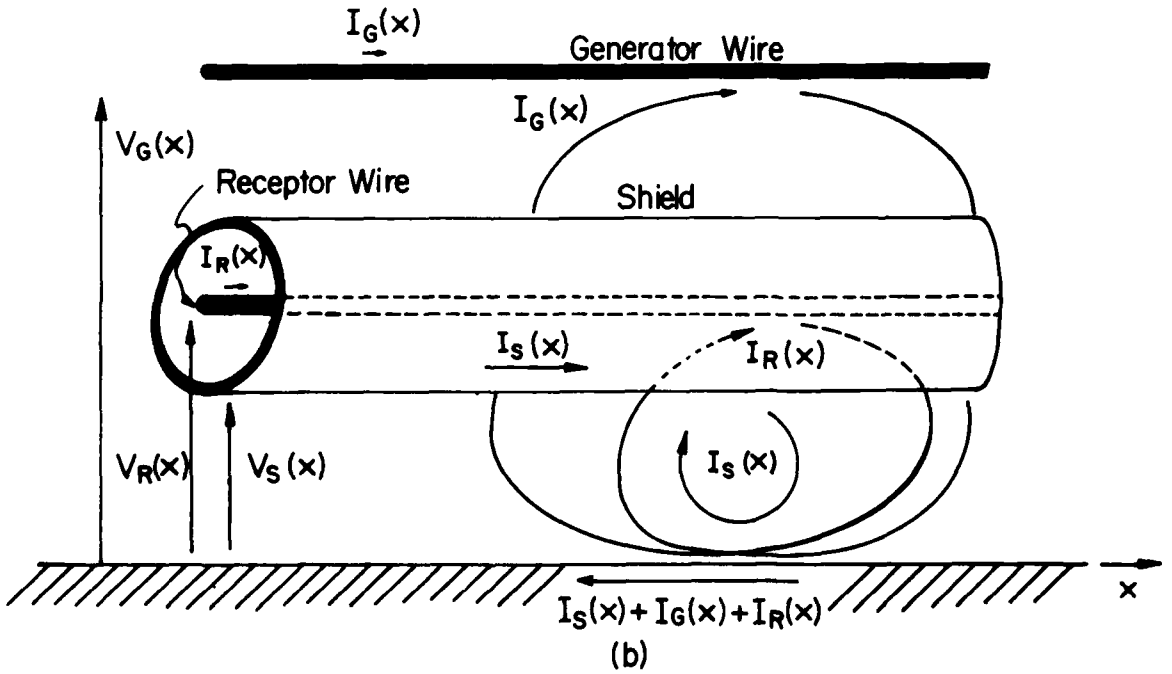

(b)

Fig. 11. The primed and unprimed variable definitions.

are the line currents.

As a fundamental assumption of the model, we will investigate the TEM or "quasi-TEM" mode of propagation. In the TEM mode field structure, the electric and magnetic field vectors lie in the transverse (y,z) plane. Clearly, since the shield cannot be assumed to be a perfect conductor (otherwise there would be no coupling to the receptor wire circuit if the shield were solid) the fields cannot lie strictly in the transverse plane. Due to the impedance of the shield as well as its surface transfer impedance, there will be components of electric field directed along the shield surfaces in the x direction. However, we will presume that the field structure is predominantly TEM or "quasi-TEM." An indication of the adequacy of this assumption will be investigated when we compare the predictions of the model to the experimental results. Assuming a TEM or "quasi-TEM" field structure, we may define voltages between the conductors as well as conductor currents [7]. It is shown in [7] that the TEM field structure satisfies a static distribution. Thus we may calculate mutual and self inductances and capacitances between the line conductors as a static (D-C) calculation. The effect of the frequency dependent shield braid impedance z_{SH} and surface transfer impedance z_T (which give rise to a non-TEM field structure) will be included in the model as an approximation.

Since the field structure is assumed to be "quasi-TEM," the conductor currents and voltages will be functions of only the line axis variable, x [7]. We have defined these voltages and currents as shown in Fig. 11(a) in order to incorporate the concept of surface transfer impedance. The generator wire current is denoted as $I'_G(x)$ and its return path is defined to be via the infinite ground plane. The generator wire voltage with respect to the ground plan is designated as $V'_G(x)$. The current $I'_S(x)$ is defined as the portion of the shield current which has its return path through the ground plane. The shield voltage $V'_S(x)$ is with respect to the ground plane. The receptor wire current, $I'_R(x)$ returns through the shield, and the receptor wire voltage $V'_R(x)$ is with respect to the shield.

The transmission line equations will be derived in terms of $I'_G(x)$, $V'_G(x)$, $I'_R(x)$, $V'_R(x)$, $I'_S(x)$, $V'_S(x)$ and converted to the more conventional variables $I_G(x)$, $V_G(x)$, $I_R(x)$, $V_R(x)$, $I_S(x)$, $V_S(s)$ shown in Fig. 11(b). The only two differences in voltage and current definitions in Fig. 11(a) and Fig. 11(b)

are that the return path for $I_R(x)$ in Fig. 11(b) is defined to be the ground plane instead of the shield as was the case for $I'_R(x)$ and the voltage $V_R(x)$ is with respect to the ground plane instead of the shield as was the case for $V'_R(x)$. If the transmission line equations are derived for the primed variables in Fig. 11(a) they may be converted to the unprimed variables in Fig. 11(b) with the following simple change of variables:

$$I_G(x) = I'_G(x) \tag{6-12a}$$

$$I_R(x) = I'_R(x) \tag{6-12b}$$

$$I_S(x) = I'_S(x) - I'_R(x) \tag{6-12c}$$

$$V_G(x) = V'_G(x) \tag{6-12d}$$

$$V_R(x) = V'_R(x) + V'_S(x) \tag{6-12e}$$

$$V_S(x) = V'_S(x) \tag{6-12f}$$

Let us now consider a Δx section of the line in Fig. 11(a) and derive the voltage change expressions. Proceeding around the generator circuit (generator wire-ground plane) we obtain

$$V'_G(x+\Delta x) - V'_G(x) = -j\omega \ell'_{GG} \Delta x\, I'_G(x) - j\omega \ell'_{GR} \Delta x\, I'_R(x) - j\omega \ell'_{GS} \Delta x\, I'_S(x) \tag{6-13}$$

where ℓ'_{GG} is the self inductance of the generator circuit, ℓ'_{GR} is the mutual inductance between the generator circuit and receptor circuit (receptor wire-shield), and ℓ'_{GS} is the mutual inductance between the generator circuit and shield circuit (shield-ground plane). Dividing both sides by Δx and taking the limit as $\Delta x \to 0$ we obtain the first transmission line equation:

$$\dot{V}'_G(x) = -j\omega \ell'_{GG} I'_G(x) - j\omega \ell'_{GR} I'_R(x) - j\omega \ell'_{GS} I'_S(s) \tag{6-14}$$

where the dot ($\cdot$) denotes the ordinary derivative with respect to x. Similarly, around the receptor circuit (following the path of I'_R) we obtain

$$\dot{V}_R'(x) = -j\omega\ell_{GR}'I_G'(x) - j\omega\ell_{RR}'I_R'(x) - j\omega\ell_{RS}'I_S'(x) \tag{6-15}$$

Additional terms are required in (6-15). The self impedance of the shield introduces an additional voltage drop according to (6-5) of $-z_{SH}I_R'(x)$. Similarly the surface transfer impedance introduces a voltage source in this loop in accordance with (6-5) of $z_T I_S'(x)$. Thus (6-15) becomes

$$\begin{aligned}\dot{V}_R'(x) = &-j\omega\ell_{GR}'I_G'(x) - j\omega\ell_{RR}'I_R'(x) \\ &-j\omega\ell_{RS}'I_S'(x) - z_{SH}I_R'(x) + z_T I_S'(x)\end{aligned} \tag{6-16}$$

Similarly, around the shield circuit (following the path of I_S') we obtain

$$\begin{aligned}\dot{V}_S'(x) = &-j\omega\ell_{GS}'I_G'(x) - j\omega\ell_{RS}'I_R'(x) \\ &-j\omega\ell_{SS}'I_S'(x) - z_{SH}I_S'(x) + z_T I_R'(x)\end{aligned} \tag{6-17}$$

where the self impedance and surface transfer impedance are included in accordance with (6-5).

Equations (6-14), (6-16) and (6-17) can be written in matrix form as

$$\dot{\underline{V}}^{S'}(x) = -(\underset{\sim}{Z}^{S'} + j\omega\underset{\sim}{L}^{S'})\,\underline{I}^{S'}(x) \tag{6-18}$$

where

$$\underline{V}^{S'}(x) = \begin{bmatrix} V_G'(x) \\ V_R'(x) \\ V_S'(x) \end{bmatrix} \tag{6-19a}$$

$$\underline{I}^{S'}(x) = \begin{bmatrix} I_G'(x) \\ I_R'(x) \\ I_S'(x) \end{bmatrix} \tag{6-19b}$$

The 3 x 3 matrices $\underset{\sim}{Z}^{S'}$ and $\underset{\sim}{L}^{S'}$ are given by

$$\underset{\sim}{Z}'^{S} = \begin{bmatrix} 0 & 0 & 0 \\ 0 & z_{SH} & -z_T \\ 0 & -z_T & z_{SH} \end{bmatrix} \tag{6-20a}$$

$$\underset{\sim}{L}'^{S} = \begin{bmatrix} \ell'_{GG} & \ell'_{GR} & \ell'_{GS} \\ \ell'_{GR} & \ell'_{RR} & \ell'_{RS} \\ \ell'_{GS} & \ell'_{RS} & \ell'_{SS} \end{bmatrix} \tag{6-20b}$$

In the above, we have clearly neglected the impedance of the generator and receptor wires, i.e., we have considered these to be perfect conductors. Obviously we could not do so for the shield.

Let us now change variables from the primed quantities to the unprimed quantities illustrated in Fig. 11(b) via the transformations in (6-12):

$$\underbrace{\begin{bmatrix} I'_G \\ I'_R \\ I'_S \end{bmatrix}}_{\underset{\sim}{I}'^{S}} = \underbrace{\begin{bmatrix} 1 & 0 & 0 \\ 0 & 1 & 0 \\ 0 & 1 & 1 \end{bmatrix}}_{\underset{\sim}{T}_I} \underbrace{\begin{bmatrix} I_G \\ I_R \\ I_S \end{bmatrix}}_{\underset{\sim}{I}^{S}} \tag{6-21a}$$

$$\underbrace{\begin{bmatrix} V'_G \\ V'_R \\ V'_S \end{bmatrix}}_{\underset{\sim}{V}'^{S}} = \underbrace{\begin{bmatrix} 1 & 0 & 0 \\ 0 & 1 & -1 \\ 0 & 0 & 1 \end{bmatrix}}_{\underset{\sim}{T}_V} \underbrace{\begin{bmatrix} V_G \\ V_R \\ V_S \end{bmatrix}}_{\underset{\sim}{V}^{S}} \tag{6-21b}$$

Substituting (6-21) into (6-18) we obtain

$$\dot{\underset{\sim}{V}}^{S}(x) = -(\underset{\sim}{Z}^{S} + j\omega\underset{\sim}{L}^{S})\underset{\sim}{I}^{S}(x) \tag{6-22}$$

where

$$\underset{\sim}{Z}^{S} = \underset{\sim}{T}_V^{-1}\, \underset{\sim}{Z}^{'S}\, \underset{\sim}{T}_I$$

$$= \begin{bmatrix} 0 & 0 & 0 \\ 0 & 2(z_{SH} - z_T) & (z_{SH} - z_T) \\ 0 & (z_{SH} - z_T) & z_{SH} \end{bmatrix} \tag{6-23a}$$

$$\underset{\sim}{L}^{S} = \underset{\sim}{T}_V^{-1}\, \underset{\sim}{L}^{'S}\, \underset{\sim}{T}_I$$

$$= \begin{bmatrix} \ell'_{GG} & (\ell'_{GR} + \ell'_{GS}) & \ell'_{GS} \\ (\ell'_{GR} + \ell'_{GS}) & (\ell'_{RR} + 2\ell'_{RS} + \ell'_{SS}) & (\ell'_{RS} + \ell'_{SS}) \\ \ell'_{GS} & (\ell'_{RS} + \ell'_{SS}) & \ell'_{SS} \end{bmatrix} \tag{6-23b}$$

and

$$\underline{V}^{S}(x) = \begin{bmatrix} V_G(x) \\ V_R(x) \\ V_S(x) \end{bmatrix} \tag{6-23c}$$

$$\underline{I}^{S}(x) = \begin{bmatrix} I_G(x) \\ I_R(x) \\ I_S(x) \end{bmatrix} \tag{6-23d}$$

The inverse of $\underset{\sim}{T}_V$ is given by

$$\underset{\sim}{T}_V^{-1} = \begin{bmatrix} 1 & 0 & 0 \\ 0 & 1 & 1 \\ 0 & 0 & 1 \end{bmatrix} \tag{6-23e}$$

It should be pointed out that we assumed that the surface transfer impedances z_{io} and z_{oi} in (6-1) were equal and these were designated as z_T. Also we assumed that the shield inner surface and outer surface self im-

pedances, z_{ii} and z_{oo} in (6-..., were equal. These were designated as z_{SH}. If we do not make these assumptions one can show that $\underset{\sim}{Z}'^{S}$ in (6-20a) becomes

$$\underset{\sim}{Z}'^{S} = \begin{bmatrix} 0 & 0 & 0 \\ 0 & z_{ii} & -z_{io} \\ 0 & -z_{oi} & z_{oo} \end{bmatrix} \tag{6-24a}$$

and $\underset{\sim}{Z}^{S}$ in (6-23a) becomes

$$\underset{\sim}{Z}^{S} = \begin{bmatrix} 0 & 0 & 0 \\ 0 & (z_{ii} + z_{oo} - z_{io} - z_{oi}) & (z_{oo} - z_{io}) \\ 0 & (z_{oo} - z_{oi}) & z_{oo} \end{bmatrix} \tag{6-24b}$$

Note also that as the frequency is decreased $z_{SH} \cong z_T$. When $z_{SH} = z_T$, (6-23a) becomes

$$\underset{\sim}{Z}^{S} \cong \begin{bmatrix} 0 & 0 & 0 \\ 0 & 0 & 0 \\ 0 & 0 & z_{SH} \end{bmatrix} \tag{6-24c}$$

(low frequency)

and the shield impedance term appears only in the voltage change expression of the shield circuit which is a logical result [7]. In fact, the voltage change transmission line equations can be derived directly from the unprimed circuit in Fig. 11(b) with no conceptual difficulties when the frequency is small enough that $z_T = z_{SH}$ [7].

A few comments are in order concerning these inductance parameters. Consider Fig. 12(a) in which we have shown cross sections of the line. The per-unit-length inductance matrix, $\underset{\sim}{L}'^{S}$, is defined by

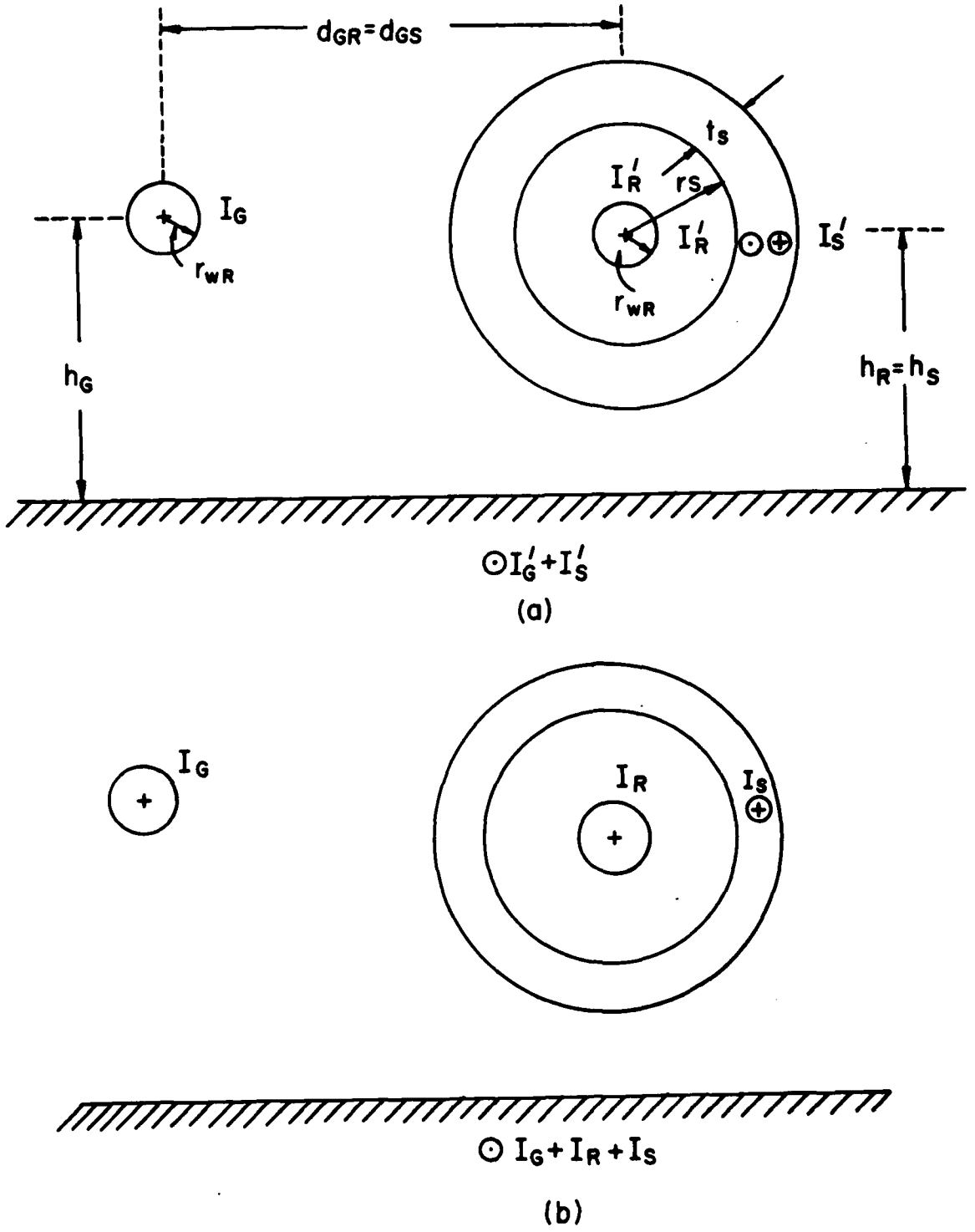

Fig. 12. A cross-section of the line illustrating the primed and unprimed current variables.

$$\begin{bmatrix} \phi'_G \\ \phi'_R \\ \phi'_S \end{bmatrix} = \underset{\sim}{L}^{S'} \begin{bmatrix} I'_G \\ I'_R \\ I'_S \end{bmatrix} \tag{6-25}$$

where ϕ'_G, ϕ'_R, ϕ'_S are the magnetic fluxes linking the appropriate primed circuits. From (6-20b) and (6-25) we obtain

$$\ell'_{GG} = \left.\frac{\phi'_G}{I'_G}\right|_{I'_R = I'_S = 0} \tag{6-26}$$

Recalling that the TEM mode assumption permits a D-C calculation for these inductance parameters, this result becomes (approximately) [7]

$$\ell'_{GG} \cong \frac{\mu_v}{2\pi} \ell n \left(\frac{2h_G}{r_{wG}}\right) \tag{6-27}$$

where r_{wG} is the radius of the generator wire and h_G is the height of this wire above the ground plane. The mutual inductance ℓ'_{GR} becomes

$$\ell'_{GR} = \left.\frac{\phi'_G}{I'_R}\right|_{I'_G = I'_S = 0} \tag{6-28}$$

From a consideration of Fig. 12(a) we obtain (approximately)

$$\ell'_{GR} \cong 0 \tag{6-29}$$

Next we have

$$\ell'_{GS} = \left.\frac{\phi'_G}{I'_S}\right|_{I'_G = I'_R = 0} \tag{6-30}$$

which becomes (approximately) [7]

$$\ell'_{GS} \cong \frac{\mu_v}{4\pi} \ell n\left[1 + \frac{4h_G h_S}{d_{GS}^2}\right] \tag{6-31}$$

Similarly we obtain [7]

$$\ell'_{RR} = \left.\frac{\phi'_R}{I'_R}\right|_{I'_G = I'_S = 0}$$

$$= \frac{\mu_v}{2\pi} \ell n\left(\frac{r_s}{r_{wR}}\right) \tag{6-32}$$

where r_s is the shield internal radius and r_{wR} is the receptor wire radius. Also,

$$\ell'_{RS} = \ell'_{SR}$$

$$= \left.\frac{\phi'_S}{I'_R}\right|_{I'_G = I'_S = 0} \tag{6-33}$$

$$\cong 0$$

and [7]

$$\ell'_{SS} = \left.\frac{\phi'_S}{I'_S}\right|_{I'_G = I'_R = 0}$$

$$\cong \frac{\mu_v}{2\pi} \ell n\left(\frac{2h_S}{r_s + t_s}\right) \tag{6-34}$$

If we write $\underset{\sim}{L}$ in (6-23b) as

$$\underset{\sim}{L} = \begin{bmatrix} \ell_{GG} & \ell_{GR} & \ell_{GS} \\ \ell_{GR} & \ell_{RR} & \ell_{RS} \\ \ell_{GS} & \ell_{RS} & \ell_{SS} \end{bmatrix} \tag{6-35}$$

we identify

$$\ell_{GG} = \ell'_{GG}$$

$$= \frac{\mu_v}{2\pi} \ell n\left(\frac{2h_G}{r_{wG}}\right) \tag{6-36}$$

$$\ell_{GR} = \ell'_{GR} + \ell'_{GS}$$

$$= 0 + \frac{\mu_v}{4\pi} \ell n[1 + \frac{4h_G h_S}{d_{GS}^2}] \qquad (6\text{-}37)$$

$$\ell_{GS} = \ell'_{GS}$$

$$= \ell_{GR} \qquad (6\text{-}38)$$

$$= \frac{\mu_v}{4\pi} \ell n[1 + \frac{4h_G h_S}{d_{GS}^2}]$$

$$\ell_{RR} = \ell'_{RR} + 2\ell'_{RS} + \ell'_{SS}$$

$$= \frac{\mu_v}{2\pi} \ell n(\frac{r_s}{r_{wR}}) + \frac{\mu_v}{2\pi} \ell n(\frac{2h_S}{r_s + t_s}) \qquad (6\text{-}39)$$

$$\cong \frac{\mu_v}{2\pi} \ell n(\frac{2h_S}{r_{wR}})$$

(for shield walls whose thickness is small in comparison with the shield radius)

$$\ell_{RS} = \ell'_{RS} + \ell'_{SS}$$

$$= \frac{\mu_v}{2\pi} \ell n(\frac{2h_S}{r_s + t_s}) \qquad (6\text{-}40)$$

$$\ell_{SS} = \ell'_{SS}$$

$$= \frac{\mu_v}{2\pi} \ell n(\frac{2h_S}{r_s + t_s}) \qquad (6\text{-}41)$$

$$= \ell_{RS}$$

Note that $\ell_{SS} = \ell_{RS}$. This is a reasonable result as discussed in Section IV since the self inductance of the shield-ground plane circuit, ℓ_{SS}, relates the flux passing between the shield and the ground plane to the shield current, and the mutual inductance between the receptor wire-ground plane circuit and the shield-ground plane circuit, ℓ_{RS}, relates the flux linking the shield circuit to the receptor current. Clearly, the two are equivalent (or approximately so) since for the purposes of calculating ℓ_{SS}, we may concentrate the shield current at the center of the shield (the position of the receptor wire) and in both cases the flux passing between the shield and the ground plane is to be computed.

Now let us derive the current change expression. A cross section of the line with appropriate per-unit-length capacitances for a solid shield is shown in Fig. 13(a). The appropriate self and mutual capacitances between the various conductors are indicated. Note that there is no mutual capacitance, c_{GR}, between the generator wire and receptor wire and there is no self capacitance, c_{RR}, between the receptor wire and ground plane -both reasonable results for solid, (assumed for this calculation to be perfectly conducting) shields. (For a proof of this result, see Appendix F.)

The corresponding diagram is shown for braided shields in Fig. 13(b). For braided shields, the holes in the shield allow the mutual capacitance c_{GR} and self capacitance c_{RR} to be present due to the penetration of the electric field lines through these holes. The quantities $j\omega c_{GR}$ and $j\omega c_{RR}$ may be thought of as the shield transfer admittances [14,16]. A typical calculation in (6-11b) for a braided shield of the same physical characteristics as the shield used in this investigation indicates that c_{RR} would be on the order of 10^{-14} F/m. The values of the other capacitances (in the absence of the holes) are on the order of 10^{-11} F/m. Thus we choose to ignore the effects of the shield holes on the capacitive transfer.

From Fig. 13(a) in terms of the unprimed voltage variables we may obtain the current change expression in the limit as $\Delta x \to 0$ [7]

$$\underline{\dot{I}}^S(x) = -j\omega \underset{\sim}{C}^S \underline{V}^S(x) \tag{6-42}$$

where $\underline{I}^S(x)$ and $\underline{V}^S(x)$ are given by (6-23d) and

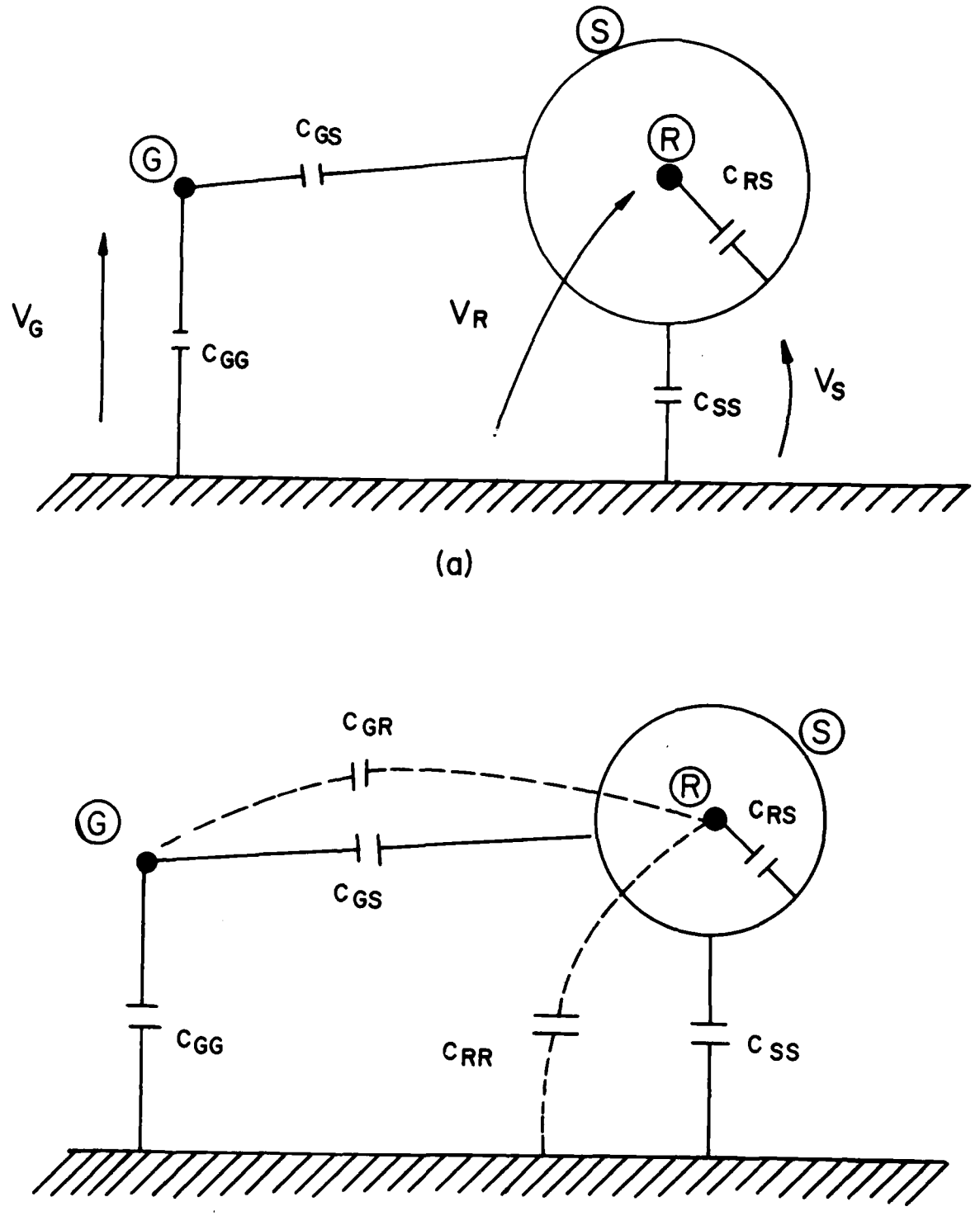

Fig. 13. A cross-section of the line illustrating the per-unit-length capacitances. (a) solid shields (b) braided shields.

$$\underset{\sim}{C}^S = \begin{bmatrix} (c_{GG} + c_{GS}) & 0 & -c_{GS} \\ 0 & c_{RS} & -c_{RS} \\ -c_{GS} & -c_{RS} & (c_{SS} + c_{RS} + c_{GS}) \end{bmatrix} \tag{6-43a}$$

(Formulating the node-voltage equations for Fig. 13(a) is a simple way of obtaining the entries in $\underset{\sim}{C}^S$ given in (6-43a).) The entries in $\underset{\sim}{C}^S$ are computed via the following [7]

$$\begin{bmatrix} (c_{GG} + c_{GS}) & -c_{GS} \\ -c_{GS} & (c_{SS} + c_{GS}) \end{bmatrix} = \mu_v \varepsilon_v \begin{bmatrix} \ell_{GG} & \ell_{GS} \\ \ell_{GS} & \ell_{SS} \end{bmatrix}^{-1} \tag{6-43b}$$

$$c_{RS} = \frac{2\pi\varepsilon}{\ell n(\frac{r_s}{r_w})} \tag{6-43c}$$

The equation in (6-43b) results from the computation of c_{GG}, c_{SS}, c_{GS} as the per-unit-length capacitance matrix of two wires, one the generator wire and the other a wire of radius equal to the shield radius, in free space [7]. Equation (6-43c) is the familiar per-unit-length capacitance of a coaxial line filled with a dielectric having permittivity $\varepsilon = \varepsilon_r \varepsilon_v$ [7].

Thus the coupled transmission line equations are given by (6-22) and (6-43)

$$\underline{\dot{V}}^S(x) = -(\underset{\sim}{Z}^S + j\omega\underset{\sim}{L}^S)\underline{I}^S(x) \tag{6-44a}$$

$$\underline{\dot{I}}^S(x) = -j\omega\underset{\sim}{C}^S\underline{V}^S(x) = -\underset{\sim}{Y}^S\underline{V}(x) \tag{6-44b}$$

where

$$\underset{\sim}{Y}^S = j\omega\underset{\sim}{C}^S \tag{6-44c}$$

We may relate the line voltages and currents at one end of a line of length ℓ_s to the voltages and currents at the other end as shown in Fig. 14 by solving (6-44) and obtaining the chain parameter matrix [7]:

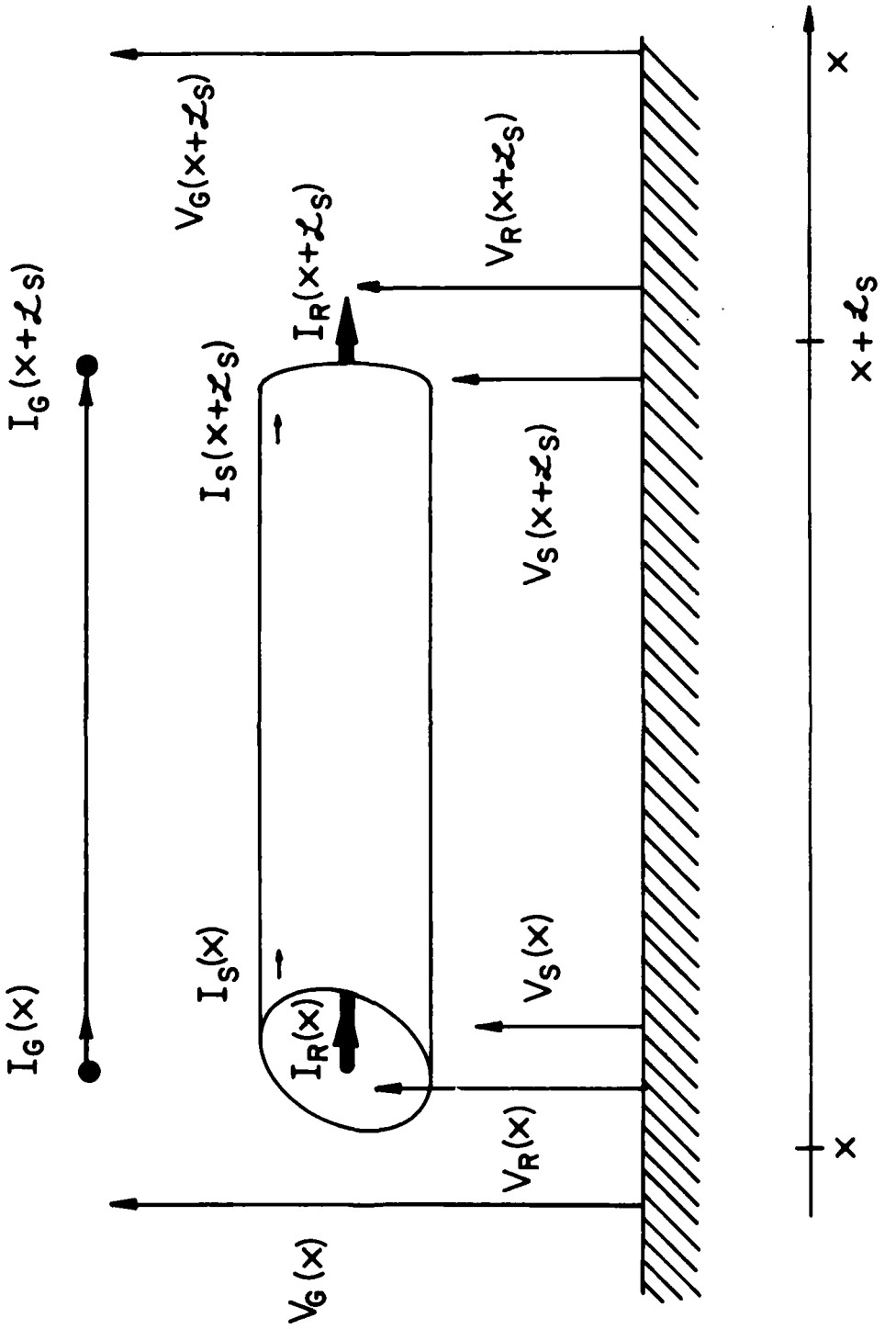

Fig. 14. The shielded section and terminal variable definitions.

$$\begin{bmatrix} \underline{V}^S(x + \ell_s) \\ \underline{I}^S(x + \ell_s) \end{bmatrix} = \underbrace{\begin{bmatrix} \underset{\sim}{\phi}^S_{11}(\ell_s) & \underset{\sim}{\phi}^S_{12}(\ell_s) \\ \underset{\sim}{\phi}^S_{21}(\ell_s) & \underset{\sim}{\phi}^S_{22}(\ell_s) \end{bmatrix}}_{\underset{\sim}{\phi}^S(\ell_s)} \begin{bmatrix} \underline{V}^S(x) \\ \underline{I}^S(x) \end{bmatrix} \tag{6-45a}$$

The 3 x 3 $\underset{\sim}{\phi}^S_{ij}(\ell_s)$ submatrices are given by [7]

$$\underset{\sim}{\phi}^S_{11}(\ell_s) = \frac{1}{2} \underset{\sim}{Y}^{S^{-1}} \underset{\sim}{T} (\underset{\sim}{e}^{\underset{\sim}{\gamma}\ell_s} + \underset{\sim}{e}^{-\underset{\sim}{\gamma}\ell_s}) \underset{\sim}{T}^{-1} \underset{\sim}{Y}^S \tag{6-45b}$$

$$\underset{\sim}{\phi}^S_{12}(\ell_s) = -\frac{1}{2} \underset{\sim}{Y}^{S^{-1}} \underset{\sim}{T} \underset{\sim}{\gamma} (\underset{\sim}{e}^{\underset{\sim}{\gamma}\ell_s} - \underset{\sim}{e}^{-\underset{\sim}{\gamma}\ell_s}) \underset{\sim}{T}^{-1} \tag{6-45c}$$

$$\underset{\sim}{\phi}^S_{21}(\ell_s) = -\frac{1}{2} \underset{\sim}{T} (\underset{\sim}{e}^{\underset{\sim}{\gamma}\ell_s} - \underset{\sim}{e}^{-\underset{\sim}{\gamma}\ell_s}) \underset{\sim}{\gamma}^{-1} \underset{\sim}{T}^{-1} \underset{\sim}{Y}^S \tag{6-45d}$$

$$\underset{\sim}{\phi}^S_{22}(\ell_s) = \frac{1}{2} \underset{\sim}{T} (\underset{\sim}{e}^{\underset{\sim}{\gamma}\ell_s} + \underset{\sim}{e}^{-\underset{\sim}{\gamma}\ell_s}) \underset{\sim}{T}^{-1} \tag{6-45e}$$

The various matrices in (6-45) are defined as follows [7]. First compute the 3 x 3 transformation matrix $\underset{\sim}{T}$ as

$$\underset{\sim}{T}^{-1} (\underset{\sim}{Y}^S)(\underset{\sim}{Z}^S + j\omega \underset{\sim}{L}^S) \underset{\sim}{T} = \underset{\sim}{\gamma}^2 \tag{6-45f}$$

where $\underset{\sim}{\gamma}^2$ is a 3 x 3 diagonal matrix. $\underset{\sim}{\gamma}$ is the square root of $\underset{\sim}{\gamma}^2$ with main diagonal entries γ_i. The matrix exponential $\underset{\sim}{e}^{\underset{\sim}{\gamma}\ell_s}$ is diagonal with entries $e^{\gamma_i \ell_s}$.

To find the propagation constants, γ_i, via (6-45f), we must obtain the matrix product

$$\underset{\sim}{Y}^S(\underset{\sim}{Z}^S + j\omega \underset{\sim}{L}^S) = j\omega \underset{\sim}{C}^S \underset{\sim}{Z}^S - \omega^2 \underset{\sim}{C}^S \underset{\sim}{L}^S \tag{6-46}$$

One can show, with the entries in $\underset{\sim}{L}^S$ given by (6-35) through (6-41) and the entries in $\underset{\sim}{C}^S$ given by (6-43), that the matrix product $\underset{\sim}{C}^S \underset{\sim}{L}^S$ becomes

$$\underset{\sim}{C}^S \underset{\sim}{L}^S = \begin{bmatrix} \mu_v \epsilon_v & 0 & 0 \\ 0 & \mu_v \epsilon_v & 0 \\ 0 & \mu_v \epsilon_v (1 - \epsilon_r) & \mu_v \epsilon_v \epsilon_r \end{bmatrix} \tag{6-47a}$$

If the interior of the shielded cable is filled with air, $\varepsilon = \varepsilon_v$, we have a four conductor line in a homogeneous medium (free space) and (6-47a) reduces to

$$\underset{\sim}{C}^S\underset{\sim}{L}^S = \mu_v\varepsilon_v\,\underset{\sim}{1}_3 \qquad (\varepsilon_r = 1) \tag{6-47b}$$

a sensible result [7]. With the form of $\underset{\sim}{C}^S\underset{\sim}{L}^S$ in (6-47a), the matrix product in (6-46) may be easily computed, a' priori.

6.2 Incorporating the Pigtail Sections

The primary concern is to formulate a transmission line model of the unshielded to shielded case shown in Fig. 3(b). Thus we need to incorporate pigtail sections into the previously developed transmission line model for a shielded section of line.

The basic idea is illustrated in Fig. 15. We developed the chain parameter matrix of the shielded section in the previous section. This chain parameter matrix related the conductor voltages V_G, V_R, V_S and the conductor currents I_G, I_R, I_S at one end of the shielded section of the line to the corresponding variables at the other end of the section. If we relate the terminal voltages and currents of the pigtail sections in a similar fashion, we may obtain the overall matrix chain parameters of the entire line by multiplying (in the proper sequence) the chain parameter matrices of the two pigtail sections and the shielded section. Then we incorporate the terminal (load) constraints and solve for the terminal voltages and currents of the entire line. This is the essence of our procedure.

First we need to obtain the chain parameter matrices of the pigtail sections. Both sections are identical in characteristics and length in this investigation so we shall consider one section shown in Fig. 16. We may write the transmission line equations for the pigtail section and solve for the chain parameter matrix $\underset{\sim}{\phi}^P(\ell_p)$ of a section of length ℓ_p as was done for the shielded section. If we ignore the dielectric insulations surrounding the generator and receptor wires (the pigtail wire was bare) we may obtain the chain parameter matrices of the pigtail sections as [7]

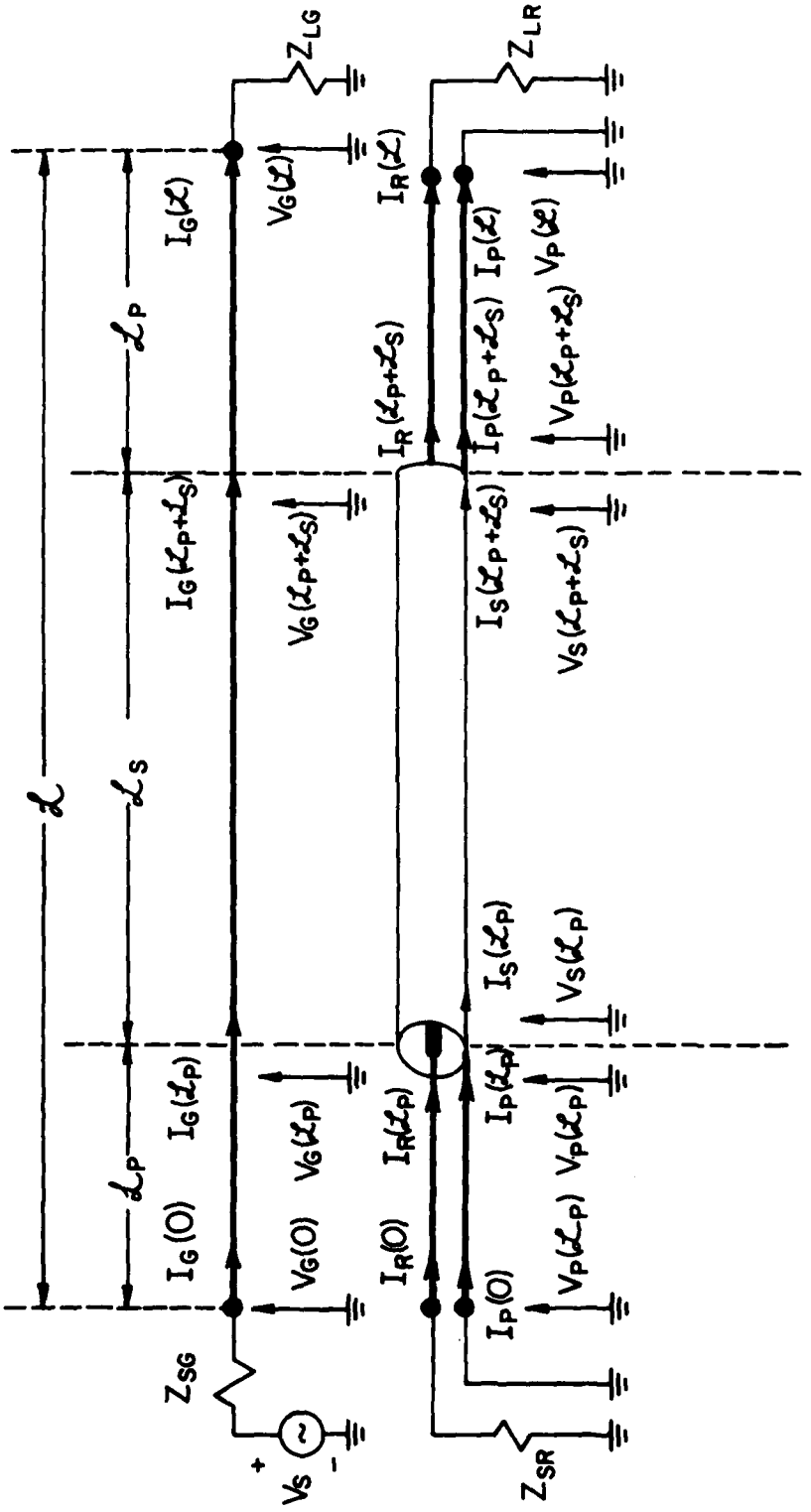

Fig. 15. Variable definitions for the overall line.

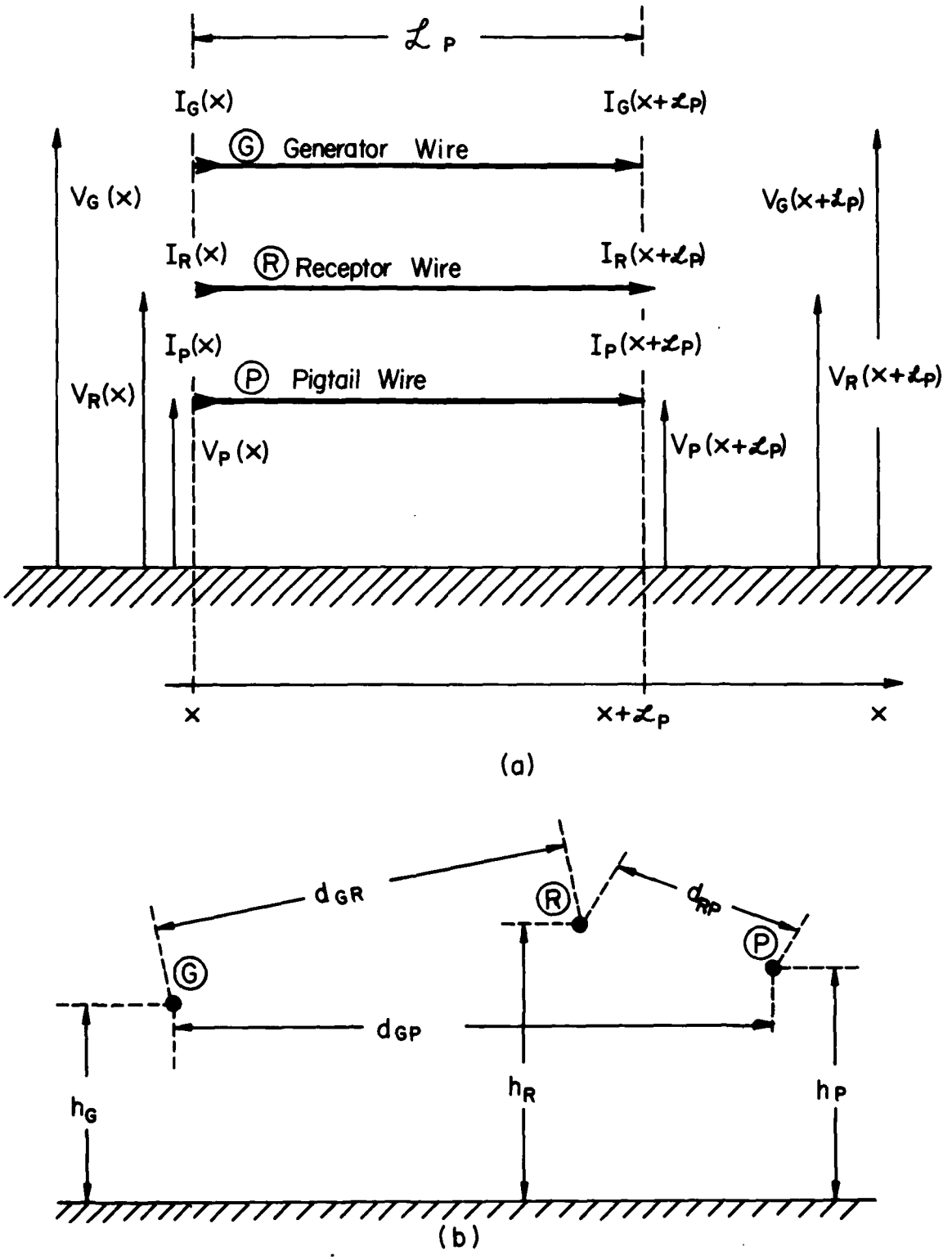

Fig. 16. The pigtail sections and variable definitions.

$$\begin{bmatrix} \underline{V}^P(x + \ell_p) \\ \underline{I}^P(x + \ell_p) \end{bmatrix} = \underbrace{\begin{bmatrix} \underset{\sim}{\phi}^P_{11}(\ell_p) & \underset{\sim}{\phi}^P_{12}(\ell_p) \\ \underset{\sim}{\phi}^P_{21}(\ell_p) & \underset{\sim}{\phi}^P_{22}(\ell_p) \end{bmatrix}}_{\underset{\sim}{\phi}^P(\ell_p)} \begin{bmatrix} \underline{V}^P(x) \\ \underline{I}^P(x) \end{bmatrix} \tag{6-48}$$

where $\underline{V}^P(x)$ and $\underline{I}^P(x)$ are given by

$$\underline{V}^P(x) = \begin{bmatrix} V_G(x) \\ V_R(x) \\ V_P(x) \end{bmatrix} \tag{6-49a}$$

$$\underline{I}^P(x) = \begin{bmatrix} I_G(x) \\ I_R(x) \\ I_P(x) \end{bmatrix} \tag{6-49b}$$

and $V_p(x)$ and $I_p(x)$ are the pigtail wire voltage (with respect to ground) and current, respectively. The 3 x 3 $\underset{\sim}{\phi}^P_{ij}(\ell_p)$ submatrices of $\underset{\sim}{\phi}^P(\ell_p)$ are given by [7]

$$\underset{\sim}{\phi}^P_{11}(\ell_p) = \cos(\beta \ell_p)\ \underset{\sim}{1}_3 \tag{6-50a}$$

$$\underset{\sim}{\phi}^P_{12}(\ell_p) = -jv \sin(\beta \ell_p)\ \underset{\sim}{L}^P \tag{6-50b}$$

$$\underset{\sim}{\phi}^P_{21}(\ell_p) = -jv \sin(\beta \ell_p)\ \underset{\sim}{C}^P \tag{6-50c}$$

$$\underset{\sim}{\phi}^P_{22}(\ell_p) = \cos(\beta \ell_p)\ \underset{\sim}{1}_3 \tag{6-50d}$$

and $\underset{\sim}{1}_3$ is the 3 x 3 identity matrix with ones on the main diagonal and zeros elsewhere. The quantity β is the phase constant given by

$$\beta = \omega/v \tag{6-51}$$

and v is the phase velocity of propagation in the surrounding (free space) medium

$$v = \frac{1}{\sqrt{\mu_v \varepsilon_v}} = 3 \times 10^8 \text{ m/s} \tag{6-52}$$

The 3 x 3 matrices $\underset{\sim}{L}^P$ and $\underset{\sim}{C}^P$ are the per-unit-length inductance and capacitance matrices of the pigtail sections given by

$$\underset{\sim}{L}^P = \begin{bmatrix} \ell_{GG} & \ell_{GR} & \ell_{GP} \\ \ell_{GR} & \ell_{RR} & \ell_{RP} \\ \ell_{GP} & \ell_{RP} & \ell_{PP} \end{bmatrix} \tag{6-53a}$$

$$\underset{\sim}{C}^P = \begin{bmatrix} (c_{GG}+c_{GR}+c_{GP}) & -c_{GR} & -c_{GP} \\ -c_{GR} & (c_{RR}+c_{GR}+c_{RP}) & -c_{RP} \\ -c_{GP} & -c_{RP} & (c_{PP}+c_{RP}+c_{GP}) \end{bmatrix} \tag{6-53b}$$

In $\underset{\sim}{L}^P$, ℓ_{GG}, ℓ_{RR} and ℓ_{GR} are the same as for the shielded section and ℓ_{GP}, ℓ_{RP} and ℓ_{PP} are given by [7] (see Fig. 16(b))

$$\ell_{GP} = \frac{\mu_v}{4\pi} \ell n[1 + \frac{4h_G h_P}{d_{GP}^2}] \tag{6-54a}$$

$$\ell_{RP} = \frac{\mu_v}{4\pi} \ell n[1 + \frac{4h_R h_P}{d_{RP}^2}] \tag{6-54b}$$

$$\ell_{PP} = \frac{\mu_v}{2\pi} \ell n[\frac{2h_P}{r_{wp}}] \tag{6-54c}$$

The 3 x 3 per-unit-length capacitance matrix $\underset{\sim}{C}^P$ is obtained via [7]

$$\underset{\sim}{C}^P = \mu_v \varepsilon_v \underset{\sim}{L}^{P^{-1}} \tag{6-53c}$$

Now consider Fig. 15. From Fig. 15 and the previous results we have, over the shielded section,

$$\begin{bmatrix} \underline{V}^S(\mathcal{I}_p + \mathcal{I}_s) \\ \underline{I}^S(\mathcal{I}_p + \mathcal{I}_s) \end{bmatrix} = \underset{\sim}{\phi}^S(\mathcal{I}_s) \begin{bmatrix} \underline{V}^S(\mathcal{I}_p) \\ \underline{I}^S(\mathcal{I}_p) \end{bmatrix} \tag{6-55}$$

Similarly we observe that, over the pigtail sections

$$\begin{bmatrix} \underline{V}^P(\ell) \\ \underline{I}^S(\ell) \end{bmatrix} = \underset{\sim}{\phi}^P(\ell_p) \begin{bmatrix} \underline{V}^P(\ell_p + \ell_s) \\ \underline{I}^P(\ell_p + \ell_s) \end{bmatrix} \tag{6-56}$$

and

$$\begin{bmatrix} \underline{V}^P(\ell_p) \\ \underline{I}^P(\ell_p) \end{bmatrix} = \underset{\sim}{\phi}^P(\ell_p) \begin{bmatrix} \underline{V}^P(0) \\ \underline{I}^P(0) \end{bmatrix} \tag{6-57}$$

Noting that, because of the sequencing of the variables in $\underline{V}^S$, $\underline{I}^S$, $\underline{V}^P$ and $\underline{I}^P$,

$$\underline{V}^P(\ell_p + \ell_s) = \underline{V}^S(\ell_p + \ell_s) \tag{6-58a}$$

$$\underline{I}^P(\ell_p + \ell_s) = \underline{I}^S(\ell_p + \ell_s) \tag{6-58b}$$

$$\underline{V}^S(\ell_p) = \underline{V}^P(\ell_p) \tag{6-58c}$$

$$\underline{I}^S(\ell_p) = \underline{I}^P(\ell_p) \tag{6-58d}$$

we have

$$\begin{bmatrix} \underline{V}^P(\ell) \\ \underline{I}^P(\ell) \end{bmatrix} = \underbrace{\underset{\sim}{\phi}^P(\ell_p)\ \underset{\sim}{\phi}^S(\ell_s)\ \underset{\sim}{\phi}^P(\ell_p)}_{\underset{\sim}{\phi}(\ell)} \begin{bmatrix} \underline{V}^P(0) \\ \underline{I}^P(0) \end{bmatrix} \tag{6-59a}$$

where

$$\begin{aligned} \underset{\sim}{\phi} &= \underset{\sim}{\phi}^P(\ell_p)\ \underset{\sim}{\phi}^S(\ell_s)\ \underset{\sim}{\phi}^P(\ell_p) \\ &= \begin{bmatrix} \underset{\sim}{\phi}_{11}(\ell) & \underset{\sim}{\phi}_{12}(\ell) \\ \underset{\sim}{\phi}_{21}(\ell) & \underset{\sim}{\phi}_{22}(\ell) \end{bmatrix} \end{aligned} \tag{6-59b}$$

From the terminal conditions in Fig. 15 we also obtain

$$\underline{V}^P(0) = \underline{V}_S - \underline{\underline{Z}}_S \underline{I}^P(0) \tag{6-60a}$$

$$\underline{V}^P(\ell) = \underline{\underline{Z}}_L \underline{I}^P(\ell) \tag{6-60b}$$

where, for the shield grounded at both ends, we obtain

$$\underline{V}_S = \begin{bmatrix} V_S \\ 0 \\ 0 \end{bmatrix} \tag{6-61a}$$

$$\underline{\underline{Z}}_S = \begin{bmatrix} Z_{SG} & 0 & 0 \\ 0 & Z_{SR} & 0 \\ 0 & 0 & 0 \end{bmatrix} \tag{6-61b}$$

$$\underline{\underline{Z}}_L = \begin{bmatrix} Z_{LG} & 0 & 0 \\ 0 & Z_{LR} & 0 \\ 0 & 0 & 0 \end{bmatrix} \tag{6-61c}$$

The zeros in the (3,3) positions of $\underline{\underline{Z}}_S$ and $\underline{\underline{Z}}_L$ account for the fact that the load impedances on the pigtail wires are short circuits. Combining (6-59) and (6-60) we obtain a matrix equation for the line currents at the source (x = 0) end of the line [7]

$$[\underline{\underline{Z}}_L \underline{\underline{\phi}}_{22} - \underline{\underline{Z}}_L \underline{\underline{\phi}}_{21} \underline{\underline{Z}}_S - \underline{\underline{\phi}}_{12} + \underline{\underline{\phi}}_{11} \underline{\underline{Z}}_S] \underline{I}^P(0) = [\underline{\underline{\phi}}_{11} - \underline{\underline{Z}}_L \underline{\underline{\phi}}_{21}] \underline{V}_S \tag{6-62a}$$

Once (6-62a) is solved for $\underline{I}^P(0)$ we obtain the terminal currents at the load end, $\underline{I}^P(\ell)$, from [7]

$$\underline{I}^P(\ell) = \underline{\underline{\phi}}_{21} \underline{V}_S + [\underline{\underline{\phi}}_{22} - \underline{\underline{\phi}}_{21} \underline{\underline{Z}}_S] \underline{I}^P(0) \tag{6-62b}$$

The terminal voltages are obtained from (6-60). In particular, we are interested in the voltage of the receptor wire across Z_{SR}, $V_R(0)$.

The shielded to unshielded configuration in which the source voltage is in series with Z_{SR} instead of Z_{SG} can be handled similarly in a trivial fashion. Clearly the chain parameter matrix of the entire line is unchanged. The only change is in the vector $\underline{V}_S$ in (6-61a). For the shielded to unshielded case, V_S appears in the second row of $\underline{V}_S$ instead of the first.

If the shield (pigtail wire) is grounded at only one end or neither end one can obtain a similar incorporation of these terminal conditions. For example, if the right end of the shield (pigtail wire) is ungrounded but the left end is grounded, we may write an alternate Norton equivalent expression for (6-60a) (since the impedance of an open circuit is infinite) as

$$\underline{I}^P(\ell) = \underset{\sim}{Y}_L \underline{V}^P(\ell) \tag{6-63a}$$

where

$$\underset{\sim}{Y}_L = \begin{bmatrix} 1/Z_{LG} & 0 & 0 \\ 0 & 1/Z_{LR} & 0 \\ 0 & 0 & 0 \end{bmatrix} \tag{6-63b}$$

since the admittance of the open circuit is zero. Equation (6-62a) becomes, by multiplying both sides by $\underset{\sim}{Y}_L = \underset{\sim}{Z}_L^{-1}$,

$$[\underset{\sim}{\phi}_{22} - \underset{\sim}{\phi}_{21}\,\underset{\sim}{Z}_S - \underset{\sim}{Y}_L\,\underset{\sim}{\phi}_{12} + \underset{\sim}{Y}_L\,\underset{\sim}{\phi}_{11}\,\underset{\sim}{Z}_S]\,\underline{I}^P(0) = [\underset{\sim}{Y}_L\,\underset{\sim}{\phi}_{11} - \underset{\sim}{\phi}_{21}]\,\underline{V}_S \tag{6-63c}$$

Similar modifications can be made if the left end is ungrounded but the right end is grounded or if both ends are ungrounded.

6.3 The MTL Equations for the Shielded to Shielded Case

The transmission line equations may be similarly derived for the shielded to shielded configuration in Fig. 3(c). First we obtain the transmission line equations for the shielded section.

Consider Fig. 17 in which we have defined the primed voltage and current variables in a manner similar to the unshielded to shielded case discussed

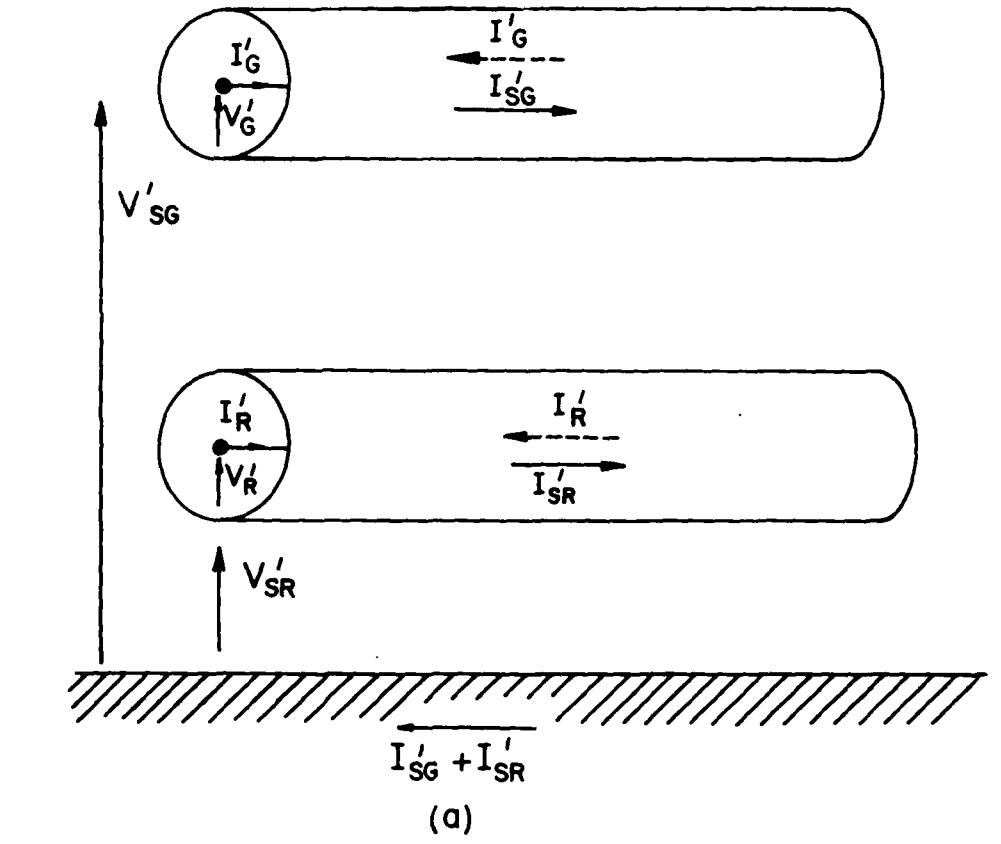

(a)

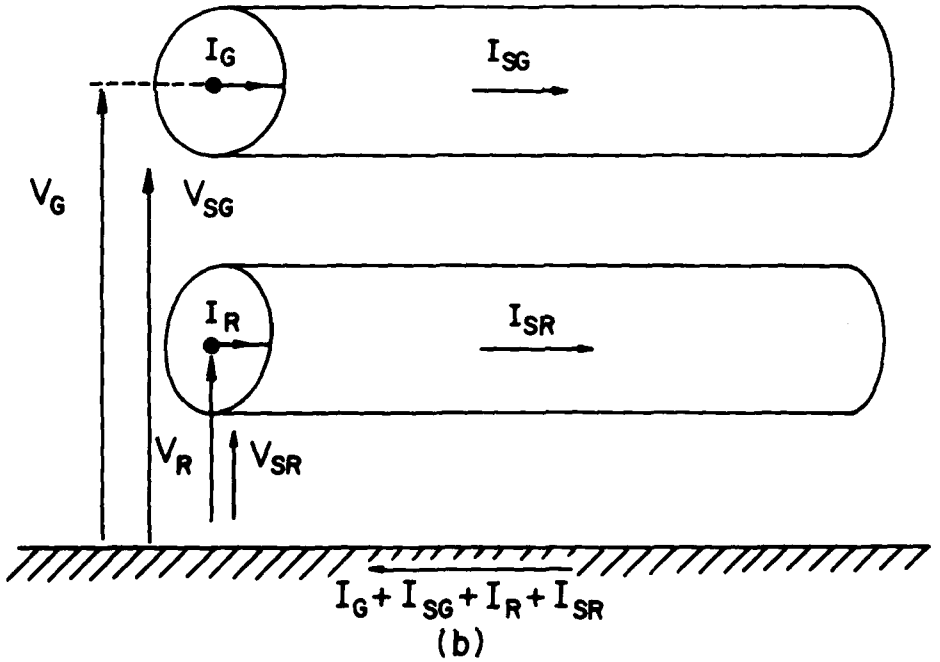

(b)

Fig. 17. The primed and unprimed variable definitions for shielded to shielded.

in Section 6.1. The return paths for the generator and receptor wire currents, I'_G and I'_R, are again defined to be the appropriate shields. Similarly, the generator and receptor wire voltages, V'_G and V'_R, are defined for each wire with respect to the appropriate shield. The shield currents of the generator circuit shield, I'_{SG}, and the receptor circuit shield, I'_{SR}, are defined to return via the ground plane. The shield voltages, V'_{SG} and V'_{SR}, are defined with respect to the ground plane. We may obtain, in a similar fashion to the unshielded to shielded case in Section 6.1, the voltage change transmission line equations as

$$\underline{\dot{V}}^{'S}(x) = - (\underset{\sim}{Z}^{'S} + j\omega \underset{\sim}{L}^{'S}) \underline{I}^{'S}(x) \tag{6-64}$$

where

$$\underline{V}^{'S}(x) = \begin{bmatrix} V'_G(x) \\ V'_R(x) \\ V'_{SG}(x) \\ V'_{SR}(x) \end{bmatrix} \tag{6-65a}$$

$$\underline{I}^{'S}(x) = \begin{bmatrix} I'_G(x) \\ I'_R(x) \\ I'_{SG}(x) \\ I'_{SR}(x) \end{bmatrix} \tag{6-65b}$$

and

$$\underset{\sim}{L}^{'S} = \begin{bmatrix} \ell'_{GG} & \ell'_{GR} & \ell'_{GSG} & \ell'_{GSR} \\ \ell'_{GR} & \ell'_{RR} & \ell'_{RSG} & \ell'_{RSR} \\ \ell'_{GSG} & \ell'_{RSG} & \ell'_{SGSG} & \ell'_{SGSR} \\ \ell'_{GSR} & \ell'_{RSR} & \ell'_{SGSR} & \ell'_{SRSR} \end{bmatrix} \tag{6-66a}$$

$$\underset{\sim}{Z}^{S'} = \begin{bmatrix} z_{SH} & 0 & -z_T & 0 \\ 0 & z_{SH} & 0 & -z_T \\ -z_T & 0 & z_{SH} & 0 \\ 0 & -z_T & 0 & z_{SH} \end{bmatrix} \tag{6-66b}$$

In obtaining (6-66b), we assume both shields to be identical so that $z_{SH}^{G} = z_{SH}^{R}$. In addition, we assume that the shield self impedances of the inner and outer surfaces to be equal, and the shield transfer impedances inside to outside and outside to inside are also assumed to be identical. Equation (6-66b) can be easily derived even when the assumptions are not made by employing the principles outlined in Section 6.1.

The unprimed variables are shown in Fig. 17(b). All unprimed currents are defined to return through the ground plane, and all unprimed voltages are with respect to the ground plane. The primed and unprimed variables may be related from Fig. 17 as

$$\begin{aligned} V_G &= V'_G + V'_{SG} \\ V_{SG} &= V'_{SG} \\ V_R &= V'_R + V'_{SR} \\ V_{SR} &= V'_{SR} \\ I_G &= I'_G \\ I_{SG} &= I'_{SG} - I'_G \\ I_R &= I'_R \\ I_{SR} &= I'_{SR} - I'_R \end{aligned} \tag{6-67}$$

or in matrix notation

$$\underline{V}^{S'} = \underset{\sim}{T}_V \, \underline{V}^{S} \tag{6-68a}$$

$$\underline{I}^{S'} = \underset{\sim}{T}_I \, \underline{I}^{S} \tag{6-68b}$$

where

$$\underset{\sim}{T}_V = \begin{bmatrix} 1 & 0 & -1 & 0 \\ 0 & 1 & 0 & -1 \\ 0 & 0 & 1 & 0 \\ 0 & 0 & 0 & 1 \end{bmatrix} \tag{6-68c}$$

$$\underset{\sim}{T}_I = \begin{bmatrix} 1 & 0 & 0 & 0 \\ 0 & 1 & 0 & 0 \\ 1 & 0 & 1 & 0 \\ 0 & 1 & 0 & 1 \end{bmatrix} \tag{6-68d}$$

The voltage change transmission line equations in terms of the unprimed variables become

$$\underline{\dot{V}}^S(x) = - (\underset{\sim}{Z}^S + j\omega \underset{\sim}{L}^S) \underline{I}^S(x) \tag{6-69}$$

where

$$\underline{V}^S(x) = \begin{bmatrix} V_G(x) \\ V_R(x) \\ V_{SG}(x) \\ V_{SR}(x) \end{bmatrix} \tag{6-70a}$$

$$\underline{I}^S(x) = \begin{bmatrix} I_G(x) \\ I_R(x) \\ I_{SG}(x) \\ I_{SR}(x) \end{bmatrix} \tag{6-70b}$$

and

$$\underset{\sim}{L}^S = \underset{\sim}{T}_V^{-1} \underset{\sim}{L}^{S'} \underset{\sim}{T}_I$$

$$= \begin{bmatrix} \ell_{GG} & \ell_{GR} & \ell_{GSG} & \ell_{GSR} \\ \ell_{GR} & \ell_{RR} & \ell_{RSG} & \ell_{RSR} \\ \ell_{GSG} & \ell_{RSG} & \ell_{SGSG} & \ell_{SGSR} \\ \ell_{GSR} & \ell_{RSR} & \ell_{SGSR} & \ell_{SRSR} \end{bmatrix} \tag{6-71a}$$

$$\underset{\sim}{Z}^{S} = \underset{\sim}{T}_V^{-1}\ \underset{\sim}{Z}^{S'}\ \underset{\sim}{T}_I \tag{6-71b}$$

$$= \begin{bmatrix} 2(z_{SH} - z_T) & 0 & (z_{SH} - z_T) & 0 \\ 0 & 2(z_{SH} - z_T) & 0 & (z_{SH} - z_T) \\ (z_{SH} - z_T) & 0 & z_{SH} & 0 \\ 0 & (z_{SH} - z_T) & 0 & z_{SH} \end{bmatrix}$$

Note than when the frequency is sufficiently small so that $z_T \cong z_{SH}$, (6-71b) becomes

$$\underset{\sim}{Z}^{S} \cong \begin{bmatrix} 0 & 0 & 0 & 0 \\ 0 & 0 & 0 & 0 \\ 0 & 0 & z_{SH} & 0 \\ 0 & 0 & 0 & z_{SH} \end{bmatrix} \tag{6-71c}$$

(low frequency)

and the shield impedance appears only in the voltage change expression for the shield circuits: again a logical result.

The per-unit-length mutual inductances in (6-71a) can be derived in a straightforward fashion similar to the unshielded to shielded case [7]. These become

$$\ell_{GG} = \frac{\mu_v}{2\pi} \ell n\left(\frac{2h_G}{r_{wG}}\right) \tag{6-72a}$$

$$\ell_{GR} = \frac{\mu_v}{4\pi} \ell n \left[1 + \frac{4h_G h_R}{d_{GR}^2}\right] \tag{6-72b}$$

$$\ell_{GSG} = \frac{\mu_v}{2\pi} \ell n \left(\frac{2h_G}{r_{sG} + t_{sG}}\right) \tag{6-72c}$$

$$\ell_{GSR} = \ell_{GR} \tag{6-72d}$$

$$\ell_{RR} = \frac{\mu_v}{2\pi} \ell n \left(\frac{2h_R}{r_{wR}}\right) \tag{6-72e}$$

$$\ell_{RSG} = \ell_{GR} \tag{6-72f}$$

$$\ell_{RSR} = \frac{\mu_v}{2\pi} \ell n \left(\frac{2h_R}{r_{sR} + t_{sR}} \right) \tag{6-72g}$$

$$\ell_{SGSG} = \frac{\mu_v}{2\pi} \ell n \left(\frac{2h_G}{r_{sG} + t_{sG}} \right) \tag{6-72h}$$

$$\ell_{SGSR} = \ell_{GR} \tag{6-72i}$$

$$\ell_{SRSR} = \frac{\mu_v}{2\pi} \ell n \left(\frac{2h_R}{r_{sR} + t_{sR}} \right) \tag{6-72j}$$

The current change expression (neglecting the shield transfer admittances assuming a solid shield) becomes

$$\begin{aligned} \underline{\dot{I}}^S &= - j\omega \, \underset{\sim}{C}^S \, \underline{V}^S \\ &= - \underset{\sim}{Y}^S \, \underline{V}^S \end{aligned} \tag{6-73}$$

where $\underset{\sim}{C}^S$ is derived from Fig. 18 as

$$\underset{\sim}{C}^S = \begin{bmatrix} c_{GSG} & 0 & -c_{GSG} & 0 \\ 0 & c_{RSR} & 0 & -c_{RSR} \\ -c_{GSG} & 0 & (c_{GSG} + c_{SGSG} + c_{SGSR}) & -c_{SGSR} \\ 0 & -c_{RSR} & -c_{SGSR} & (c_{SRSR} + c_{RSR} + c_{SGSR}) \end{bmatrix} \tag{6-74a}$$

Again, the entries in $\underset{\sim}{C}^S$ may be obtained quite easily by writing the node voltage equations for Fig. 18. The values of the specific entries are computed as

$$\begin{bmatrix} (c_{SGSG} + c_{SGSR}) & -c_{SGSR} \\ -c_{SGSR} & (c_{SRSR} + c_{SGSR}) \end{bmatrix} = \mu_v \varepsilon_v \begin{bmatrix} \ell_{SGSG} & \ell_{SGSR} \\ \ell_{SGSR} & \ell_{SRSR} \end{bmatrix}^{-1} \tag{6-74b}$$

$$c_{GSG} = \frac{2\pi\varepsilon}{\ell n \left(\frac{r_{sG}}{r_{wG}} \right)} \tag{6-74c}$$

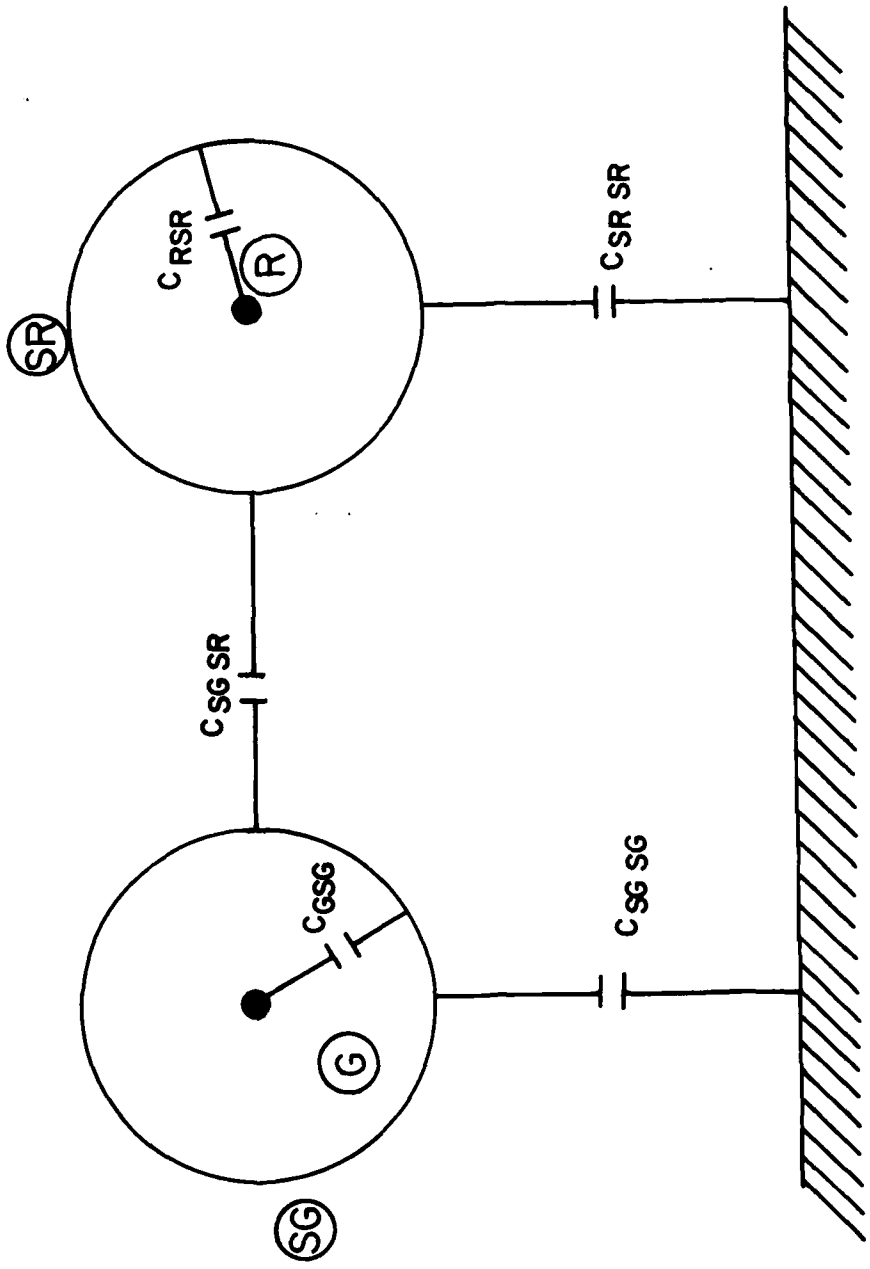

Fig. 18. A cross section of the line illustrating the per-unit-length capacitances.

$$C_{RSR} = \frac{2\pi\epsilon}{\ell n\left(\frac{r_{sR}}{r_{wR}}\right)} \tag{6-74d}$$

The chain parameter matrix of the shielded section of length ℓ_s can similarly be calculated as

$$\begin{bmatrix} \underline{V}^S(x+\ell_s) \\ \underline{I}^S(x+\ell_s) \end{bmatrix} = \underset{\sim}{\phi}^S(\ell_s) \begin{bmatrix} \underline{V}^S(x) \\ \underline{I}^S(x) \end{bmatrix} \tag{6-75}$$

where the entries of the 8 x 8 chain parameter matrix $\underset{\sim}{\phi}^S(\ell_s)$ are 4 x 4 submatrices. This is expressed as

$$\underset{\sim}{\phi}^S(\ell_s) = \begin{bmatrix} \underset{\sim}{\phi}^S_{11}(\ell_s) & \underset{\sim}{\phi}^S_{12}(\ell_s) \\ \underset{\sim}{\phi}^S_{21}(\ell_s) & \underset{\sim}{\phi}^S_{22}(\ell_s) \end{bmatrix} \tag{6-76}$$

and are given by (6-45) where the matrices in (6-45) are now 4 x 4.

The 8 x 8 chain parameter matrix of the pigtail sections (both shields have pigtail wires attached in this case) may be similarly computed as

$$\begin{bmatrix} \underline{V}^P(x+\ell_p) \\ \underline{I}^P(x+\ell_p) \end{bmatrix} = \underset{\sim}{\phi}^P(\ell_p) \begin{bmatrix} \underline{V}^P(x) \\ \underline{I}^P(x) \end{bmatrix} \tag{6-77}$$

where

$$\underline{V}^P(x) = \begin{bmatrix} V_G(x) \\ V_R(x) \\ V_{PG}(x) \\ V_{PR}(x) \end{bmatrix} \tag{6-78a}$$

$$\underline{I}^P(x) = \begin{bmatrix} I_G(x) \\ I_R(x) \\ I_{PG}(x) \\ I_{PR}(x) \end{bmatrix} \tag{6-78b}$$

The generator and receptor wire voltages and currents V_G, V_R, I_G, I_R are defined in the same fashion as for the shielded section. The voltages V_{PG} and V_{PR} are the voltages of the pigtail wires of the generator and receptor shields, respectively, with respect to the ground plane. Similarly, I_{PG} and I_{PR} are the appropriate pigtail wire currents. The entries in $\underset{\sim}{\phi}^P(\boldsymbol{\mathcal{L}}_p)$ are given by

$$\underset{\sim}{\phi}^P(\boldsymbol{\mathcal{L}}_p) = \begin{bmatrix} \underset{\sim}{\phi}^P_{11}(\boldsymbol{\mathcal{L}}_p) & \underset{\sim}{\phi}^P_{12}(\boldsymbol{\mathcal{L}}_p) \\ \underset{\sim}{\phi}^P_{21}(\boldsymbol{\mathcal{L}}_p) & \underset{\sim}{\phi}^P_{22}(\boldsymbol{\mathcal{L}}_p) \end{bmatrix} \tag{6-79}$$

where the entries in the 4 x 4 submatrices are

$$\underset{\sim}{\phi}^P_{11}(\boldsymbol{\mathcal{L}}_p) = \cos(\beta \boldsymbol{\mathcal{L}}_p)\ \underset{\sim}{1}_4 \tag{6-80a}$$

$$\underset{\sim}{\phi}^P_{12}(\boldsymbol{\mathcal{L}}_p) = -\,jv \sin(\beta \boldsymbol{\mathcal{L}}_p)\ \underset{\sim}{L}^P \tag{6-80b}$$

$$\underset{\sim}{\phi}^P_{21}(\boldsymbol{\mathcal{L}}_p) = -jv \sin(\beta \boldsymbol{\mathcal{L}}_p)\ \underset{\sim}{C}^P \tag{6-80c}$$

$$\underset{\sim}{\phi}^P_{22}(\boldsymbol{\mathcal{L}}_p) = \cos(\beta \boldsymbol{\mathcal{L}}_p)\ \underset{\sim}{1}_4 \tag{6-80d}$$

The per-unit-length inductance matrix is defined by

$$\underset{\sim}{L}^P = \begin{bmatrix} \ell_{GG} & \ell_{GR} & \ell_{GPG} & \ell_{GPR} \\ \ell_{GR} & \ell_{RR} & \ell_{RPG} & \ell_{RPR} \\ \ell_{GPG} & \ell_{RPG} & \ell_{PGPG} & \ell_{PGPR} \\ \ell_{GPR} & \ell_{RPR} & \ell_{PGPR} & \ell_{PRPR} \end{bmatrix} \tag{6-81}$$

and

$$\underset{\sim}{C}^P = \mu_v \epsilon_v\ \underset{\sim}{L}^{P^{-1}} \tag{6-82}$$

The entries in $\underset{\sim}{L}^P$ are given by the following with reference to Fig. 19:

$$\ell_{GG} = \frac{\mu_v}{2\pi} \ell n \left(\frac{2h_G}{r_{wG}} \right) \tag{6-83a}$$

$$\ell_{GR} = \frac{\mu_v}{4\pi} \ell n \left(1 + \frac{4h_G h_R}{d_{GR}^2} \right) \tag{6-83b}$$

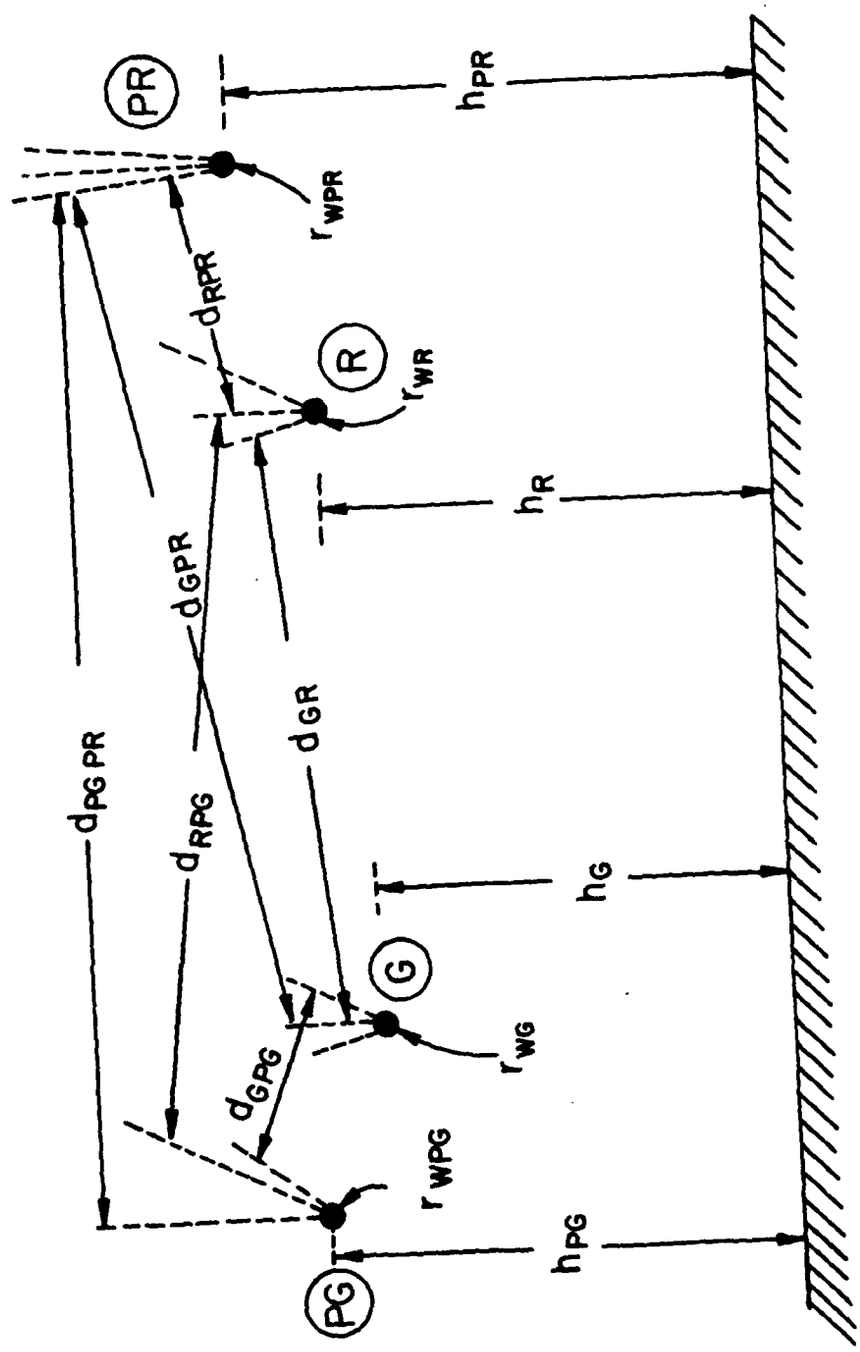

Fig. 19. The variable definitions for the pigtail sections.

$$\ell_{GPG} = \frac{\mu_v}{4\pi} \ell n \left(1 + \frac{4h_G h_{PG}}{d_{GPG}^2}\right) \tag{6-83c}$$

$$\ell_{GPR} = \frac{\mu_v}{4\pi} \ell n \left(1 + \frac{4h_G h_{PR}}{d_{GPR}^2}\right) \tag{6-83d}$$

$$\ell_{RR} = \frac{\mu_v}{2\pi} \ell n \left(\frac{2h_R}{r_{wR}}\right) \tag{6-83e}$$

$$\ell_{RPG} = \frac{\mu_v}{4\pi} \ell n \left(1 + \frac{4h_R h_{PG}}{d_{RPG}^2}\right) \tag{6-83f}$$

$$\ell_{RPR} = \frac{\mu_v}{4\pi} \ell n \left(1 + \frac{4h_R h_{PR}}{d_{RPR}^2}\right) \tag{6-83g}$$

$$\ell_{PGPG} = \frac{\mu_v}{2\pi} \ell n \left(\frac{2h_{PG}}{r_{wPG}}\right) \tag{6-83h}$$

$$\ell_{PGPR} = \frac{\mu_v}{4\pi} \ell n \left(1 + \frac{4h_{PG} h_{PR}}{d_{PGPR}^2}\right) \tag{6-83i}$$

$$\ell_{PRPR} = \frac{\mu_v}{2\pi} \ell n \left(\frac{2h_{PR}}{r_{wPR}}\right) \tag{6-83j}$$

The chain parameter matrix for the complete line for the shielded to shielded configuration in Fig. 3(c) can be obtained in a fashion similar to the unshielded to shielded case by multiplying these appropriate chain parameter matrices together. Thus we obtain

$$\begin{bmatrix} \underline{V}^P(\mathcal{L}) \\ \underline{I}^P(\mathcal{L}) \end{bmatrix} = \underset{\sim}{\phi}^P(\mathcal{L}_p)\ \underset{\sim}{\phi}^S(\mathcal{L}_s)\ \underset{\sim}{\phi}^P(\mathcal{L}_p) \begin{bmatrix} \underline{V}^P(0) \\ \underline{I}^P(0) \end{bmatrix} \tag{6-84}$$

The terminal conditions are again written as

$$\underline{V}^P(0) = \underline{V}_S - \underset{\sim}{Z}_S\ \underline{I}^P(0) \tag{6-85a}$$

$$\underline{V}^P(\ell) = \underset{\sim}{Z}_L \, \underline{I}^P(\ell) \tag{6-85b}$$

where, for both shields grounded at both ends,

$$\underline{V}_S = \begin{bmatrix} V_S \\ 0 \\ 0 \\ 0 \end{bmatrix} \tag{6-86a}$$

$$\underset{\sim}{Z}_S = \begin{bmatrix} Z_{SG} & 0 & 0 & 0 \\ 0 & Z_{SR} & 0 & 0 \\ 0 & 0 & 0 & 0 \\ 0 & 0 & 0 & 0 \end{bmatrix} \tag{6-86b}$$

$$\underset{\sim}{Z}_L = \begin{bmatrix} Z_{LG} & 0 & 0 & 0 \\ 0 & Z_{LR} & 0 & 0 \\ 0 & 0 & 0 & 0 \\ 0 & 0 & 0 & 0 \end{bmatrix} \tag{6-86c}$$

Again, the equations to be solved for the terminal currents are given by (6-62) where the matrices and vectors are now of dimension 4. The desired voltage across Z_{SR} is given by

$$V_{out} = - Z_{SR} \, I_R(0) \tag{6-87}$$

VII. Predictions of the Multiconductor Transmission Line (MTL) Model

In this section, the predictions of the multiconductor transmission line (MTL) model discussed in the previous section will be compared to the appropriate experimental results. These comparisons are shown in Appendix E. The comparisons for the unshielded to shielded case in Fig. 3(b) are given in Fig. E-1 through Fig. E-32. The comparisons for the shielded to shielded case in Fig. 3(c) are given in Fig. E-33 through Fig. E-38.

First consider the results for the unshielded to shielded configuration, 0.5 cm pigtails, 1.5 cm separation (WIDE) and R = 50Ω shown in Fig. E-1 through Fig. E-4. Note in Fig. E-1 for both ends of the shield grounded, the MTL model provides prediction accuracies within 1dB below 1MHz and within approximately 6dB for higher frequencies. For the other shield grounding configurations shown in Fig. E-2, E-3, E-4, the MTL model provides similar prediction accuracies although these tend to be somewhat better above 1MHz than for the double-end grounded case.

The corresponding results for R = 1kΩ are shown in Fig. E-5 through Fig. E-8. Again we obtain rather remarkable prediction accuracies similar to the R = 50Ω case. The small discrepancy in Fig. E-8 is explained in Appendix G.

The results for R = 50Ω, 8cm pigtails and 1.5cm separation (WIDE) are given in Fig. E-9 through Fig. E-12. The corresponding results for R =1kΩ are shown in Fig. E-13 through Fig. E-16. The prediction accuracies of the MTL model for these 8cm pigtail cases are also extremely good, and above 1MHz they are even better than for the 0.5cm pigtail cases. The slight prediction error in Fig. E-16 is explained in Appendix G.

We observed that for R = 1kΩ and the shield grounded at only one end, there was a considerable difference in crosstalk above approximately 200kHz depending upon which end of the shield was grounded. The low-frequency model, of course, made no distinction in coupling according to which end of the shield was grounded since it did not account for these distributed effects prevalant when the line is not electrically short. Clearly, the MTL model predicts these distributed affects and predicts them remarkably well.

The above results for the TOUCHING separation are shown in Fig. E-17 through Fig. E-32. For R = 50Ω and the 0.5 pigtails shown in Fig. E-17 through Fig. E-20, the prediction accuracies are very similar to the corresponding results for the WIDE separation. The results for R = 1kΩ shown in Fig. E-21

through Fig. E-24 show similar prediction accuracies although the predictions in the "standing wave region" (> 10 MHz) are somewhat poorer than for the corresponding R = 50Ω cases. Also for the case of the shielded ungrounded shown in Fig. E-24, the experimental results are above the MTL predictions for low frequencies by an almost consistent amount of some 6 dB. The reason for this sudden departure in prediction accuracy of the MTL model is due to our neglecting the wire dielectric insulations in computing the per-unit-length capacitances as is explained in Appendix G. Including the wire dielectric would result in prediction errors of only approximately 1.5 dB. This is supported by the fact that no such prediction errors were uncovered for the R = 50Ω cases (in which case inductive coupling is predominant) or for the WIDE separations. (See Fig. E-1 through Fig. E-16. In particular, see Fig. E-8 and Fig. E-16.)

The results for the 8 cm pigtails, TOUCHING separation and R = 50Ω are shown in Fig. E-25 through Fig. E-28. The prediction accuracies of the MTL model below 10 MHz are again within 1 dB, whereas above 10 MHz in the standing wave region the prediction accuracies of the MTL model are slightly poorer although they are typically within 6 dB. The corresponding results for R = 1kΩ are shown in Fig. E-29 through Fig. E-32. Again for this TOUCHING separation and R = 1kΩ we observe that the MTL model predicts less coupling than the experimental results show by an almost consistent amount of some 3-6 dB for the low frequencies. Again this is due to neglecting the wire insulation in the calculation of the per-unit-length capacitances as is shown in Appendix G. Including the wire insulation dielectric will result in modest prediction errors of 1 dB to 2 dB.

In the remaining figures of Appendix E, we will investigate the prediction accuracies of the MTL model for the shielded to shielded configuration of Fig. 3(c). The results for R = 50Ω, TOUCHING separation and 0.5 cm pigtails are shown in Fig. E-33. Note that below 10 MHz, the MTL model provides rather remarkable prediction accuracies which are typically within 1.5 dB. Recall that the predictions of the low-frequency model were typically some 8 dB above the experimental results when pigtail coupling is dominant (above approximately 200 kHz in Fig. E-33). This was attributed to the effect of the pigtail wires. The low-frequency model neglects the interaction between the pigtail wires and the generator and receptor wires over

the pigtail sections whereas the MTL model does not. For the unshielded to shielded case both models provided accurate predictions when pigtail coupling is dominant. Thus it seems clear that the pigtail wires have a substantial effect. The corresponding results for $R = 1k\Omega$ are shown in Fig. E-34 where we observe prediction accuracies similar to the previous $R = 50\Omega$ case. Note that for $R = 1k\Omega$ in Fig. E-34 for frequencies greater than 20 kHz, the predictions of the MTL model are below the experimental results by some 6 dB. In this frequency range, pigtail coupling is dominant (see Fig. C-15) and the prediction errors are a result of neglecting the wire dielectric as discussed in Appendix G. Inclusion of the dielectric will result in modest prediction errors of 1 dB to 2 dB.

The results for the 8 cm pigtails are given for $R = 50\Omega$ in Fig. E-35 and for $R = 1k\Omega$ in Fig. E-36. We again observe prediction accuracies for these longer pigtails which are similar to the 0.5 cm pigtail cases. The prediction errors for $R = 1k\Omega$ in Fig. E-36 are, once again, due to neglecting the pigtail wire dielectric insulation as discussed in Appendix G.

The corresponding results for 8 cm pigtails and the WIDE separation are shown in Fig. E-37 and Fig. E-38. The predictions for $R = 50\Omega$ in Fig. E-37 are once again within 2 dB below 10 MHz. When pigtail coupling is dominant (above approximately 100 kHz) the pigtail wires have a more substantial effect for this WIDE separation than for the TOUCHING separation over the unshielded to shielded results. (See Fig. A-23.) The MTL model however provides quite accurate predictions of this effect. For $R = 1k\Omega$ shown in Fig. E-38, the MTL model provides very accurate predictions below 10 MHz. The corresponding predictions for $R = 1k\Omega$ and the TOUCHING separations in Fig. E-34 and Fig. E-36 were not as good when pigtail coupling is dominant. This was attributed to neglecting the insulation dielectric of the generator and receptor wires in the computation of the per-unit-length capacitances. The results for the WIDE separation in Fig. E-38 tend to confirm this, since we would expect the dielectric to have much less of an effect for the WIDE separation.

In summary, we have found that the MTL model will provide prediction accuracies within 1 - 3 dB when the line is electrically short and within 6 - 10 dB when the line is electrically long although there are exceptions at isolated frequencies. However, it should be noted that when the line is suf-

ficiently short, electrically, the simpler low-frequency model provides prediction accuracies which are quite often equivalent to the MTL model. The advantage in using the low-frequency model is that due to its simplicity, certain qualitative effects are easily seen as was pointed out in Sections IV and V. The advantage in using the MTL model is that one needs not be concerned about determining whether the line is "sufficiently short, electrically" as was required in the use of the low-frequency model; the distributed effects which were ignored by the low-frequency model are included in the predictions of the MTL model. In addition the complicated interactions between all conductors are taken into account. This turned out to be significant in the shielded to shielded case for R = 50Ω where the pigtail wires had a substantial effect which was accurately predicted with the MTL model. The MTL model seems to provide prediction accuracies which are within reasonable expectations.

VIII. Effect of Pigtail Loop Area

The pigtail configuration which has been considered up to this point was chosen to simulate the method of terminating a shield in a connector as shown in Fig. 2. The shield braid is stripped back and is terminated via another wire, the pigtail wire, to a connector pin. In connector installations, this pigtail wire is routed parallel to the shielded wire as shown in Fig. 2 and simulated in Fig. 3 and our previous experiments.

However, there are cases in which the pigtail wire is not terminated (for example to structural ground) within a connector. In these cases, the pigtail wire connecting the shield braid to ground is of some uncontrolled length and its routing is random (not parallel to the shielded wire as in previous cases) as is illustrated in Fig. 20.

In this final section, we wish to examine the effect of the random orientation of the pigtail wire on our previous conclusions which were obtained for the controlled, connector-configuration simulation.

Also, in the previous controlled, connector-configuration simulation, the pigtail wire was routed parallel to the shielded wire, with a physically, somewhat minimal separation between the pigtail wire and shielded wire of 0.5cm. It should be emphasized that the intent was to simulate typical routings of these pigtail wires in connector installations. In an actual connector installation, the shield is stripped back and a pigtail wire is soldered (or crimped) to the shield. This pigtail wire is then routed to a connector pin via the shortest route which places the pigtail wire parallel to and at a typically small distance (such as 0.5cm) away from the associated shielded wire. It is of interest, however, to examine the effect of placing the pigtail wire parallel to the shielded wire but at a further distance from the shielded wire. The second objective of this section is to examine this effect of increasing the area of the loop formed between the pigtail wire and the shielded wire.

In this section we will show some limited experimental data which address these two questions. It should be emphasized that these limited data are only intended to provide some general conclusions. For example, the case of random pigtail wires is a totally uncontrolled configuration. Comparing crosstalk for this configuration to that of some other configuration cannot

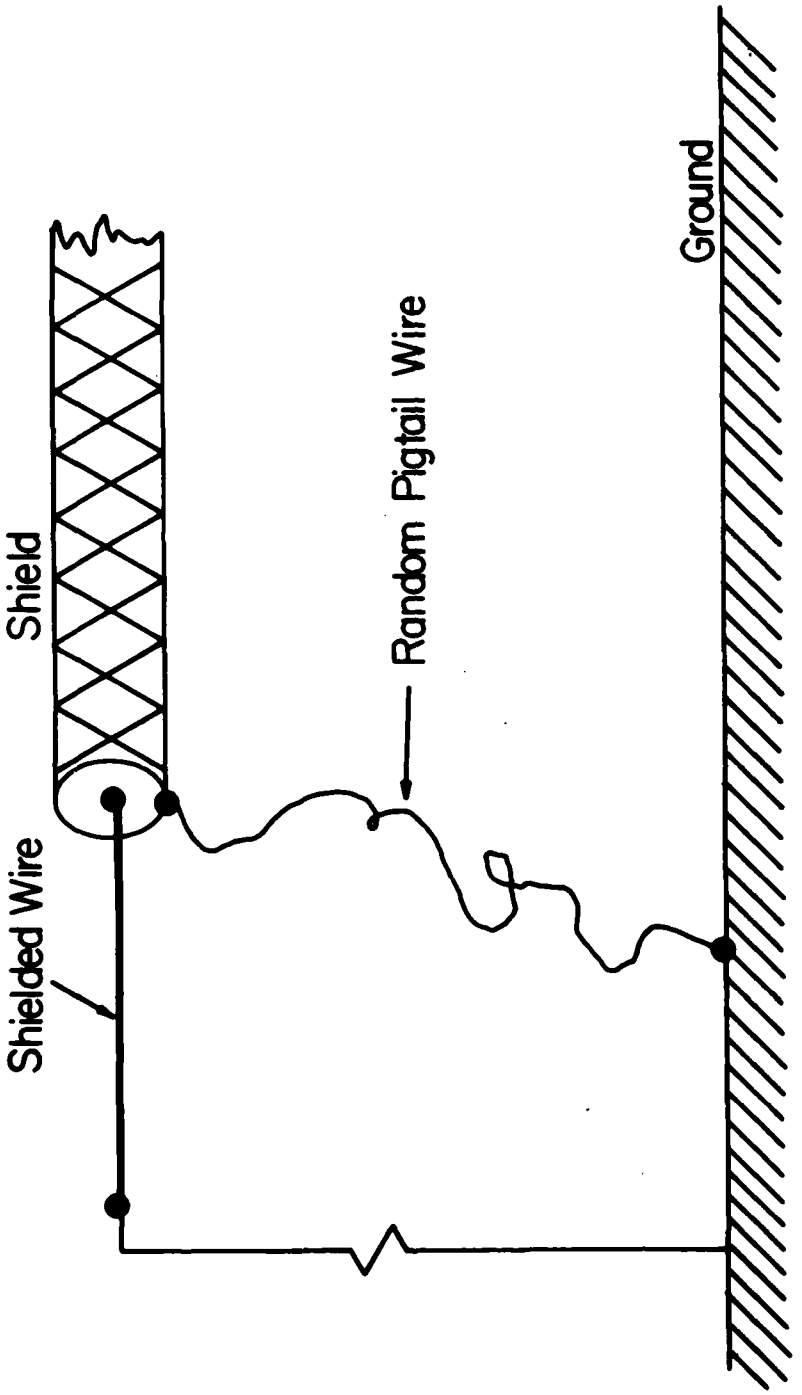

Fig. 20. The random pigtail wire configuration.

be expected to provide quantitative conclusions; only somewhat general conclusions can be obtained (more or less coupling than the controlled, 0.5cm separation, etc.).

The experimental configuration chosen is the unshielded to shielded case with 3 cm length pigtail sections. The pigtail wires are configured as the random pigtail in which the pigtail wires are approximately 30 cm in length and shown in Fig. 21(a) and three controlled configurations in which the pigtail wire is parallel to the shielded wire but separated from it by 0.5cm, 1.5cm and 3cm. The 3cm separation is shown in Fig. 21(b).

The results for R = 50Ω, TOUCHING separation and both ends of the shield grounded via the pigtail wires are shown in Fig. 22(a). Note that for the controlled configuration, moving the pigtail wire away from the shielded wire (and thus increasing the loop area between the pigtail wire and the shielded wire) results in an increase in coupling. If we denote the separation between the pigtail wire and the shielded wire as W and the length of the pigtail section as L (L = 3cm in all cases) as shown in Fig. 22(a) then there are three values of loop area:

Pigtail (I)	W = 0.5cm, L = 3cm	Area = $1.5cm^2$	(8-1a)
Pigtail (II)	W = 1.5cm, L = 3cm	Area = $4.5cm^2$	(8-1b)
Pigtail (III)	W = 3cm, L = 3cm	Area = $9cm^2$	(8-1c)

Note in Fig. 22(a) that above 100 KHz, the coupling is clearly due to the coupling over the pigtail section. This coupling increases approximately linearly with loop area. For example, at 1 MHz changing from pigtail (I) to Pigtail (II) given in (8-1) results in an increase in crosstalk by a factor of approximately 2 and the area has increased by a factor of 3. Also increasing the loop area from Pigtail (II) to Pigtail (III), an increase of a factor of 2, causes an increase in crosstalk by a factor of 1.75 at 1 MHz. Thus it is clear that the coupling to the pigtail section increases with an increase in loop area. (Actually this conclusion was evident in our previous results since for a pigtail wire separation of 0.5cm and pigtail section lengths of 0.5cm, 3cm, 8cm, the loop area also increased!)

For the random pigtail wire configuration, note that in Fig. 22(a), the crosstalk increases (above 10 KHz) by as much as 20 dB! It should be noted that in obtaining these data for the case of random pigtail wires, the

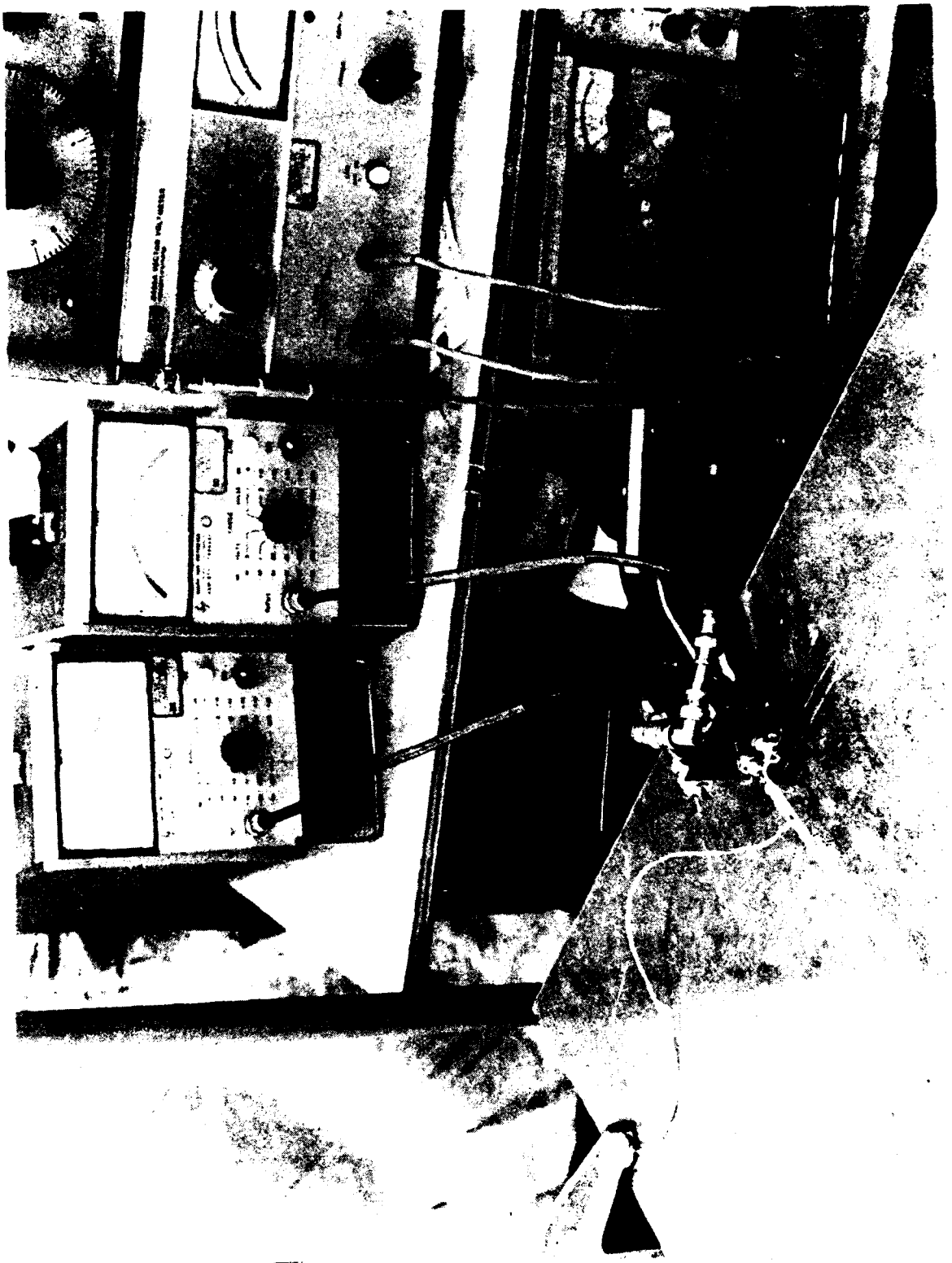

(a)

Fig. 21. The experimental configuration - random pigtail wires. (continued)

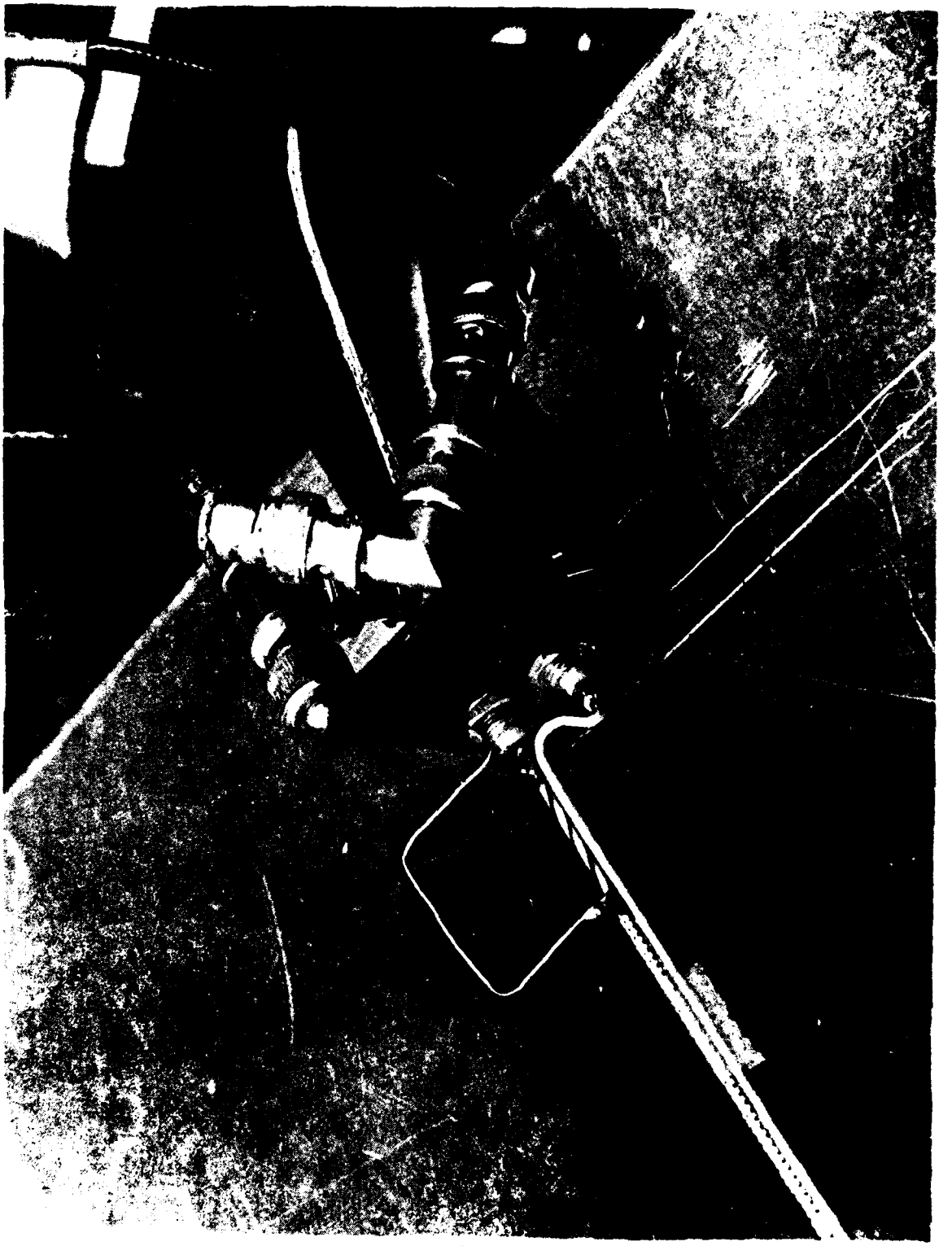

(b)

Fig. 21. The experimental configuration - 3cm x 3cm pigtail loop. (continued)

(c)

Fig. 21. The experimental configuration - random pigtail wires.

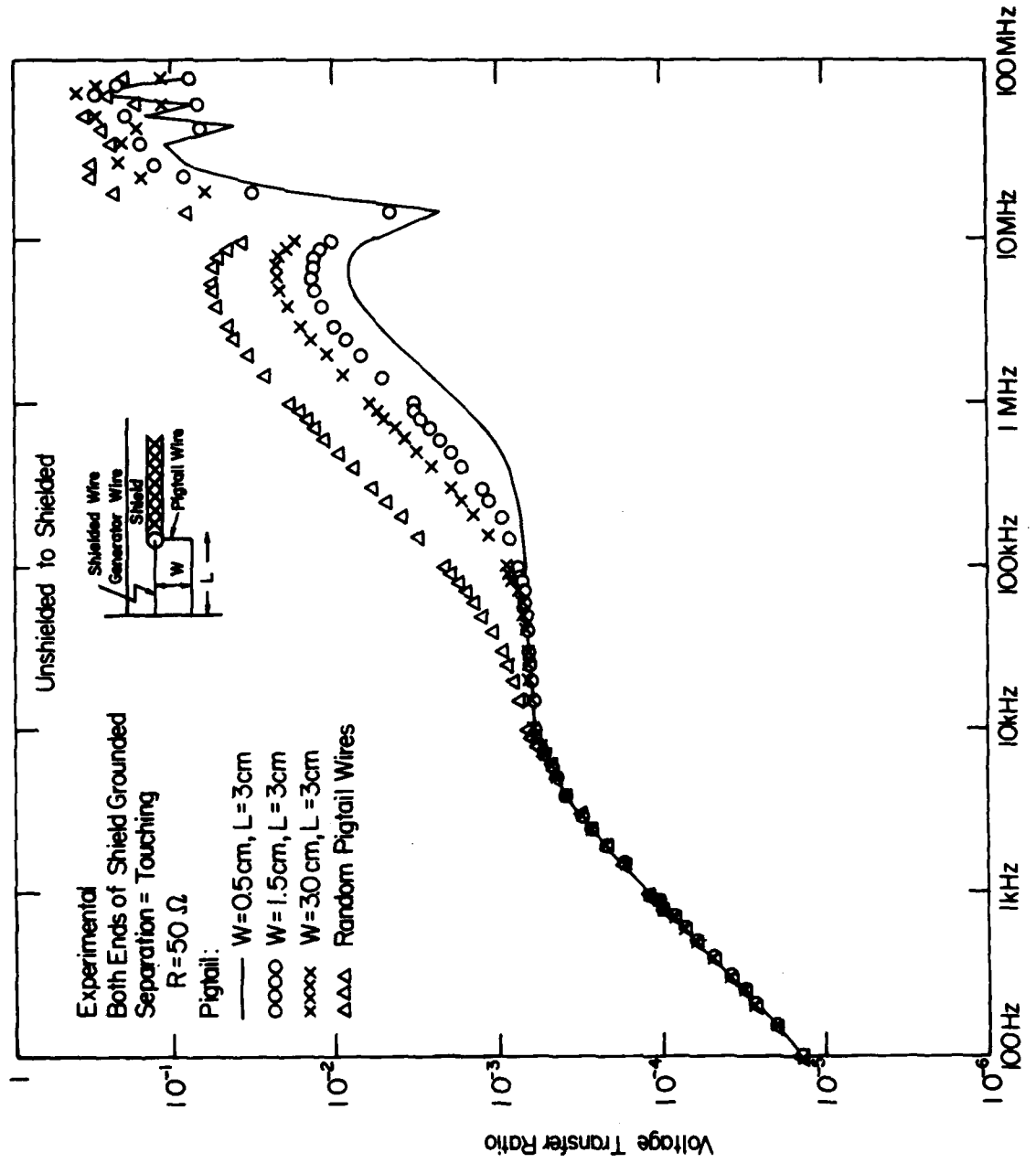
Unshielded to Shielded
Experimental
Both Ends of Shield Grounded
Separation = Touching
R = 50 Ω
Pigtail:
—— W=0.5cm, L=3cm
oooo W=1.5cm, L=3cm
xxxx W=3.0cm, L=3cm
ΔΔΔ Random Pigtail Wires
Shielded Wire
Generator Wire
Shield
Pigtail Wire
W
L
Voltage Transfer Ratio
Frequency (Hz)
100Hz
1kHz
10kHz
100kHz
1 MHz
10MHz
100MHz

(a)

Fig. 22.

results were very sensitive to the position of the pigtail wire. Simply touching this random pigtail wire and moving it slightly produced very noticeable changes in crosstalk. For example, at 1 MHz, touching the wire changed the measured voltage from 10 mV to approximately 32 mV! It is doubtful that accurate predictions of pigtail coupling for the random pigtail wire case can be obtained. The data, however, clearly show that termination of shielded wires with random pigtail wires is undesirable. IF pigtail sections cannot be avoided, the pigtail wires should be routed parallel to the exposed, shielded wire and as close as possible to it.

The corresponding results for R = 1kΩ are shown in Fig. 22(b). Note that for frequencies less than approximately 8 MHz, there is virtually no difference in crosstalk for any of the pigtail wire configurations. It is clear from Fig. A-9, that pigtail coupling is dominant above 500 kHz so that the results of Fig. 22(b) show that coupling over the pigtail sections is virtually unaffected by the pigtail wire configuration. In other words, it is clear that this invariance is not a result of the pigtail coupling being obscured by the coupling over the shielded section. This is a significant result but is reasonable to expect. Also it should be noted that the results were very insensitive to slight movements of the random pigtail wire as opposed to the R = 50Ω case. For R = 50Ω, we would presume that inductive coupling is the predominant contributor to the coupling over the pigtail sections. Thus for R = 50Ω it makes sense that varying the pigtail loop area (as defined above) would affect the crosstalk. However for R = 1kΩ, it is reasonable to expect that capacitive coupling is the predominant contributor to the coupling over the pigtail sections. For capacitive coupling, moving the pigtail wires further from the shielded wire should have less effect on the crosstalk.

Thus we observe that the configuration of the pigtail wires may or may not affect the crosstalk depending on the load impedances. For low impedance loads, the pigtail wire configuration had a drastic effect. For high impedance loads, the pigtail wire configuration had virtually no effect (for an electrically short line).

It is also of interest to observe how the shield grounding configuration affects these conclusions. The results for the shield grounded at the load end and ungrounded at the source end and R = 50Ω are shown in Fig. 23(a).

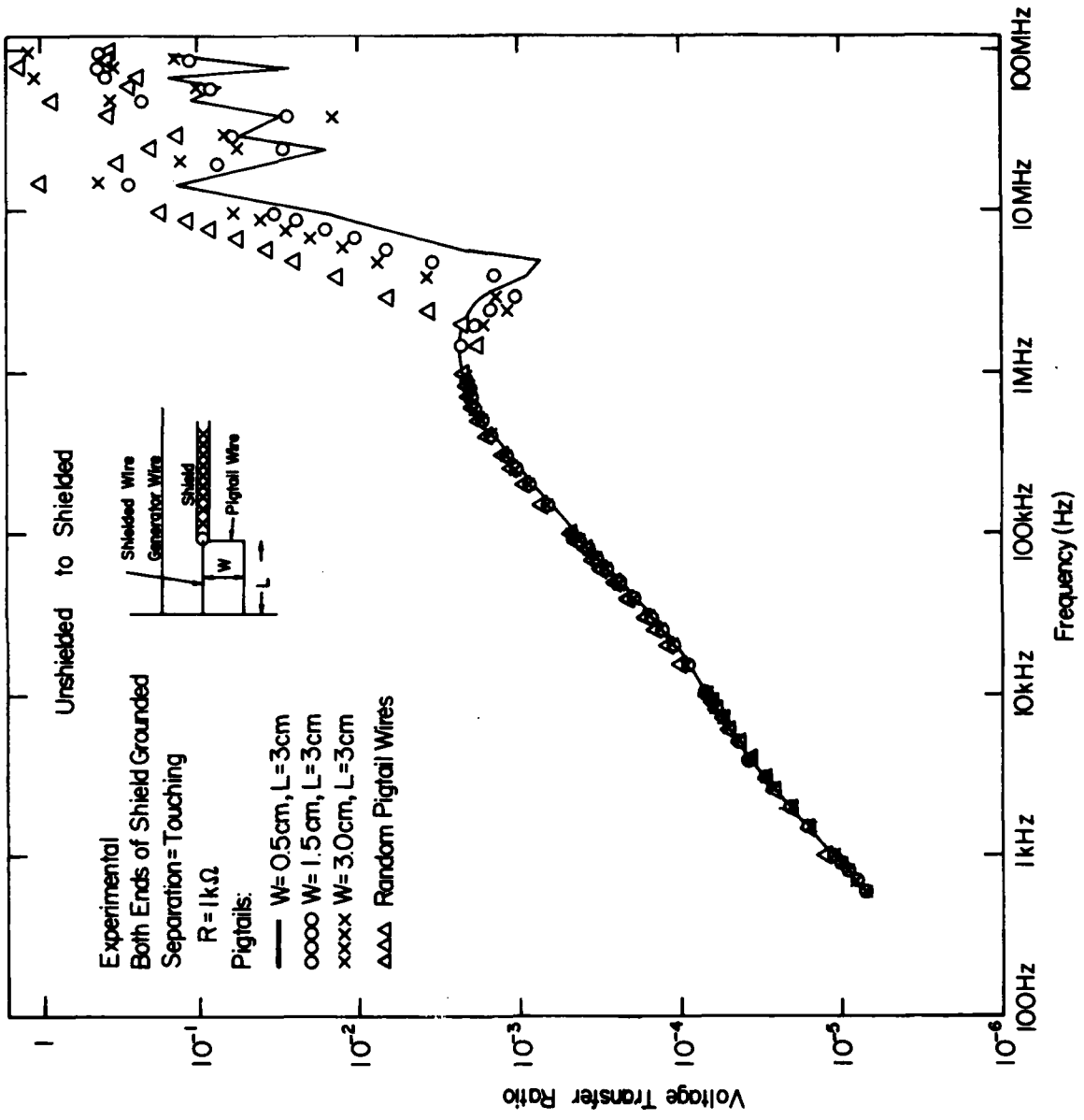
Unshielded to Shielded
Experimental
Both Ends of Shield Grounded
Separation = Touching
R = 1kΩ
Pigtails:
W = 0.5cm, L = 3cm
W = 1.5cm, L = 3cm
W = 3.0cm, L = 3cm
Random Pigtail Wires
Shielded Wire
Generator Wire
Shield
Pigtail Wire
W
L
Voltage Transfer Ratio
Frequency (Hz)
100Hz
1kHz
10kHz
100kHz
1MHz
10MHz
100MHz

(b)

Fig. 22.

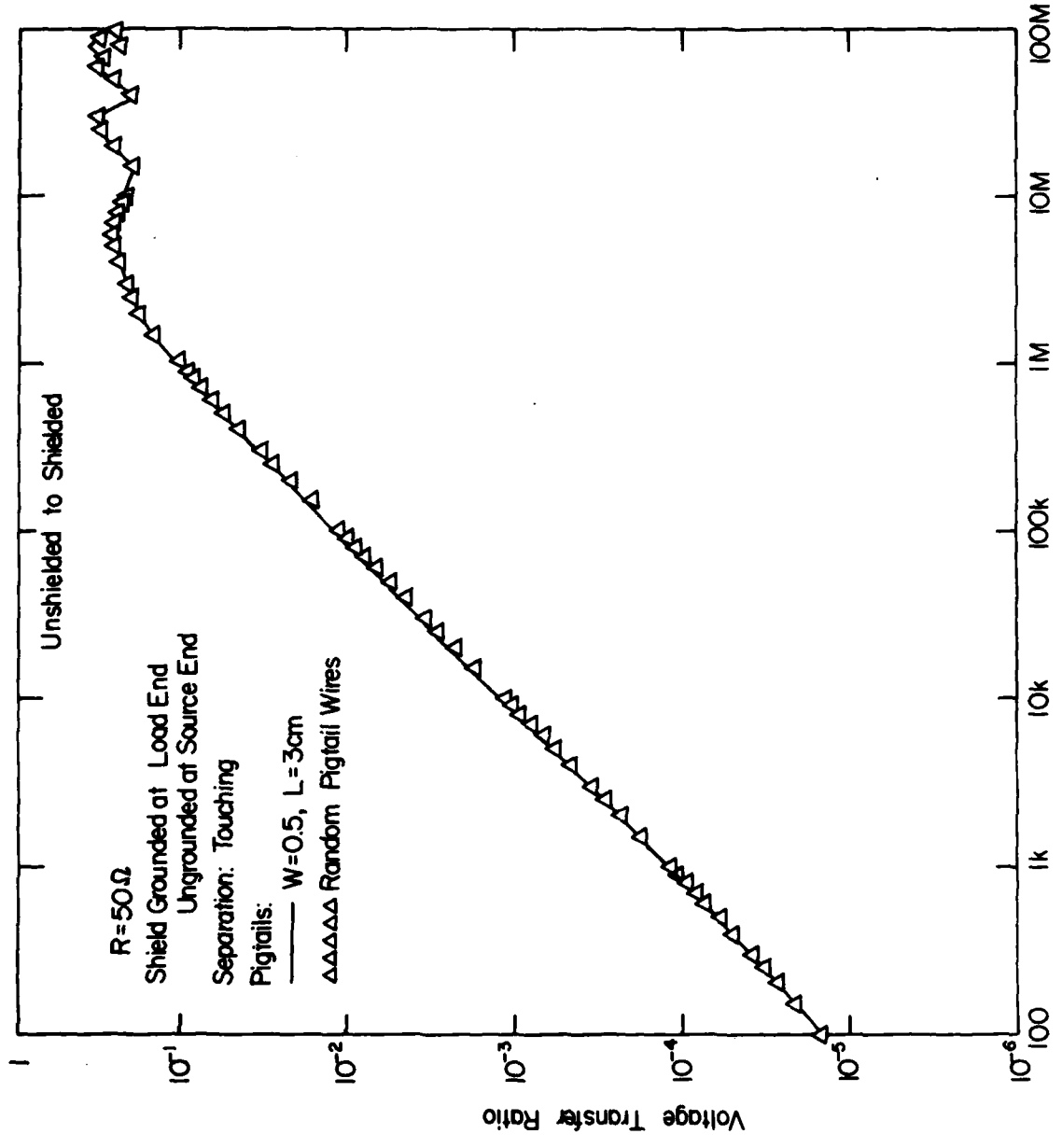
Unshielded to Shielded
R=50Ω
Shield Grounded at Load End
Ungrounded at Source End
Separation: Touching
Pigtails:
—— W=0.5, L=3cm
ΔΔΔΔΔ Random Pigtail Wires
Voltage Transfer Ratio
Frequency (Hz)
1
10⁻¹
10⁻²
10⁻³
10⁻⁴
10⁻⁵
10⁻⁶
100
1k
10k
100k
1M
10M
100M

(a)

Fig. 23.

Interestingly we find, as opposed to the double-end grounded case, that the crosstalk is independent of the pigtail wire configuration for these low impedance loads! This is again reasonable since there is no closed (physically) loop in the single-end ground case to support a current and alter the inductive coupling. The corresponding result for R = 1kΩ is shown in Fig. 23(b). Again, for the single-end grounded case, the pigtail wire configuration has virtually no effect on crosstalk.

The results for the shield grounded at the source end and ungrounded at the load end are shown for R = 50Ω in Fig. 24(a) and for R = 1kΩ in Fig. 24(b). Note that for R = 50Ω in Fig. 24(a) we again observe that even for low impedance loads, the pigtail wire configuration has no effect on crosstalk for the single-end grounded shield. For R = 1kΩ in Fig. 24(b) we observe similar conclusions except that the crosstalk is affected by the pigtail wire configuration as before. (See Fig. 22b.)

Clearly, the configuration of the pigtail wire may have an effect on crosstalk. For a double-end grounded shield and low impedance loads, there is a rather drastic dependence on configuration of the pigtail wire. However, for the common, random pigtail wire orientation, it is doubtful that one could provide reasonable predictions. The random pigtail wire configuration seems to be a hopeless case from the standpoint of prediction for low impedance loads and double-end grounded shields.

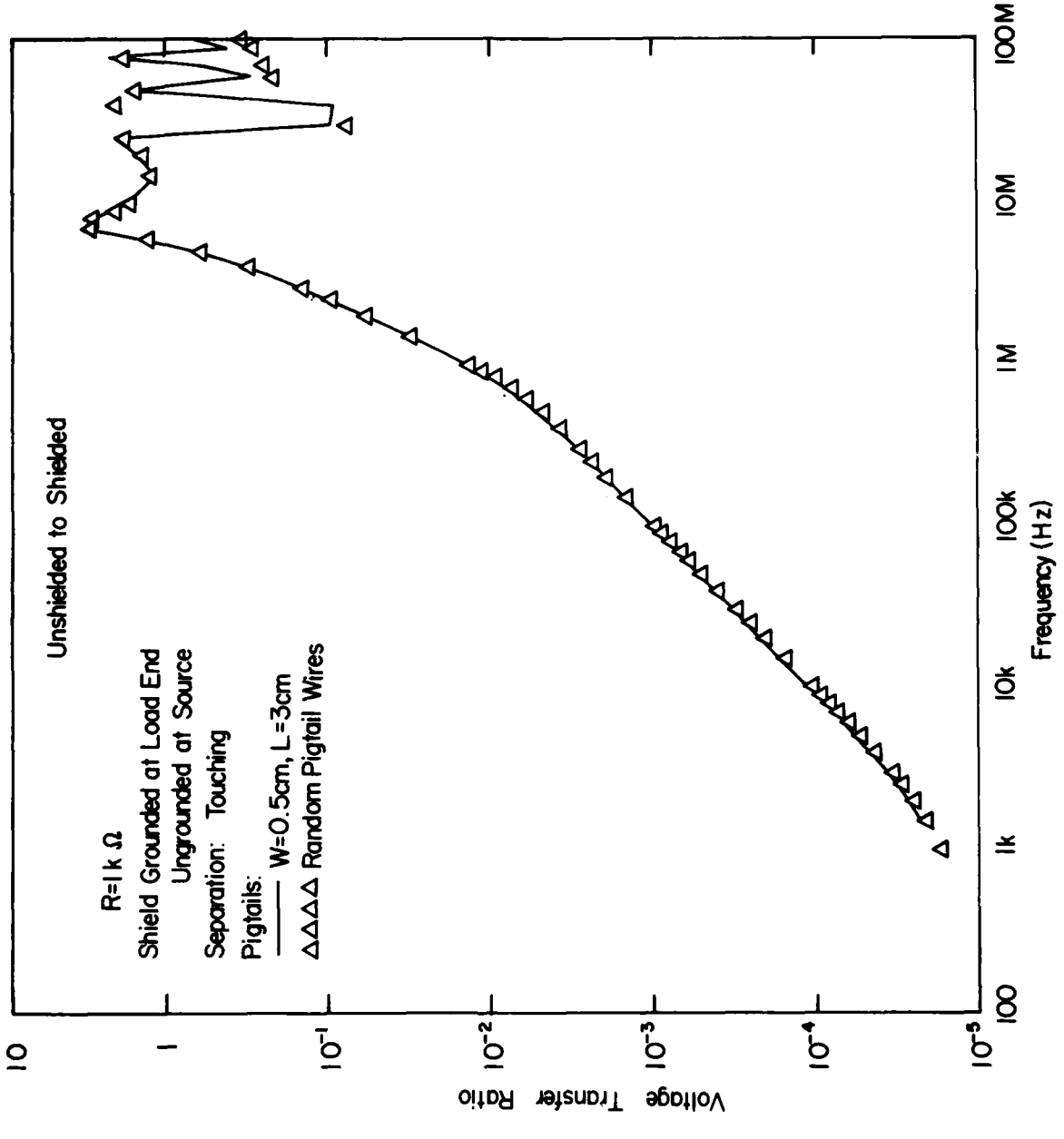
Unshielded to Shielded
R=1 k Ω
Shield Grounded at Load End
Ungrounded at Source
Separation: Touching
Pigtails:
W=0.5cm, L=3cm
Random Pigtail Wires
Voltage Transfer Ratio
Frequency (Hz)
10
1
10^{-1}
10^{-2}
10^{-3}
10^{-4}
10^{-5}
100
1k
10k
100k
1M
10M
100M

(b)

Fig. 23.

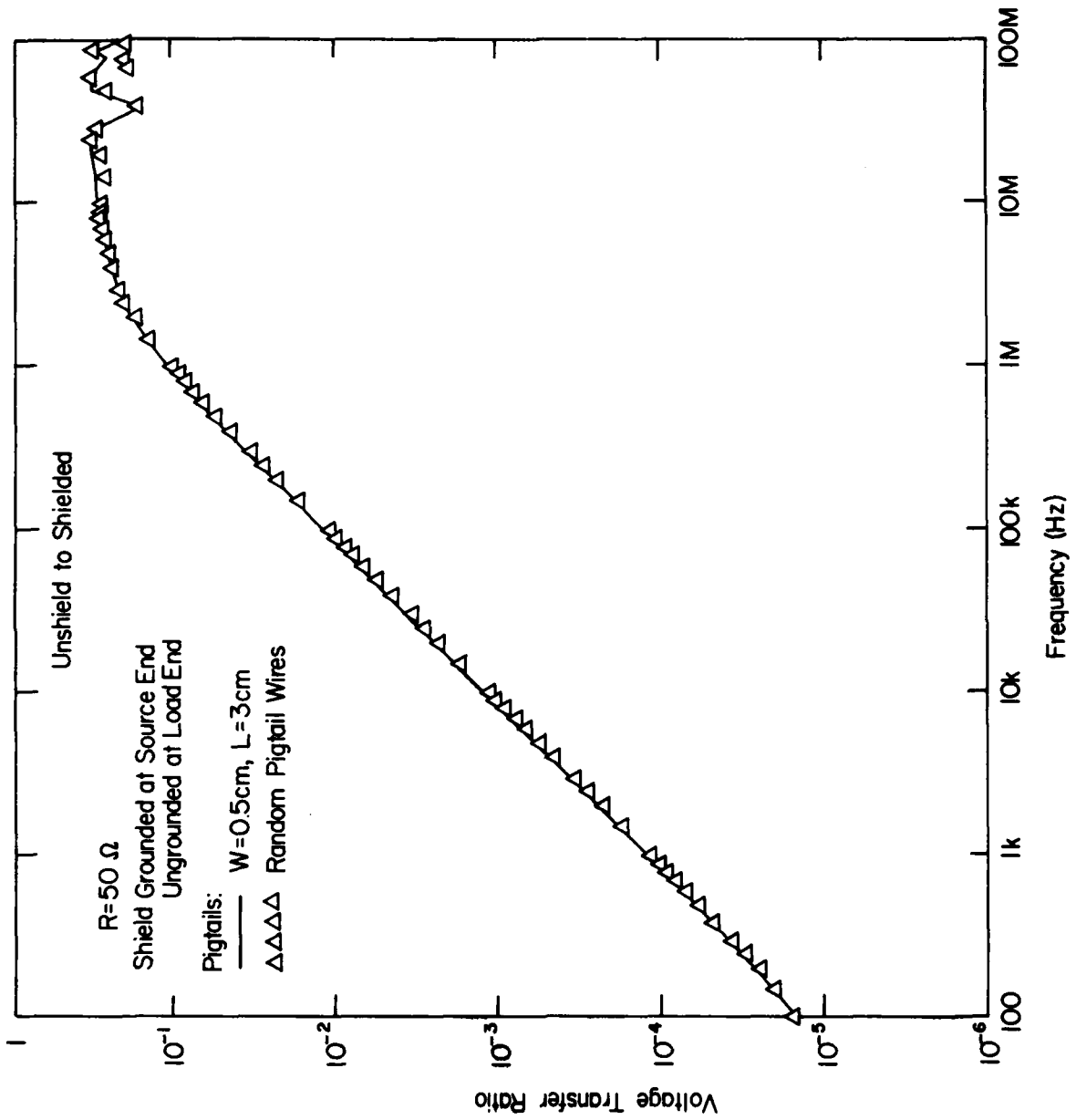
Unshield to Shielded
R=50 Ω
Shield Grounded at Source End
Ungrounded at Load End
Pigtails:
W=0.5cm, L=3cm
ΔΔΔΔ Random Pigtail Wires
Voltage Transfer Ratio
Frequency (Hz)
1
10^-1
10^-2
10^-3
10^-4
10^-5
10^-6
100
1k
10k
100k
1M
10M
100M

(a)

Fig. 24.

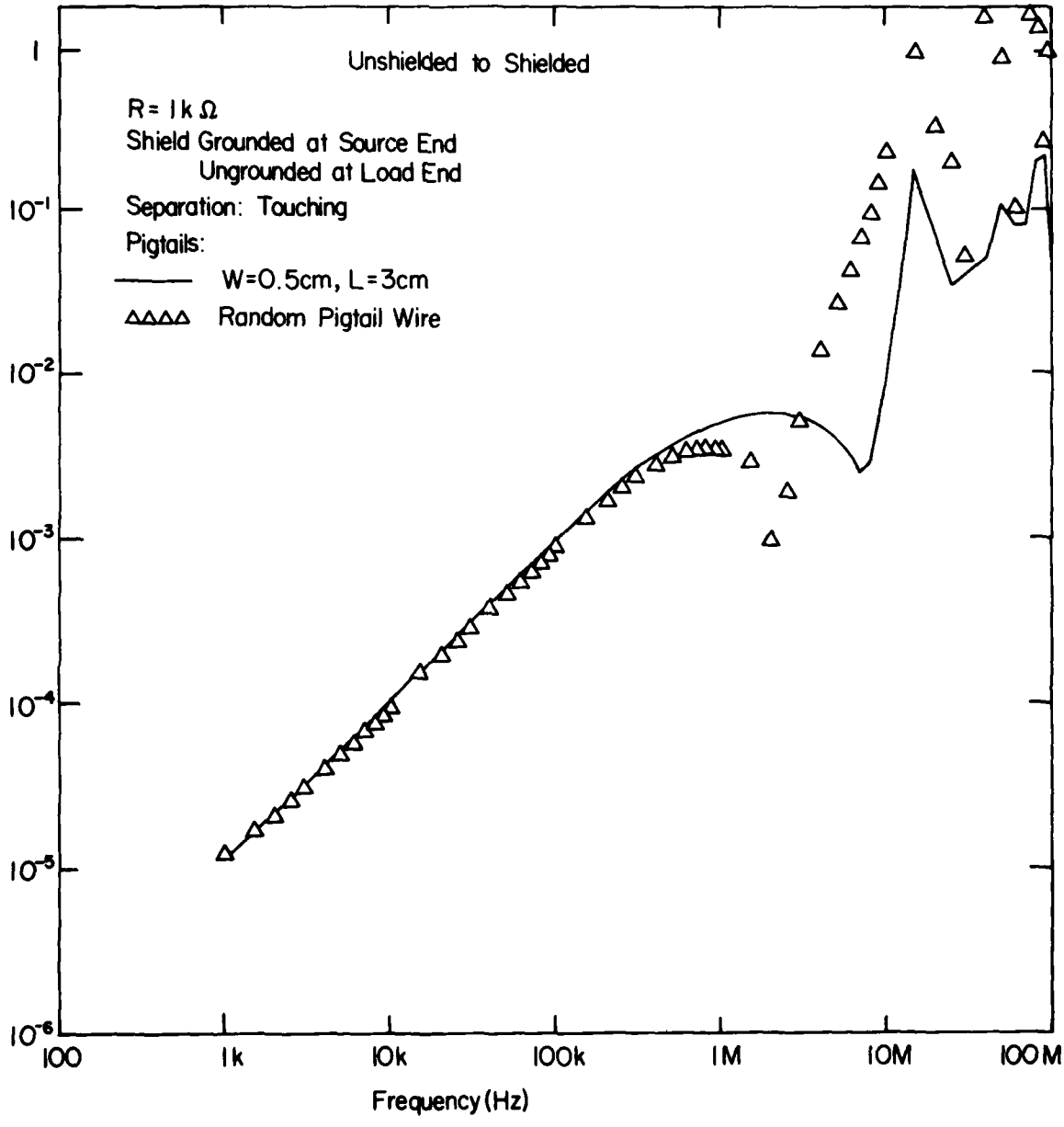
Unshielded to Shielded
R = 1 k Ω
Shield Grounded at Source End
Ungrounded at Load End
Separation: Touching
Pigtails:
W=0.5cm, L=3cm
Random Pigtail Wire
1
10⁻¹
10⁻²
10⁻³
10⁻⁴
10⁻⁵
10⁻⁶
100
1k
10k
100k
1M
10M
100M
Frequency (Hz)

(b)

Fig. 24.

IX. Summary and Conclusions

The intent of this report was to investigate coupling (crosstalk) between braided-shield cables. There were two main items to be addressed. We intended to show that pigtails on braided-shield cables such as are employed when these cables are terminated in connectors can result in a significant degradation in the effectiveness of the shield in the reduction of crosstalk. We also intended to investigate the modeling and prediction of crosstalk to or from braided-shield cables.

The effect of pigtails was dramatically illustrated with experimental results. It was observed that even though the lengths of the pigtail sections constituted only a very small fraction of the total line length (4%), the pigtails can result in an increase in crosstalk of as much as 30 dB over the case where the pigtail lengths are minimized (0.3%). Computed results support the idea that the degradation in the effectiveness of the shield comes about due to the following. For a sufficiently small frequency, we may superimpose the coupling over the pigtail sections and the shielded section to obtain the total received voltage at each end of the line. The contributions due to the pigtail sections increase linearly with frequency. The contribution over the shielded section also increases linearly with frequency up to a frequency where the shield becomes effective. Above this frequency, the coupling from an unshielded wire to a shielded wire over the shielded section remains constant with frequency. Thus the pigtail coupling contribution, although "small" at the lower frequencies, can become larger than the contribution over the shielded section in the region where the shield becomes effective. In the case of coupling between two shielded wires, this effect can be more dramatic since the coupling contribution over the shielded section when the shields become effective decreases linearly with frequency. This is to be contrasted with the coupling from an unshielded wire to a shielded wire in which the coupling becomes constant as the frequency is increased. For the case of two shielded wires, the pigtail coupling can therefore result in a larger degradation over a wider frequency range.

Clearly, the pigtails do not totally destroy the effectiveness of the shield. However, when pigtail coupling is dominant, the shield simply

serves to provide an "optical coverage" of its interior, shielded wire. Thus the exposure of the interior, shielded wire is limited to the pigtail sections. However, if the pigtails were eliminated, an additional reduction in crosstalk of at least 30 dB may be realized.

From these results, it is clear that a worthwhile objective in the installation of braided-shield cables within connectors is to eliminate or, at least, minimize, the lengths of the pigtail sections. Obviously, the elimination of pigtails in connectors is a difficult problem. However, the potential benefits in the electromagnetic compatibility of a system may be considerable.

In addition, several other interesting phenomena were observed. It was noted that the effectiveness of the shield in reducing crosstalk over the situation where a shield does not surround the interior wire was dependent on the shield grounding configuration as well as the value of the termination impedances of the cable. In the case of "low impedance loads" such as 50 Ω, it was found that the shield had virtually no effect on crosstalk unless it was grounded at both ends. In the case of "high impedance loads" such as 1 kΩ, however, a single-end grounded shield did provide considerable reduction in crosstalk, and the double-end grounded configuration provided even more reduction in crosstalk.

It was also observed that for frequencies such that the shield braid impedance is larger than the reactance of the shield-ground plane loop, the shield effectiveness was the same for all grounding configurations for low impedance loads and was the same as the single-end grounding configurations for high impedance loads. In other words, the advantage of grounding both ends of a shield is not realized unless the frequency is such that the shield-ground plane reactance is greater than the shield braid self impedance. Thus the effectiveness of a shield in reducing crosstalk is strongly dependent on its braid impedance.

The second objective of this report - examine the modeling and prediction of this coupling - led to the development of two models. The low-frequency model was valid only for a "sufficiently small" frequency. The upper limit to this frequency range was not unique but depended on the load impedances and physical configuration. However, the simplicity of this model

allowed considerable insight into this coupling phenomenon. For the purposes of providing this qualitative insight and obtaining approximate predictions, this model served a useful role.

The multiconductor transmission line (MTL) model required considerably more computational effort, and the qualitative features of the coupling which were transparent in the low-frequency model were obscured in the MTL model. The advantage of the MTL model is its prediction accuracy. With the MTL model, one need not be concerned about the limitation of the frequency being sufficiently small as was required for the low-frequency model. The prediction accuracies of the MTL model tended to be in the range of 1 dB - 3 dB when the line is electrically short and 6 dB - 10 dB when the line is electrically long.

In addition, certain effects which were of a distributed nature which were not predictable with the low-frequency model were accurately predicted with the MTL model. For example, in the case of a single-end grounded shield and high impedance loads, there was a considerable difference in crosstalk depending on which end of the shield was grounded. Clearly, this is a distributed effect not predictable by the low-frequency model. However, the MTL model predicted this result within a few dB.

The results of this investigation are intended to provide insight into the coupling to braided-shield cables. The successful application of these results to the design of interference suppression in system wire harnesses depends on the particular situation. The majority of present wire bundles may be classified as random bundles. In these types of wire bundles, the relative wire positions are unknown and uncontrolled. However, in order to provide accurate predictions of crosstalk within these bundles with, for example, the MTL model, one must not only know the relative wire positions but, in addition, these wire positions must be controlled. Also the height of this bundle above some identifiable ground plane must be constant (which usually is not the case in an actual system). Thus, for random bundles, the prediction models in this report are only useful in providing estimates of the effectiveness of shielded cables in reducing crosstalk. Nevertheless, the qualitative assessment of the effectiveness of braided-shield cables in the reduction of crosstalk should be obtainable with these models.

REFERENCES

[1] E. F. Vance, "Coupling to Cables", DNA Handbook Revision, Chapter 11, Stanford Research Institute, December 1974.

[2] AFSC DH 1-4, Electromagnetic Compatibility, Design Handbooks Branch (ASNPS-40), Air Force Systems Command, Wright-Patterson AFB, OH.

[3] Electromagnetic Compatibility Design Guide for Avionics and Related Ground Support Equipment, NAVAIR AD 1115, Naval Air Systems Command, Dept. of the Navy, Washington, D. C., Change 2, December 1975.

[4] Engineering Design Handbook, Electromagnetic Compatibility, DARCOM-P 706-410, HQ, U.S. Army Material Development and Readiness Command, Alexandria, VA, March 1977.

[5] Private communication with Mr. John Prorok, U. S. Army CORADCOM, Ft. Monmouth, NJ.

[6] Private communication with Mr. Gus Weinstock, McDonnell Aircraft Company, St. Louis, MO.

[7] C. R. Paul, Applications of Multiconductor Transmission Line Theory to the Prediction of Cable Coupling, Vol. I, Multiconductor Transmission Line Theory, Technical Report, RADC-TR-76-101, Rome Air Development Center, Griffiss AFB, NY, April 1976 (A025028).

[8] R. J. Mohr, "Coupling Between Open and Shielded Wire Lines Over a Ground Plane", IEEE Trans. on Electromagnetic Compatibility, Vol. EMC-9, No. 2, pp. 34-45, September 1967.

[9] R. J. Mohr, "Coupling Between Lines at High Frequencies", IEEE Trans. on Electromagnetic Compatibility, Vol. EMC-9, No. 3, pp. 127-129, December 1967.

[10] S. Shenfeld, "Coupling Impedance of Cylindrical Tubes", IEEE Trans. on Electromagnetic Compatibility, Vol. EMC-14, No. 1, pp. 10-16, February 1972.

[11] S. A. Schelkunoff, "The Electromagnetic Theory of Coaxial Transmission Lines and Cylindrical Shields", Bell Syst. Tech. J., Vol. 13, p. 532-579, Oct. 1934.

[12] S. A. Schelkunoff and T. M. Odarenko, "Crosstalk Between Coaxial Transmission Lines", Bell Syst. Tech. J., Vol. 16, pp. 144-164, April 1937.

[13] D. E. Merewether and T. F. Ezell, "The Effect of Mutual Inductance and Mutual Capacitance on the Transient Response of Braided-Shield Coaxial Cables", IEEE Trans. on Electromagnetic Compatibility, Vol. EMC-18, No. 1, pp. 15-20, Feb. 1976.

[14] R. W. Latham, An Approach to Certain Cable Shielding Calculations, Interaction Note 90, Air Force Weapons Lab, Albuquerque, NM, Jan. 1972.

[15] R. W. Latham, Small Holes in Cable Shields, Interaction Note 118, Air Force Weapons Lab, Albuquerque, NM, Sept. 1972.

[16] E. F. Vance, "Shielding Effectiveness of Braided-Wire Shields", IEEE Trans. on Electromagnetic Compatibility, Vol. EMC-17, No. 2, pp. 71-77, May 1975.

[17] K. S. H. Lee and C. E. Baum, "Application of Modal Analysis to Braided-Shield Cables", IEEE Trans. on Electromagnetic Compatibility, Vol. EMC-17, No. 3, pp. 159-169, August 1975.

[18] K. F. Casey and E. F. Vance, "EMP Coupling Through Cable Shields", IEEE Trans. on Electromagnetic Compatibility, Vol. EMC-20, No. 1, pp. 100-106, Feb. 1978.

[19] S. Frankel, "Terminal Response of Braided-Shield Cables to External Monochromatic Electromagnetic Fields", IEEE Trans. on Electromagnetic Compatibility, Vol. EMC-16, pp. 4-16, Feb. 1974.

[20] C. R. Paul, Applications of Multiconductor Transmission Line Theory to the Prediction of Cable Coupling, Vol. III, Prediction of Crosstalk in Random Cable Bundles, Technical Report, RADC-TR-76-101, Rome Air Development Center, Griffiss AFB, NY, Feb. 1977 (A038316).

[21] C. R. Paul, "Solution of the Transmission Line Equations for Three-Conductor Lines in Homogeneous Media", IEEE Trans. on Electromagnetic Compatibility, Vol. EMC-20, No. 1, pp. 216-222, Feb. 1978.

[22] W. C. Johnson, Transmission Lines and Networks, McGraw Hill, New York, 1950.

[23] K. F. Casey, "On the Effective Transfer Impedance of Thin Coaxial Cable Shields", IEEE Trans. on Electromagnetic Compatibility, Vol. EMC-18, No. 3, pp. 110-116, August 1976.

[24] J. R. Wait, "Electromagnetic Theory of the Loosely Braided Coaxial Cable: Part I", IEEE Trans. on Microwave Theory and Techniques, Vol.

MTT-24, No. 9, pp. 547-553, Sept. 1976.

[25] J. R. Wait, Electromagnetic Field Analysis for a Coaxial Cable With Periodic Slots, Interaction Note 265, Air Force Weapons Lab, Albuquerque, NM, Feb. 1976.

[26] L. Marin, Effects of a Dielectric Jacket of a Braided-Shield Cable on EMP Coupling Calculations, Interaction Note 178, Air Force Weapons Lab, Albuquerque, NM, May 1974.

[27] D. Kajfez and D. R. Wilton, Small Aperture on a Multiconductor Transmission Line Filled with Inhomogeneous Dielectrics, Interaction Note 347, Air Force Weapons Lab, Albuquerque, NM, Nov. 1977 .

[28] D. Kajfez, Excitation of a Terminated TEM Transmission Line Through a Small Aperture, Interaction Note 215, Air Force Weapons Lab, Albuquerque, NM, July 1974.

[29] W. C. Wells and Y. Shian, Nuclear Electromagnetic Pulse (NEMP) Hardened Cables, Technical Report, ECOM-73-0341-F, U. S. Army Electronic Command, Ft. Monmouth, NJ, April 1976.

[30] J. C. Clements and C. R. Paul, Computation of the Capacitance Matrix for Dielectric-Coated Wires, Technical Report, RADC-TR-74-59, Rome Air Development Center, Griffiss AFB, NY, March 1974 (AD778948).

[31] J. C. Clements, C. R. Paul and A. T. Adams, "Computation of the Capacitance Matrix for Systems of Dielectric-Coated Cylindrical Conductors", IEEE Trans. on Electromagnetic Compatibility, Vol. EMC-17, No. 4, pp. 238-248, November 1975.

[32] H. W. Ott, Noise Reduction Techniques in Electronic Systems, John Wiley and Sons, New York, 1976 (Chapter 2).

Acknowledgement -

The author wishes to thank Mr. P. C. Magoun for his assistance and advice throughout the experimental phase of this work.

APPENDIX A

Fig.	Configuration	Ω	Separation	Grounding	Pigtails	Page
A-1	US	50Ω	Touching	SS	0.5,3,8	114
A-2	"	"	"	SO	"	115
A-3	"	"	"	OS	"	116
A-4	"	"	"	OO	"	117
A-5	"	"	Wide	SS	"	118
A-6	"	"	"	SO	"	119
A-7	"	"	"	OS	"	120
A-8	"	"	"	OO	"	121
A-9	"	1kΩ	Touching	SS	"	122
A-10	"	"	"	SO	"	123
A-11	"	"	"	OS	"	124
A-12	"	"	"	OO	"	125
A-13	"	"	Wide	SS	"	126
A-14	"	"	"	SO	"	127
A-15	"	"	"	OS	"	128
A-16	"	"	"	OO	"	129
A-17	SS	50Ω	Touching	SS	0.5,8	130
A-18	"	1kΩ	"	SS	"	131
A-19	UU,US,SS	50Ω	"	"	0.5	132
A-20	"	"	"	"	8	133
A-21	"	1kΩ	"	"	0.5	134
A-22	"	"	"	"	8	135
A-23	"	50Ω	Wide	"	8	136
A-24	"	1kΩ	"	"	"	137

UU = unshielded to unshielded

US = unshielded to shielded

SS = shielded to shielded

O = open (shield ungrounded)

S = short (shield grounded)

First letter denotes source end of line and second letter denotes load end of line. For example, SO denotes that the shield is grounded at the source end and ungrounded at the load end.

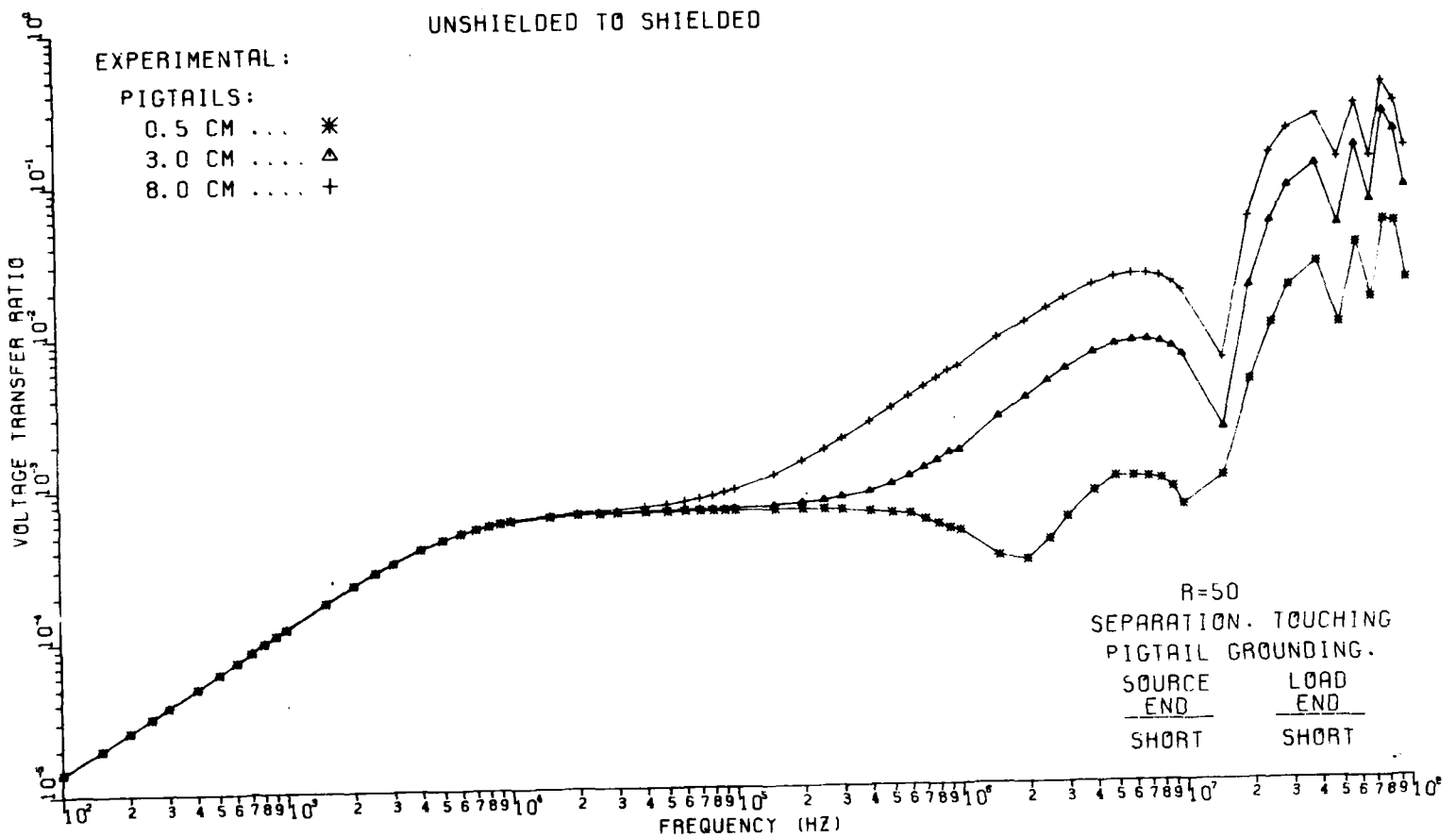
UNSHIELDED TO SHIELDED
EXPERIMENTAL:
PIGTAILS:
0.5 CM ... ✱
3.0 CM .... △
8.0 CM .... +
VOLTAGE TRANSFER RATIO
FREQUENCY (HZ)
R=50
SEPARATION. TOUCHING
PIGTAIL GROUNDING.
SOURCE END
SHORT
LOAD END
SHORT

Figure A-1.

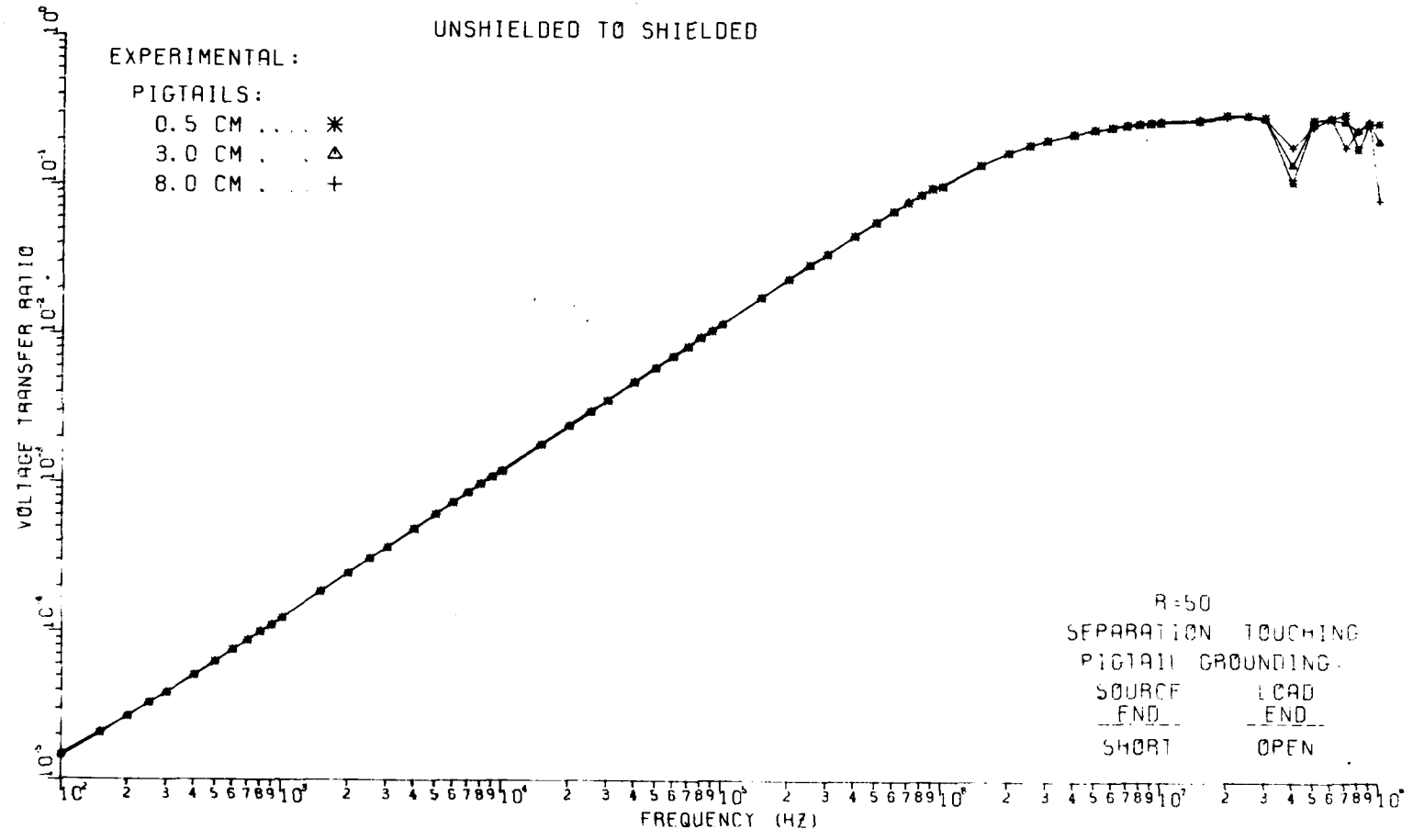
UNSHIELDED TO SHIELDED
EXPERIMENTAL:
PIGTAILS:
0.5 CM .... *
3.0 CM . . Δ
8.0 CM . . . +
VOLTAGE TRANSFER RATIO
FREQUENCY (HZ)
R=50
SEPARATION TOUCHING
PIGTAIL GROUNDING
SOURCE END SHORT
LOAD END OPEN

Figure A-2.

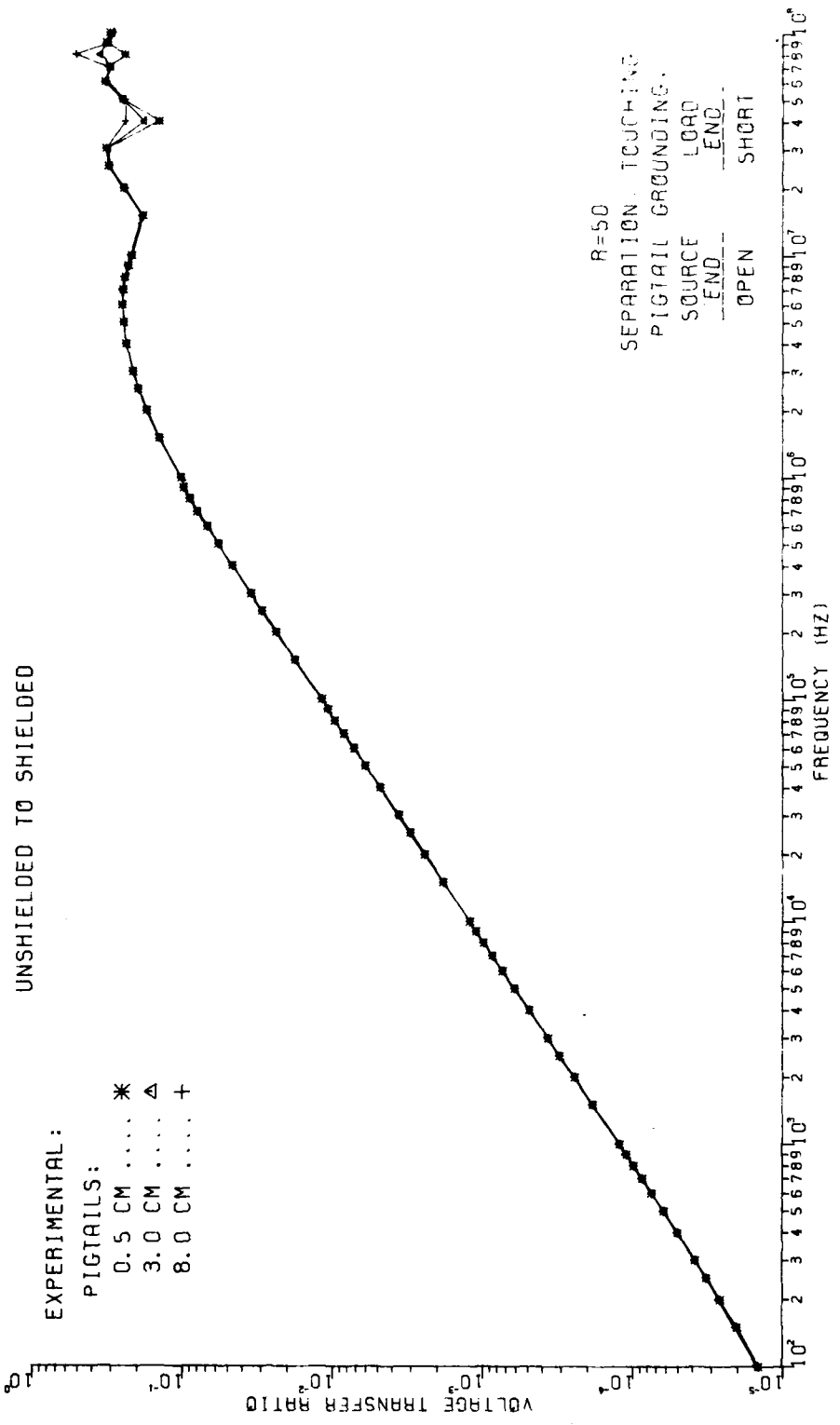
UNSHIELDED TO SHIELDED
EXPERIMENTAL:
PIGTAILS:
0.5 CM ..... *
3.0 CM ..... Δ
8.0 CM ..... +
R=50
SEPARATION TOUCHING
PIGTAIL GROUNDING
SOURCE LOAD
END END
OPEN SHORT
VOLTAGE TRANSFER RATIO
FREQUENCY (HZ)

Figure A-3.

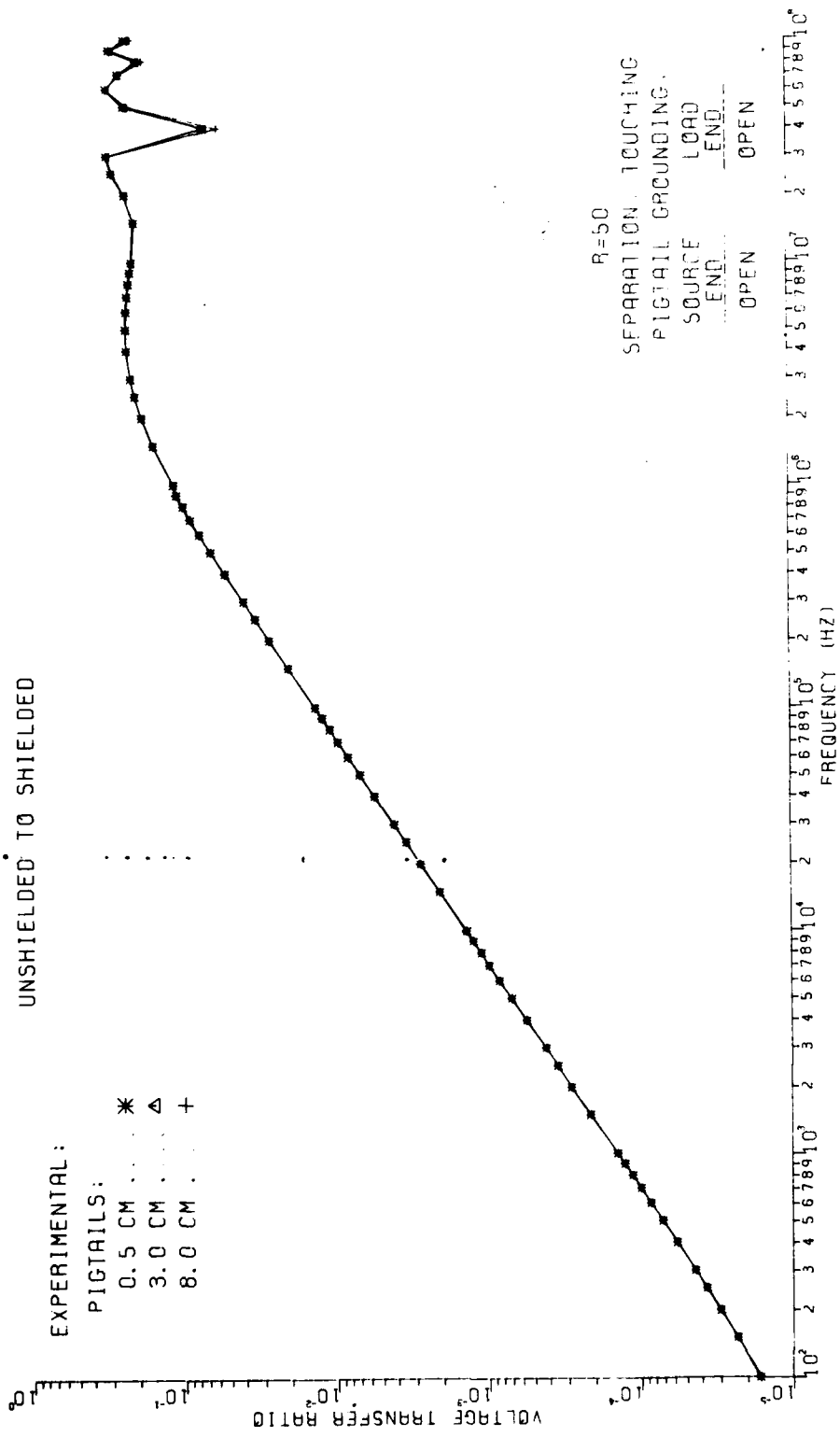
UNSHIELDED TO SHIELDED
EXPERIMENTAL:
PIGTAILS:
0.5 CM . . . *
3.0 CM . . . Δ
8.0 CM . . . +
R=50
SEPARATION, TOUCHING
PIGTAIL GROUNDING:
SOURCE END
LOAD END
OPEN
OPEN
VOLTAGE TRANSFER RATIO
FREQUENCY (HZ)

Figure A-4.

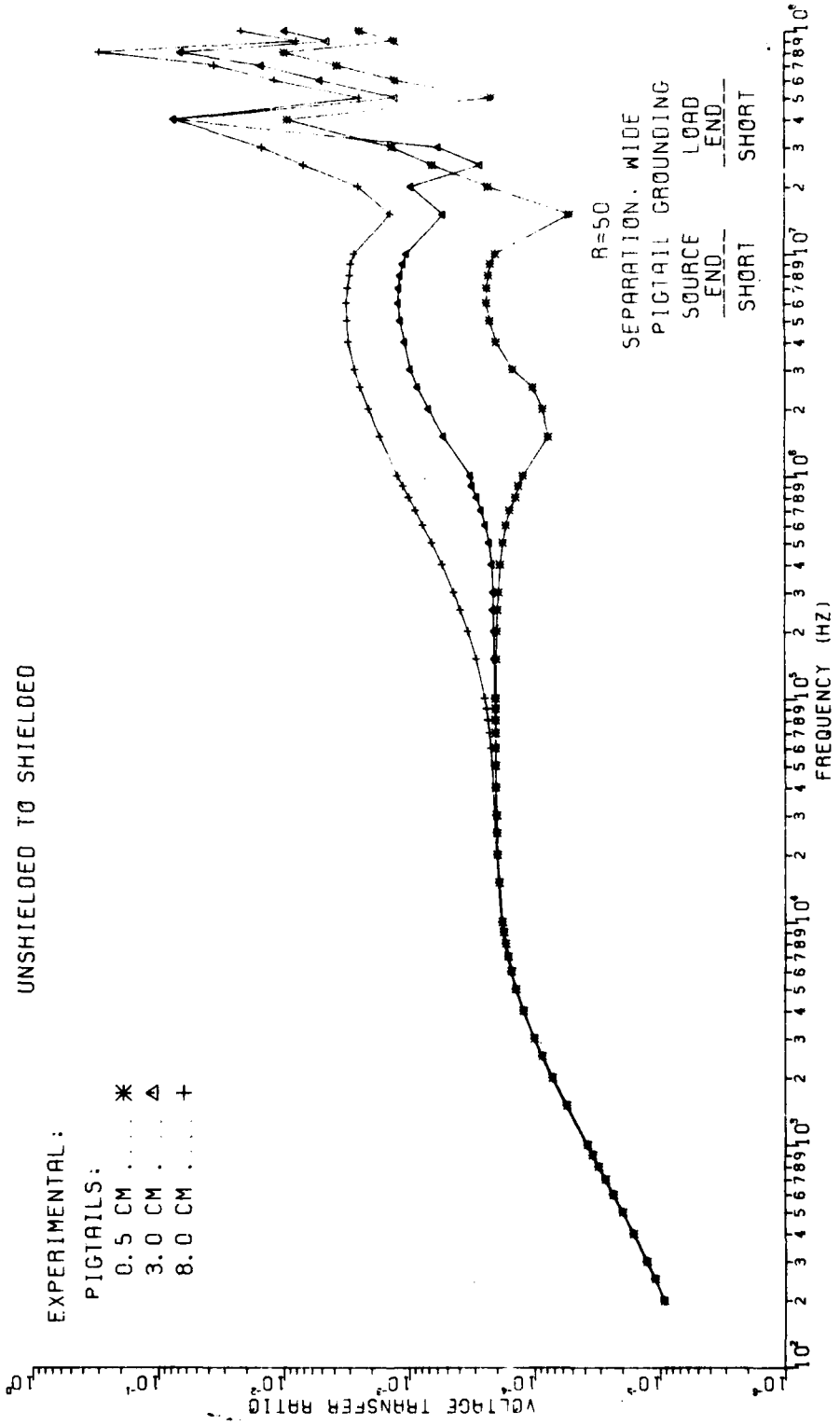
UNSHIELDED TO SHIELDED
EXPERIMENTAL:
PIGTAILS:
0.5 CM .....
3.0 CM .....
8.0 CM .....
SEPARATION. WIDE
PIGTAIL GROUNDING
SOURCE END
LOAD END
SHORT
SHORT
R=50
VOLTAGE TRANSFER RATIO
FREQUENCY (HZ)

Figure A-5.

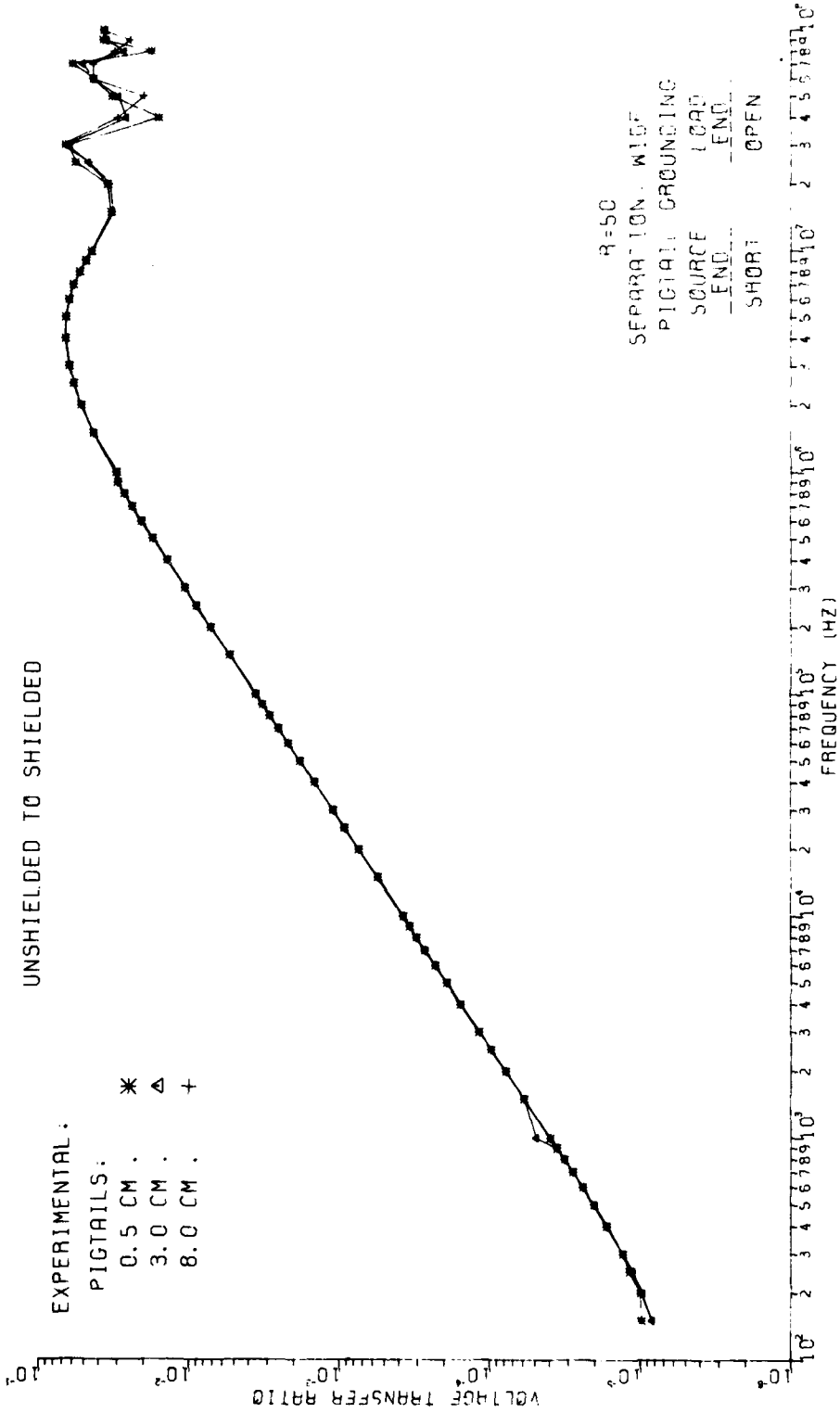
UNSHIELDED TO SHIELDED
EXPERIMENTAL:
PIGTAILS:
0.5 CM. ✱
3.0 CM. △
8.0 CM. +
R=50
SEPARATION WIDE
PIGTAIL GROUNDING
SOURCE END
LOAD END
SHORT
OPEN
VOLTAGE TRANSFER RATIO
FREQUENCY (HZ)

Figure A-6.

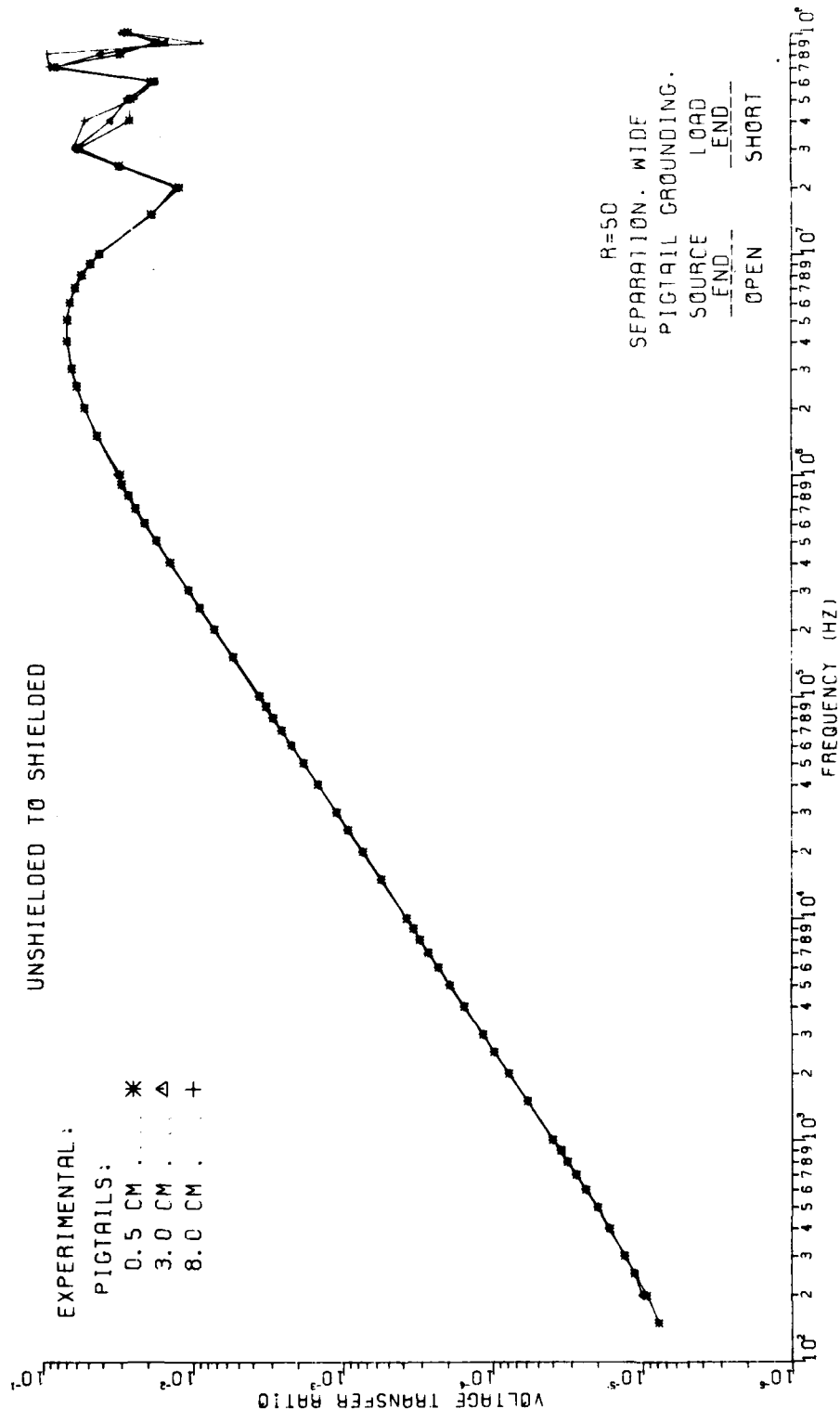
UNSHIELDED TO SHIELDED
EXPERIMENTAL:
PIGTAILS:
0.5 CM . . . . *
3.0 CM . . . Δ
8.0 CM . . . +
R=50
SEPARATION. WIDE
PIGTAIL GROUNDING.
SOURCE END
LOAD END
OPEN
SHORT
VOLTAGE TRANSFER RATIO
FREQUENCY (HZ)

Figure A-7.

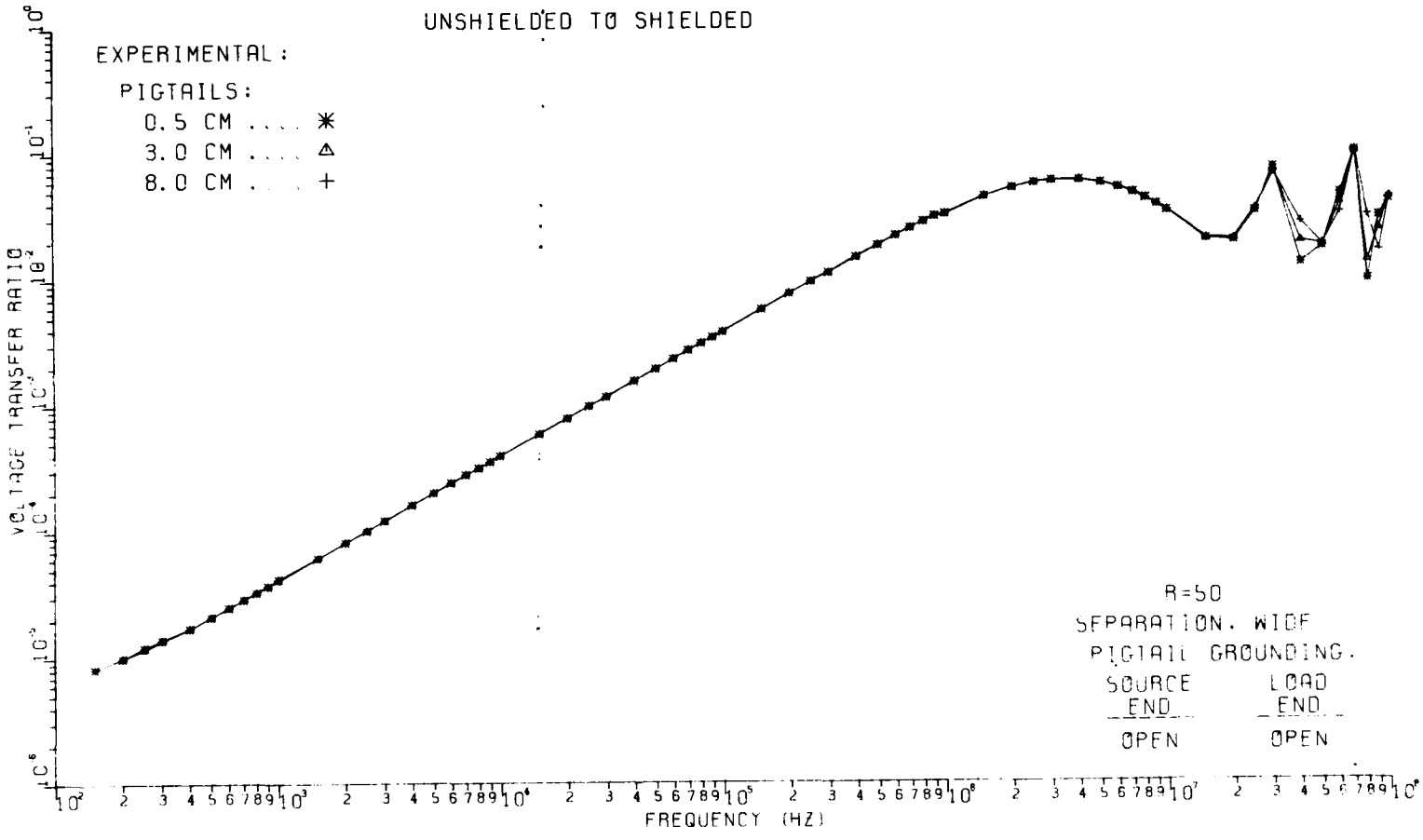
UNSHIELDED TO SHIELDED
EXPERIMENTAL:
PIGTAILS:
0.5 CM .... *
3.0 CM .... Δ
8.0 CM .... +
VOLTAGE TRANSFER RATIO
FREQUENCY (HZ)
R=50
SEPARATION. WIDE
PIGTAIL GROUNDING.
SOURCE END
LOAD END
OPEN
OPEN

Figure A-8.

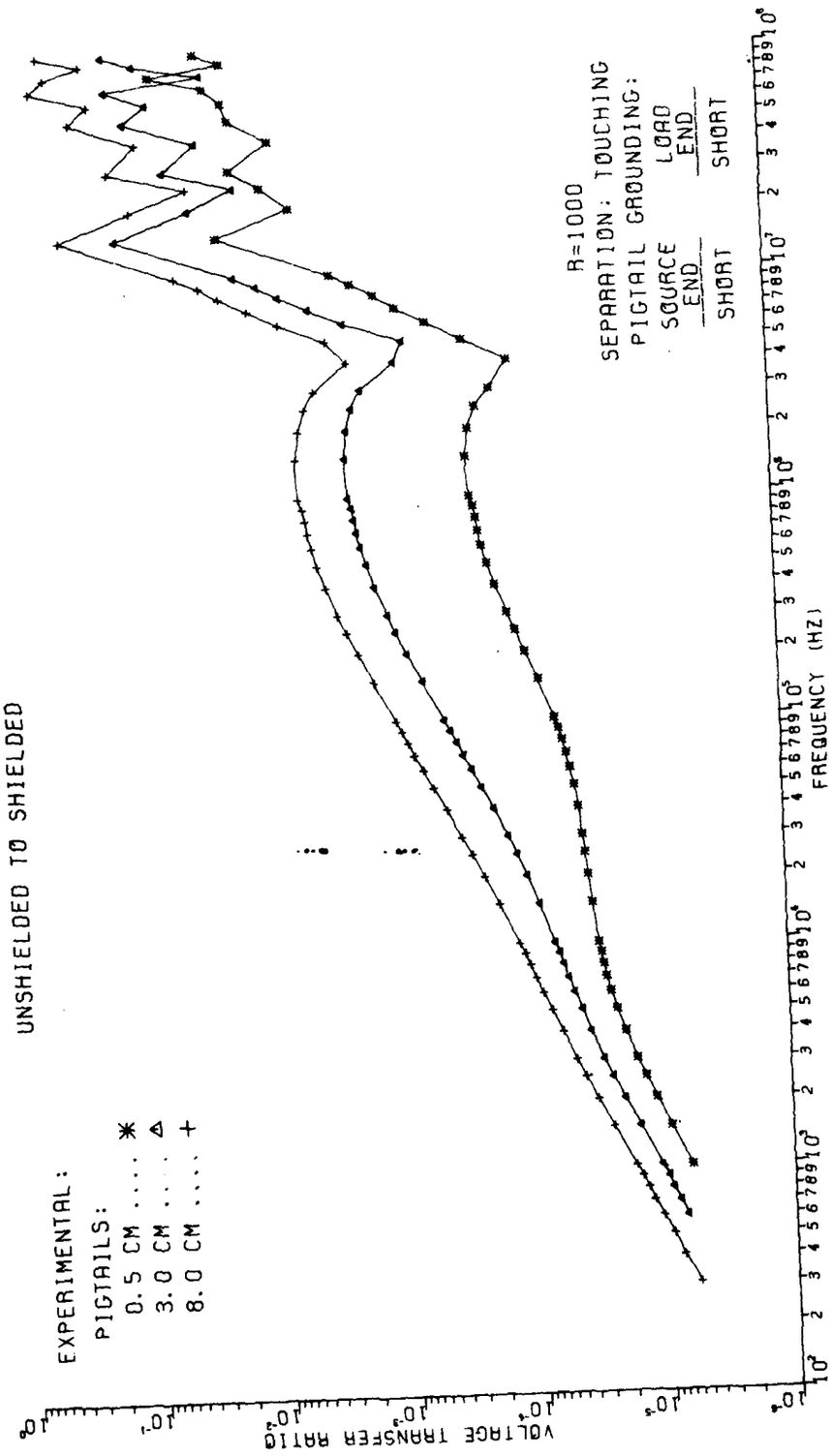
UNSHIELDED TO SHIELDED
EXPERIMENTAL:
PIGTAILS:
0.5 CM ..... *
3.0 CM ..... Δ
8.0 CM ..... +
R=1000
SEPARATION: TOUCHING
PIGTAIL GROUNDING:
SOURCE END
SHORT
LOAD END
SHORT
VOLTAGE TRANSFER RATIO
FREQUENCY (HZ)

Figure A-9.

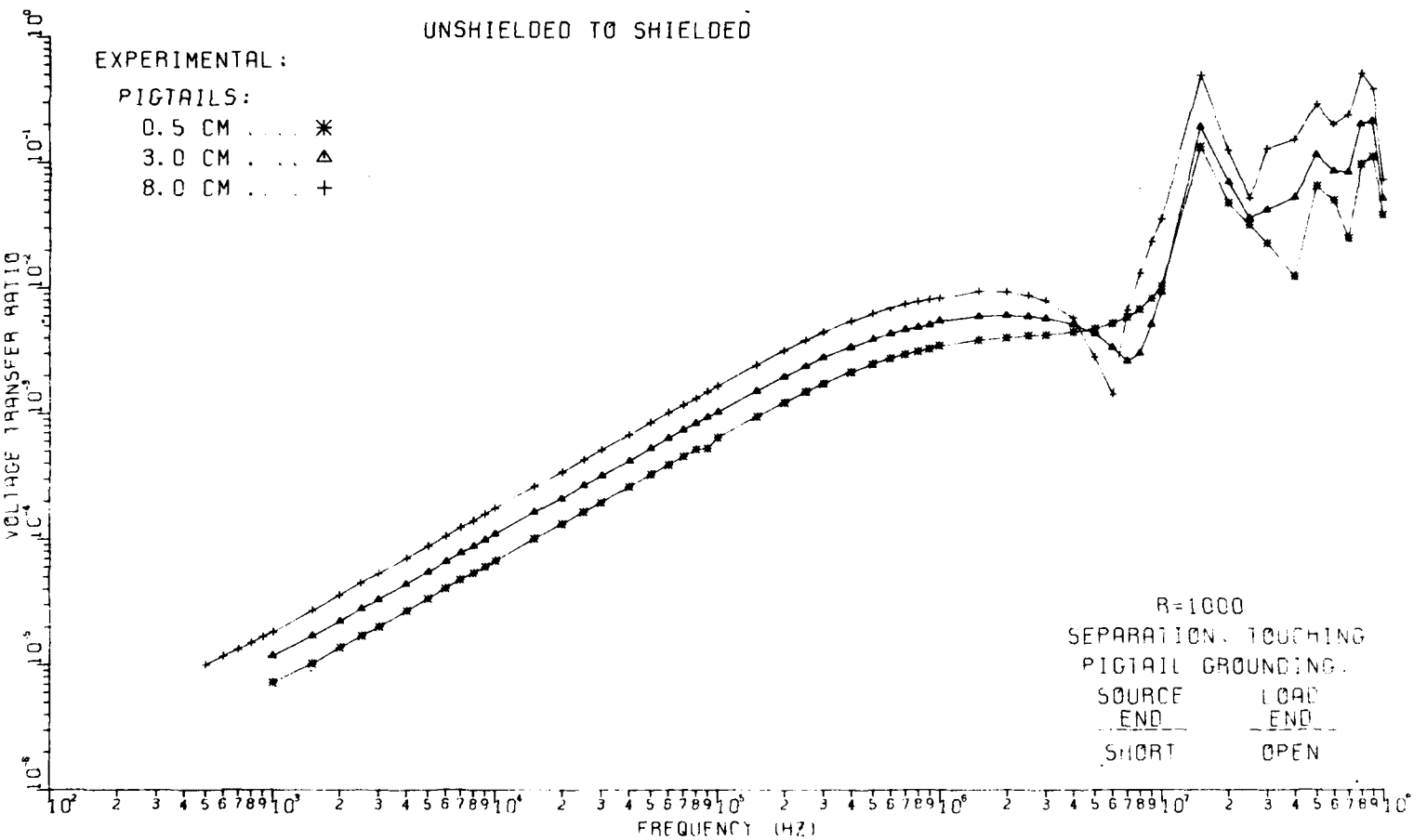
UNSHIELDED TO SHIELDED
EXPERIMENTAL:
PIGTAILS:
0.5 CM . . . ✳
3.0 CM . . . △
8.0 CM . . . +
VOLTAGE TRANSFER RATIO
FREQUENCY (HZ)
R=1000
SEPARATION, TOUCHING
PIGTAIL GROUNDING.
SOURCE END
SHORT
LOAD END
OPEN

Figure A-10.

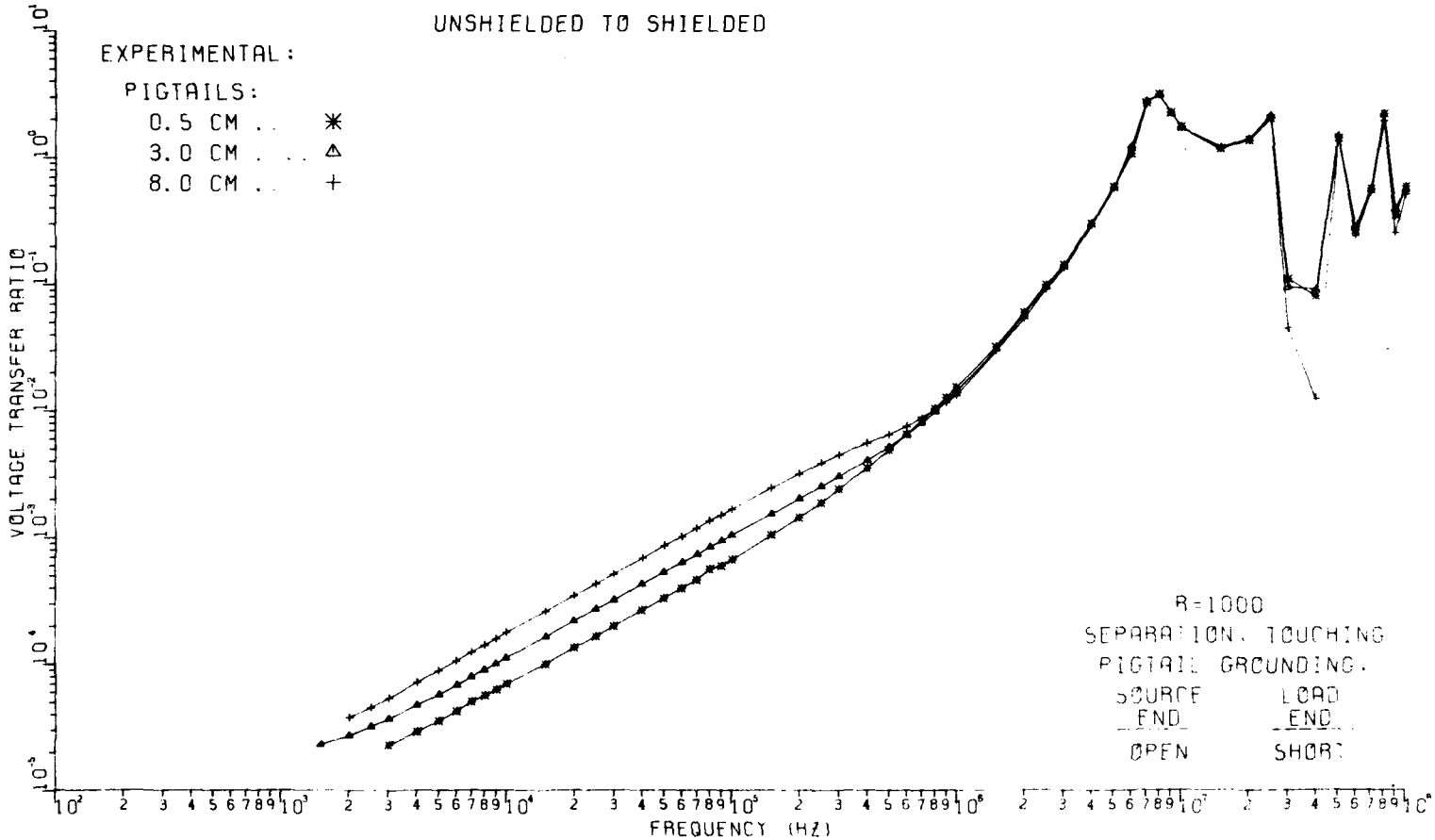
UNSHIELDED TO SHIELDED
EXPERIMENTAL:
PIGTAILS:
0.5 CM . .
3.0 CM . . .
8.0 CM . .
VOLTAGE TRANSFER RATIO
FREQUENCY (HZ)
R=1000
SEPARATION, TOUCHING
PIGTAIL GROUNDING.
SOURCE END
LOAD END
OPEN
SHORT

Figure A-11.

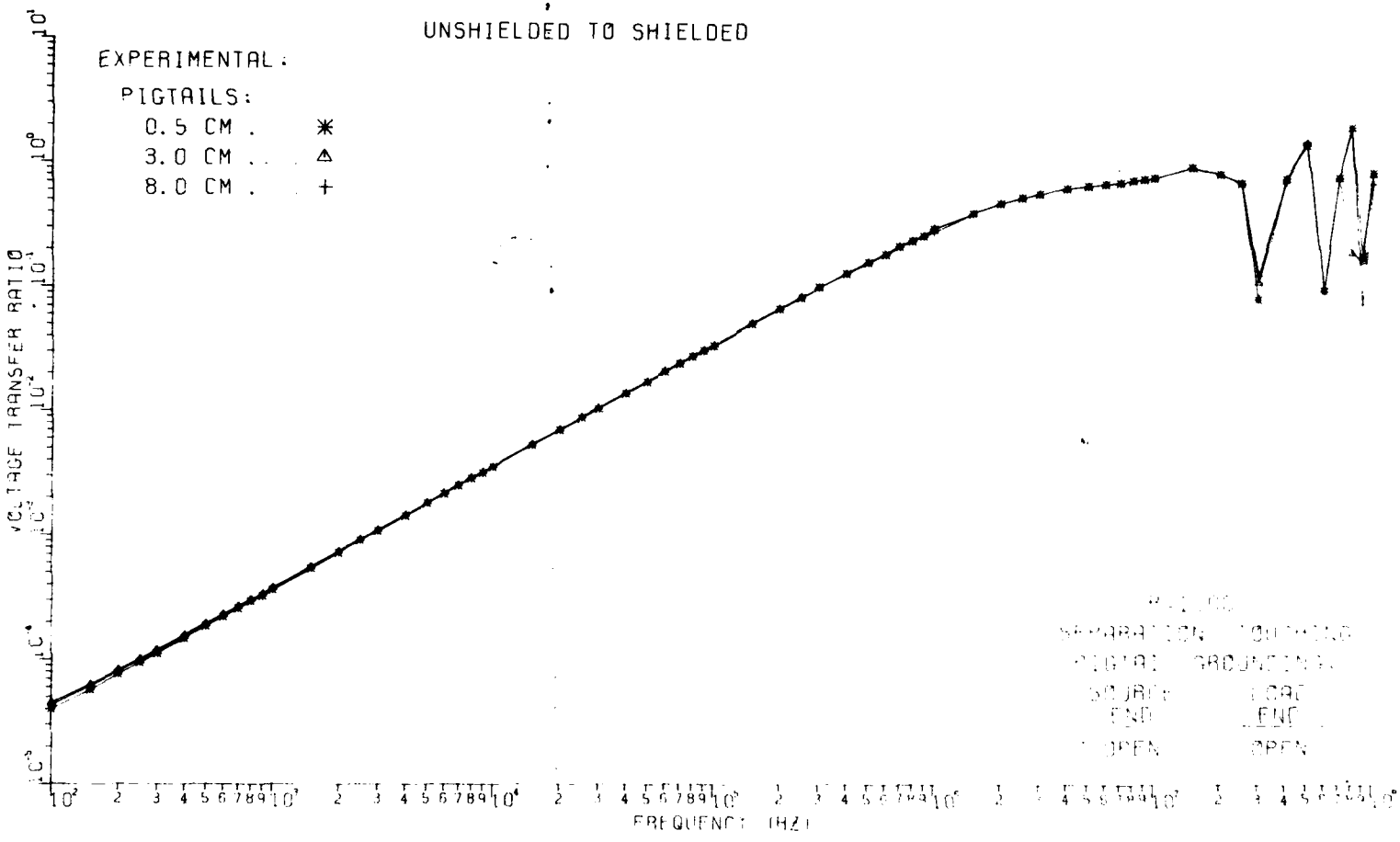
UNSHIELDED TO SHIELDED
EXPERIMENTAL:
PIGTAILS:
0.5 CM .
3.0 CM . . .
8.0 CM .
VOLTAGE TRANSFER RATIO
FREQUENCY (HZ)

Figure A-12.

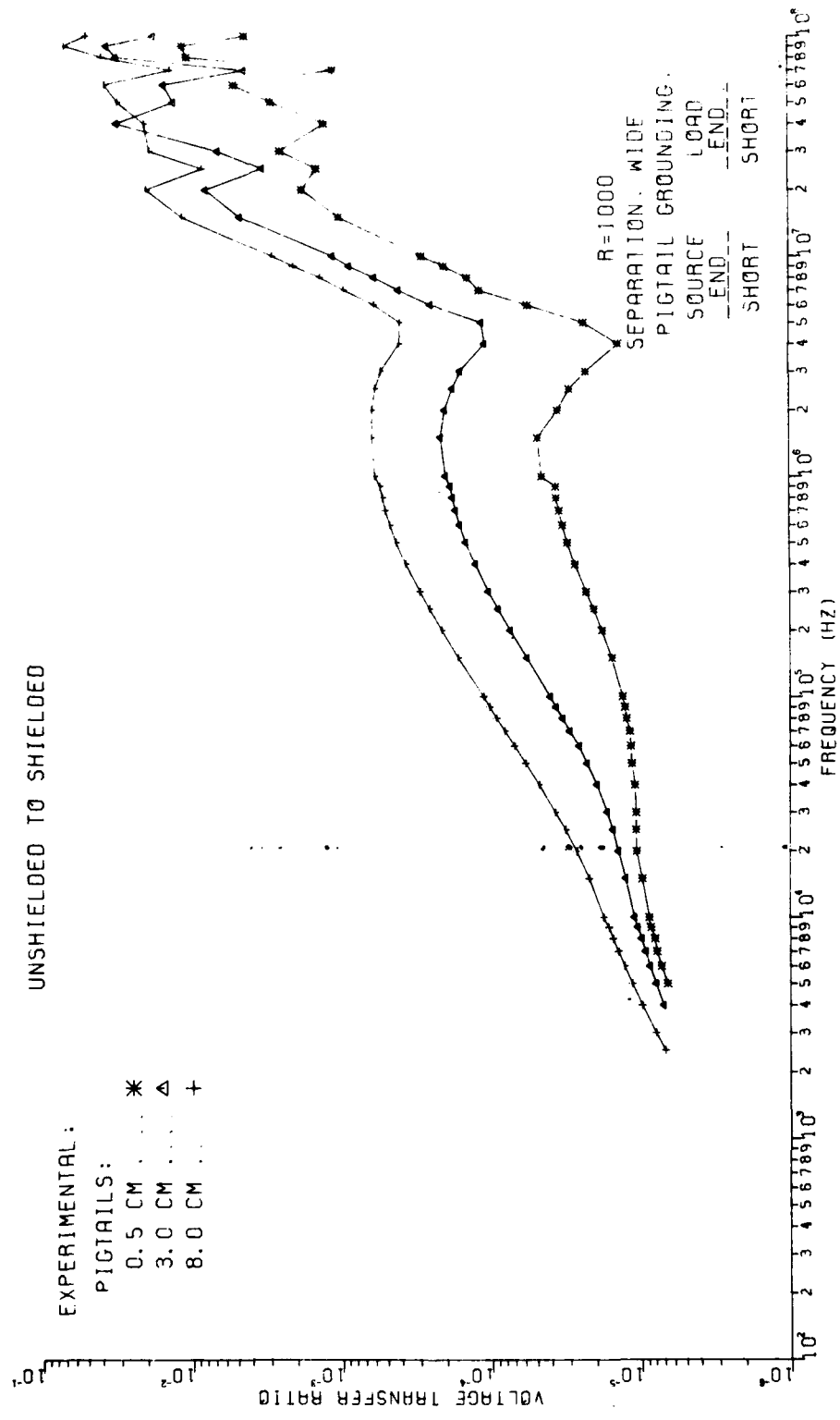
UNSHIELDED TO SHIELDED
EXPERIMENTAL:
PIGTAILS:
0.5 CM . . . *
3.0 CM . . . Δ
8.0 CM . . . +
R=1000
SEPARATION. WIDE
PIGTAIL GROUNDING.
SOURCE END
LOAD END
SHORT
SHORT
VOLTAGE TRANSFER RATIO
FREQUENCY (HZ)

Figure A-13.

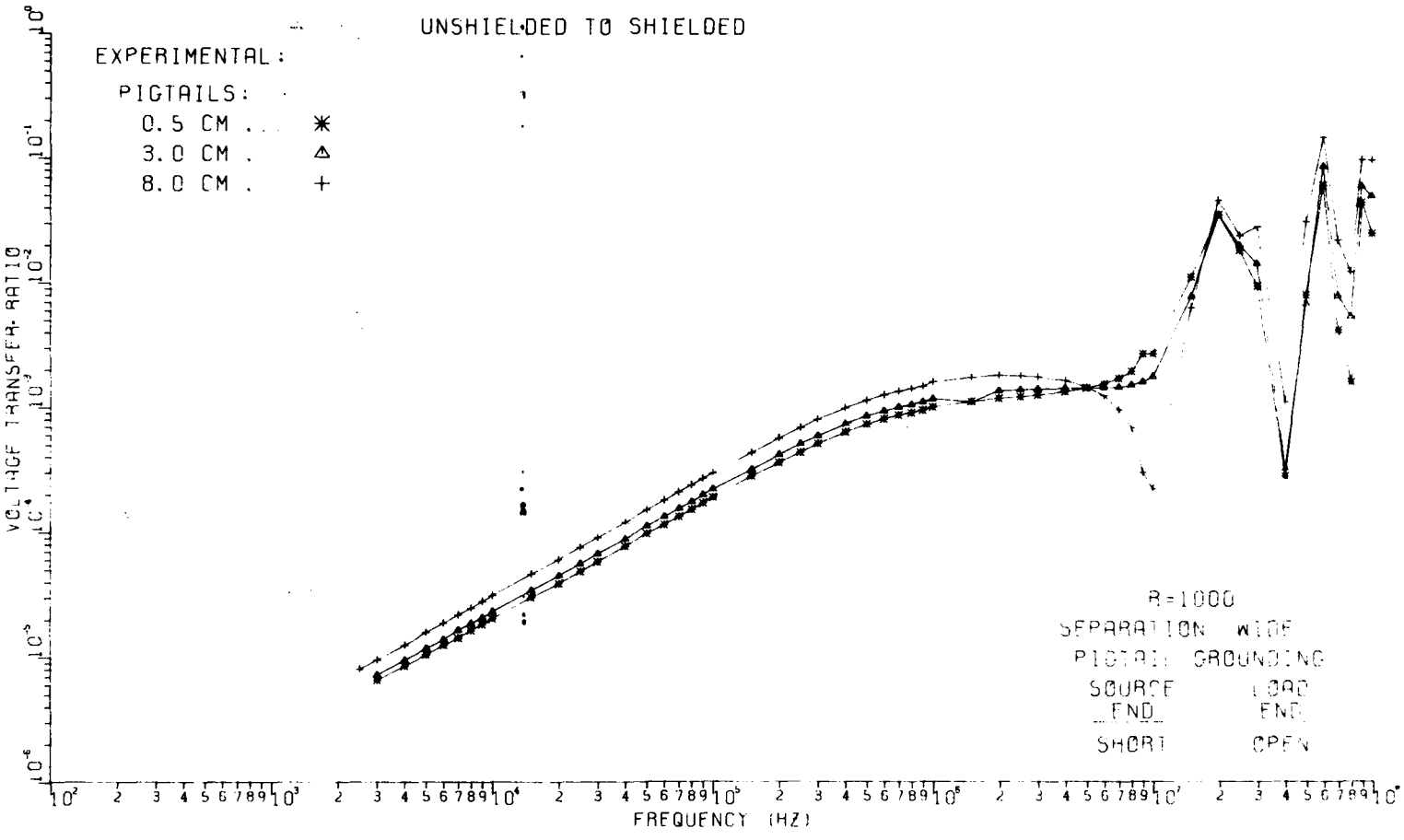
UNSHIELDED TO SHIELDED
EXPERIMENTAL:
PIGTAILS:
0.5 CM . . . *
3.0 CM . Δ
8.0 CM . +
VOLTAGE TRANSFER RATIO
FREQUENCY (HZ)
R=1000
SEPARATION WIDE
PIGTAIL GROUNDING
SOURCE END SHORT
LOAD END OPEN

Figure A-14.

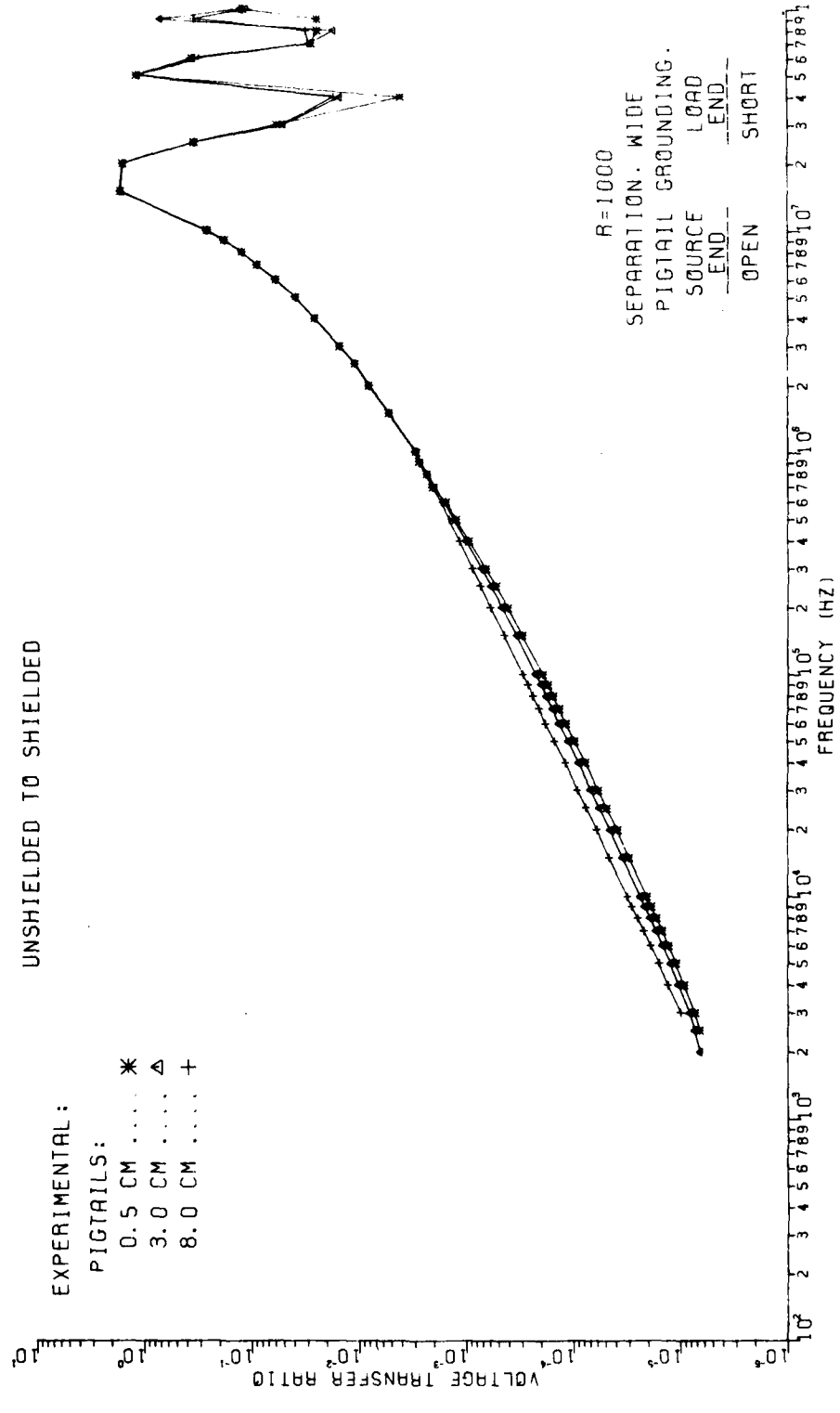
UNSHIELDED TO SHIELDED
EXPERIMENTAL:
PIGTAILS:
0.5 CM .... ✳
3.0 CM .... △
8.0 CM .... +
R=1000
SEPARATION. WIDE
PIGTAIL GROUNDING.
SOURCE LOAD
END END
OPEN SHORT
VOLTAGE TRANSFER RATIO
FREQUENCY (HZ)

Figure A-15.

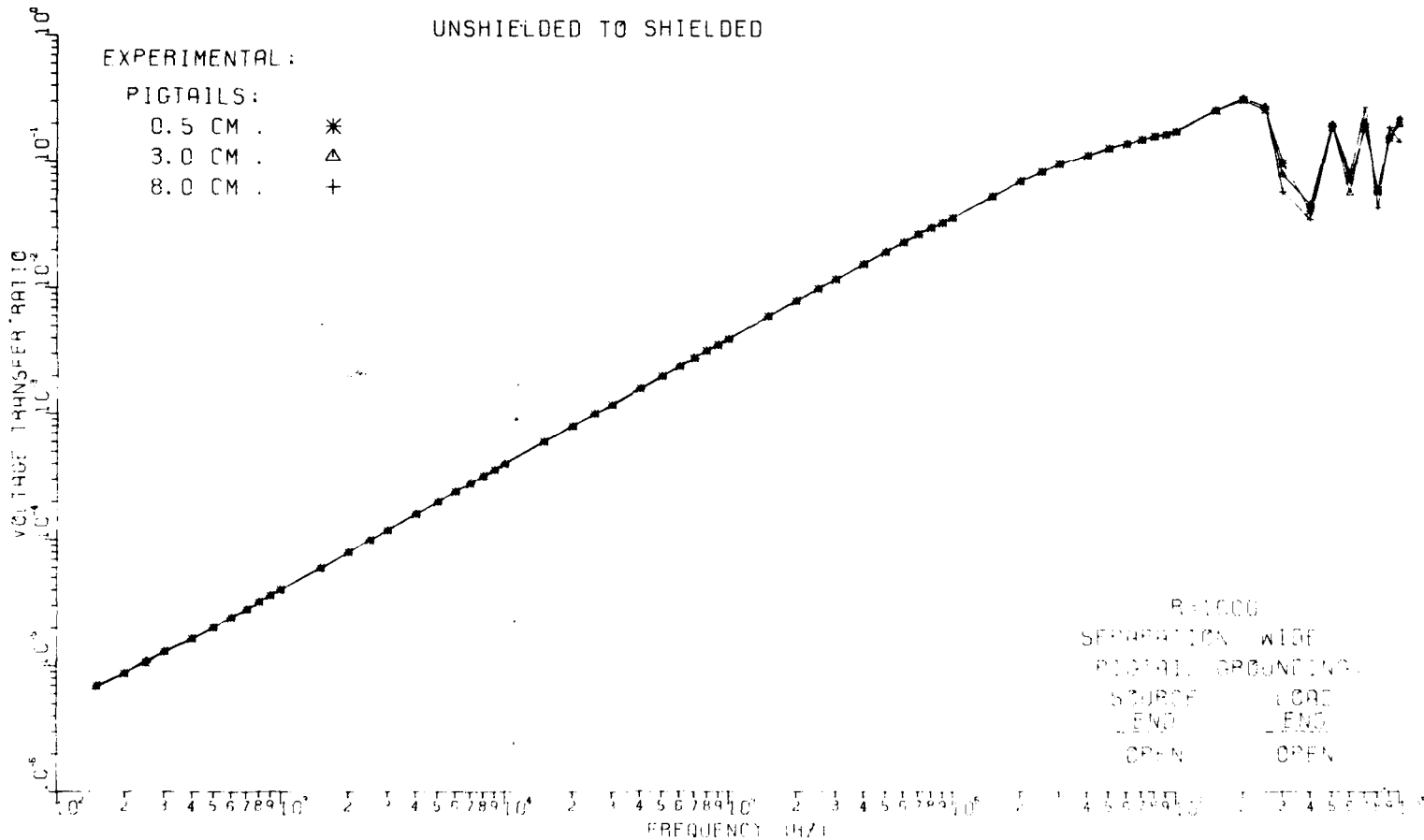
UNSHIELDED TO SHIELDED
EXPERIMENTAL:
PIGTAILS:
0.5 CM . ✳
3.0 CM . △
8.0 CM . +
VOLTAGE TRANSFER RATIO
FREQUENCY (HZ)

Figure A-16.

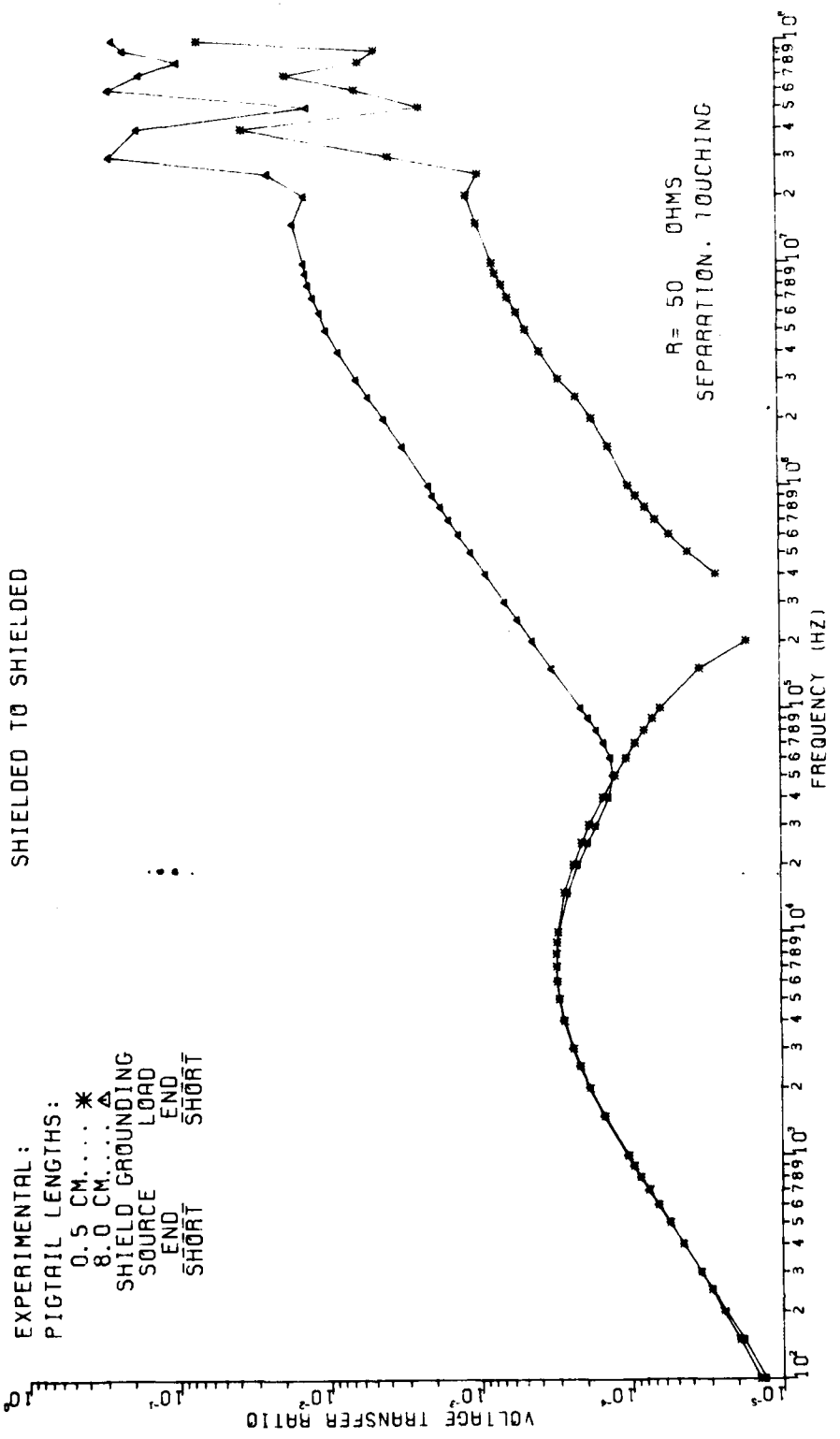
SHIELDED TO SHIELDED
EXPERIMENTAL:
PIGTAIL LENGTHS:
0.5 CM. . . . ✱
8.0 CM. . . . △
SHIELD GROUNDING
SOURCE END
SHORT
LOAD END
SHORT
R= 50 OHMS
SEPARATION. TOUCHING
VOLTAGE TRANSFER RATIO
FREQUENCY (HZ)

Figure A-17.

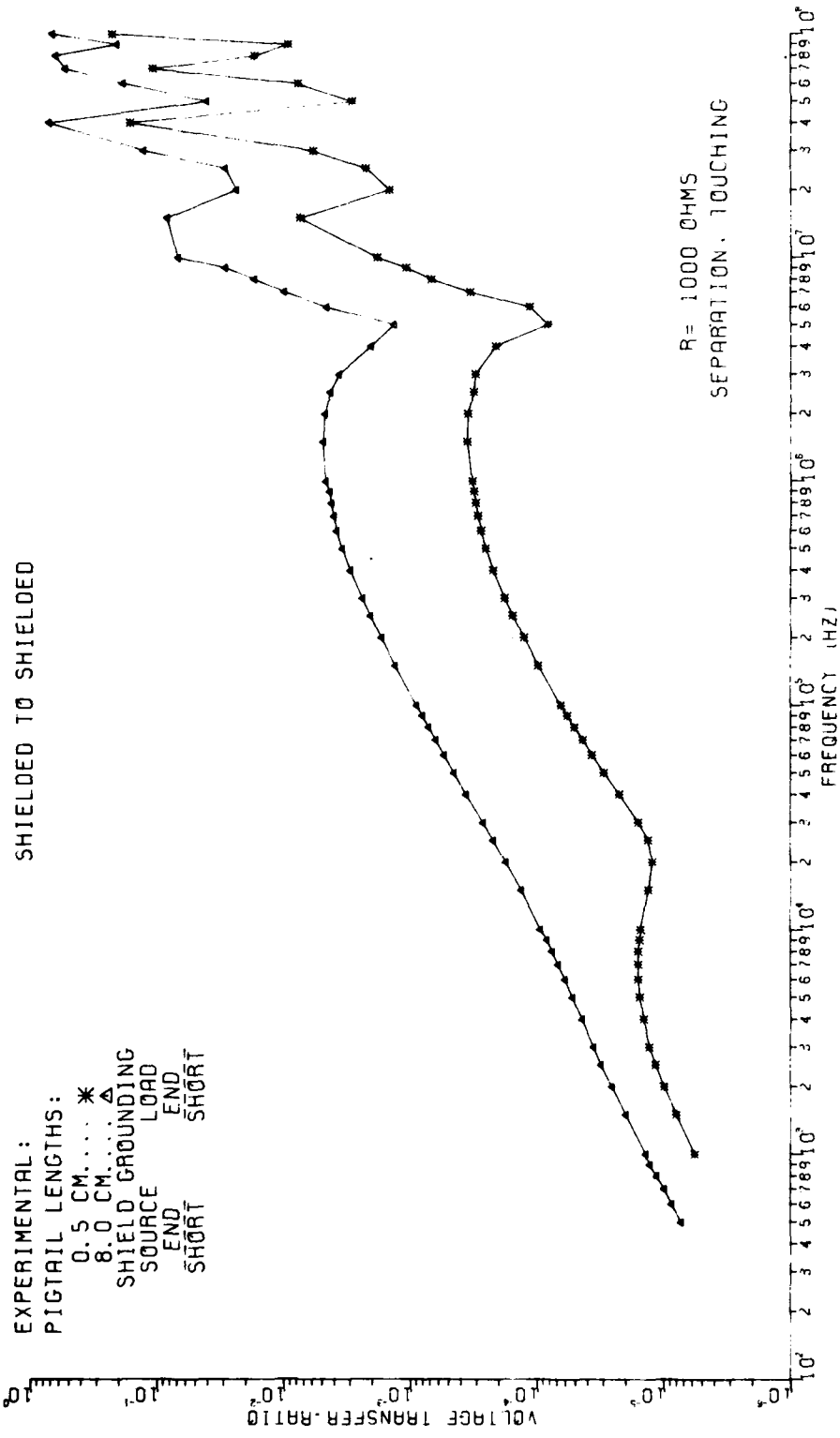
SHIELDED TO SHIELDED
EXPERIMENTAL:
PIGTAIL LENGTHS:
0.5 CM.... *
8.0 CM.... Δ
SHIELD GROUNDING
SOURCE LOAD
END END
SHORT SHORT
R= 1000 OHMS
SEPARATION. TOUCHING
VOLTAGE TRANSFER RATIO
FREQUENCY (HZ)

Figure A-18.

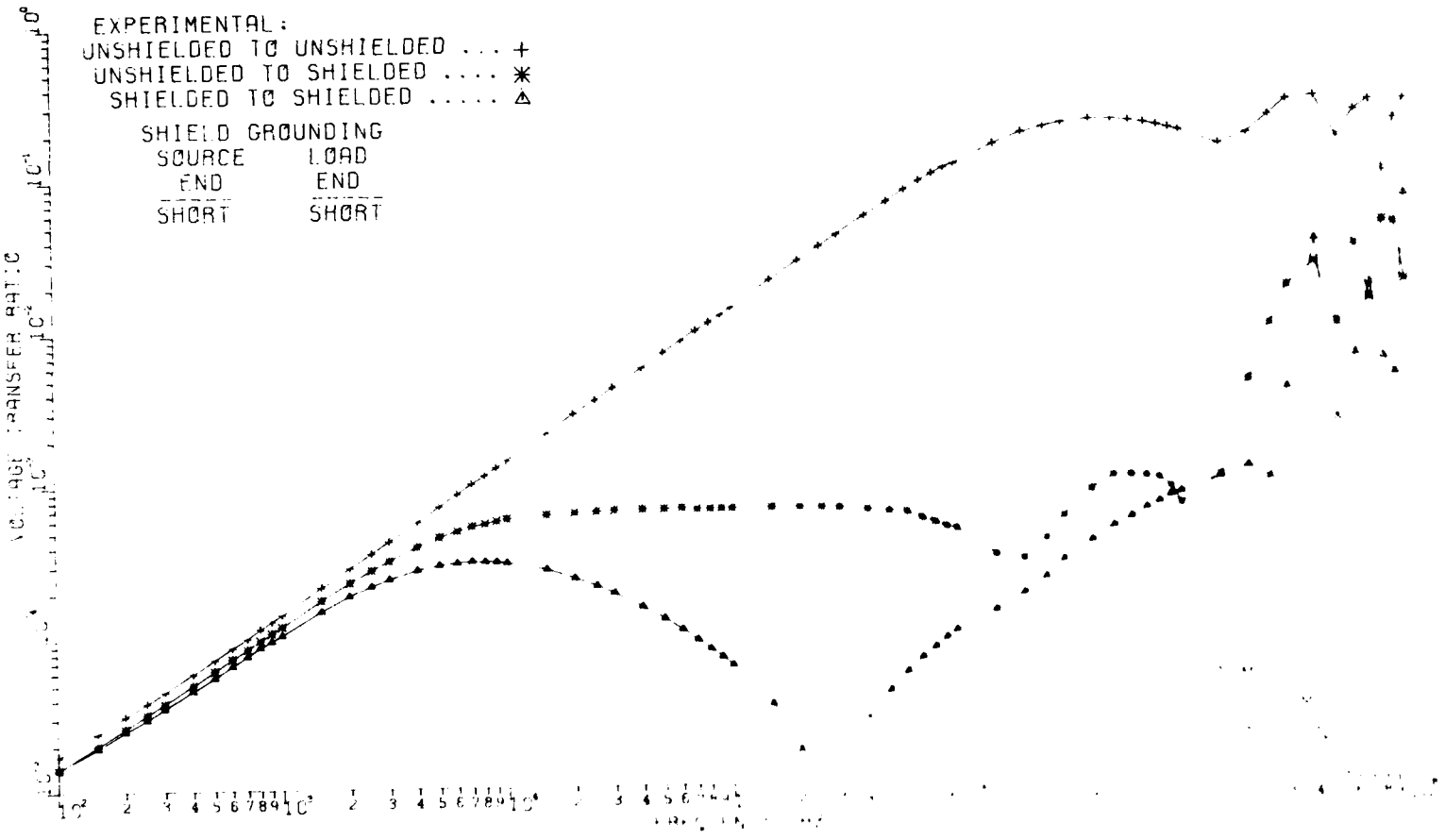
EXPERIMENTAL:
UNSHIELDED TO UNSHIELDED ... +
UNSHIELDED TO SHIELDED .... ✳
SHIELDED TO SHIELDED ..... △
SHIELD GROUNDING
SOURCE END
SHORT
LOAD END
SHORT

Figure A-19.

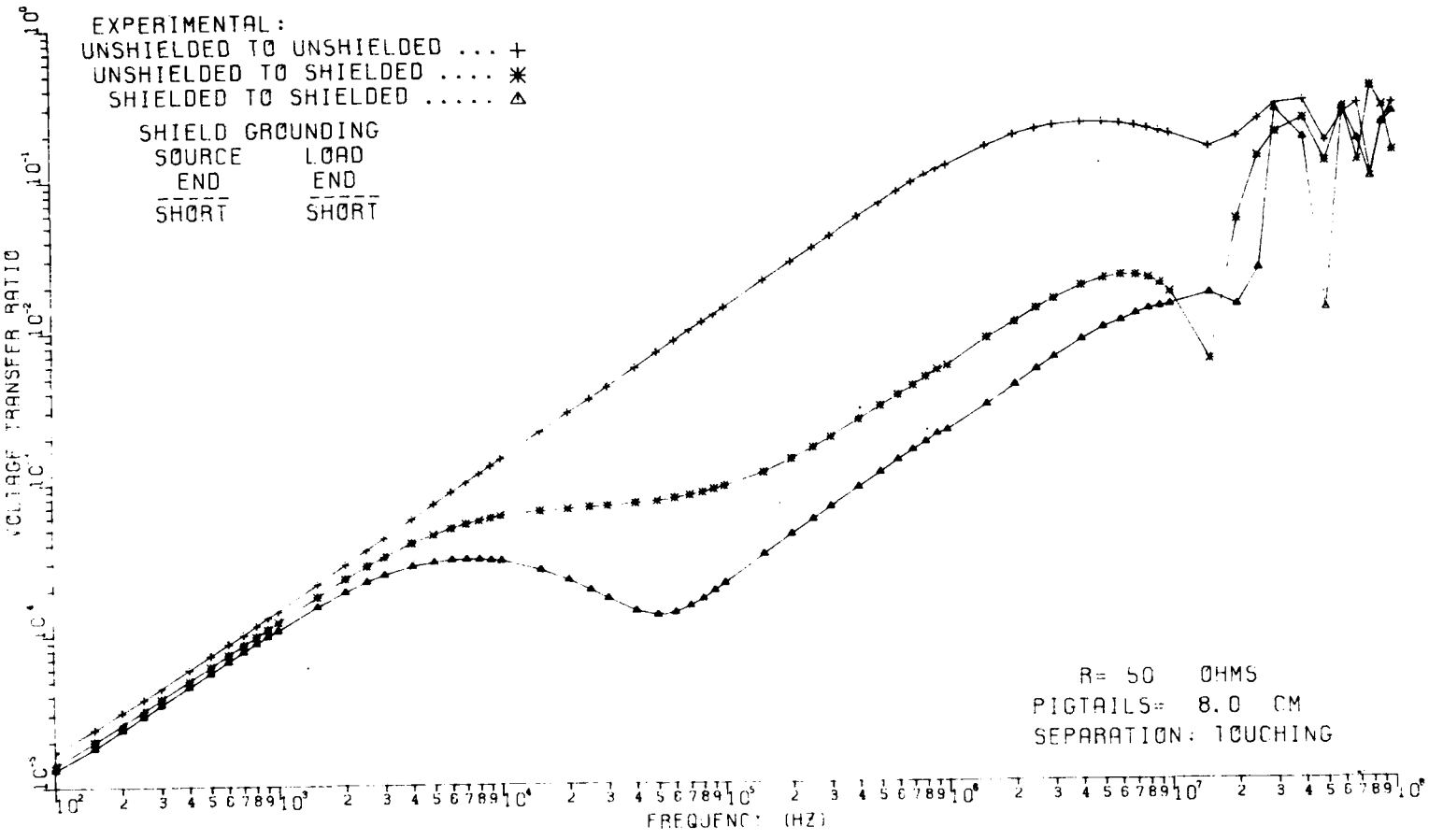
EXPERIMENTAL:
UNSHIELDED TO UNSHIELDED ... +
UNSHIELDED TO SHIELDED .... *
SHIELDED TO SHIELDED ..... Δ
SHIELD GROUNDING
SOURCE END
SHORT
LOAD END
SHORT
R= 50 OHMS
PIGTAILS= 8.0 CM
SEPARATION: TOUCHING
FREQUENCY (HZ)

Figure A-20.

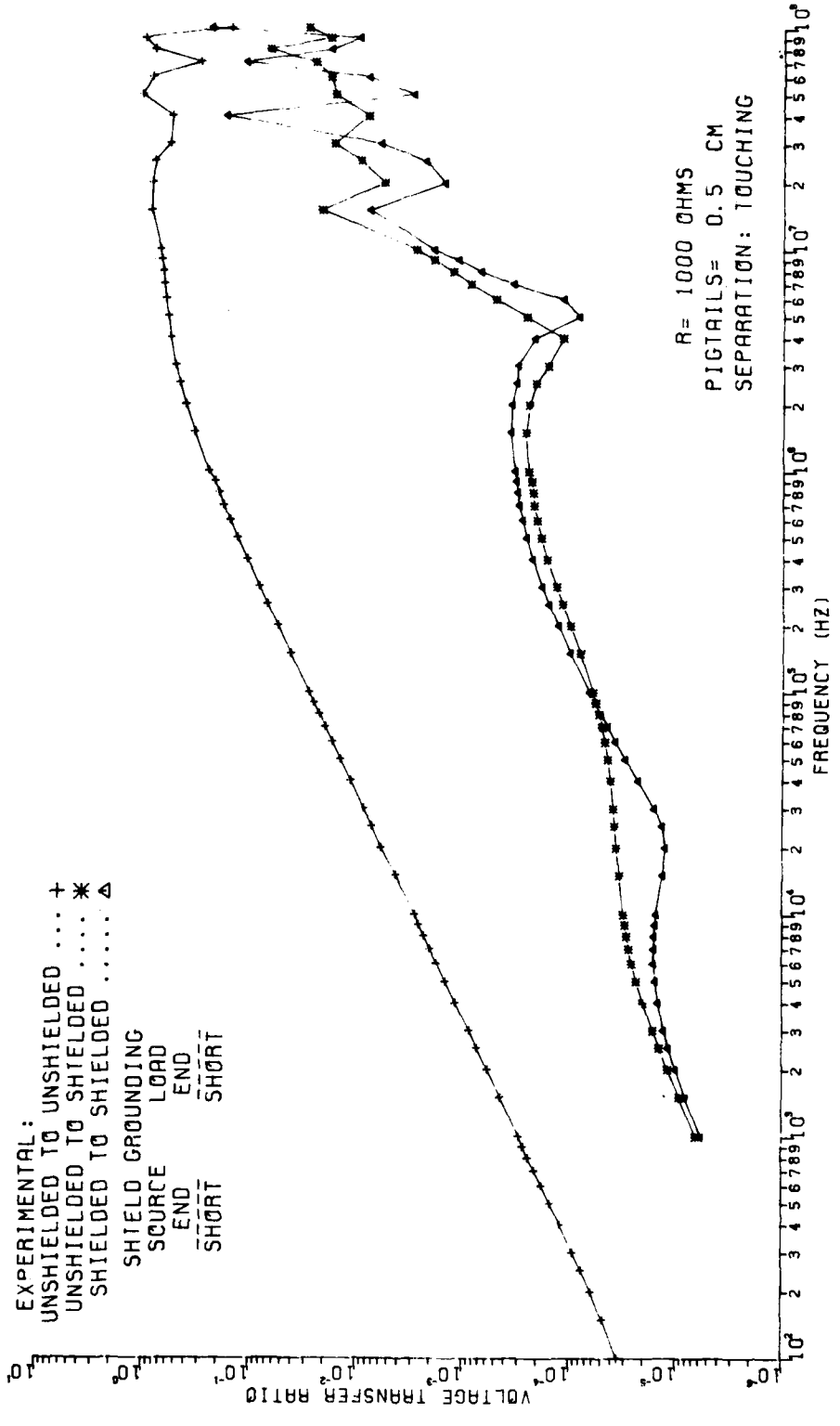
EXPERIMENTAL:
UNSHIELDED TO UNSHIELDED .... +
UNSHIELDED TO SHIELDED ..... *
SHIELDED TO SHIELDED ..... Δ
SHIELD GROUNDING
SOURCE LOAD
END END
SHORT SHORT
R= 1000 OHMS
PIGTAILS= 0.5 CM
SEPARATION: TOUCHING
VOLTAGE TRANSFER RATIO
FREQUENCY (HZ)

Figure A-21.

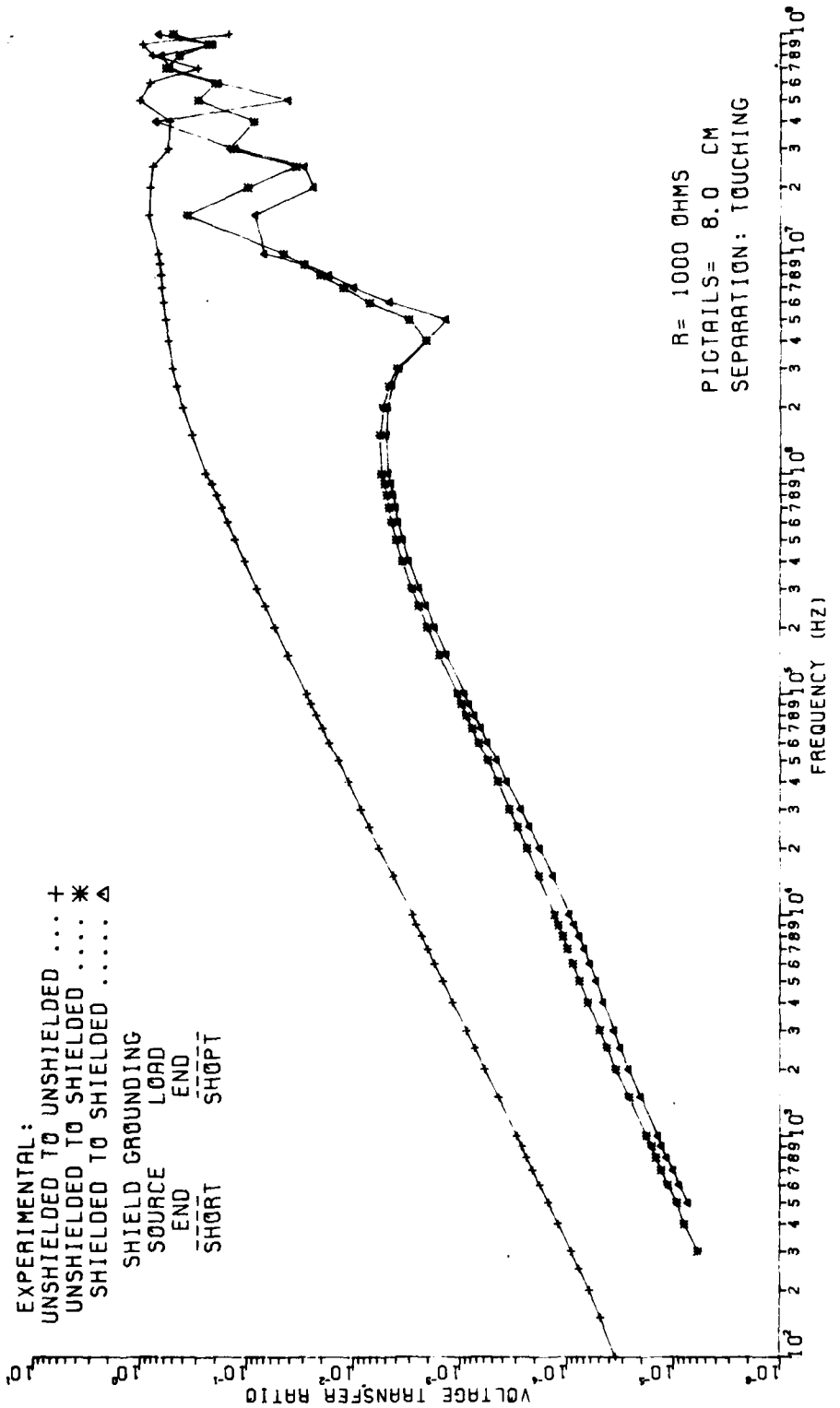
EXPERIMENTAL:
UNSHIELDED TØ UNSHIELDED ... +
UNSHIELDED TØ SHIELDED .... ✱
SHIELDED TØ SHIELDED ..... △
SHIELD GRØUNDING
SOURCE LØAD
END END
SHØRT SHØRT
R= 1000 ØHMS
PIGTAILS= 8.0 CM
SEPARATIØN: TØUCHING
VOLTAGE TRANSFER RATIO
FREQUENCY (HZ)

Figure A-22.

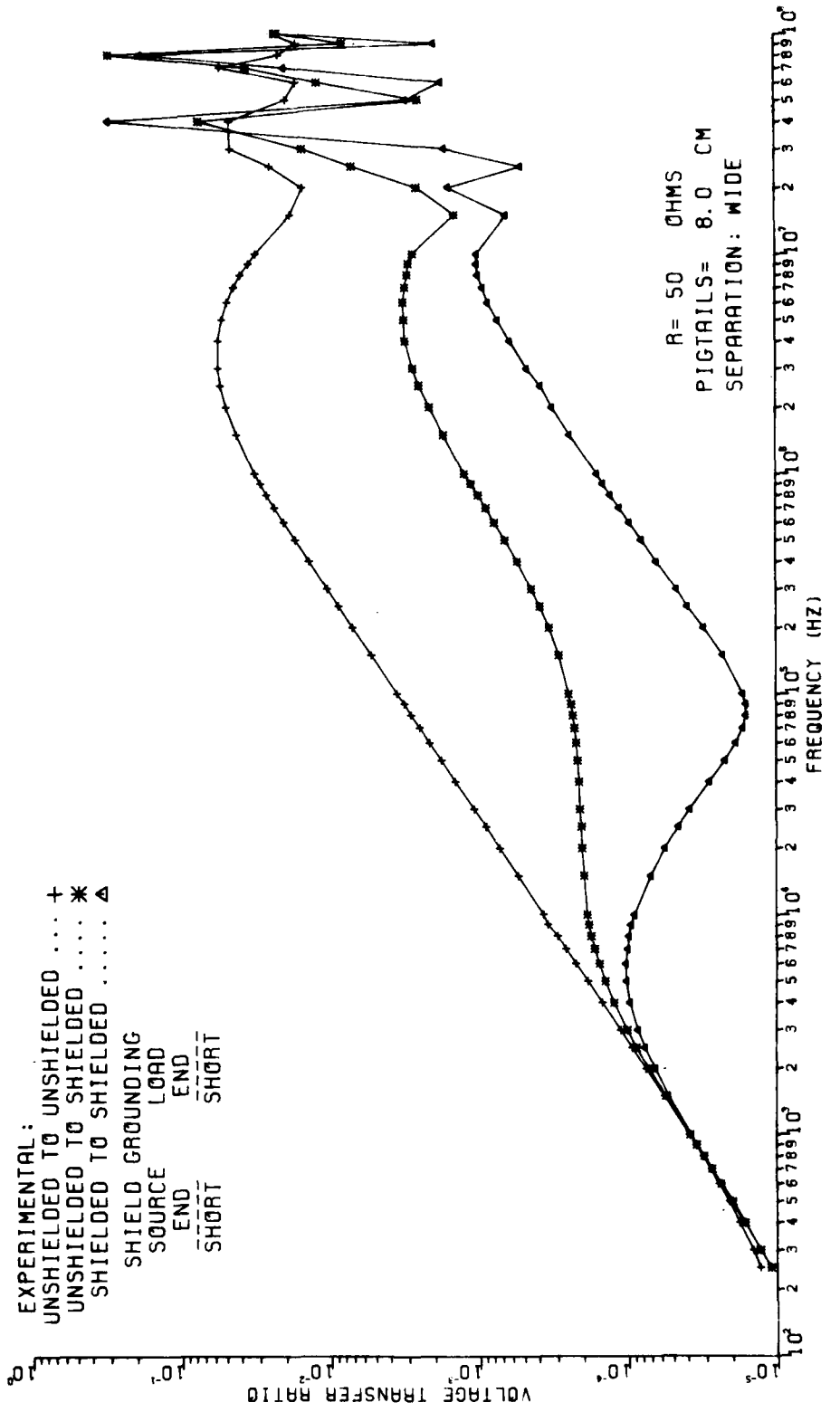
EXPERIMENTAL:
UNSHIELDED TØ UNSHIELDED .... +
UNSHIELDED TØ SHIELDED ..... ✱
SHIELDED TØ SHIELDED ..... ◁
SHIELD GROUNDING
SOURCE LØAD
END END
SHØRT SHØRT
R= 50 ØHMS
PIGTAILS= 8.0 CM
SEPARATION: WIDE
VOLTAGE TRANSFER RATIO
FREQUENCY (HZ)

Figure A-23

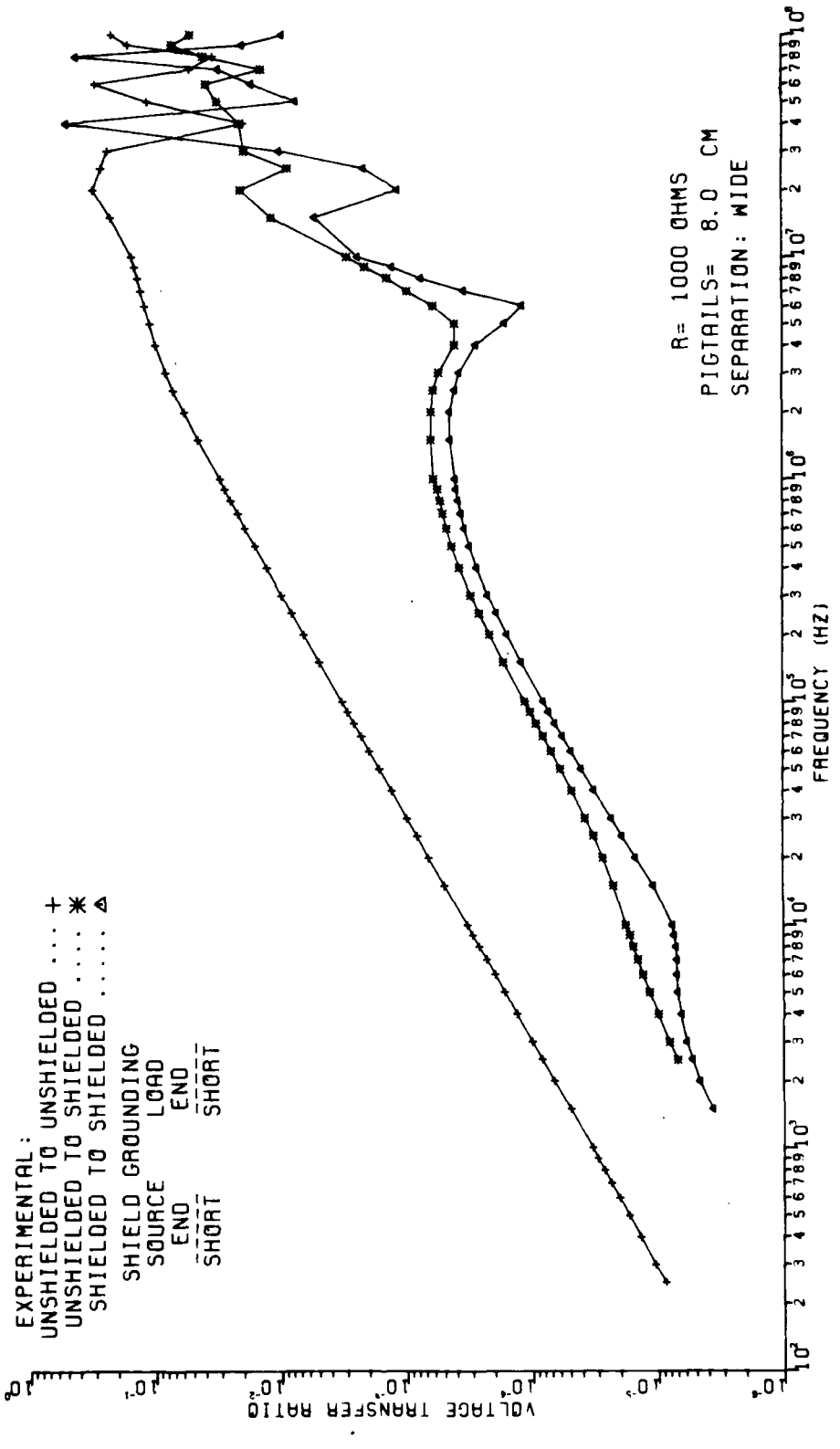
EXPERIMENTAL:
UNSHIELDED TO UNSHIELDED .... +
UNSHIELDED TO SHIELDED .... *
SHIELDED TO SHIELDED ..... Δ
SHIELD GROUNDING
SOURCE LOAD
END END
SHORT SHORT
R= 1000 OHMS
PIGTAILS= 8.0 CM
SEPARATION: WIDE
VOLTAGE TRANSFER RATIO
FREQUENCY (HZ)

Figure A-24

APPENDIX B

Fig.	Configuration	Ω	Separation	Grounding	Pigtails	Page
B-1	US,SU	50Ω	Wide	SS	0.5	140
B-2	"	"	"	OS	"	141
B-3	"	"	"	SO	"	142
B-4	"	"	"	OO	"	143
B-5	"	"	"	SS	8	144
B-6	"	"	"	OS	"	145
B-7	"	"	"	SO	"	146
B-8	"	"	"	OO	"	147
B-9	"	1kΩ	"	SS	0.5	148
B-10	"	"	"	OS	"	149
B-11	"	"	"	SO	"	150
B-12	"	"	"	OO	"	151
B-13	"	"	"	SS	8	152
B-14	"	"	"	OS	"	153
B-15	"	"	"	SO	"	154
B-16	"	"	"	OO	"	155

US = unshielded to shielded

SU = shielded to unshielded

O = open (shield ungrounded)

S = short (shield grounded)

First letter denotes source end of line and second letter denotes load end of line. For example, SO denotes that the shield is grounded at the source end and ungrounded at the load end.

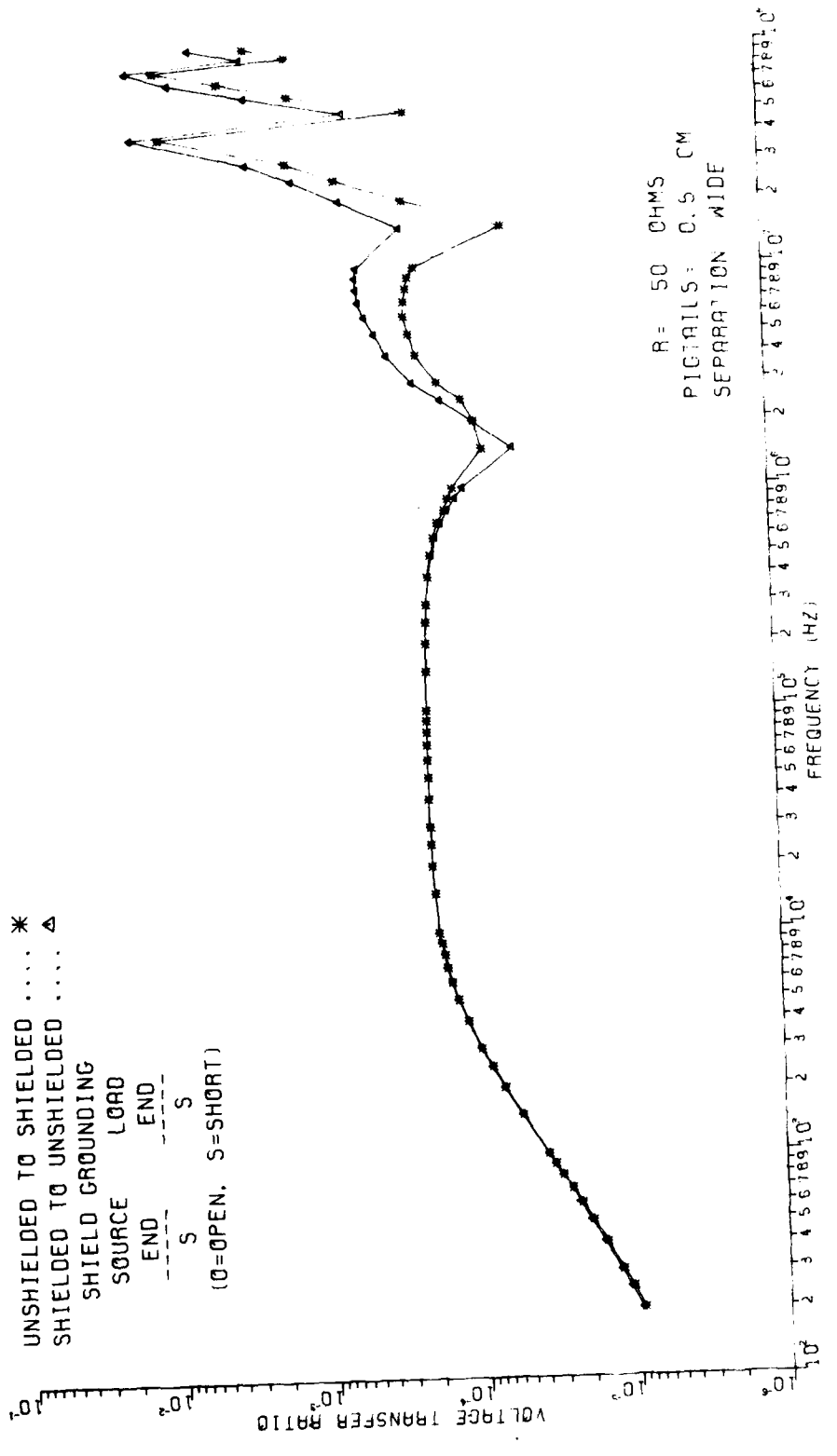
UNSHIELDED TO SHIELDED .... *
SHIELDED TO UNSHIELDED .... Δ
SHIELD GROUNDING
SOURCE LOAD
END END
S S
(0=OPEN, S=SHORT)
R= 50 OHMS
PIGTAILS: 0.5 CM
SEPARATION WIDE
VOLTAGE TRANSFER RATIO
FREQUENCY (HZ)

Figure B-1.

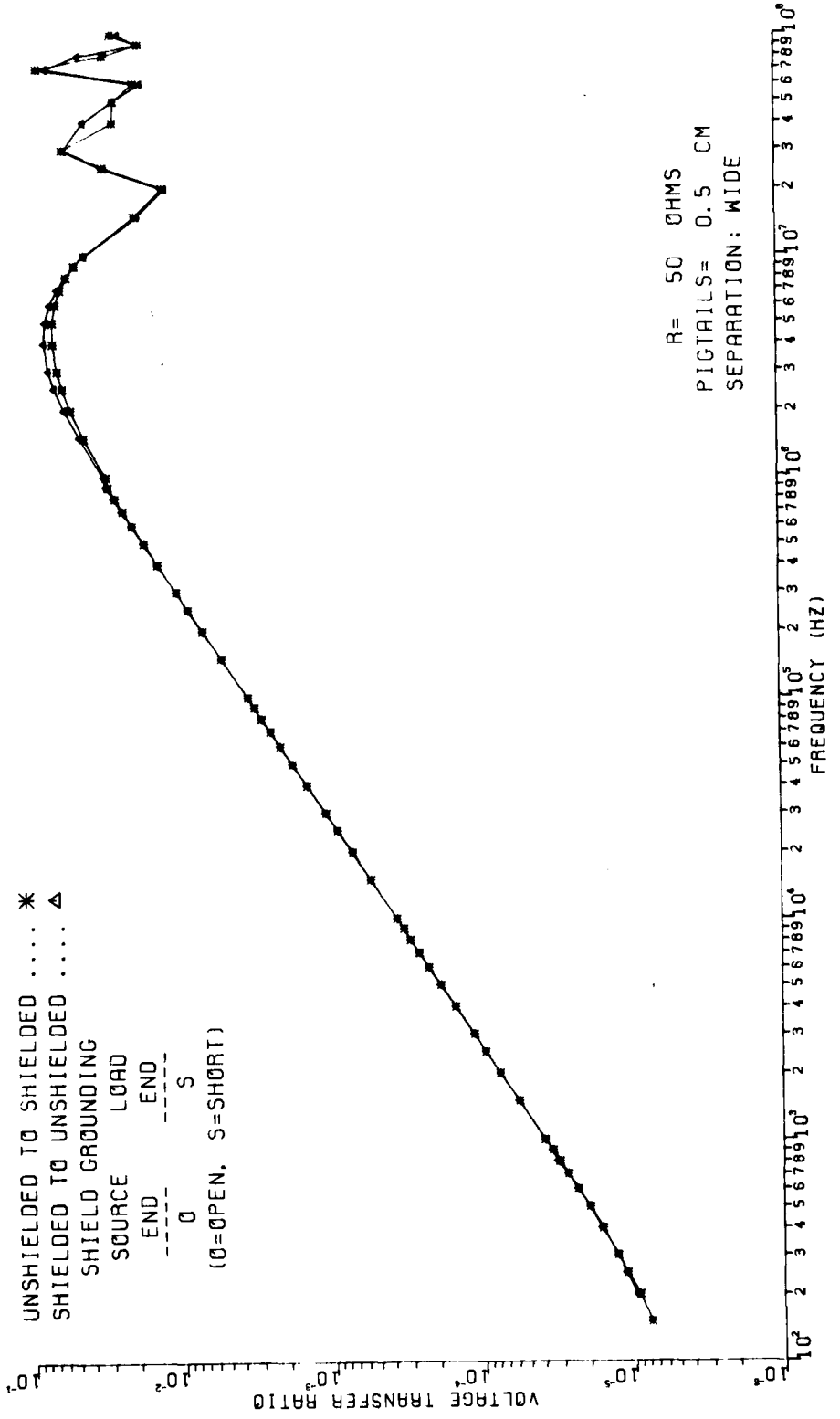
UNSHIELDED TO SHIELDED .... *
SHIELDED TO UNSHIELDED .... Δ
SHIELD GROUNDING
SOURCE LOAD
END END
0 S
(0=OPEN, S=SHORT)
R= 50 OHMS
PIGTAILS= 0.5 CM
SEPARATION: WIDE
VOLTAGE TRANSFER RATIO
FREQUENCY (HZ)

Figure B-2.

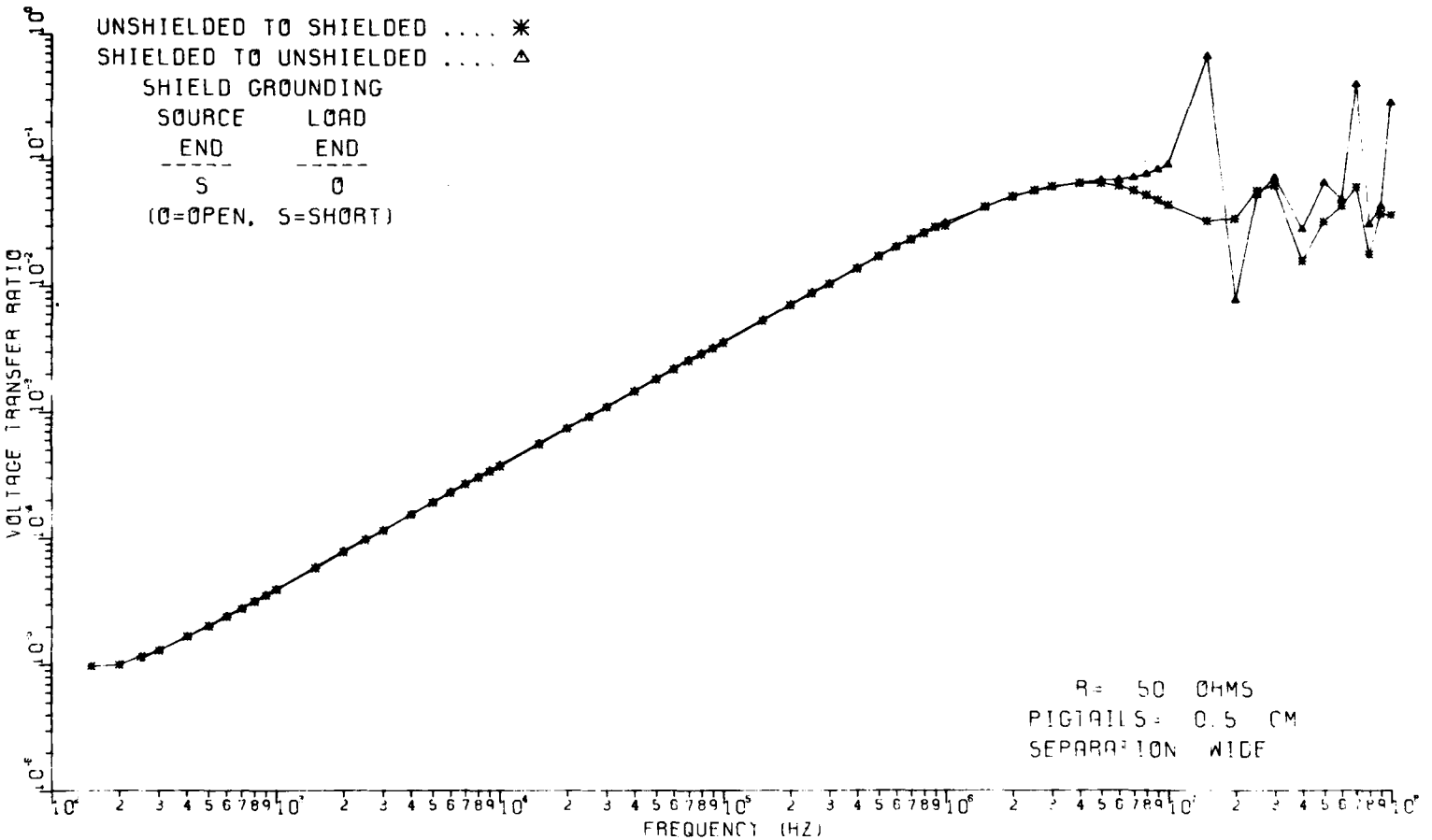
UNSHIELDED TO SHIELDED .... ✳
SHIELDED TO UNSHIELDED .... △
SHIELD GROUNDING
SOURCE END
LOAD END
S
0
(0=OPEN, S=SHORT)
VOLTAGE TRANSFER RATIO
FREQUENCY (HZ)
R= 50 OHMS
PIGTAILS= 0.5 CM
SEPARATION WIDE

Figure B-3.

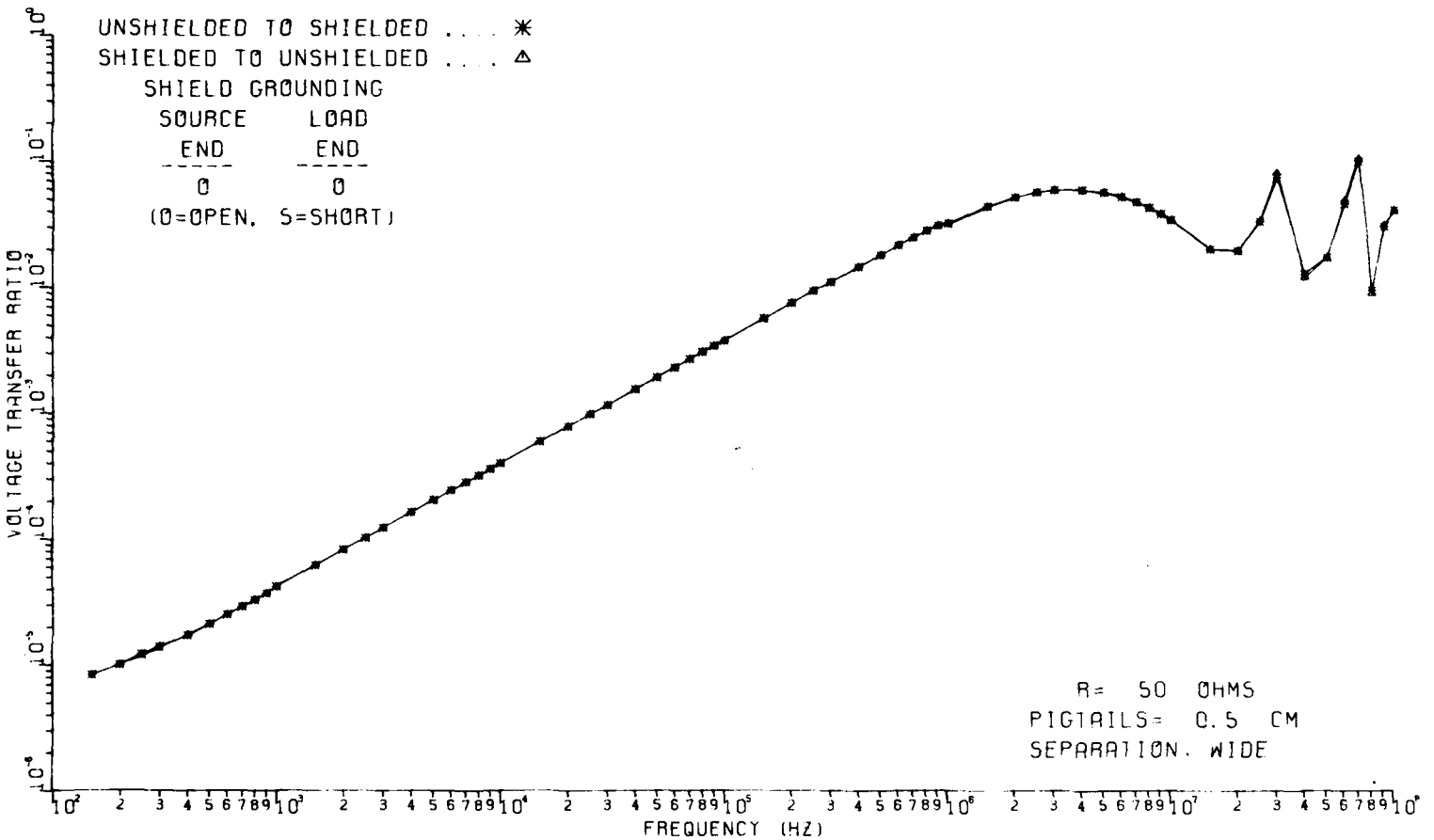
UNSHIELDED TO SHIELDED .... ✳
SHIELDED TO UNSHIELDED .... △
SHIELD GROUNDING
SOURCE END
LOAD END
0
0
(0=OPEN, S=SHORT)
VOLTAGE TRANSFER RATIO
FREQUENCY (HZ)
R= 50 OHMS
PIGTAILS= 0.5 CM
SEPARATION, WIDE

Figure B-4.

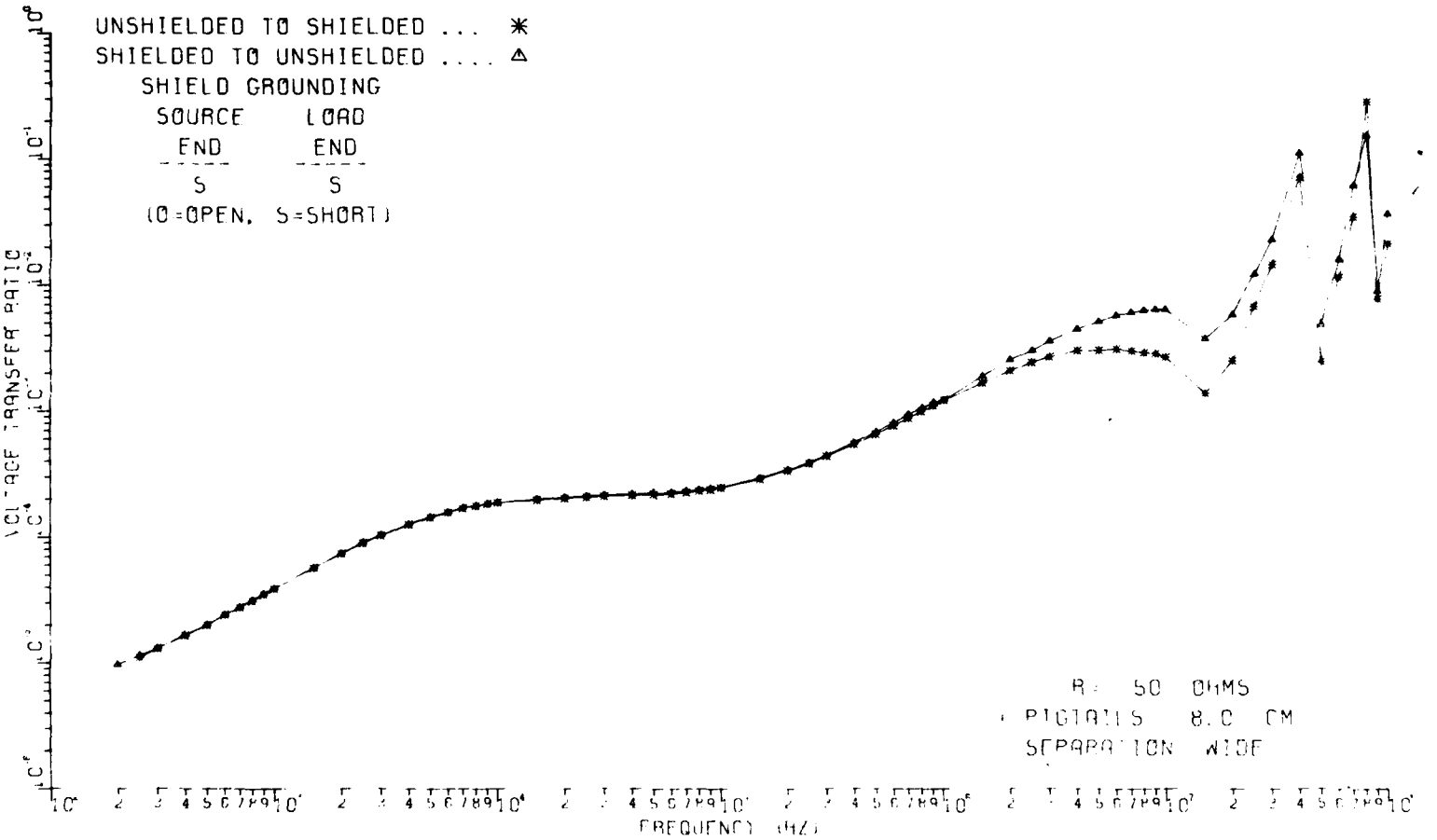
UNSHIELDED TO SHIELDED ... *
SHIELDED TO UNSHIELDED .... Δ
SHIELD GROUNDING
SOURCE END
LOAD END
S
S
(O=OPEN, S=SHORT)
R = 50 OHMS
PIGTAILS 8.0 CM
SEPARATION WIDE
FREQUENCY (HZ)

Figure B-5.

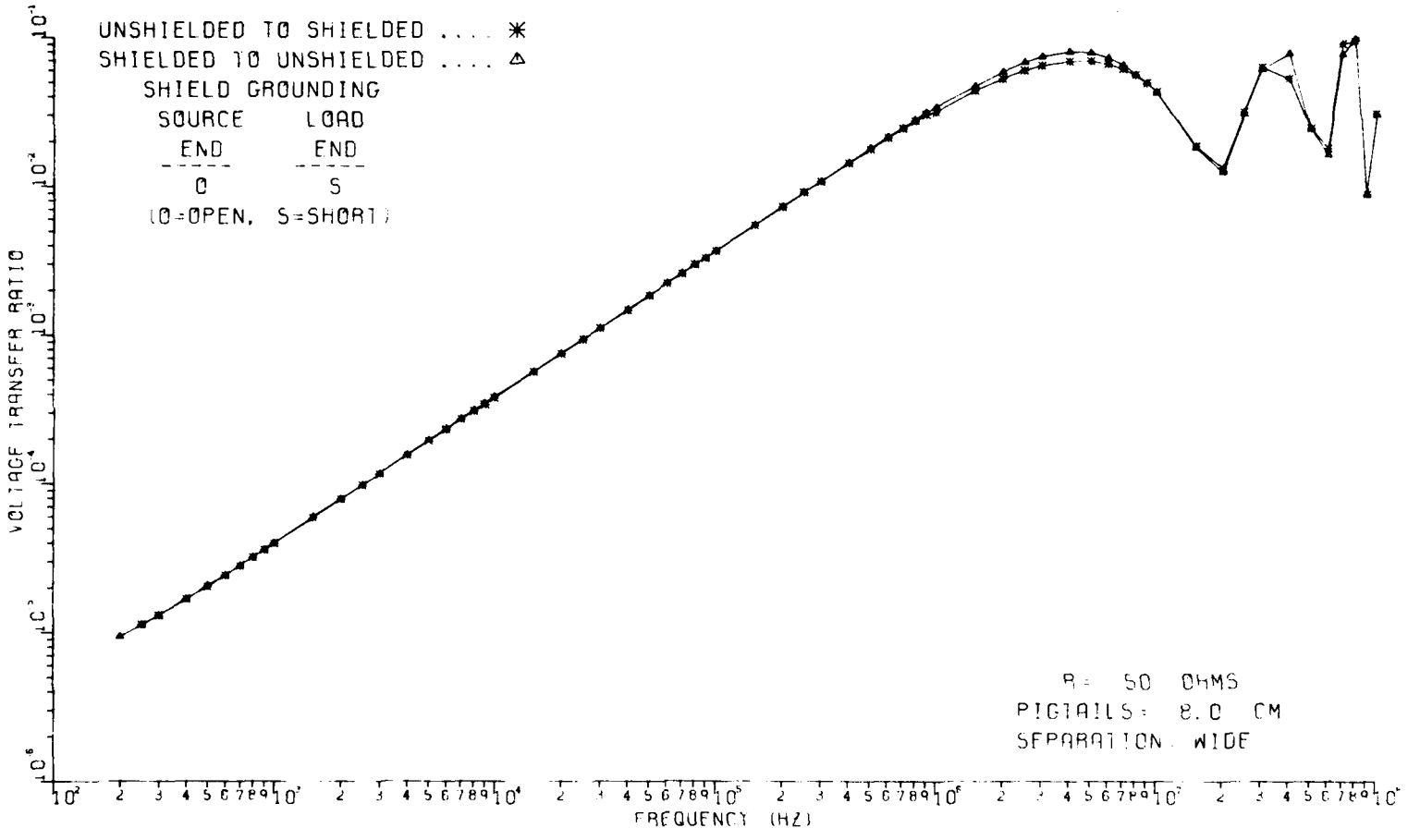
UNSHIELDED TO SHIELDED .... ✳
SHIELDED TO UNSHIELDED .... △
SHIELD GROUNDING
SOURCE END
LOAD END
0
S
(0=OPEN, S=SHORT)
VOLTAGE TRANSFER RATIO
FREQUENCY (HZ)
R= 50 OHMS
PIGTAILS= 8.0 CM
SEPARATION: WIDE

Figure B-6.

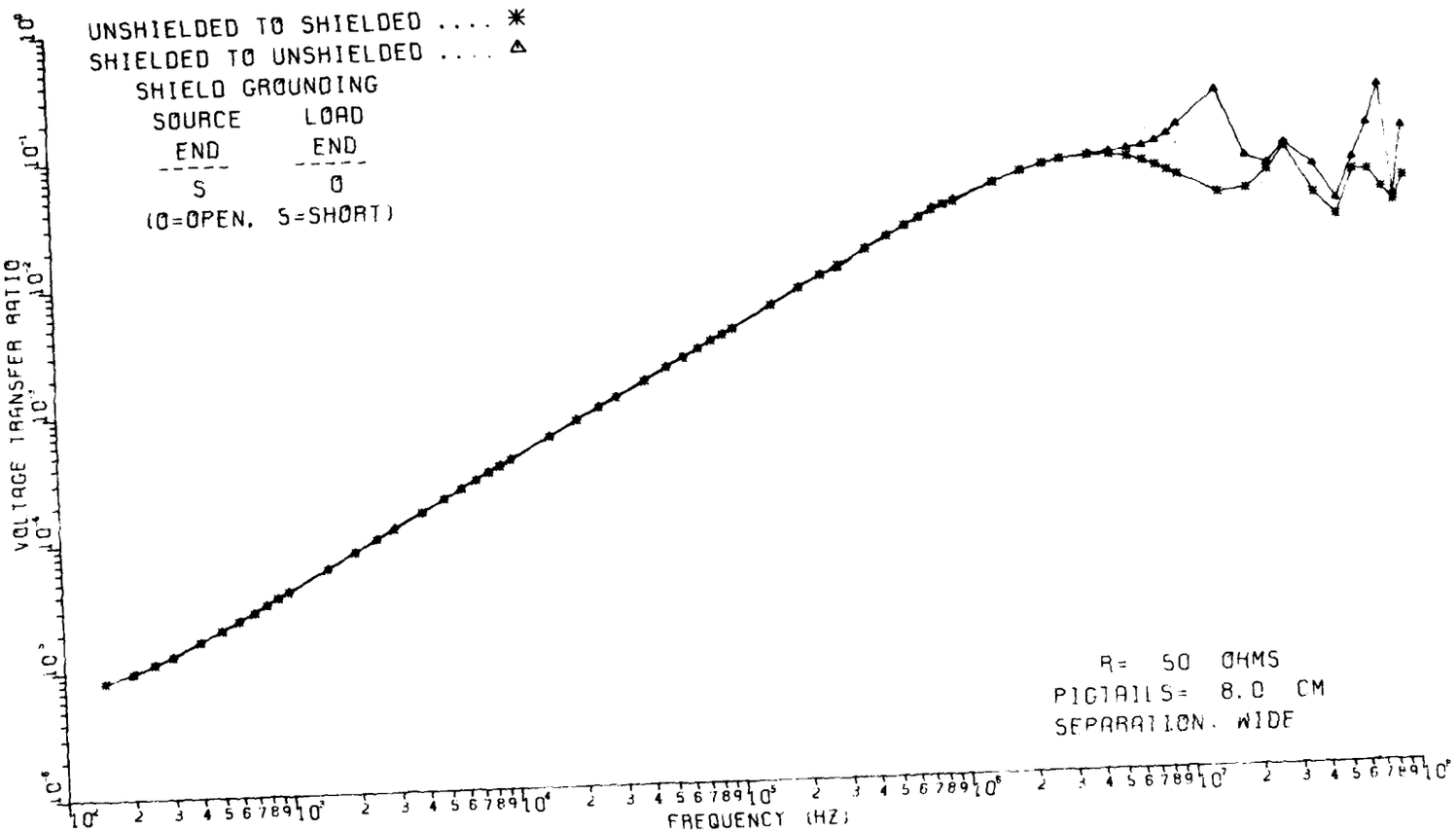
UNSHIELDED TO SHIELDED .... ✳
SHIELDED TO UNSHIELDED .... △
SHIELD GROUNDING
SOURCE END
LOAD END
S
0
(0=OPEN, S=SHORT)
VOLTAGE TRANSFER RATIO
FREQUENCY (HZ)
R= 50 OHMS
PIGTAILS= 8.0 CM
SEPARATION. WIDE

Figure B-7.

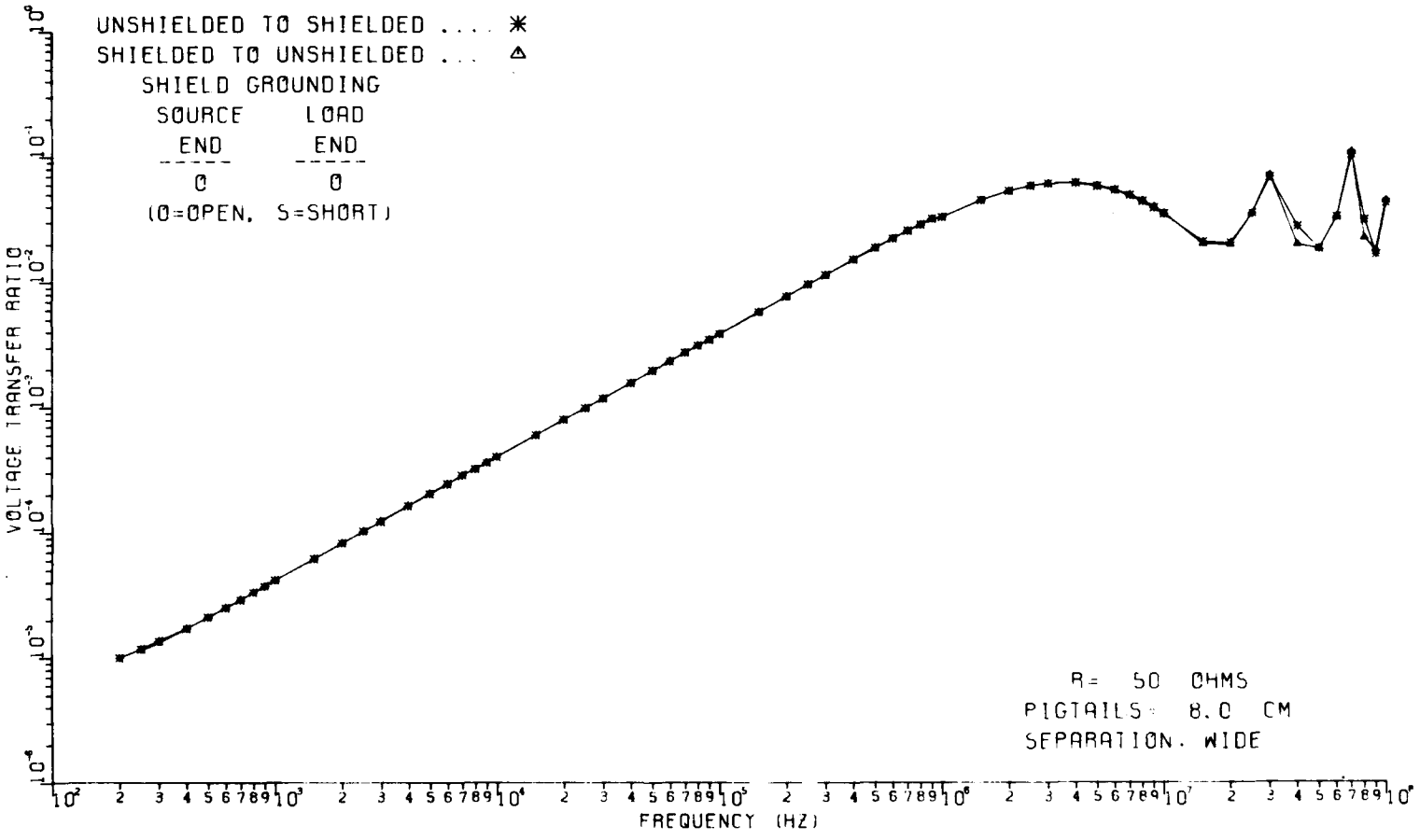
UNSHIELDED TO SHIELDED .... ✳
SHIELDED TO UNSHIELDED ... △
SHIELD GROUNDING
SOURCE END
LOAD END
0
0
(0=OPEN, S=SHORT)
VOLTAGE TRANSFER RATIO
FREQUENCY (HZ)
R= 50 OHMS
PIGTAILS= 8.0 CM
SEPARATION. WIDE

Figure B-8.

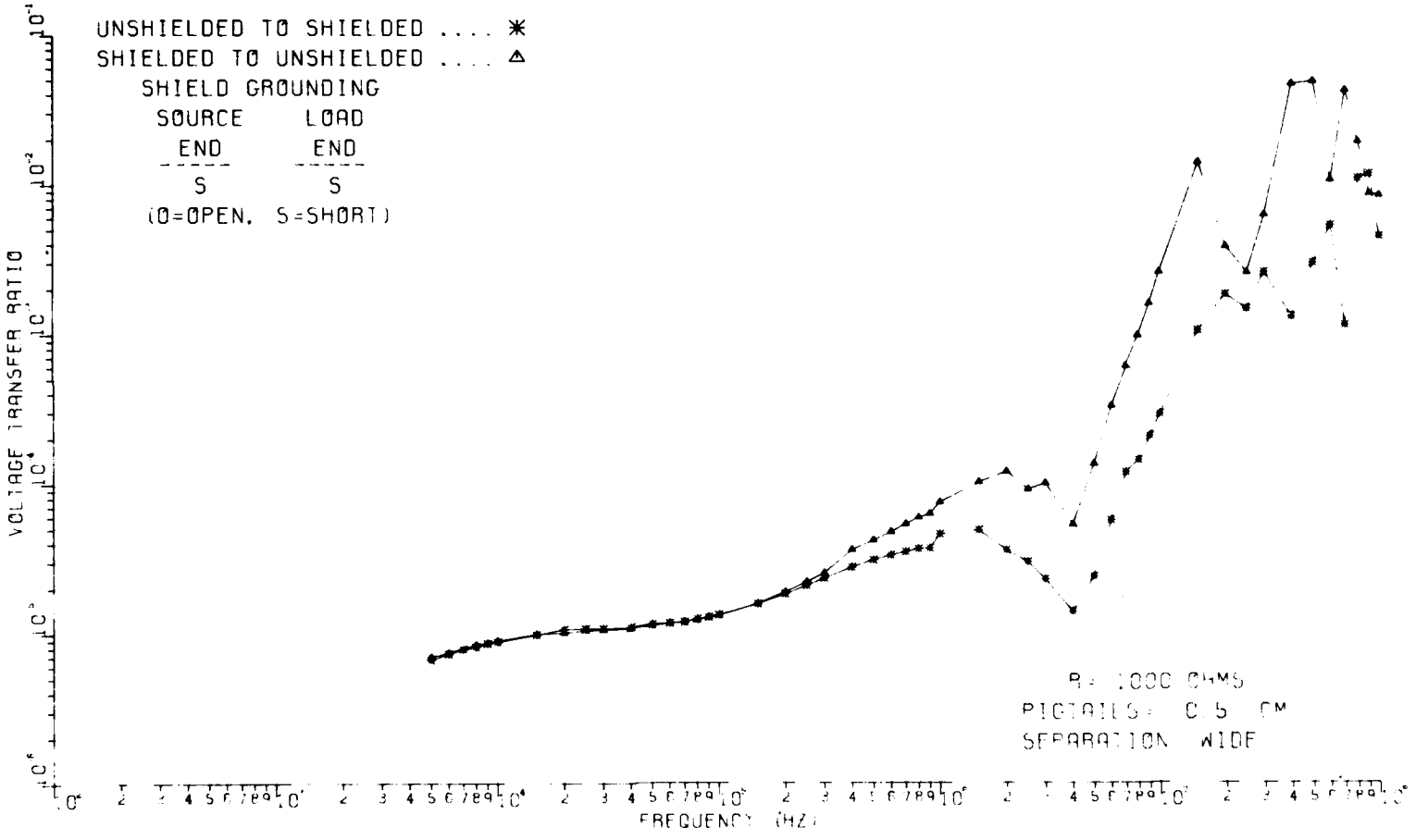
UNSHIELDED TO SHIELDED .... ✳
SHIELDED TO UNSHIELDED .... △
SHIELD GROUNDING
SOURCE END
LOAD END
S
S
(O=OPEN, S=SHORT)
VOLTAGE TRANSFER RATIO
FREQUENCY (HZ)
R= 1000 OHMS
PIGTAILS= 0.5 CM
SEPARATION WIDE

Figure B-9.

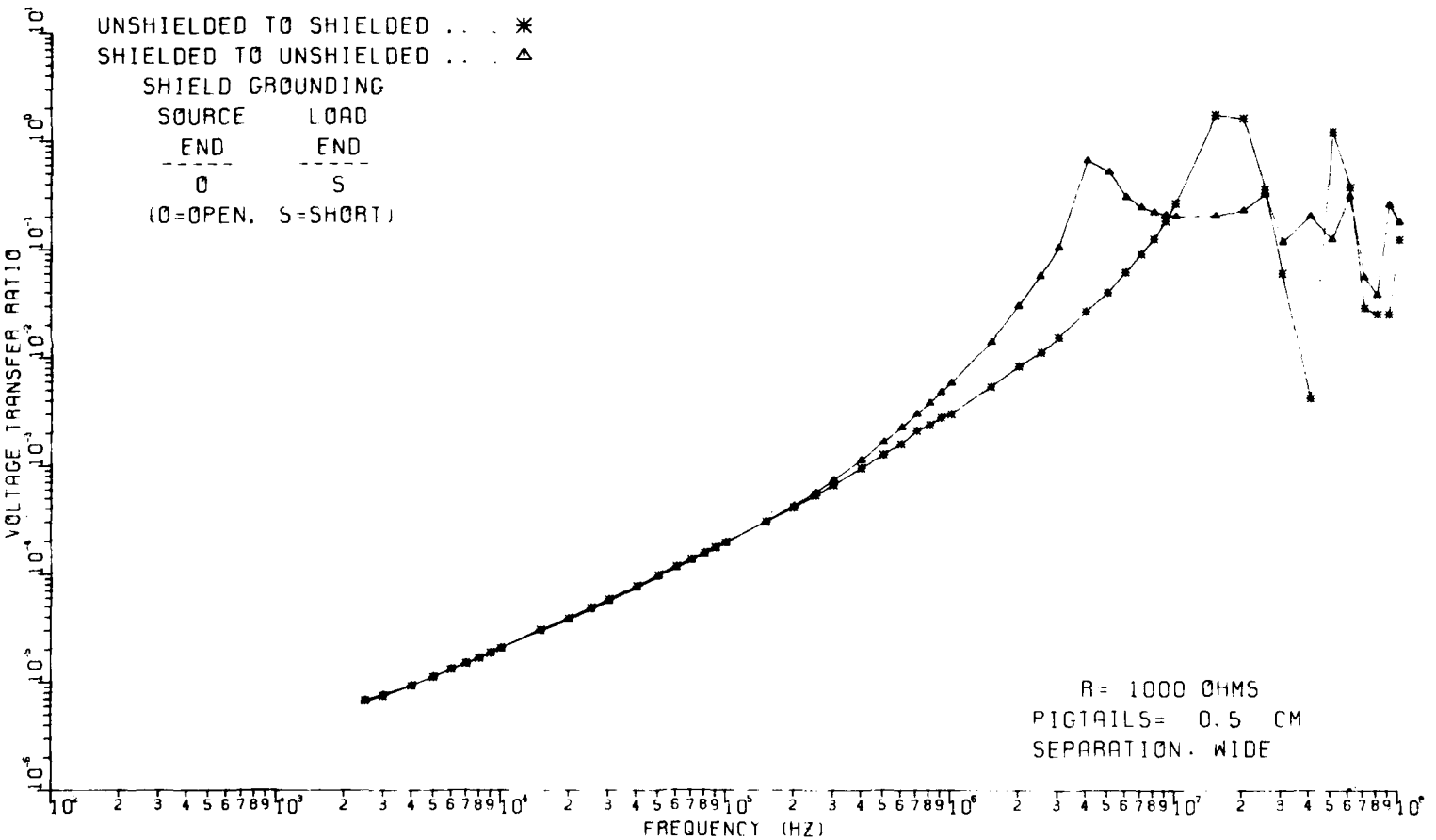
UNSHIELDED TO SHIELDED . . . *
SHIELDED TO UNSHIELDED . . . Δ
SHIELD GROUNDING
SOURCE END
LOAD END
0
S
(0=OPEN, S=SHORT)
VOLTAGE TRANSFER RATIO
FREQUENCY (HZ)
R= 1000 OHMS
PIGTAILS= 0.5 CM
SEPARATION, WIDE

Figure B-10.

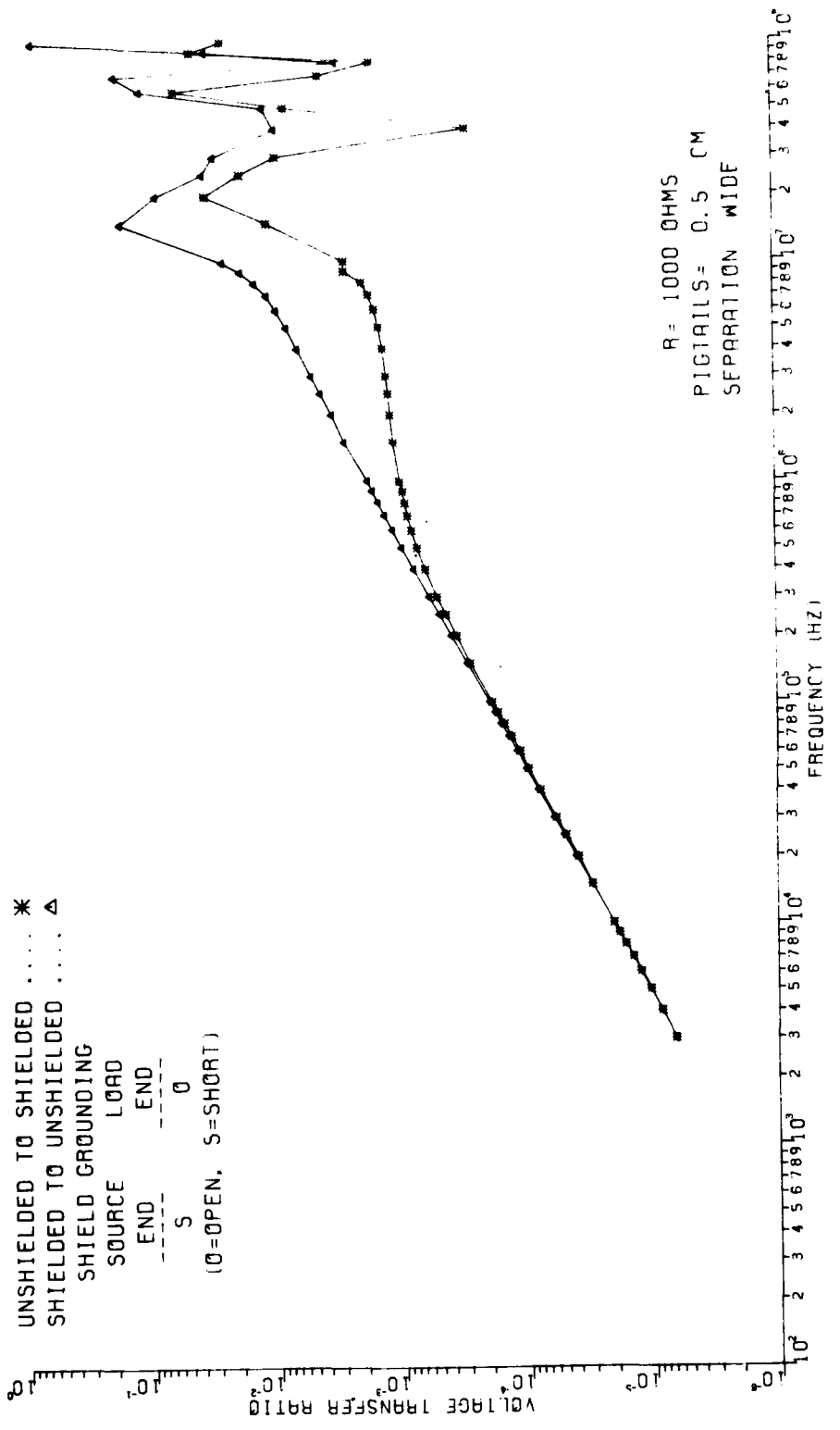
UNSHIELDED TO SHIELDED .... *
SHIELDED TO UNSHIELDED .... Δ
SHIELD GROUNDING
SOURCE LOAD
END END
S 0
(0=OPEN, S=SHORT)
R= 1000 OHMS
PIGTAILS= 0.5 CM
SEPARATION WIDE
VOLTAGE TRANSFER RATIO
FREQUENCY (HZ)

Figure B-11.

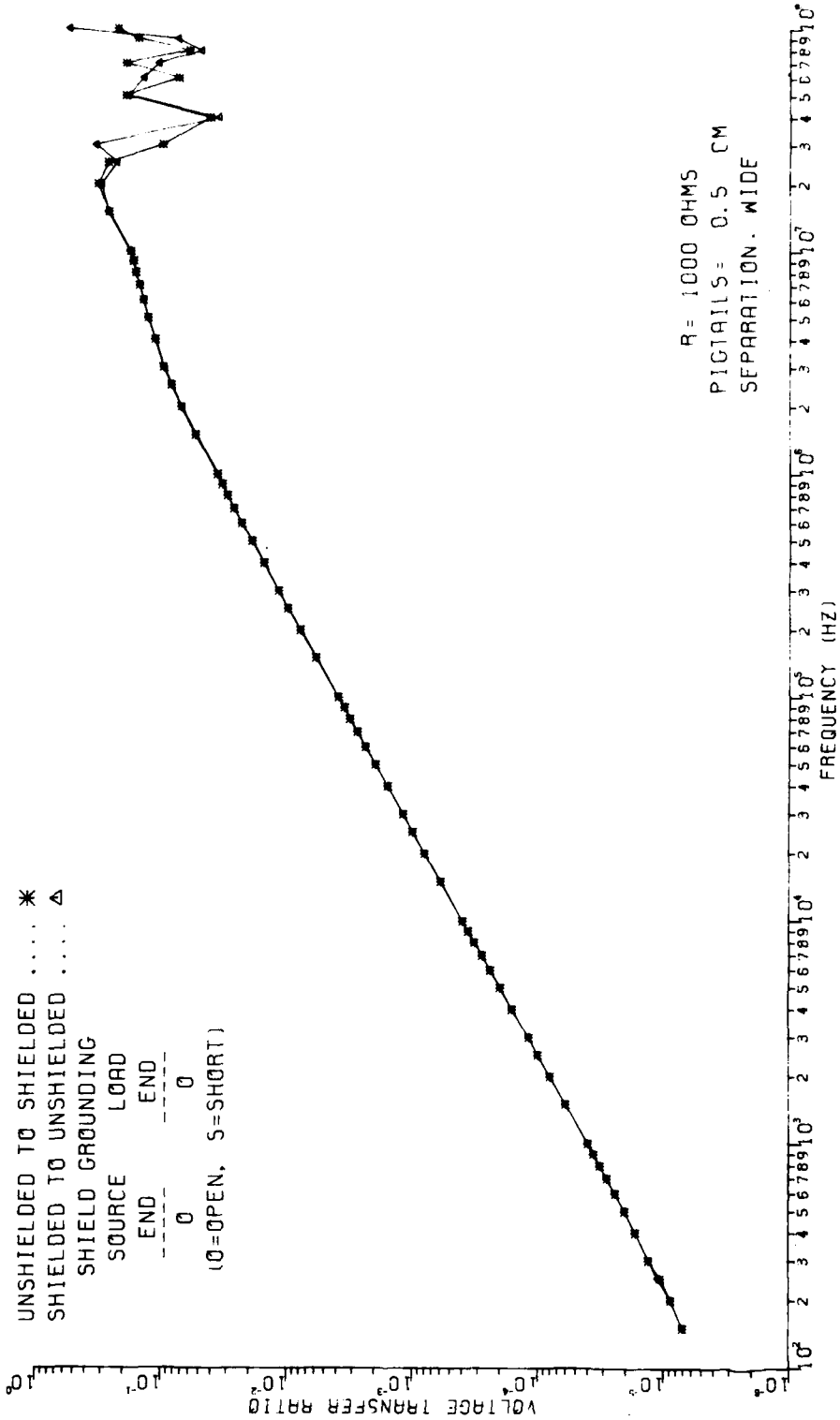
UNSHIELDED TO SHIELDED ..... *
SHIELDED TO UNSHIELDED ..... Δ
SHIELD GROUNDING
SOURCE LOAD
END END
0 0
(0=OPEN, S=SHORT)
R= 1000 OHMS
PIGTAILS= 0.5 CM
SEPARATION. WIDE
VOLTAGE TRANSFER RATIO
FREQUENCY (HZ)

Figure B-12.

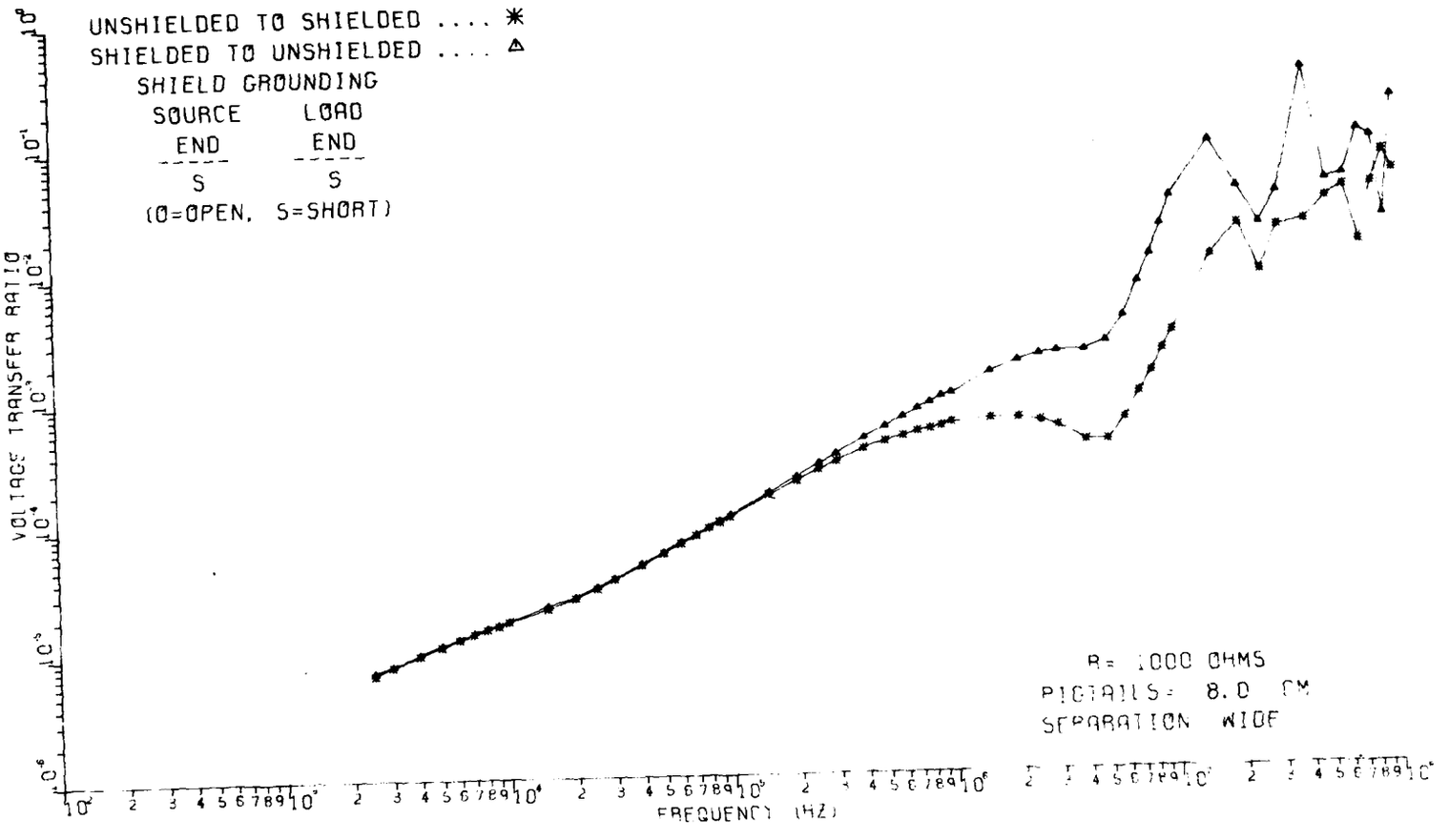
UNSHIELDED TO SHIELDED .... *
SHIELDED TO UNSHIELDED .... Δ
SHIELD GROUNDING
SOURCE END
LOAD END
S
S
(0=OPEN, S=SHORT)
VOLTAGE TRANSFER RATIO
FREQUENCY (HZ)
R= 1000 OHMS
PIGTAILS= 8.0 CM
SEPARATION WIDE

Figure B-13.

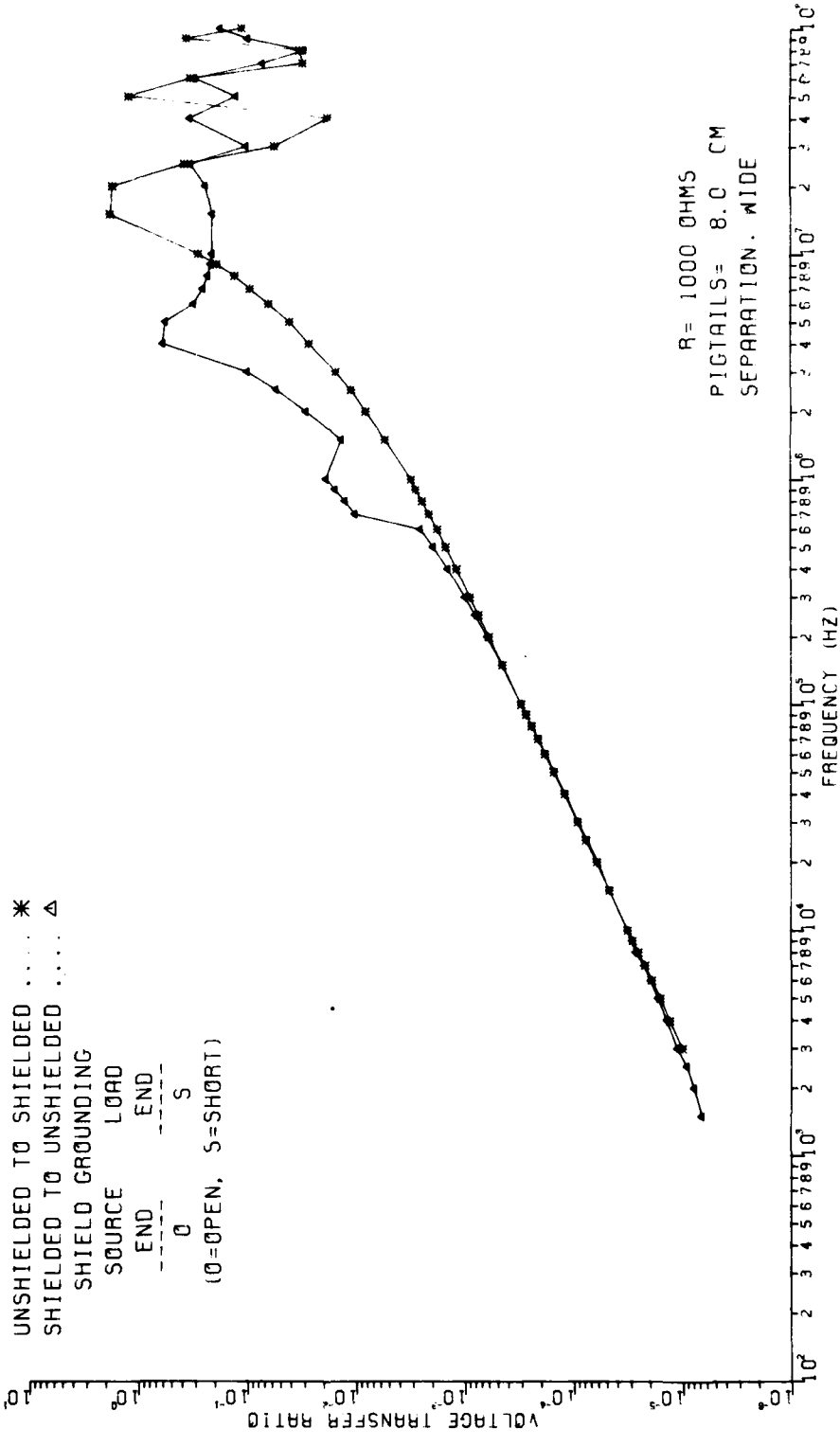
UNSHIELDED TO SHIELDED .... *
SHIELDED TO UNSHIELDED .... Δ
SHIELD GROUNDING
SOURCE LOAD
END END
0 S
(0=OPEN, S=SHORT)
R= 1000 OHMS
PIGTAILS= 8.0 CM
SEPARATION. WIDE
VOLTAGE TRANSFER RATIO
FREQUENCY (HZ)

Figure B-14.

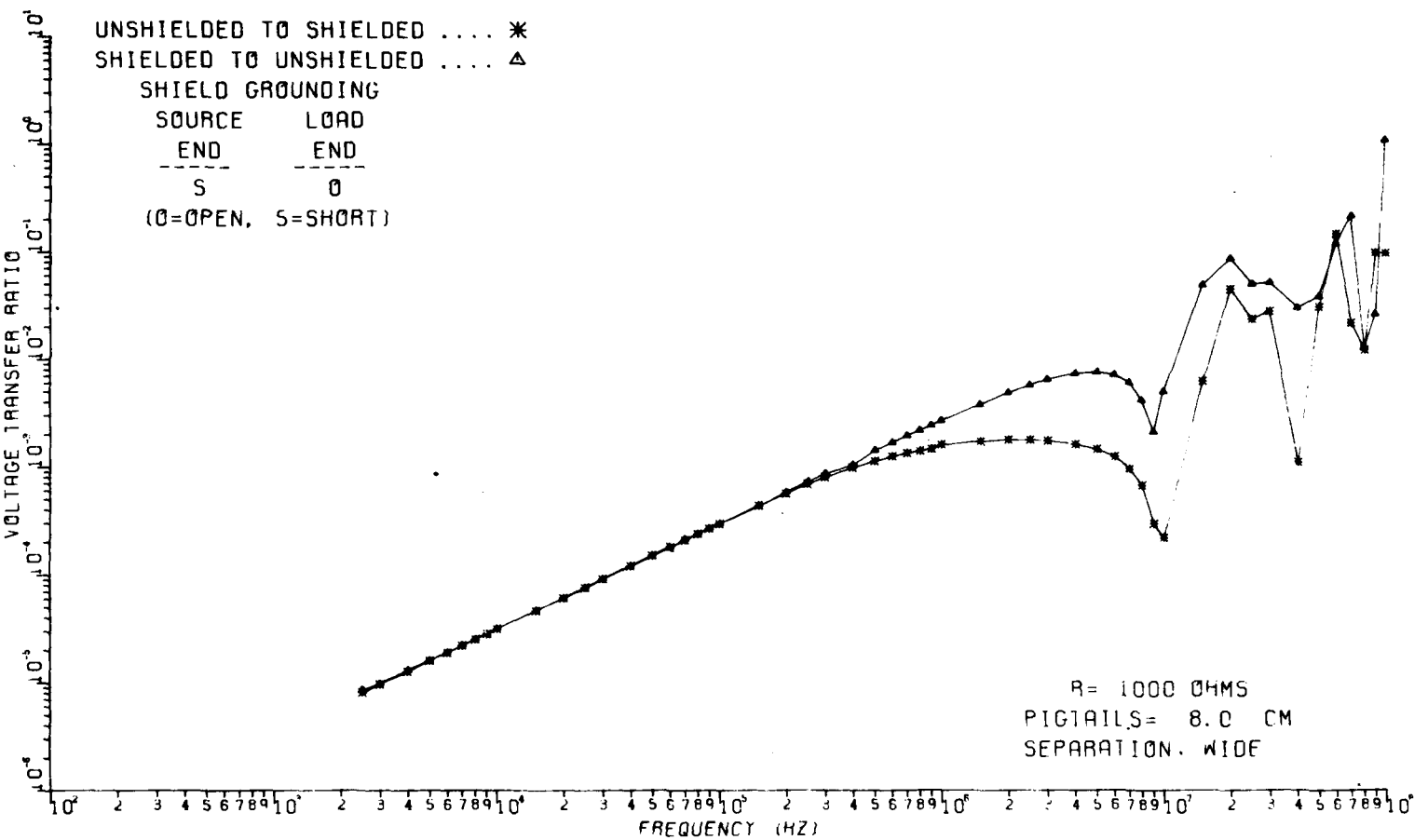
UNSHIELDED TO SHIELDED .... *
SHIELDED TO UNSHIELDED .... Δ
SHIELD GROUNDING
SOURCE END
LOAD END
S
0
(0=OPEN, S=SHORT)
VOLTAGE TRANSFER RATIO
FREQUENCY (HZ)
R= 1000 OHMS
PIGTAILS= 8.0 CM
SEPARATION, WIDE

Figure B-15.

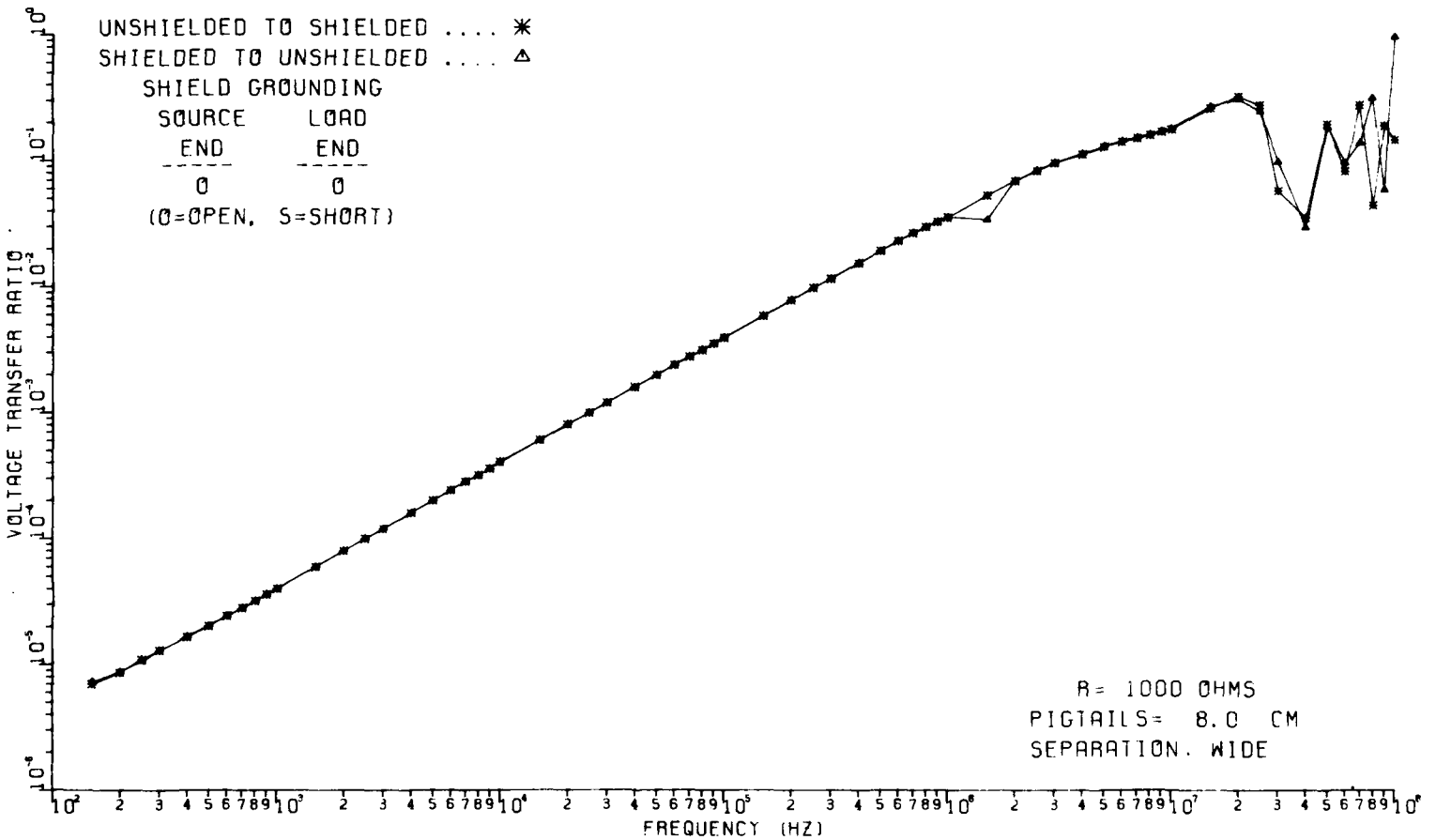
UNSHIELDED TO SHIELDED .... ✳
SHIELDED TO UNSHIELDED .... △
SHIELD GROUNDING
SOURCE END
LOAD END
0
0
(0=OPEN, S=SHORT)
VOLTAGE TRANSFER RATIO
FREQUENCY (HZ)
R= 1000 OHMS
PIGTAILS= 8.0 CM
SEPARATION. WIDE

Figure B-16.

APPENDIX C

Fig.	Configuration	Ω	Separation	Grounding	Pigtails	Page
C-1	UU	50Ω	Touching			158
C-2	"	1kΩ	"			159
C-3	"	50Ω	Wide			160
C-4	"	1kΩ	"			161
C-5	US	50Ω	Touching	SS	0.5	162
C-6	"	"	"	"	8	163
C-7	"	"	Wide	"	0.5	164
C-8	"	"	"	"	8	165
C-9	"	1kΩ	Touching	"	0.5	166
C-10	"	"	"	"	8	167
C-11	"	"	Wide	SS	0.5	168
C-12	"	"	"	"	8	169
C-13	SS	50Ω	Touching	"	0.5	170
C-14	"	"	"	"	8	171
C-15	"	1kΩ	"	"	0.5	172
C-16	"	"	"	"	8	173
C-17	"	50Ω	Wide	"	"	174
C-18	"	1kΩ	"	"	"	175

UU = unshielded to unshielded
US = unshielded to shielded
SS = shielded to shielded
O = open (shield ungrounded)
S = short (shield grounded)
First letter denotes source end of line and second letter denotes load end of line. For example, SO denotes that the shield is grounded at the source end and ungrounded at the load end.

NOTE: The solid lines on the following figures represent the various components (capacitive or inductive) of the low-frequency prediction model.

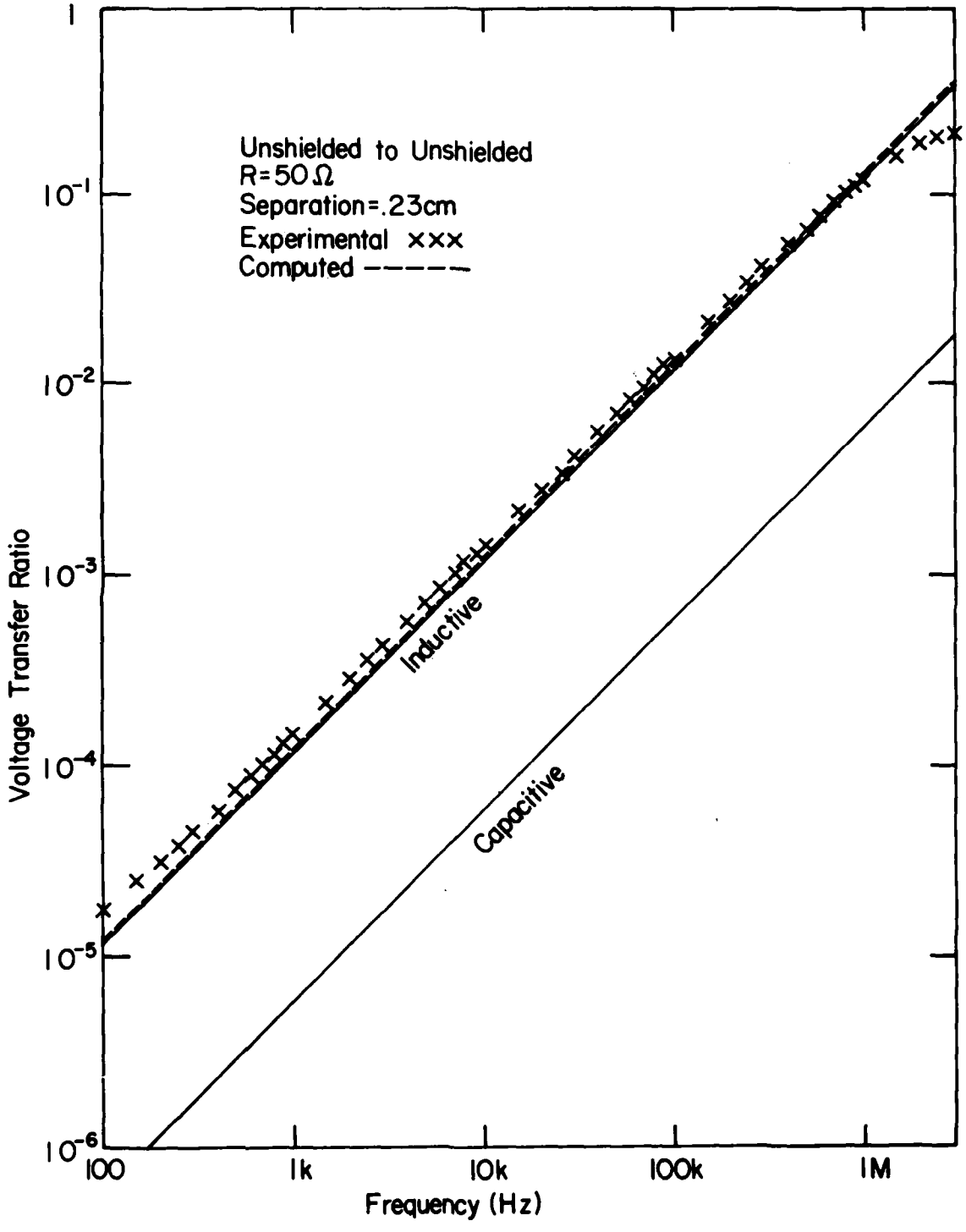
Unshielded to Unshielded
R=50Ω
Separation=.23cm
Experimental xxx
Computed -----
Inductive
Capacitive
Voltage Transfer Ratio
1
10-1
10-2
10-3
10-4
10-5
10-6
100
1k
10k
100k
1M
Frequency (Hz)

Figure C-1.

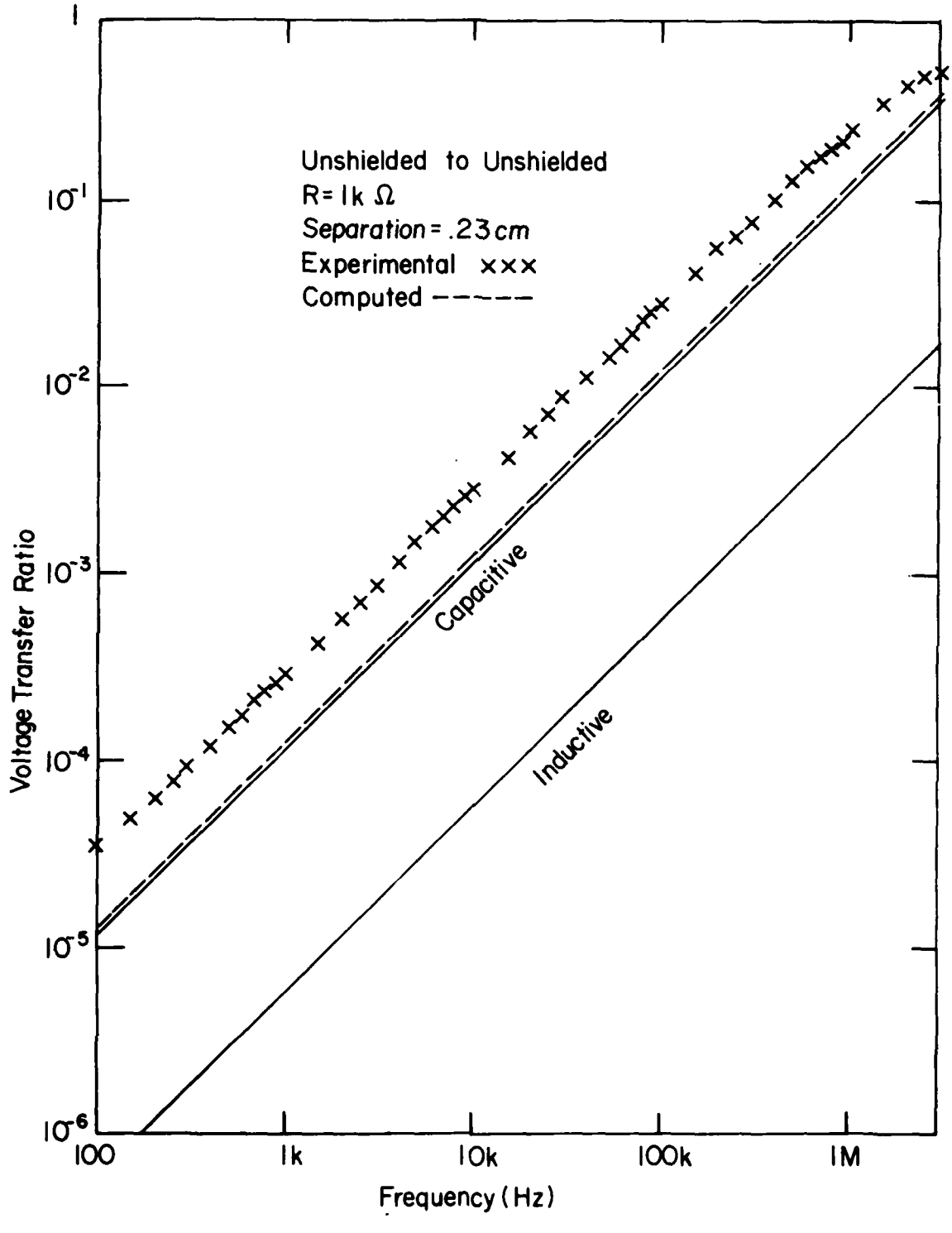
Unshielded to Unshielded
R= 1k Ω
Separation = .23cm
Experimental xxx
Computed ------
Capacitive
Inductive
Voltage Transfer Ratio
1
10-1
10-2
10-3
10-4
10-5
10-6
100
1k
10k
100k
1M
Frequency (Hz)

Figure C-2.

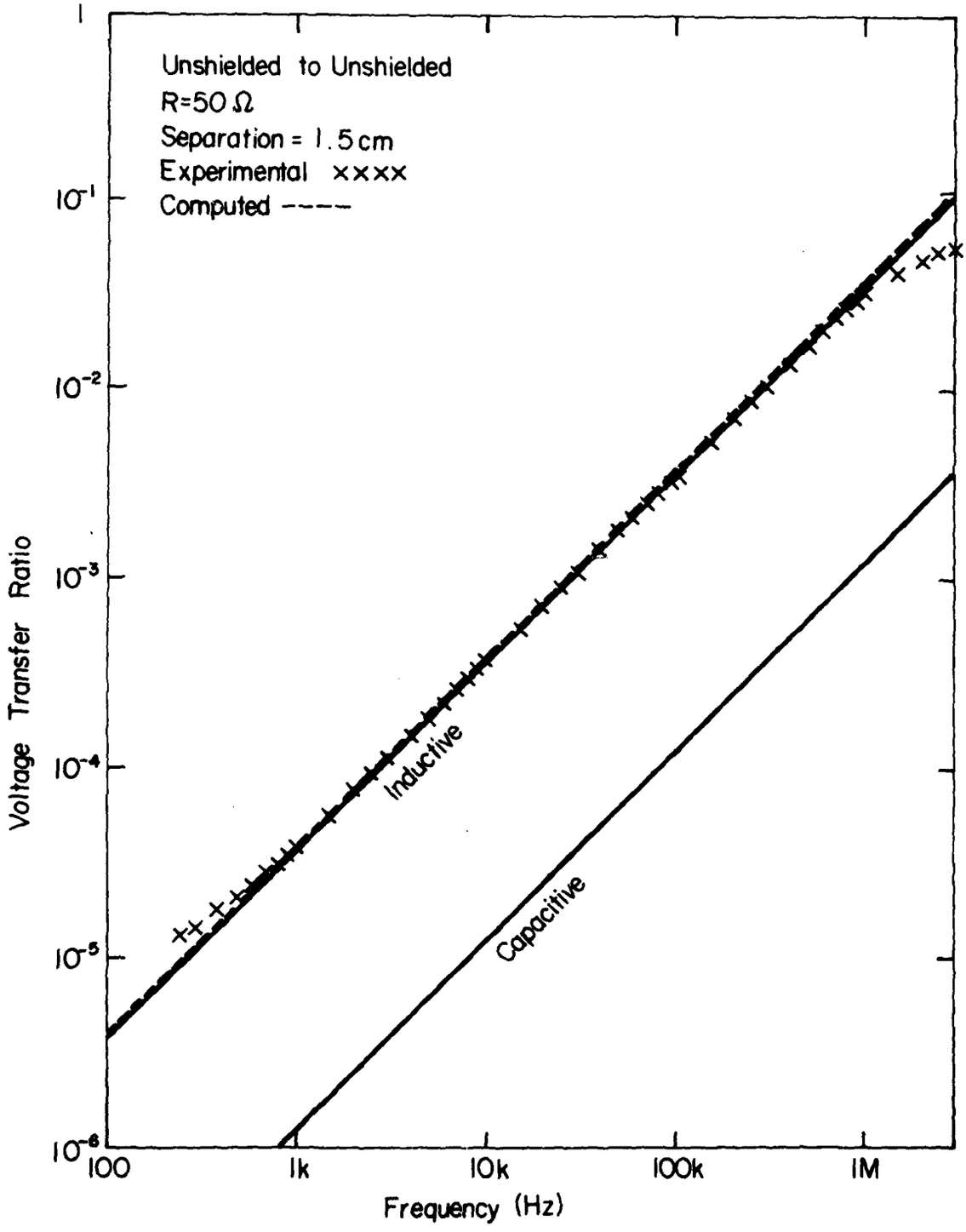
Unshielded to Unshielded
R=50 Ω
Separation = 1.5 cm
Experimental ××××
Computed ----
Inductive
Capacitive
Voltage Transfer Ratio
1
10⁻¹
10⁻²
10⁻³
10⁻⁴
10⁻⁵
10⁻⁶
100
1k
10k
100k
1M
Frequency (Hz)

Figure C-3

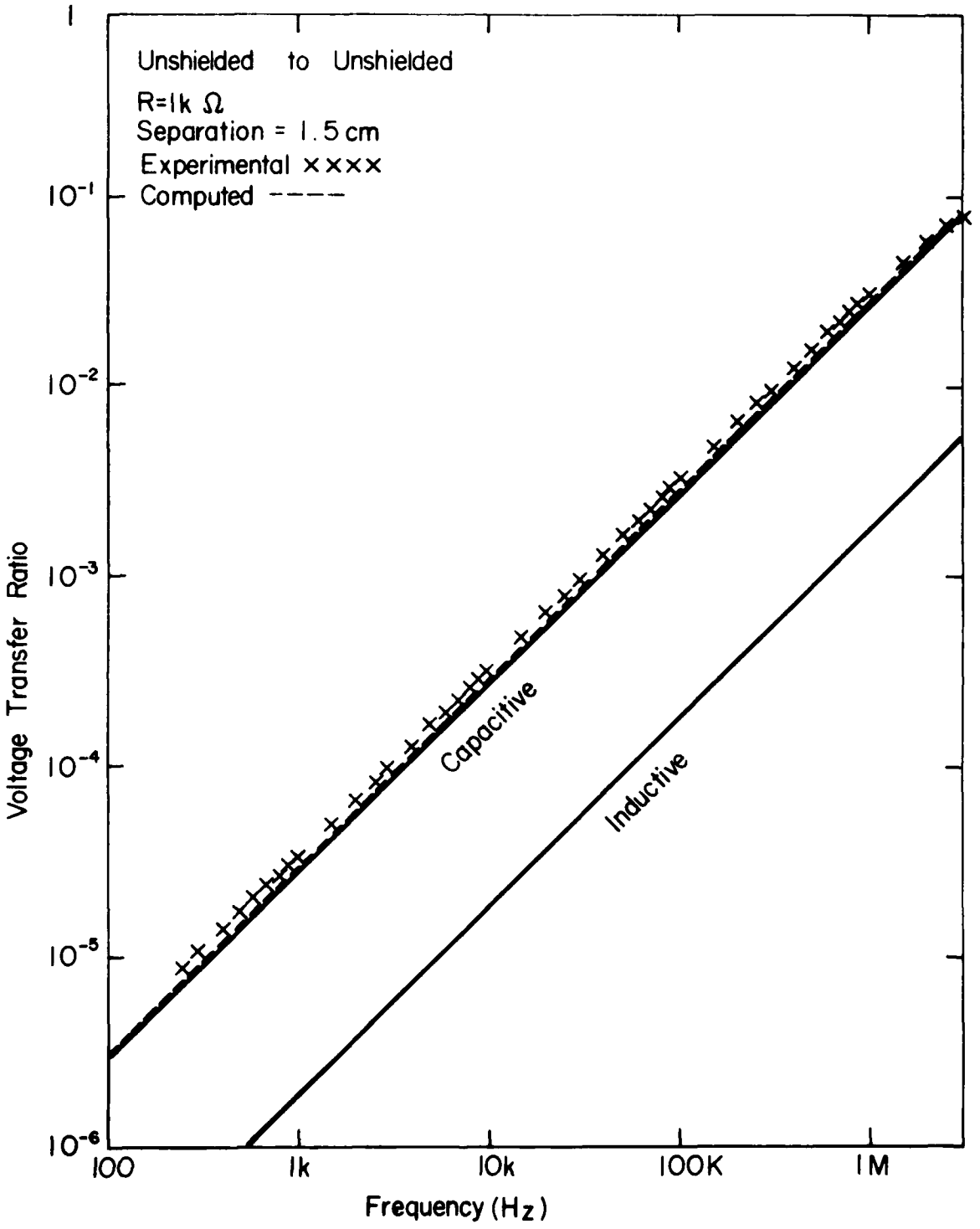
Unshielded to Unshielded
R=1k Ω
Separation = 1.5 cm
Experimental ××××
Computed ----
Capacitive
Inductive
Voltage Transfer Ratio
1
10⁻¹
10⁻²
10⁻³
10⁻⁴
10⁻⁵
10⁻⁶
100
1k
10k
100K
1M
Frequency (Hz)

Figure C-4

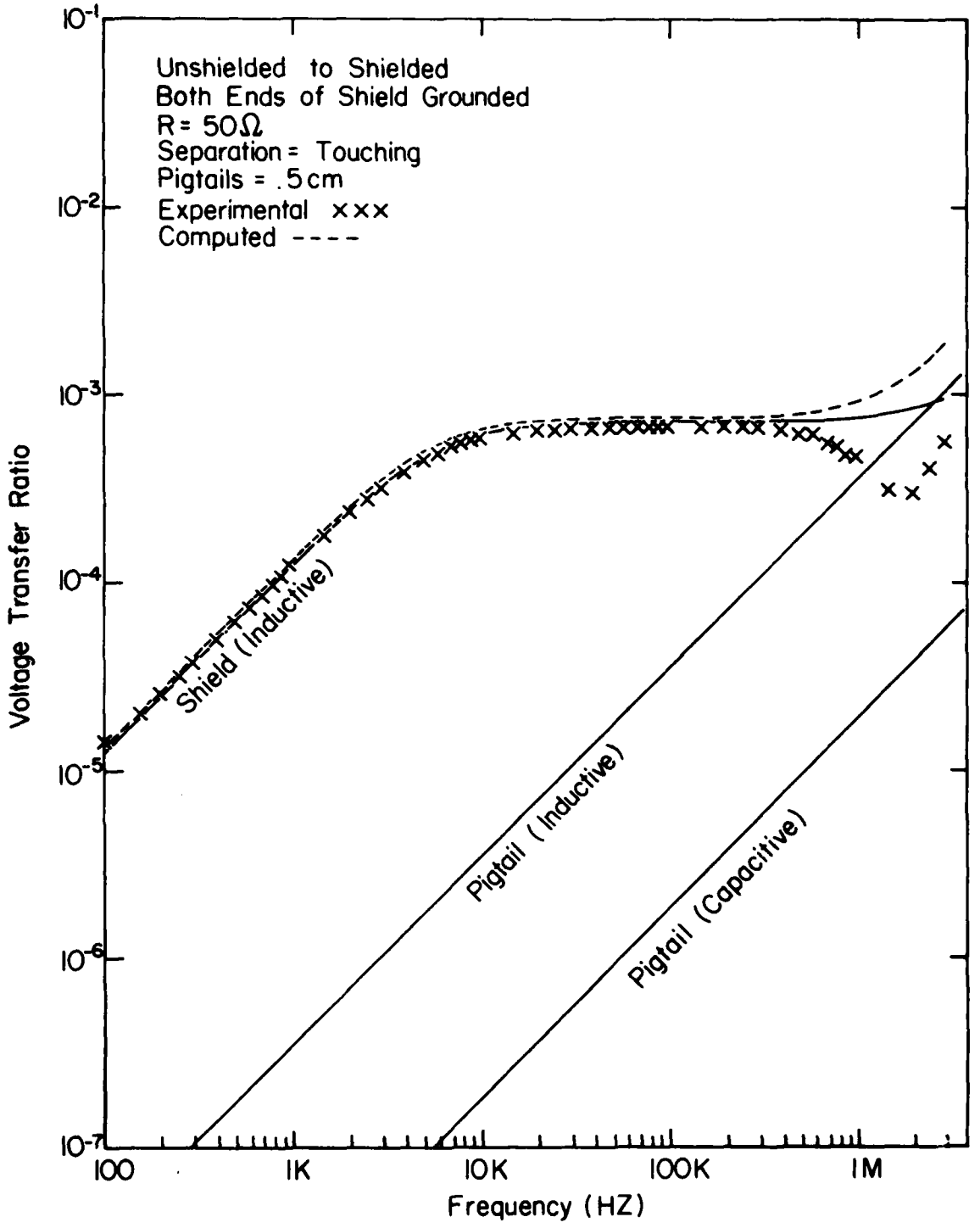
Unshielded to Shielded
Both Ends of Shield Grounded
R = 50Ω
Separation = Touching
Pigtails = .5 cm
Experimental ×××
Computed ----
Voltage Transfer Ratio
10-1
10-2
10-3
10-4
10-5
10-6
10-7
Shield (Inductive)
Pigtail (Inductive)
Pigtail (Capacitive)
100
1K
10K
100K
1M
Frequency (HZ)

Figure C-5.

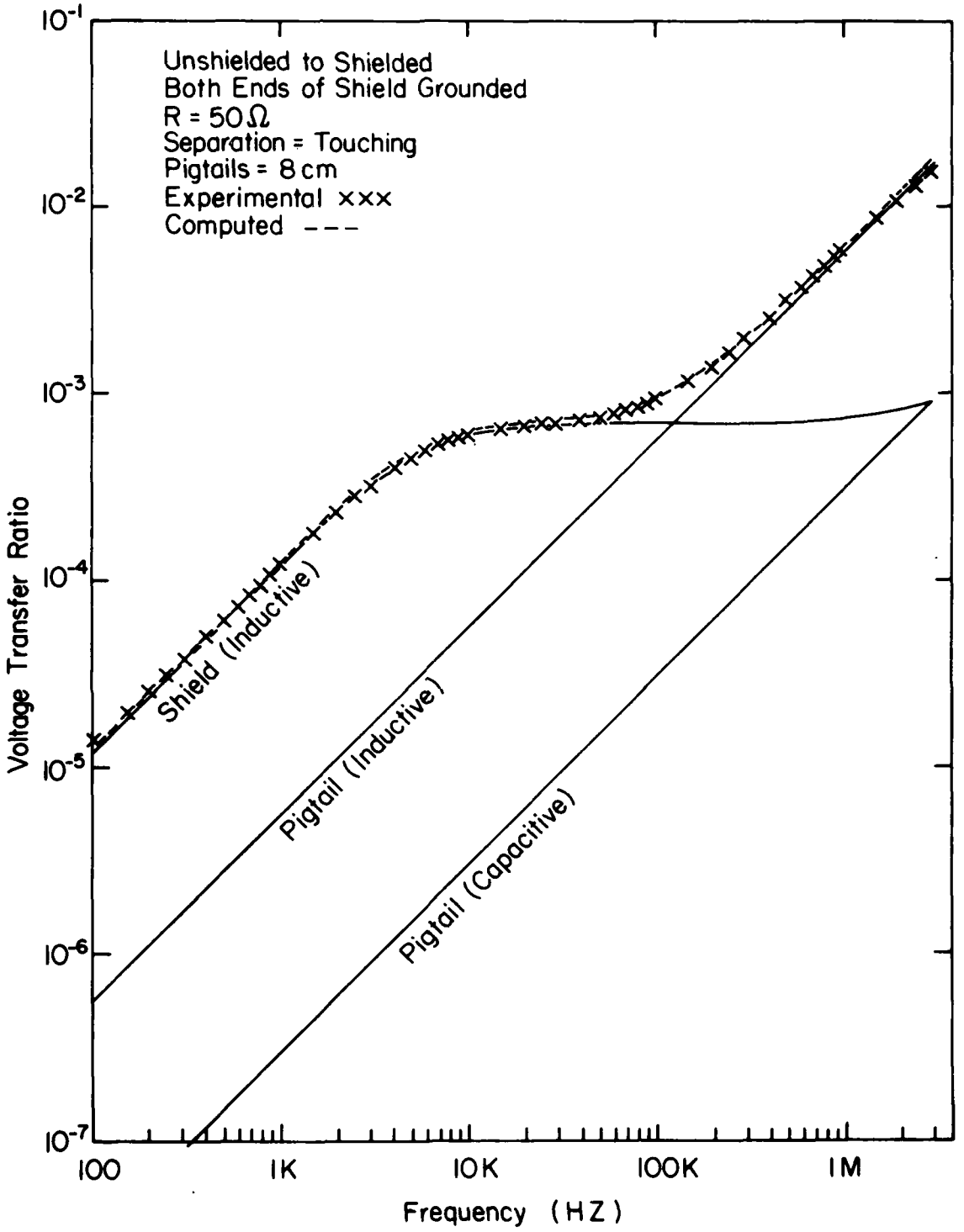
Unshielded to Shielded
Both Ends of Shield Grounded
R = 50Ω
Separation = Touching
Pigtails = 8 cm
Experimental xxx
Computed ---
Voltage Transfer Ratio
10-1
10-2
10-3
10-4
10-5
10-6
10-7
Shield (Inductive)
Pigtail (Inductive)
Pigtail (Capacitive)
100
1K
10K
100K
1M
Frequency (HZ)

Figure C-6.

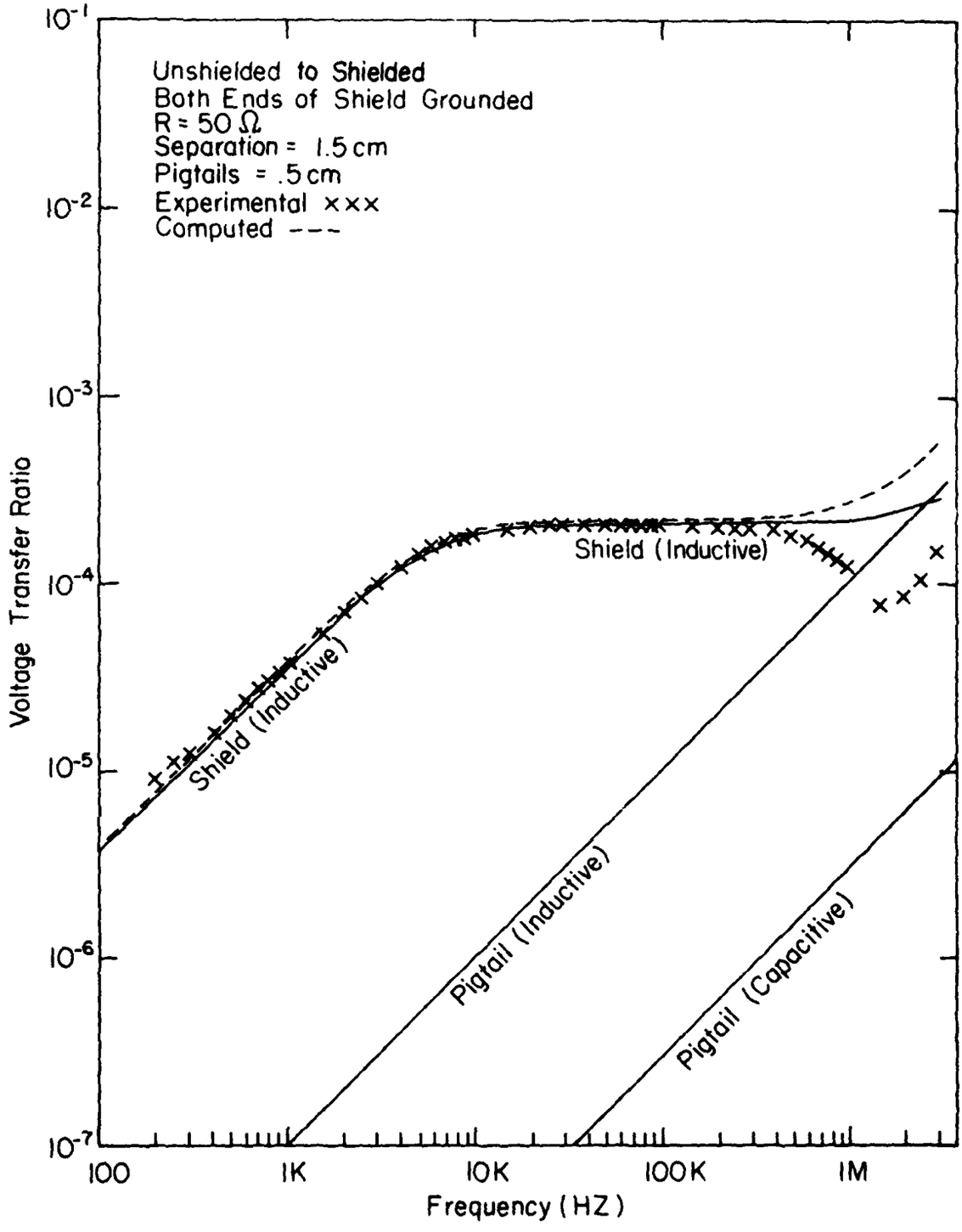
Unshielded to Shielded
Both Ends of Shield Grounded
R = 50 Ω
Separation = 1.5 cm
Pigtails = .5 cm
Experimental ×××
Computed ---
Shield (Inductive)
Shield (Inductive)
Pigtail (Inductive)
Pigtail (Capacitive)
Voltage Transfer Ratio
Frequency (HZ)
10^-1
10^-2
10^-3
10^-4
10^-5
10^-6
10^-7
100
1K
10K
100K
1M

Figure C-7.

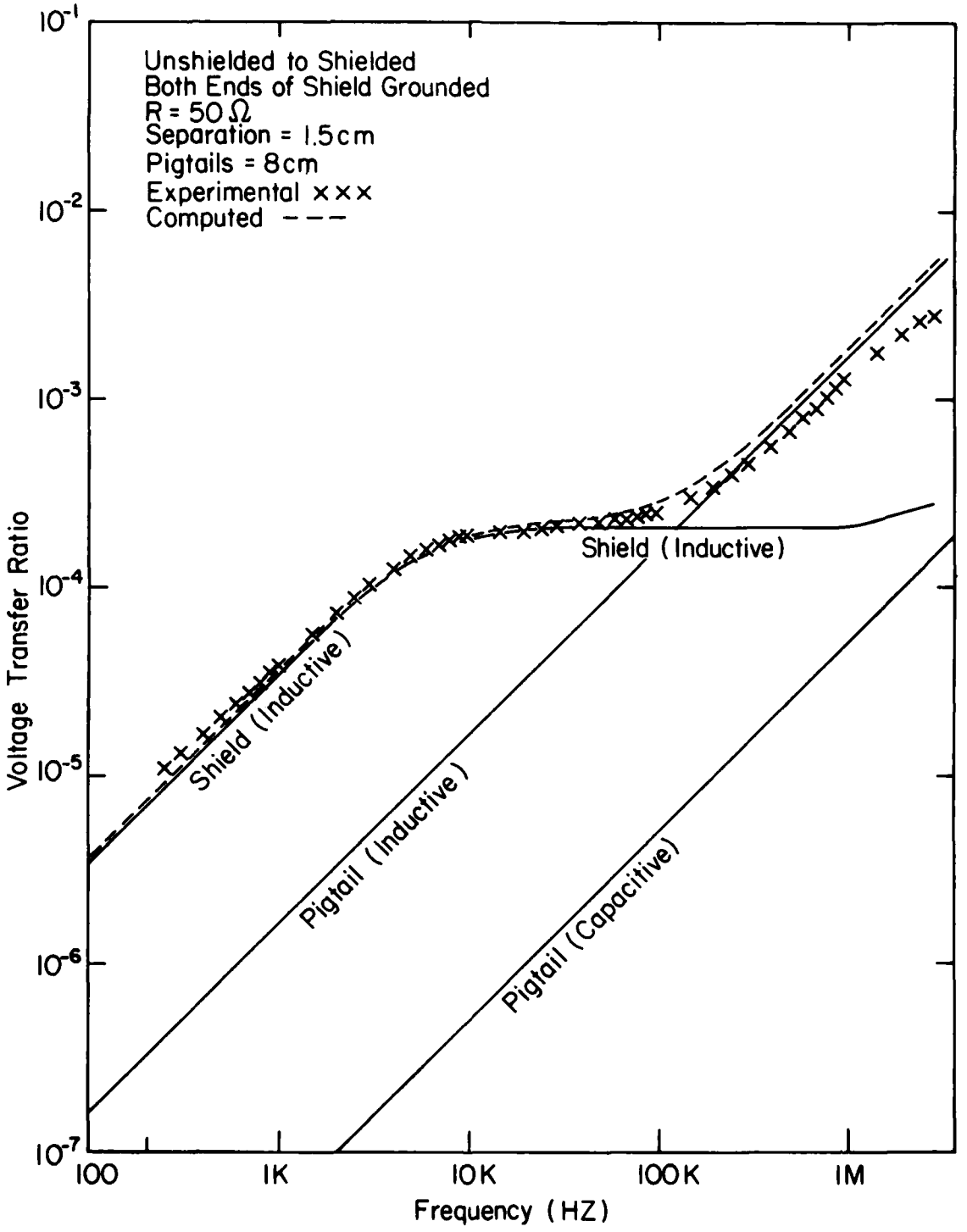
Unshielded to Shielded
Both Ends of Shield Grounded
R = 50 Ω
Separation = 1.5 cm
Pigtails = 8 cm
Experimental ×××
Computed – – –
Shield (Inductive)
Shield (Inductive)
Pigtail (Inductive)
Pigtail (Capacitive)
Voltage Transfer Ratio
10⁻¹
10⁻²
10⁻³
10⁻⁴
10⁻⁵
10⁻⁶
10⁻⁷
100
1K
10K
100K
1M
Frequency (HZ)

Figure C-8

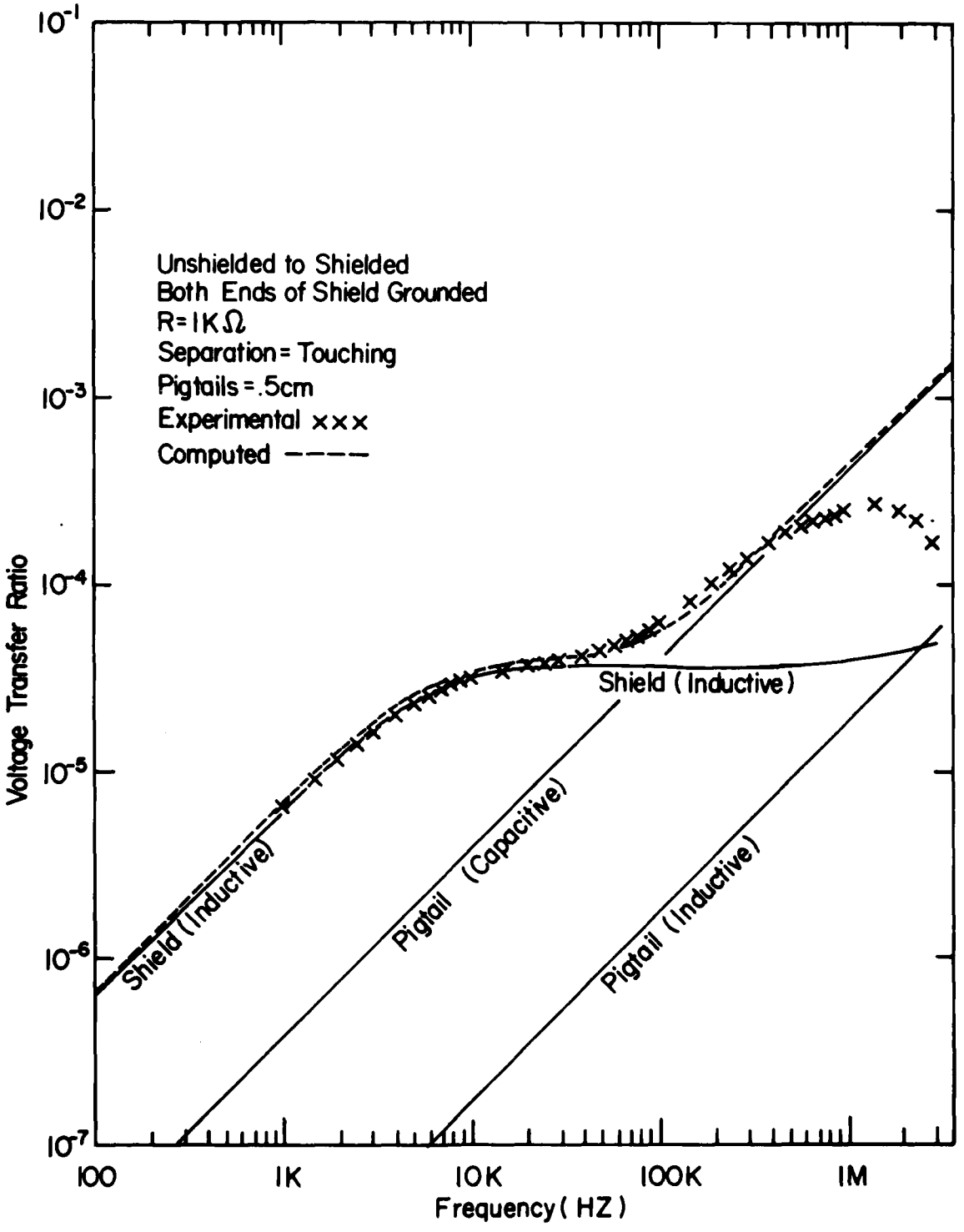
Unshielded to Shielded
Both Ends of Shield Grounded
R=1KΩ
Separation = Touching
Pigtails = .5cm
Experimental ×××
Computed ----
Shield (Inductive)
Pigtail (Capacitive)
Pigtail (Inductive)
Voltage Transfer Ratio
10⁻¹
10⁻²
10⁻³
10⁻⁴
10⁻⁵
10⁻⁶
10⁻⁷
100
1K
10K
100K
1M
Frequency (HZ)

Figure C-9

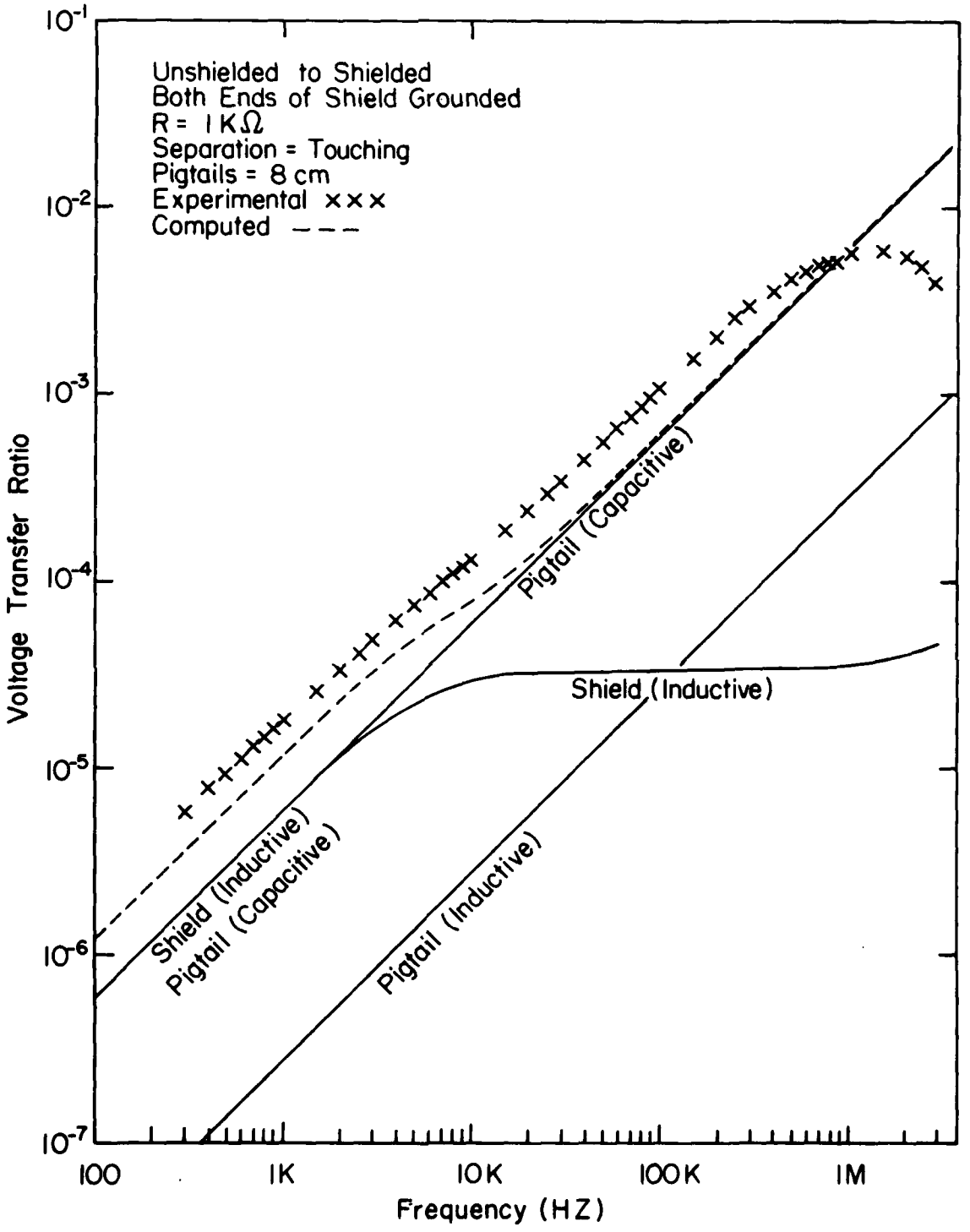
Unshielded to Shielded
Both Ends of Shield Grounded
R = 1 KΩ
Separation = Touching
Pigtails = 8 cm
Experimental ×××
Computed – – –
Voltage Transfer Ratio
10-1
10-2
10-3
10-4
10-5
10-6
10-7
Pigtail (Capacitive)
Shield (Inductive)
Shield (Inductive)
Pigtail (Capacitive)
Pigtail (Inductive)
100
1K
10K
100K
1M
Frequency (HZ)

Figure C-10

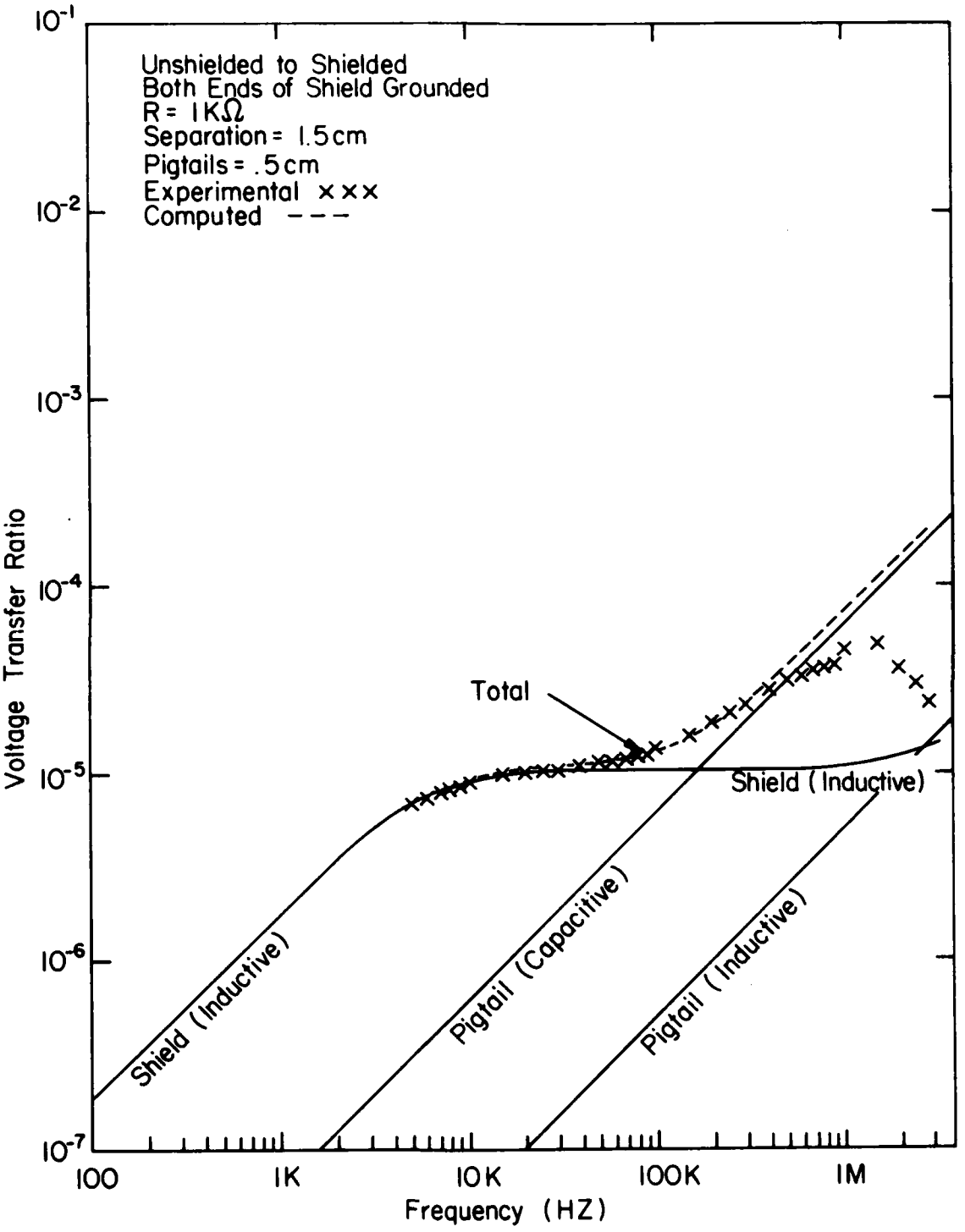
Unshielded to Shielded
Both Ends of Shield Grounded
R = 1KΩ
Separation = 1.5cm
Pigtails = .5cm
Experimental ×××
Computed – – –
Voltage Transfer Ratio
10⁻¹
10⁻²
10⁻³
10⁻⁴
10⁻⁵
10⁻⁶
10⁻⁷
Total
Shield (Inductive)
Shield (Inductive)
Pigtail (Capacitive)
Pigtail (Inductive)
100
1K
10K
100K
1M
Frequency (HZ)

Figure C-11

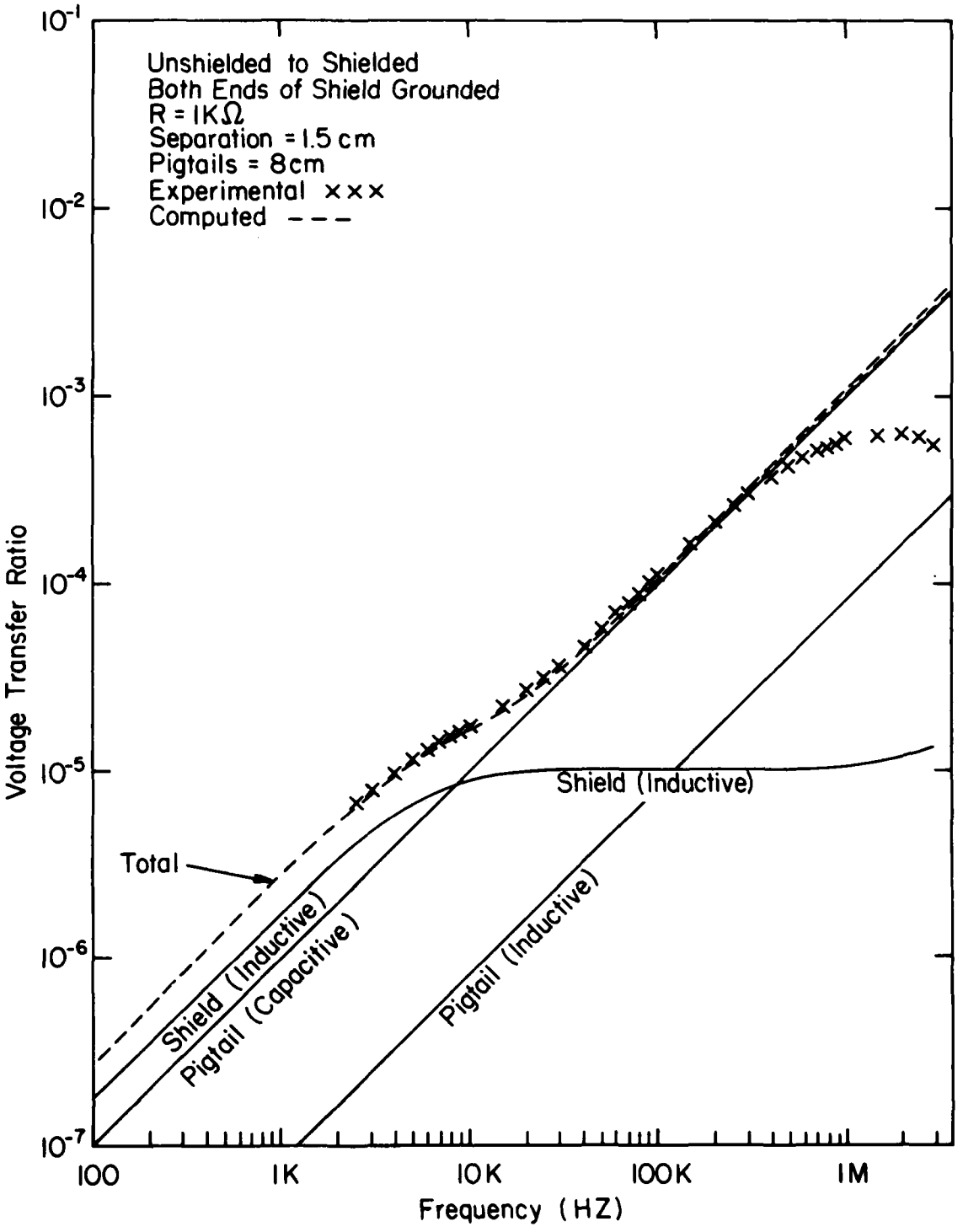
Unshielded to Shielded
Both Ends of Shield Grounded
R = 1KΩ
Separation = 1.5 cm
Pigtails = 8cm
Experimental ×××
Computed – – –
Voltage Transfer Ratio
10-1
10-2
10-3
10-4
10-5
10-6
10-7
Total
Shield (Inductive)
Pigtail (Capacitive)
Shield (Inductive)
Pigtail (Inductive)
100
1K
10K
100K
1M
Frequency (HZ)

Figure C-12.

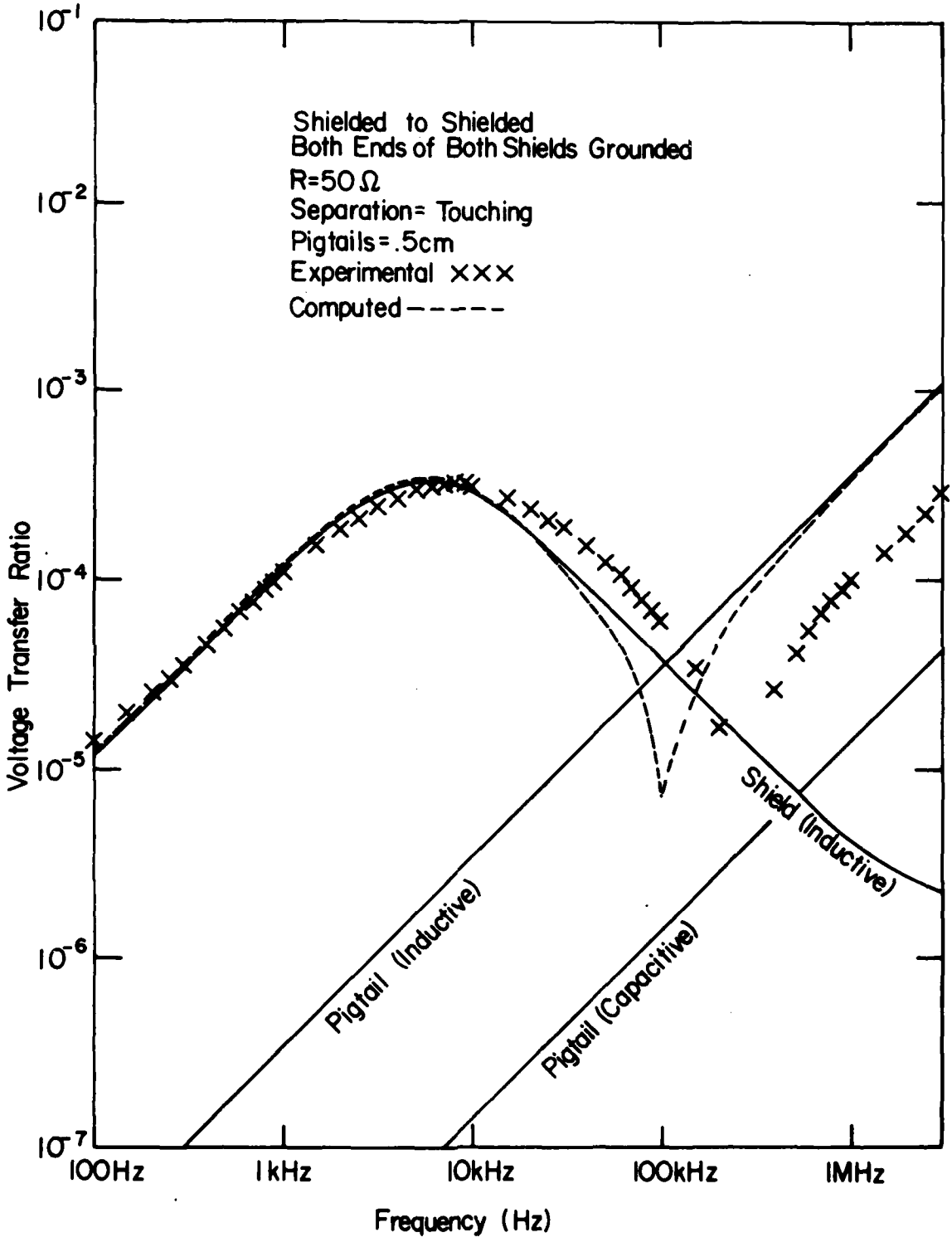
Shielded to Shielded
Both Ends of Both Shields Grounded
R=50Ω
Separation= Touching
Pigtails=.5cm
Experimental ×××
Computed -----
Voltage Transfer Ratio
10⁻¹
10⁻²
10⁻³
10⁻⁴
10⁻⁵
10⁻⁶
10⁻⁷
100Hz
1kHz
10kHz
100kHz
1MHz
Frequency (Hz)
Shield (Inductive)
Pigtail (Inductive)
Pigtail (Capacitive)

Figure C-13.

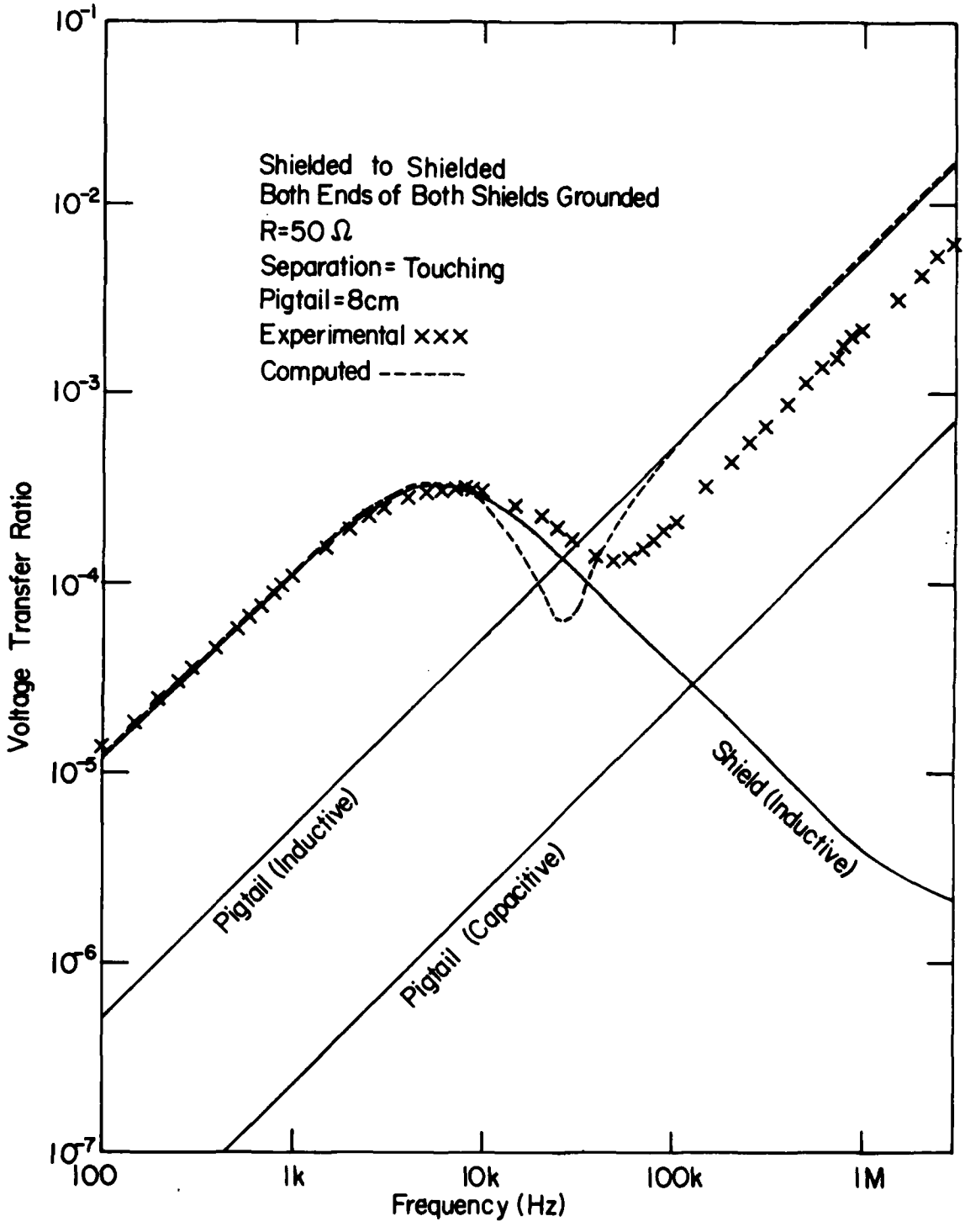
Shielded to Shielded
Both Ends of Both Shields Grounded
R=50 Ω
Separation= Touching
Pigtail=8cm
Experimental ×××
Computed ------
Voltage Transfer Ratio
10⁻¹
10⁻²
10⁻³
10⁻⁴
10⁻⁵
10⁻⁶
10⁻⁷
Pigtail (Inductive)
Pigtail (Capacitive)
Shield (Inductive)
100
1k
10k
100k
1M
Frequency (Hz)

Figure C-14.

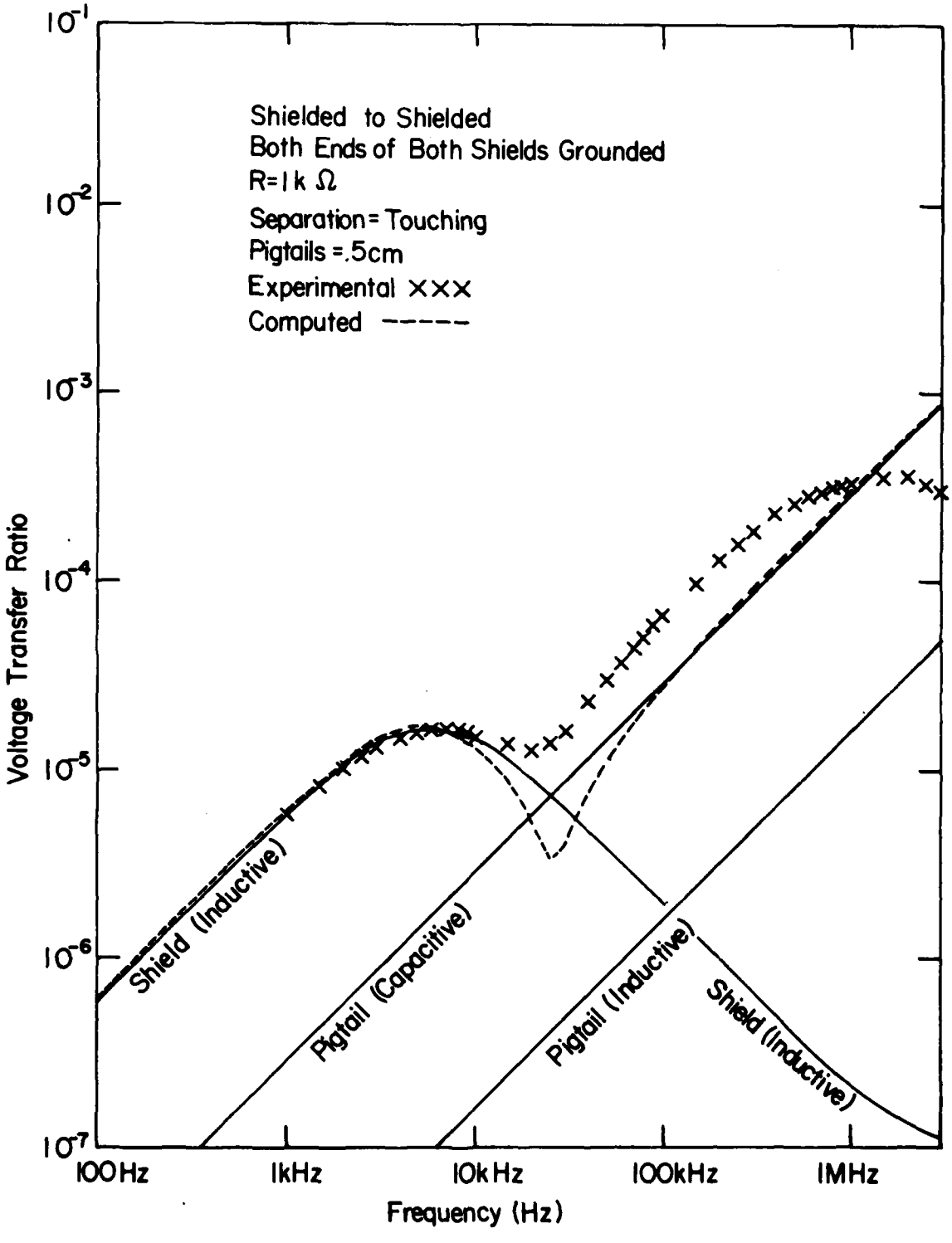
Shielded to Shielded
Both Ends of Both Shields Grounded
R=1 k Ω
Separation = Touching
Pigtails = .5cm
Experimental ×××
Computed -----
Voltage Transfer Ratio
10⁻¹
10⁻²
10⁻³
10⁻⁴
10⁻⁵
10⁻⁶
10⁻⁷
Shield (Inductive)
Pigtail (Capacitive)
Pigtail (Inductive)
Shield (Inductive)
100 Hz
1kHz
10k Hz
100kHz
1MHz
Frequency (Hz)

Figure C-15.

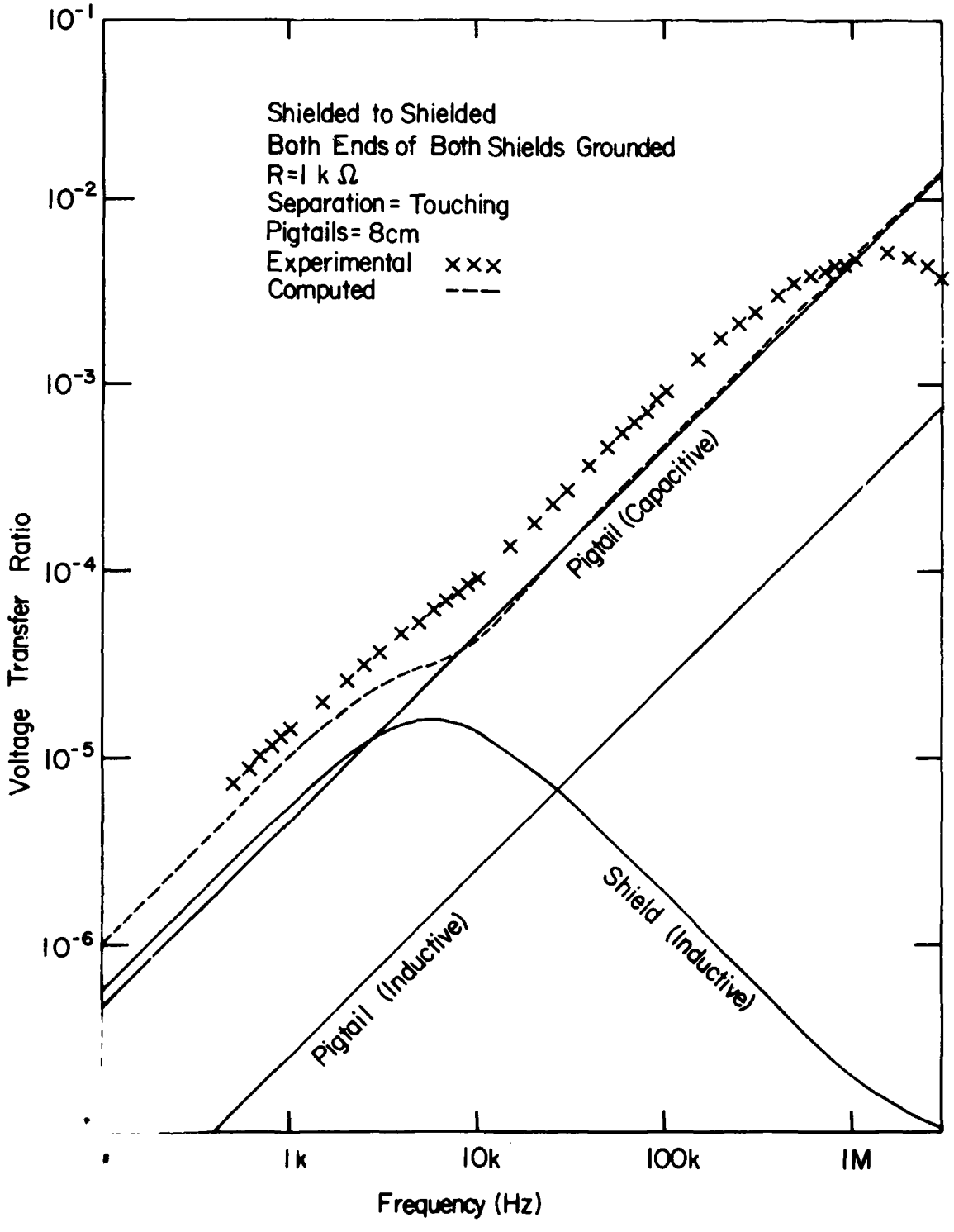
Shielded to Shielded
Both Ends of Both Shields Grounded
R=1 k Ω
Separation = Touching
Pigtails = 8cm
Experimental ×××
Computed ---
Pigtail (Capacitive)
Pigtail (Inductive)
Shield (Inductive)
Voltage Transfer Ratio
Frequency (Hz)
10^-1
10^-2
10^-3
10^-4
10^-5
10^-6
1k
10k
100k
1M

Figure C-16.

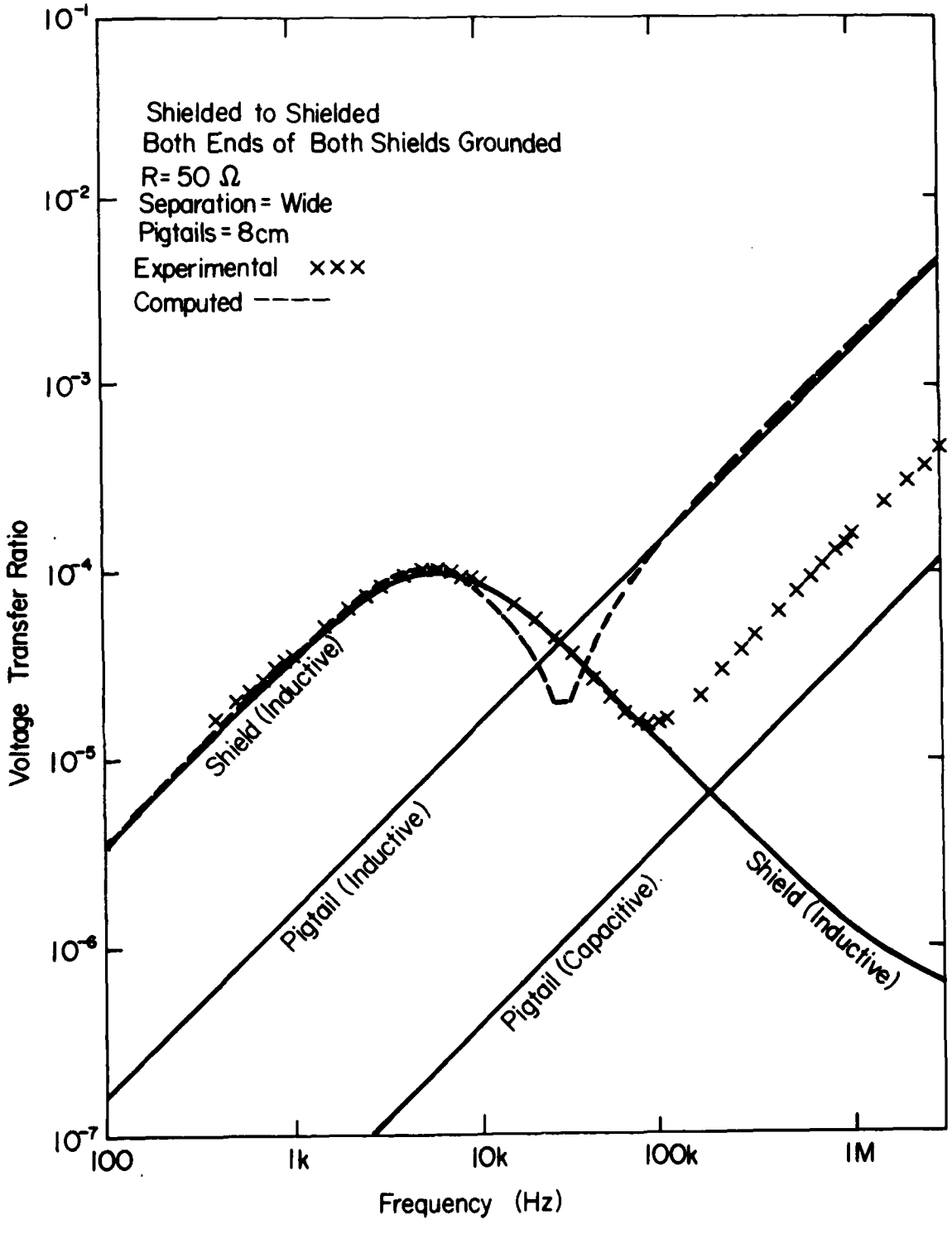
Shielded to Shielded
Both Ends of Both Shields Grounded
R= 50 Ω
Separation = Wide
Pigtails = 8cm
Experimental ×××
Computed ----
Voltage Transfer Ratio
10⁻¹
10⁻²
10⁻³
10⁻⁴
10⁻⁵
10⁻⁶
10⁻⁷
Shield (Inductive)
Pigtail (Inductive)
Pigtail (Capacitive)
Shield (Inductive)
100
1k
10k
100k
1M
Frequency (Hz)

Figure C-17.

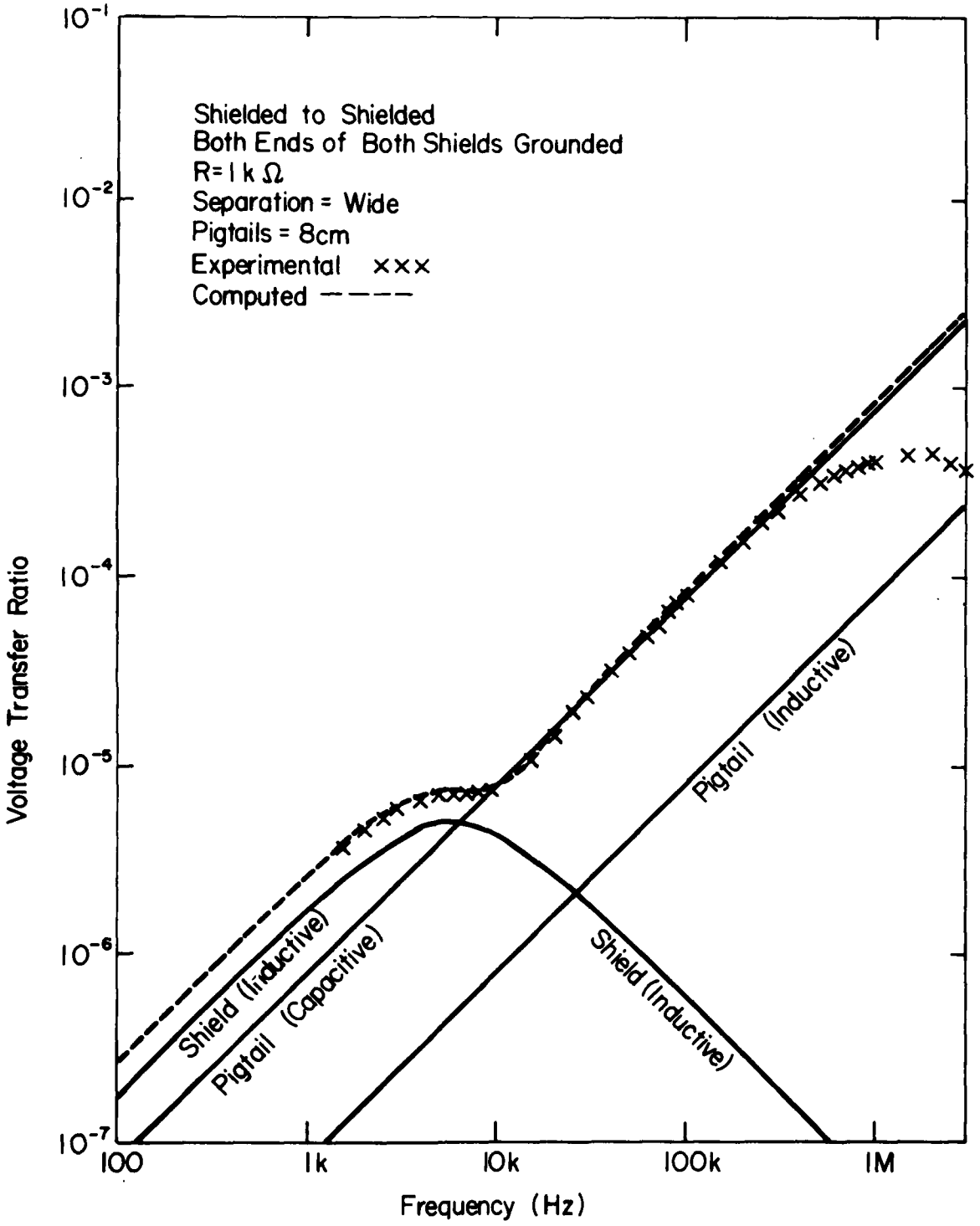
Shielded to Shielded
Both Ends of Both Shields Grounded
R= 1 k Ω
Separation = Wide
Pigtails = 8cm
Experimental ×××
Computed ————
Voltage Transfer Ratio
10⁻¹
10⁻²
10⁻³
10⁻⁴
10⁻⁵
10⁻⁶
10⁻⁷
100
1k
10k
100k
1M
Frequency (Hz)
Shield (Inductive)
Pigtail (Capacitive)
Pigtail (Inductive)
Shield (Inductive)

Figure C-18.

APPENDIX D

Fig.	Configuration	Ω	Separation	Grounding	Pigtails	Page
D-1	US	50Ω	Touching	SS,OS,SO,OO	0.5	178
D-2	"	"	"	"	3.0	179
D-3	"	"	"	"	8.0	180
D-4	"	"	Wide	"	0.5	181
D-5	"	"	"	"	3.0	182
D-6	"	"	"	"	8.0	183
D-7	"	1kΩ	Touching	"	0.5	184
D-8	"	"	"	"	3.0	185
D-9	"	"	"	"	8.0	186
D-10	"	"	Wide	"	0.5	187
D-11	"	"	"	"	3.0	188
D-12	"	"	"	"	8.0	189
D-13	SU	50Ω	Wide	"	0.5	190
D-14	"	"	"	"	8.0	191
D-15	"	1kΩ	"	"	0.5	192
D-16	"	"	"	"	8.0	193

US = unshielded to shielded
SU = shielded to unshielded
O = open (shield ungrounded)
S = short (shield grounded)
First letter denotes source end of line and second letter denotes load end of line. For example, SO denotes that the shield is grounded at the source end and ungrounded at the load end.

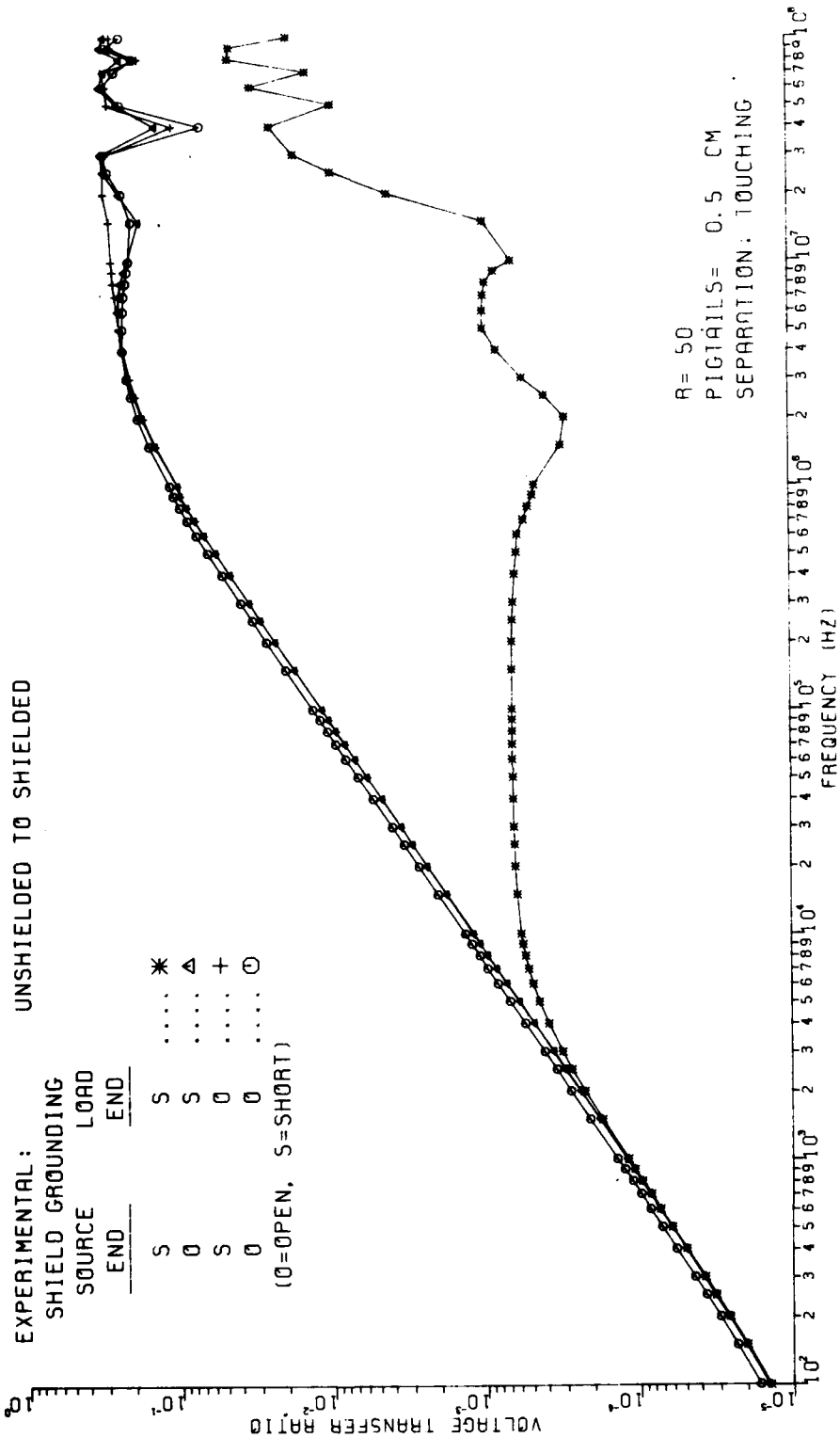
EXPERIMENTAL: UNSHIELDED TO SHIELDED
SHIELD GROUNDING
SOURCE END
LOAD END
S S
0 S
S 0
0 0
(0=OPEN, S=SHORT)
R= 50
PIGTAILS= 0.5 CM
SEPARATION: TOUCHING
VOLTAGE TRANSFER RATIO
FREQUENCY (HZ)

Figure D-1.

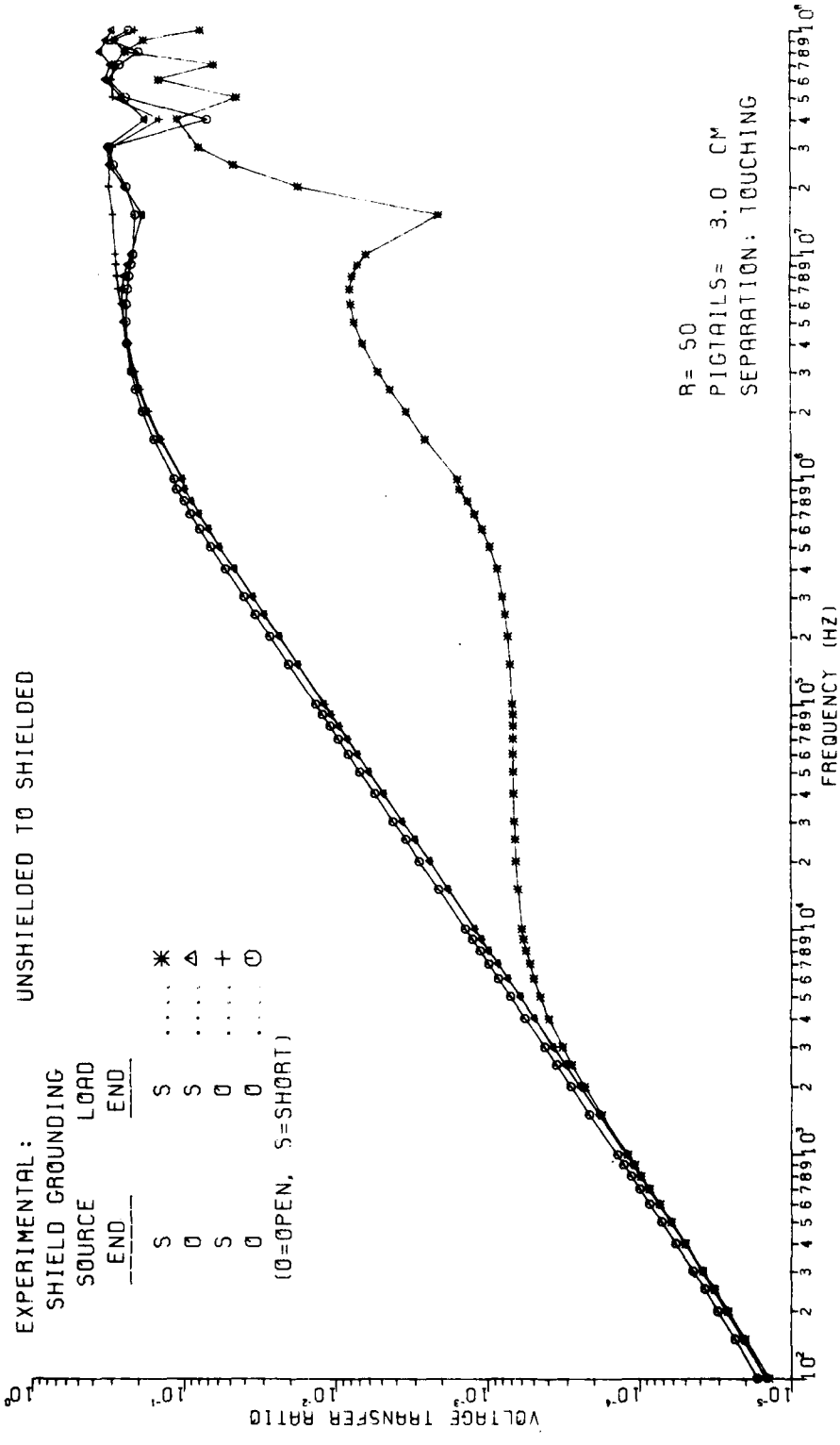
EXPERIMENTAL:
UNSHIELDED TO SHIELDED
SHIELD GROUNDING
SOURCE END
LOAD END
S S
0 S
S 0
0 0
(0=OPEN, S=SHORT)
R= 50
PIGTAILS= 3.0 CM
SEPARATION: TOUCHING
VOLTAGE TRANSFER RATIO
FREQUENCY (HZ)

Figure D-2.

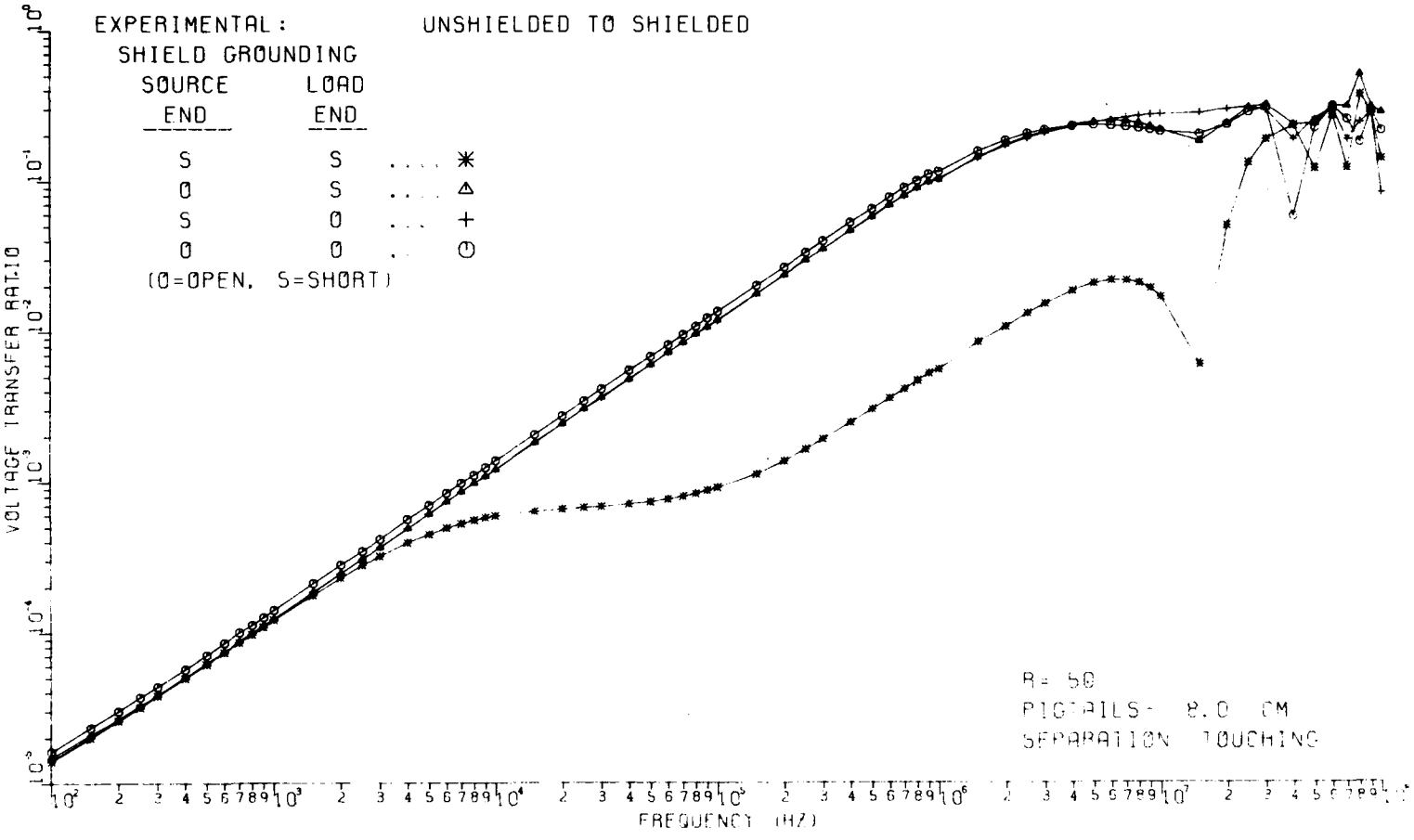
EXPERIMENTAL :
UNSHIELDED TO SHIELDED
SHIELD GROUNDING
SOURCE END
LOAD END
S S
0 S
S 0
0 0
(0=OPEN, S=SHORT)
VOLTAGE TRANSFER RATIO
FREQUENCY (HZ)
R= 50
PIGTAILS- 8.0 CM
SEPARATION TOUCHING

Figure D-3.

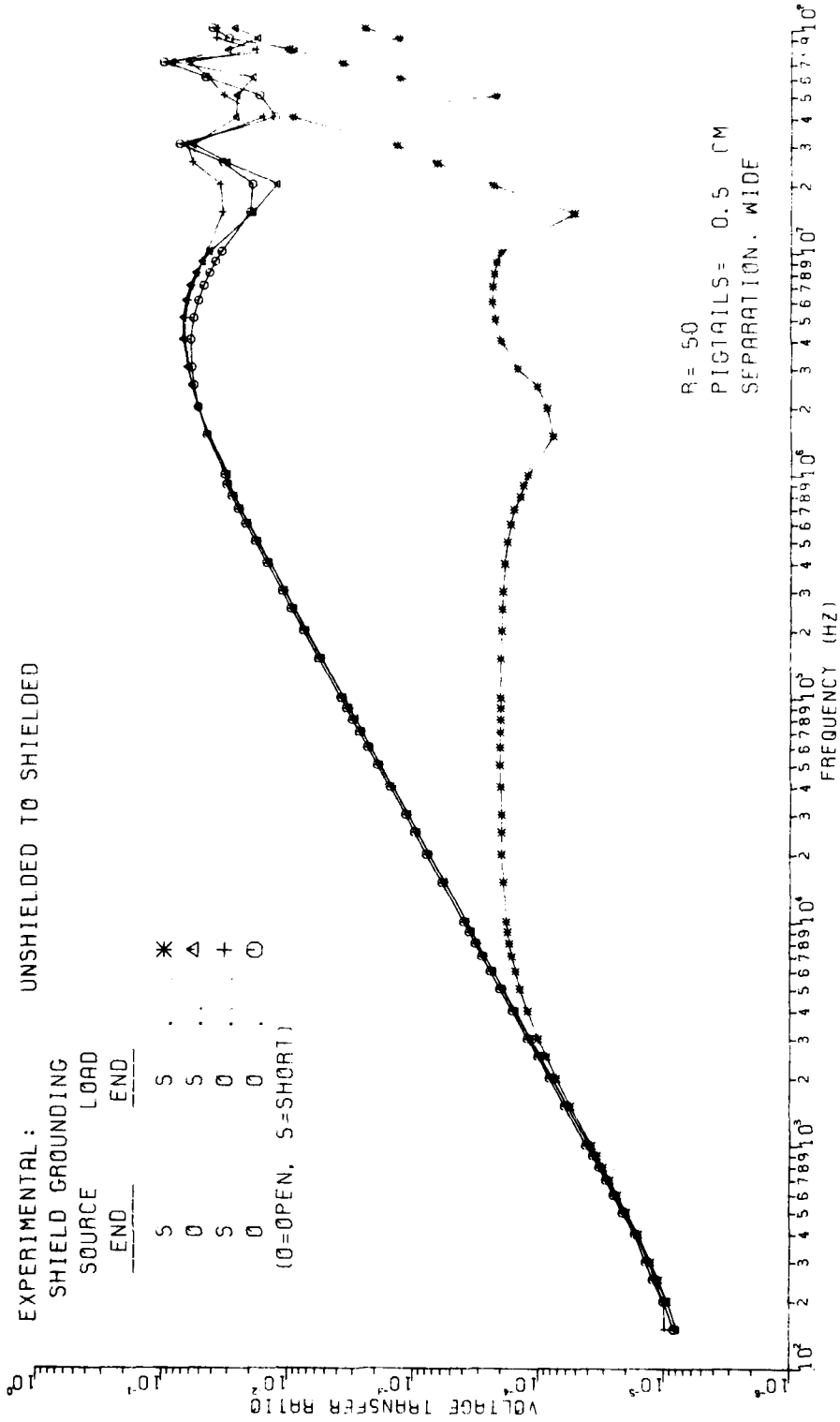
EXPERIMENTAL:
UNSHIELDED TO SHIELDED
SHIELD GROUNDING
SOURCE END
LOAD END
S S
0 S
S 0
0 0
(0=OPEN, S=SHORT)
R= 50
PIGTAILS= 0.5 CM
SEPARATION. WIDE
VOLTAGE TRANSFER RATIO
FREQUENCY (HZ)

Figure D-4.

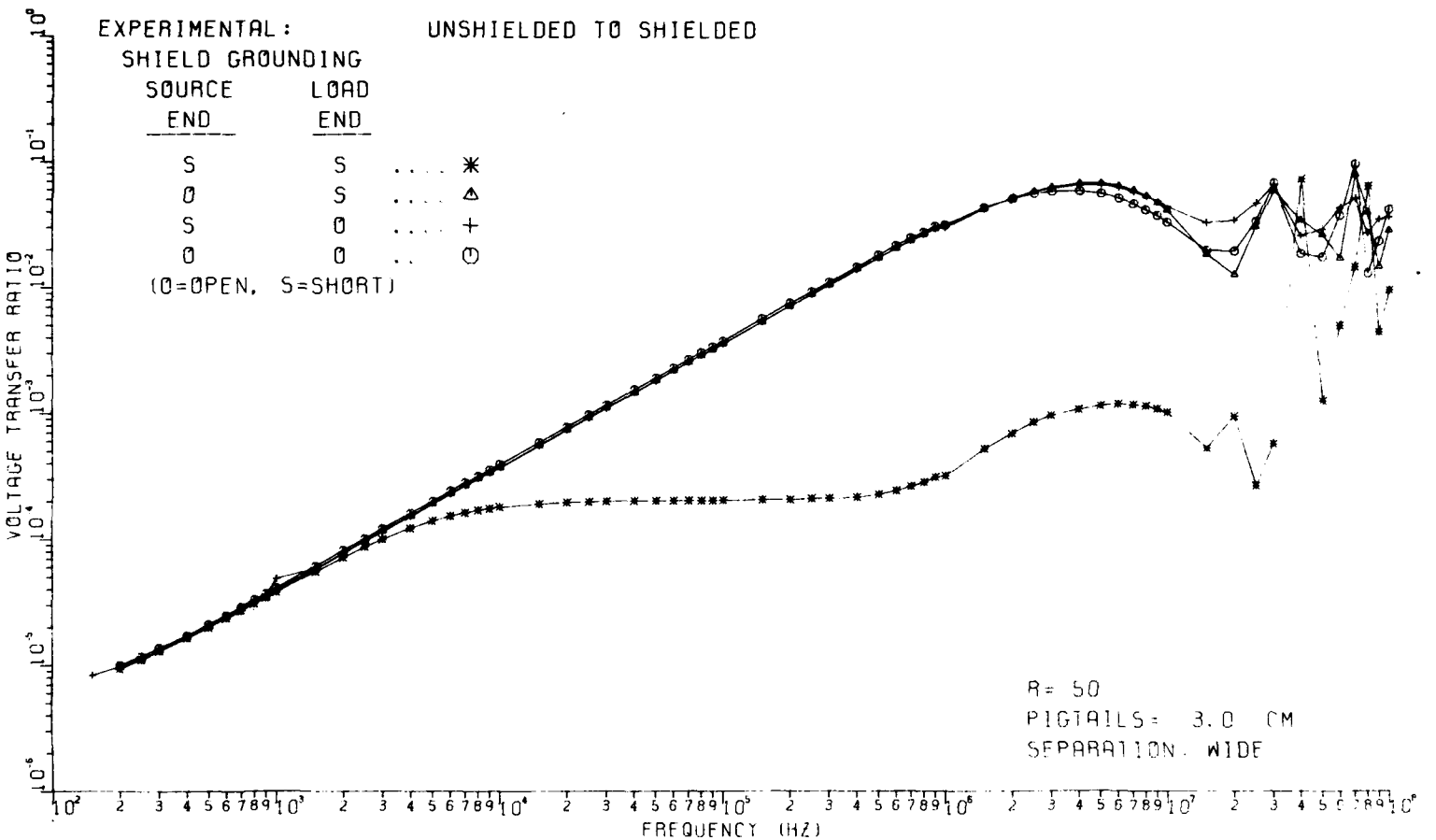
EXPERIMENTAL:
UNSHIELDED TO SHIELDED
SHIELD GROUNDING
SOURCE END
LOAD END
S S
0 S
S 0
0 0
(0=OPEN, S=SHORT)
VOLTAGE TRANSFER RATIO
FREQUENCY (HZ)
R= 50
PIGTAILS= 3.0 CM
SEPARATION: WIDE

Figure D-5.

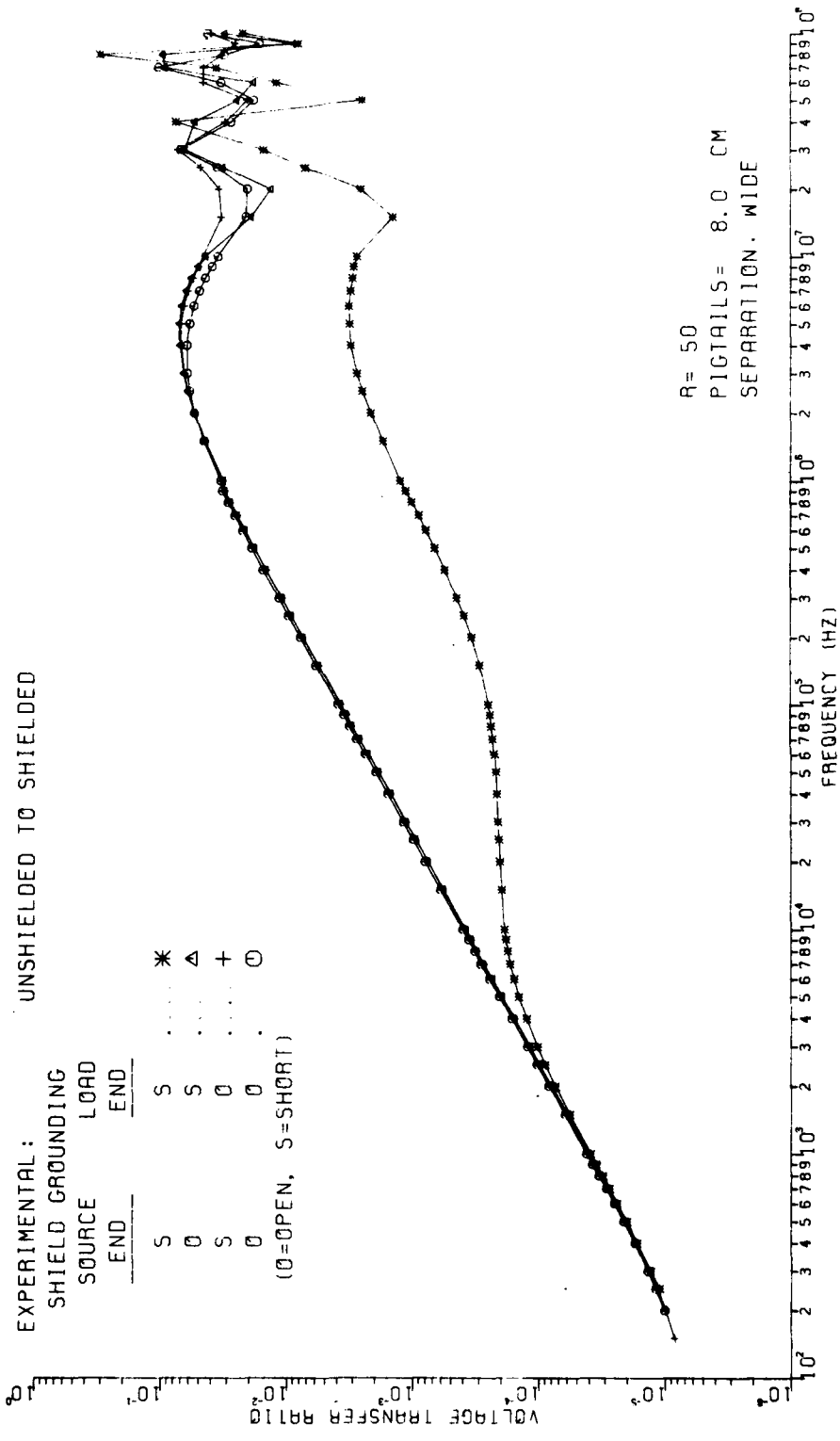
EXPERIMENTAL:
UNSHIELDED TO SHIELDED
SHIELD GROUNDING
SOURCE END
LOAD END
S S
0 S
S 0
0 0
(0=OPEN, S=SHORT)
R= 50
PIGTAILS= 8.0 CM
SEPARATION. WIDE
VOLTAGE TRANSFER RATIO
FREQUENCY (HZ)

Figure D-6.

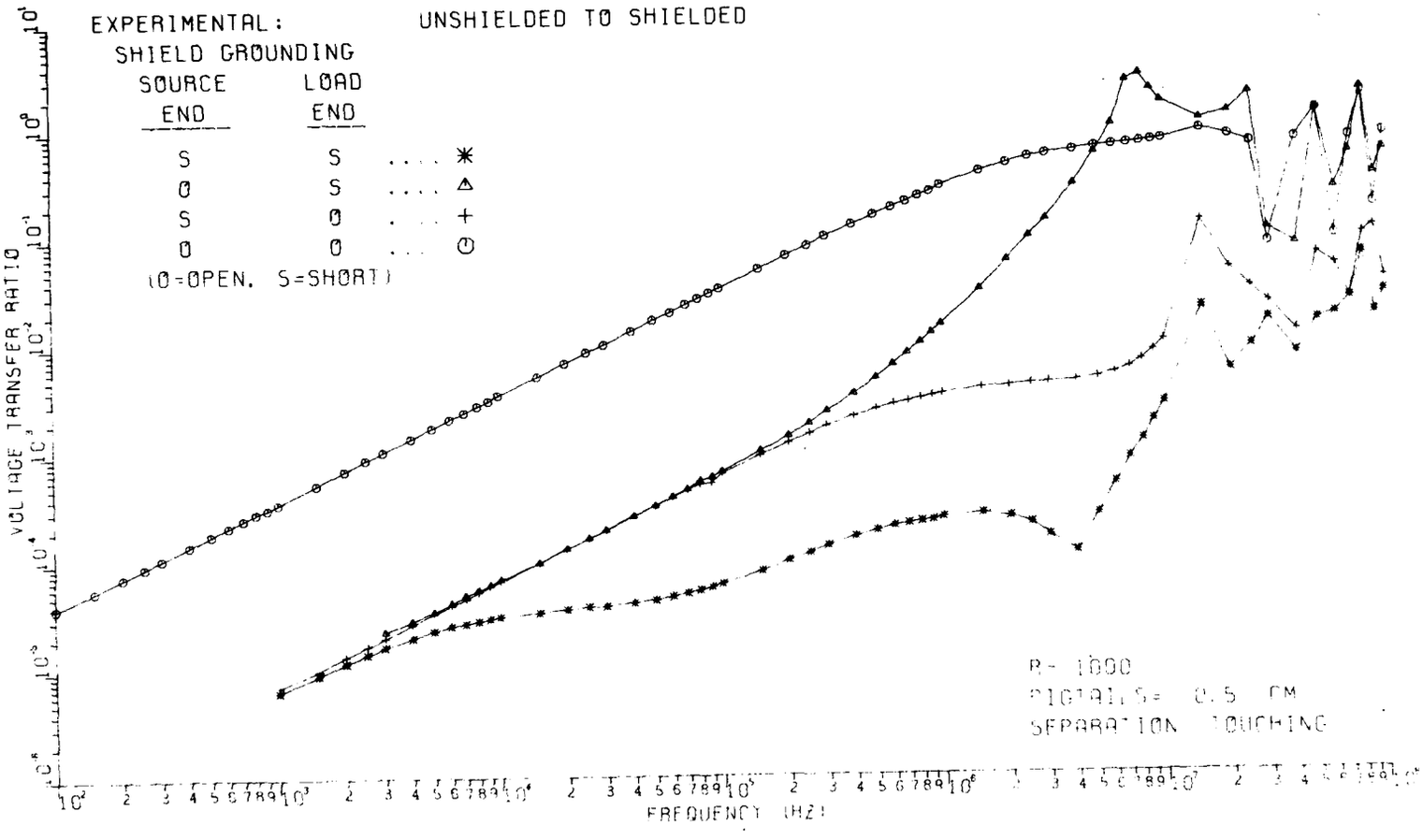
EXPERIMENTAL:
UNSHIELDED TO SHIELDED
SHIELD GROUNDING
SOURCE END
LOAD END
S S
0 S
S 0
0 0
(0=OPEN, S=SHORT)
VOLTAGE TRANSFER RATIO
FREQUENCY (HZ)
R= 1000
SEPARATION TOUCHING

Figure D-7.

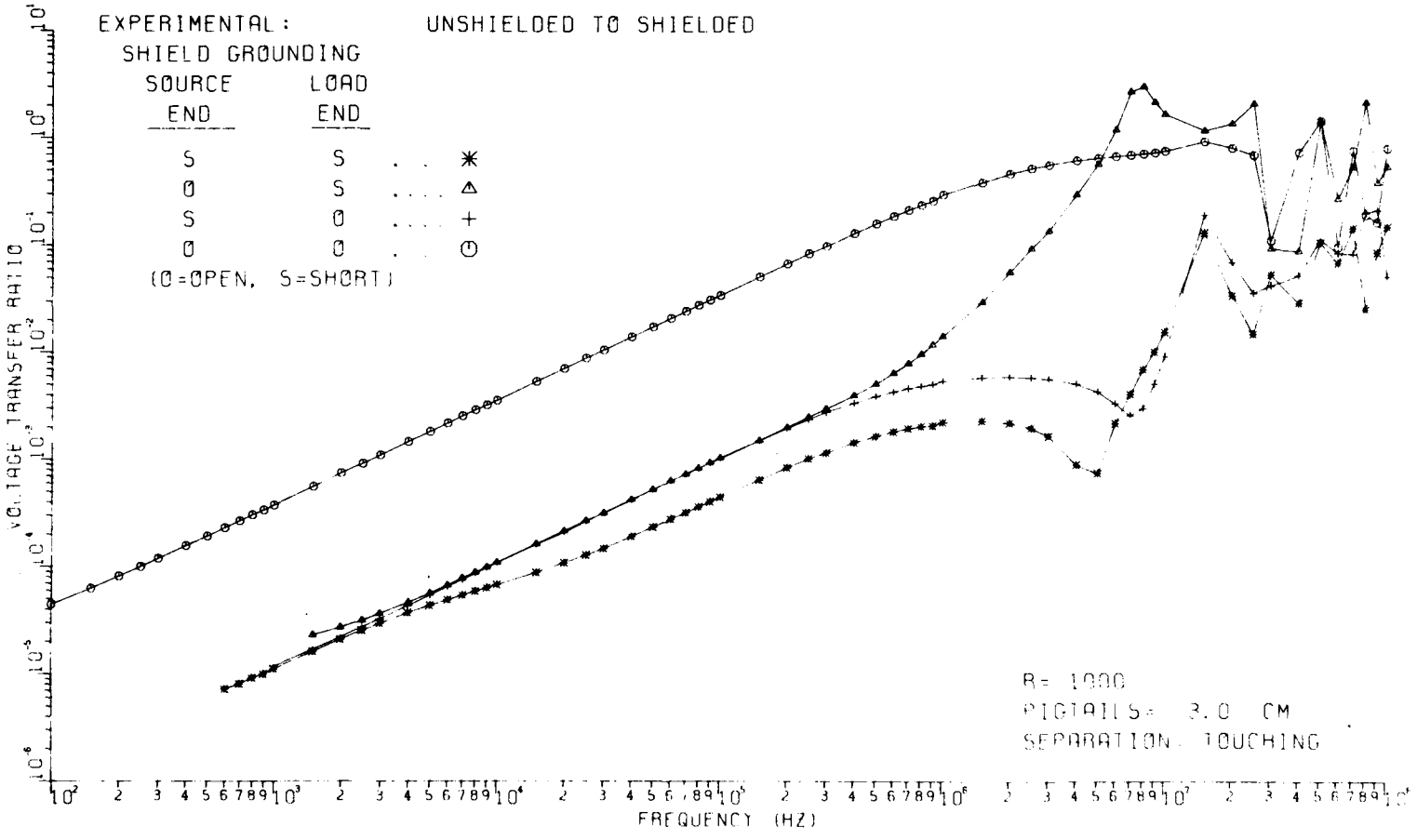
EXPERIMENTAL: UNSHIELDED TO SHIELDED
SHIELD GROUNDING
SOURCE END
LOAD END
S S
0 S
S 0
0 0
(0=OPEN, S=SHORT)
VOLTAGE TRANSFER RATIO
FREQUENCY (HZ)
R= 1000
PIGTAILS= 3.0 CM
SEPARATION: TOUCHING

Figure D-8.

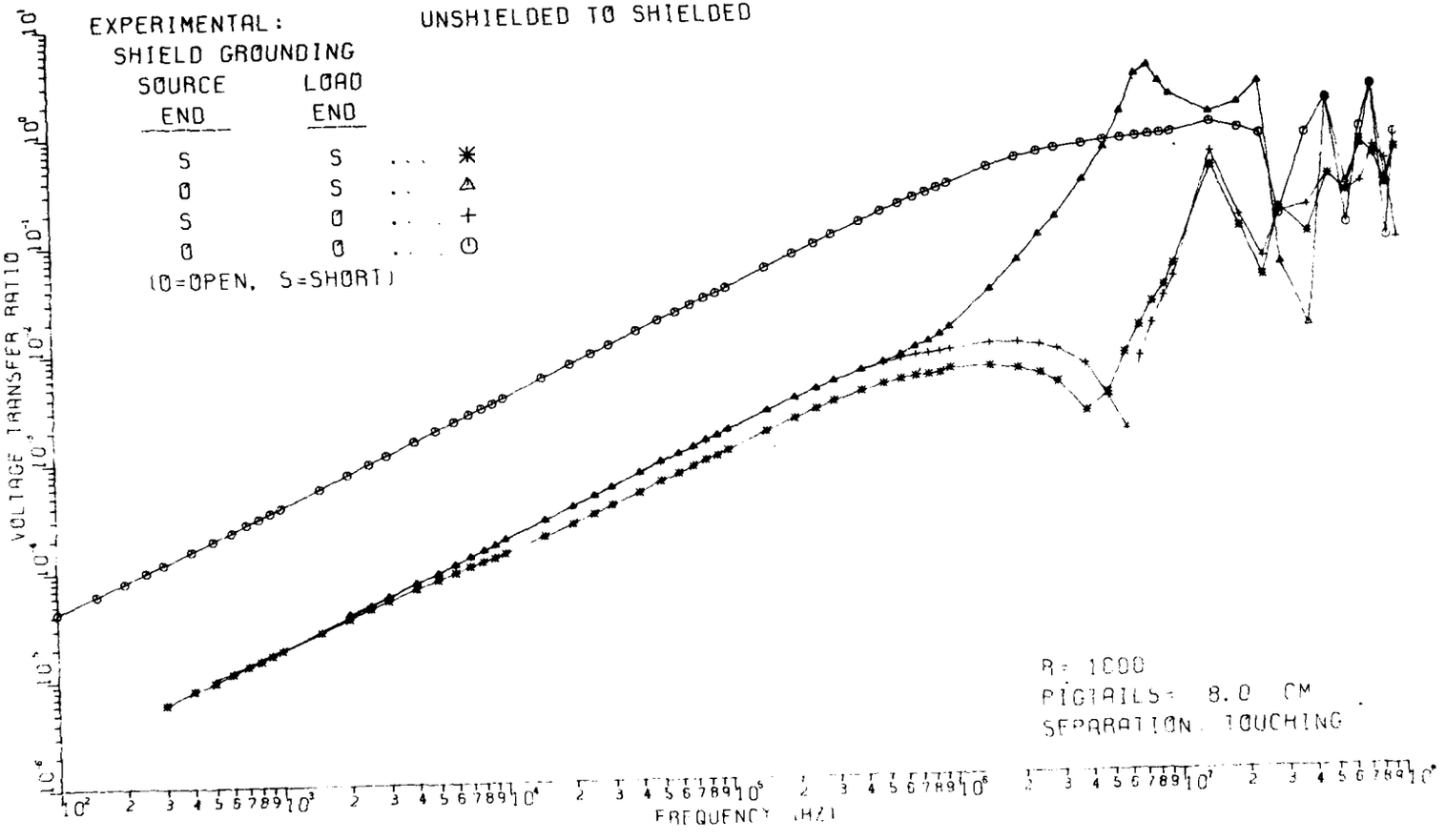
EXPERIMENTAL:
UNSHIELDED TO SHIELDED
SHIELD GROUNDING
SOURCE END
LOAD END
S S
0 S
S 0
0 0
(0=OPEN, S=SHORT)
VOLTAGE TRANSFER RATIO
FREQUENCY (HZ)
R= 1000
PIGTAILS= 8.0 CM
SEPARATION: TOUCHING

Figure D-9.

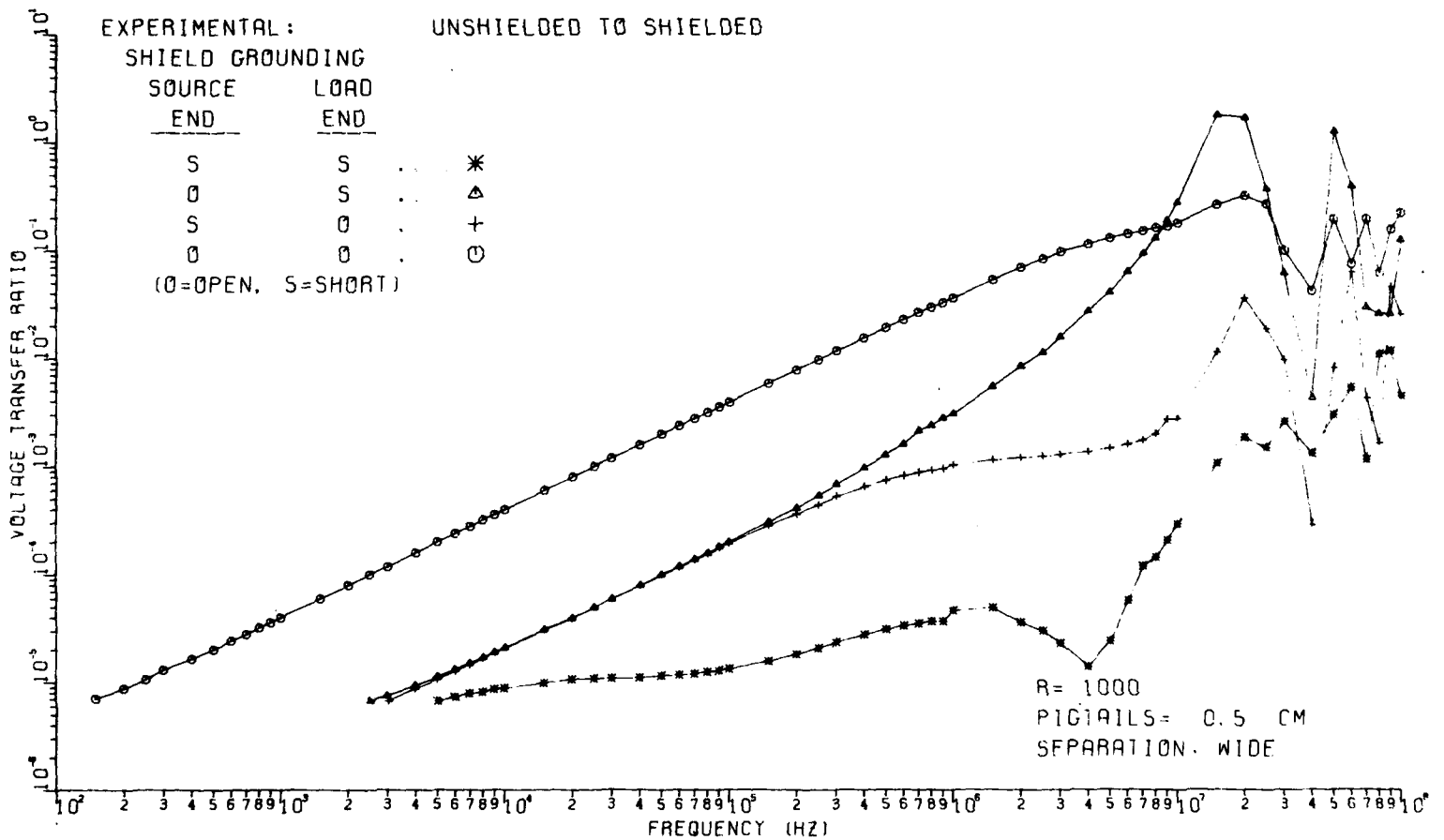
EXPERIMENTAL: UNSHIELDED TO SHIELDED
SHIELD GROUNDING
SOURCE END
LOAD END
S S
0 S
S 0
0 0
(0=OPEN, S=SHORT)
VOLTAGE TRANSFER RATIO
FREQUENCY (HZ)
R= 1000
PIGTAILS= 0.5 CM
SEPARATION. WIDE

Figure D-10.

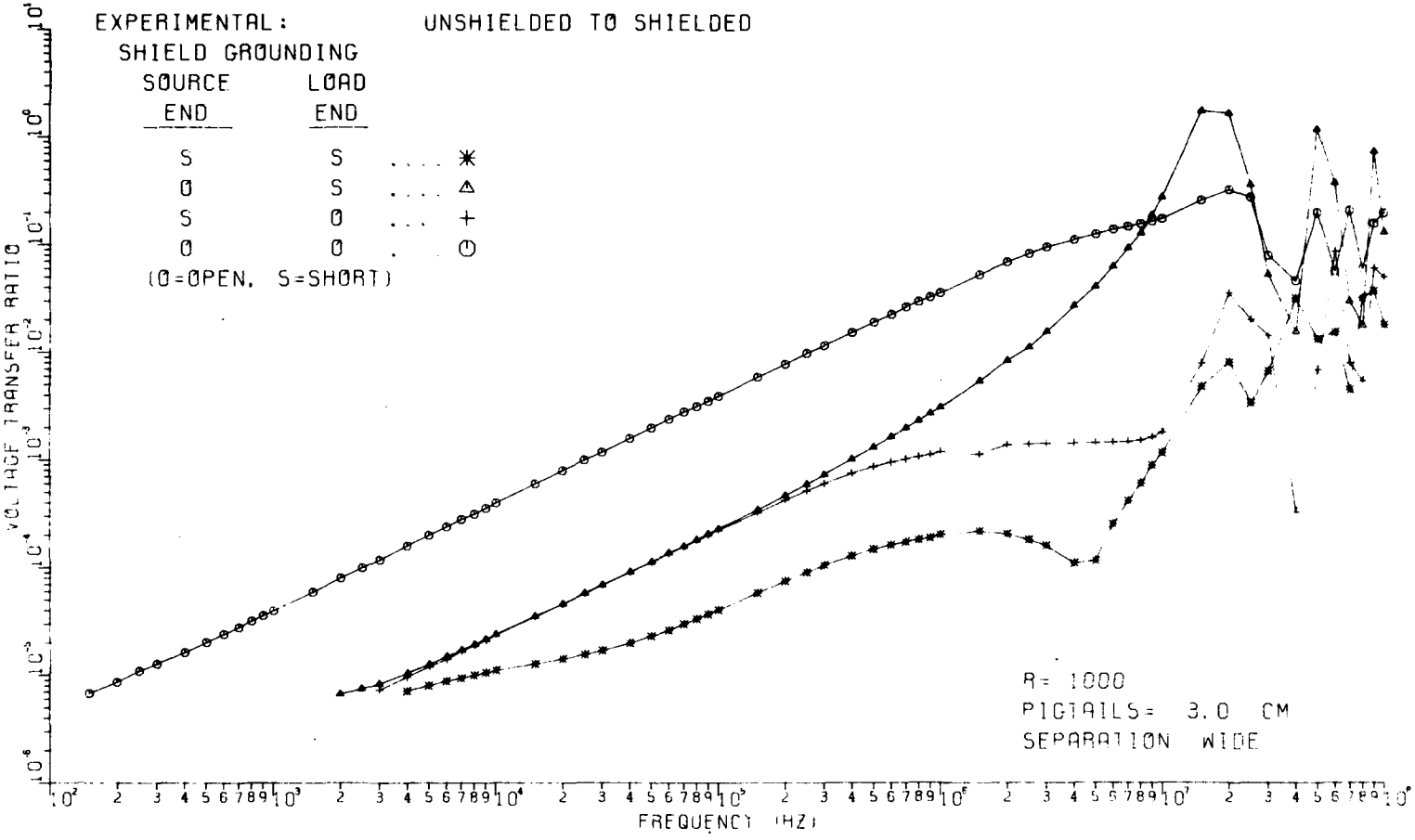
EXPERIMENTAL: UNSHIELDED TO SHIELDED
SHIELD GROUNDING
SOURCE END
LOAD END
S S
0 S
S 0
0 0
(0=OPEN, S=SHORT)
R= 1000
PIGTAILS= 3.0 CM
SEPARATION WIDE
FREQUENCY (HZ)

Figure D-11.

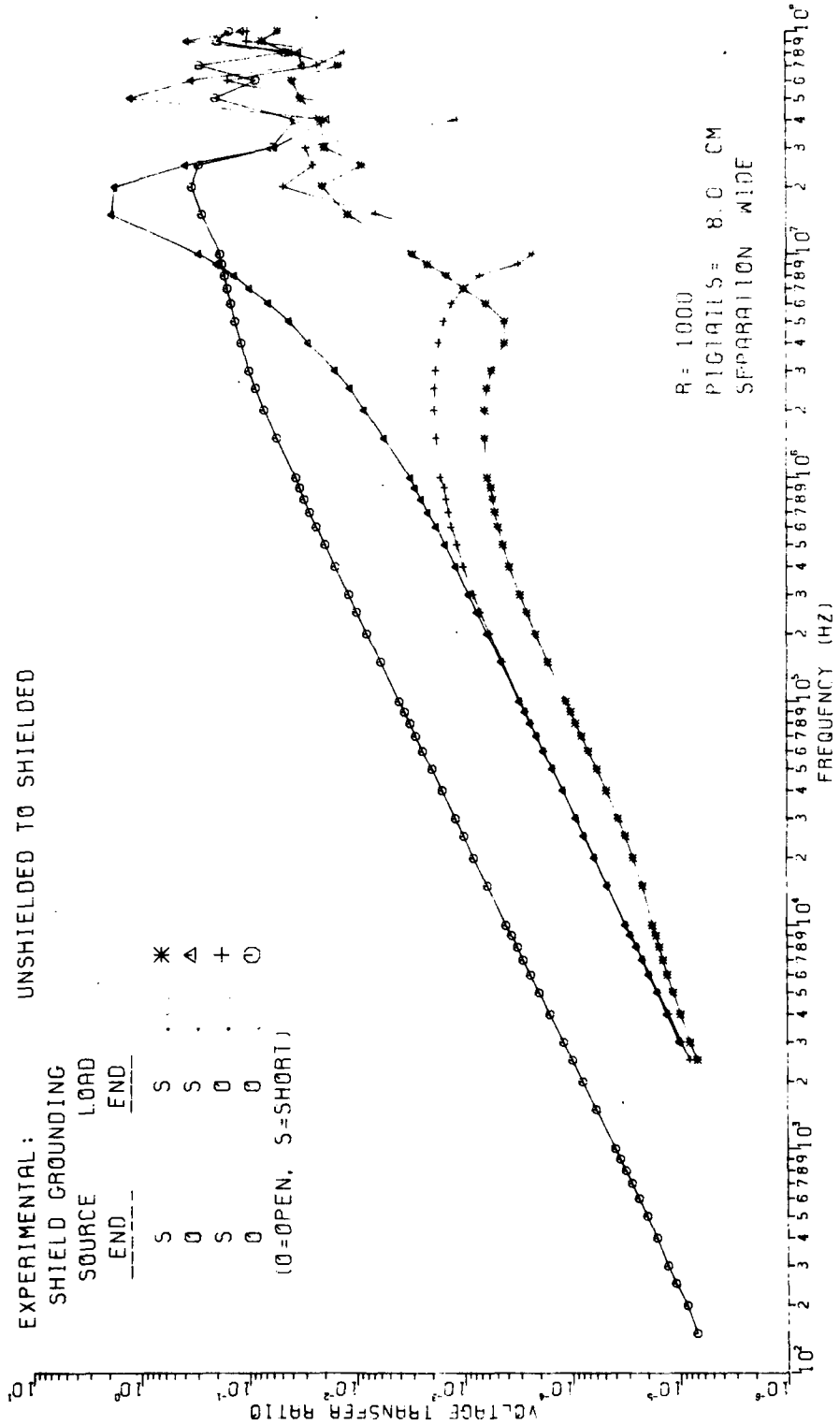
EXPERIMENTAL:
UNSHIELDED TO SHIELDED
SHIELD GROUNDING
SOURCE END
LOAD END
S S *
0 S Δ
S 0 +
0 0 ⊙
(0=OPEN, S=SHORT)
R= 1000
PICKUP SEPARATION WIDE
8.0 CM
VOLTAGE TRANSFER RATIO
FREQUENCY (HZ)

Figure D-12.

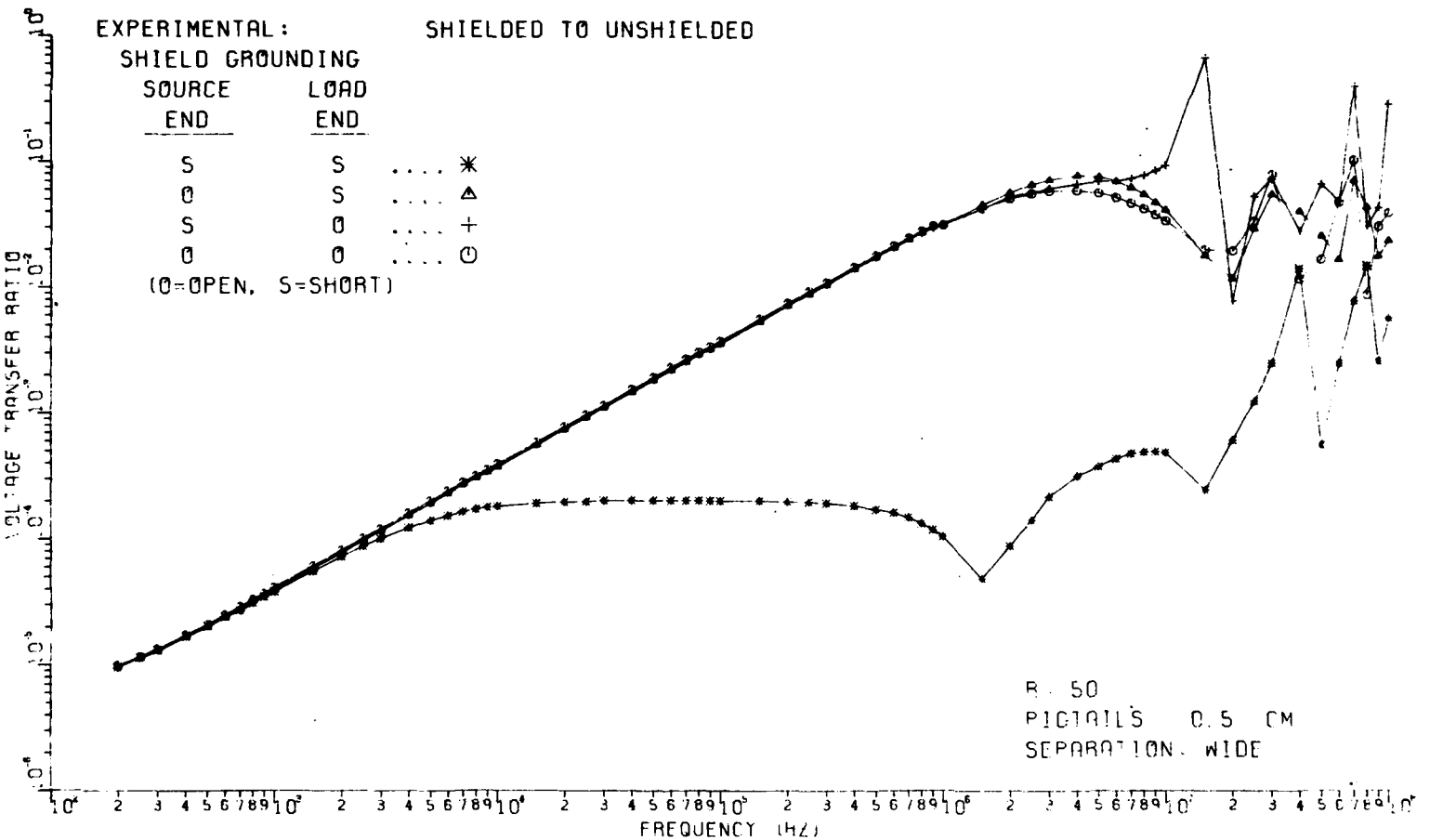
EXPERIMENTAL:
SHIELDED TO UNSHIELDED
SHIELD GROUNDING
SOURCE END
LOAD END
S S .... *
0 S .... Δ
S 0 .... +
0 0 .... ○
(0=OPEN, S=SHORT)
R = 50
PIGTAILS 0.5 CM
SEPARATION, WIDE
FREQUENCY (HZ)

Figure D-13.

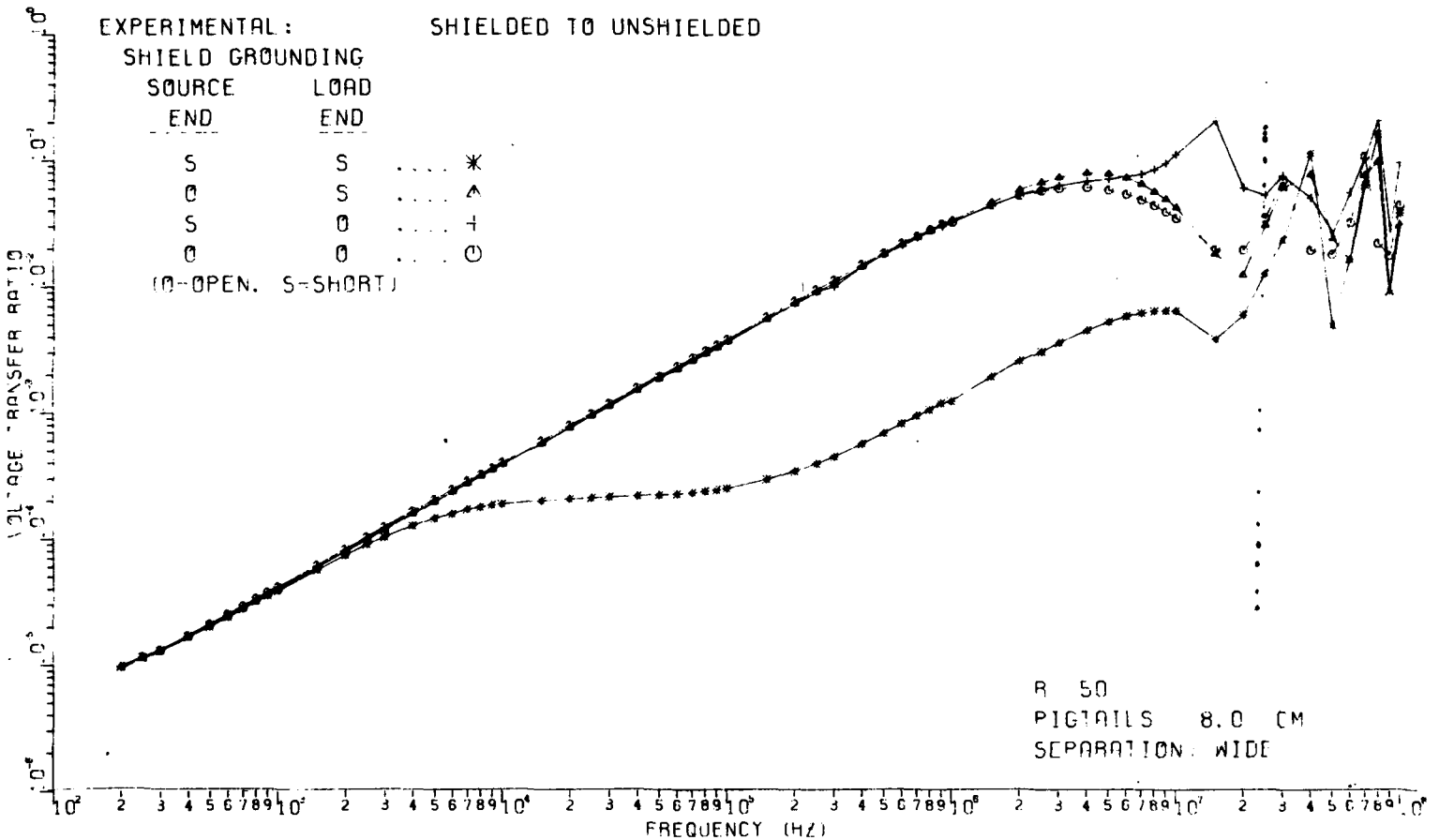
EXPERIMENTAL:
SHIELDED TO UNSHIELDED
SHIELD GROUNDING
SOURCE END
LOAD END
S S
0 S
S 0
0 0
(0-OPEN, S-SHORT)
R 50
PIGTAILS 8.0 CM
SEPARATION: WIDE
FREQUENCY (HZ)

Figure D-14.

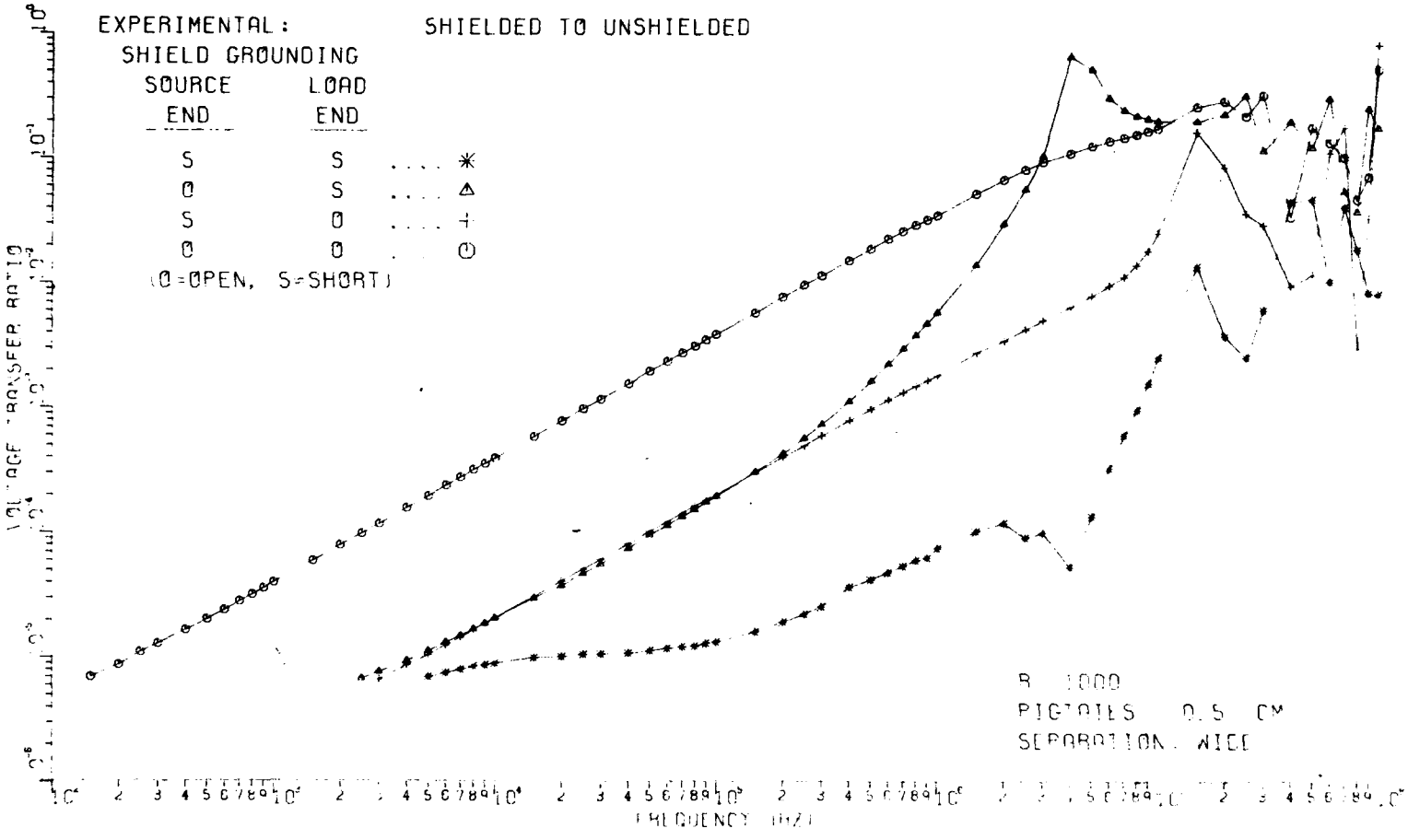
EXPERIMENTAL:
SHIELD GROUNDING
SOURCE END
LOAD END
S S
0 S
S 0
0 0
(0=OPEN, S=SHORT)
SHIELDED TO UNSHIELDED
R 1000
PIGTAILS 0.5 CM
SEPARATION WIDE
FREQUENCY (HZ)

Figure D-15.

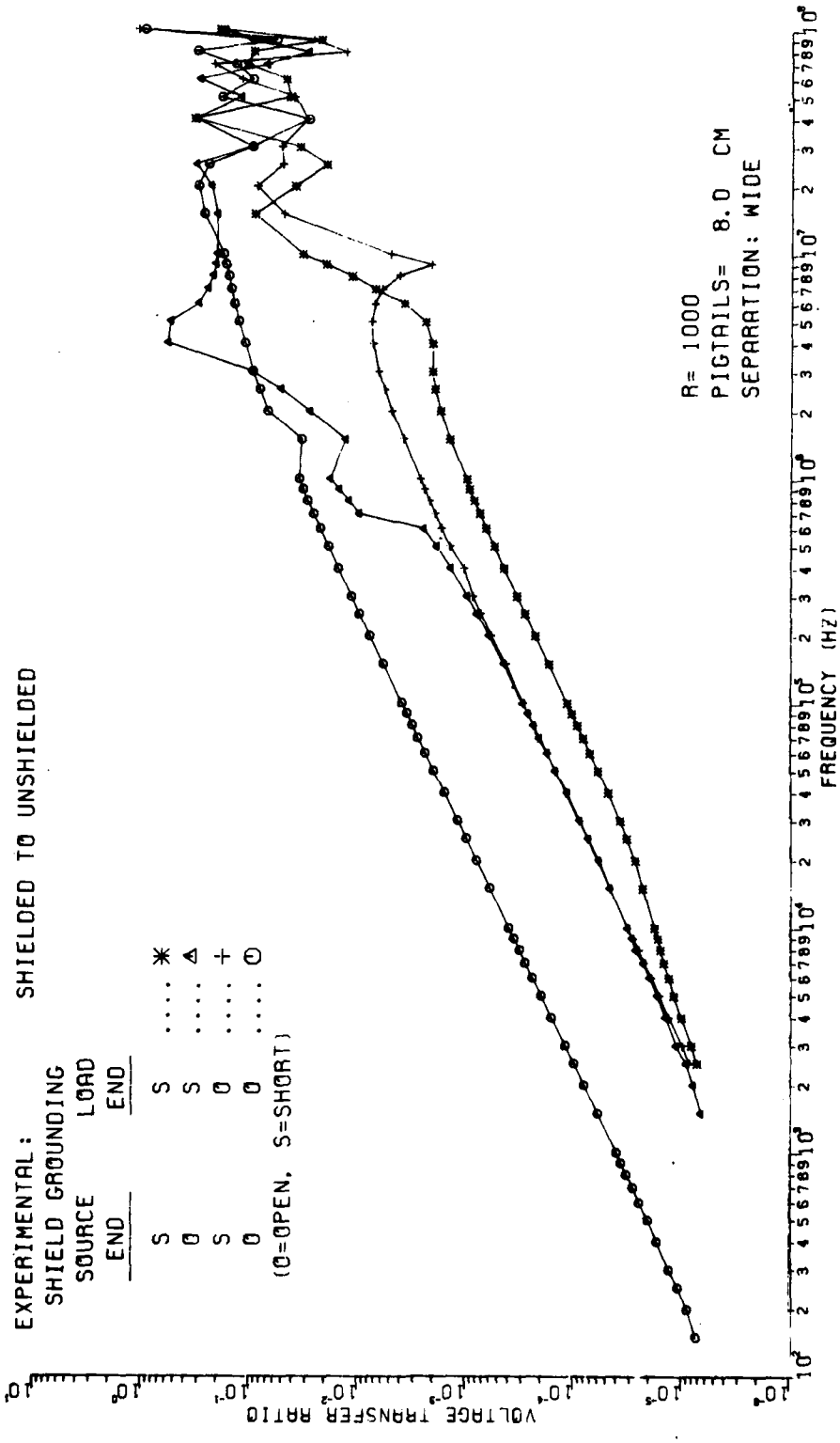
EXPERIMENTAL:
SHIELD GROUNDING
SOURCE END
LOAD END
S S
0 S
S 0
0 0
(0=OPEN, S=SHORT)
SHIELDED TO UNSHIELDED
R= 1000
PIGTAILS= 8.0 CM
SEPARATION: WIDE
VOLTAGE TRANSFER RATIO
FREQUENCY (HZ)

Figure D-16.

APPENDIX E

Fig.	Configuration	Ω	Separation	Grounding	Pigtails	Page
E-1	US	50Ω	Wide	SS	0.5	197
E-2	"	"	"	SO	"	198
E-3	"	"	"	OS	"	199
E-4	"	"	"	OO	"	200
E-5	"	1kΩ	"	SS	"	201
E-6	"	"	"	SO	"	202
E-7	"	"	"	OS	"	203
E-8	"	"	"	OO	"	204
E-9	"	50Ω	"	SS	8.0	205
E-10	"	"	"	SO	"	206
E-11	"	"	"	OS	"	207
E-12	"	"	"	OO	"	208
E-13	"	1kΩ	"	SS	"	209
E-14	"	"	"	SO	"	210
E-15	"	"	"	OS	"	211
E-16	"	"	"	OO	"	212
E-17	"	50Ω	Touching	SS	0.5	213
E-18	"	"	"	SO	"	214
E-19	"	"	"	OS	"	215
E-20	"	"	"	OO	"	216
E-21	"	1kΩ	"	SS	"	217
E-22	"	"	"	SO	"	218
E-23	"	"	"	OS	"	219
E-24	"	"	"	OO	"	220
E-25	"	50Ω	"	SS	8.0	221
E-26	"	"	"	SO	"	222
E-27	"	"	"	OS	"	223
E-28	"	"	"	OO	"	224
E-29	"	1kΩ	"	SS	"	225
E-30	"	"	"	SO	"	226
E-31	"	"	"	OS	"	227
E-32	"	"	"	OO	"	228
E-33	SS	50Ω	"	SS	0.5	229

Fig.	Configuration	Ω	Separation	Grounding	Pigtails	Page
E-34	SS	1kΩ	Touching	SS	0.5	230
E-35	"	50Ω	"	"	8.0	231
E-36	"	1kΩ	"	"	"	232
E-37	"	50Ω	Wide	"	"	233
E-38	"	1kΩ	"	"	"	234

US = unshielded to shielded

SS = shielded to shielded

O = open (shield ungrounded)

S = short (shield grounded)

First letter denotes source end of line and second letter denotes load end of line. For example, SO denotes that the shield is grounded at the source end and ungrounded at the load end.

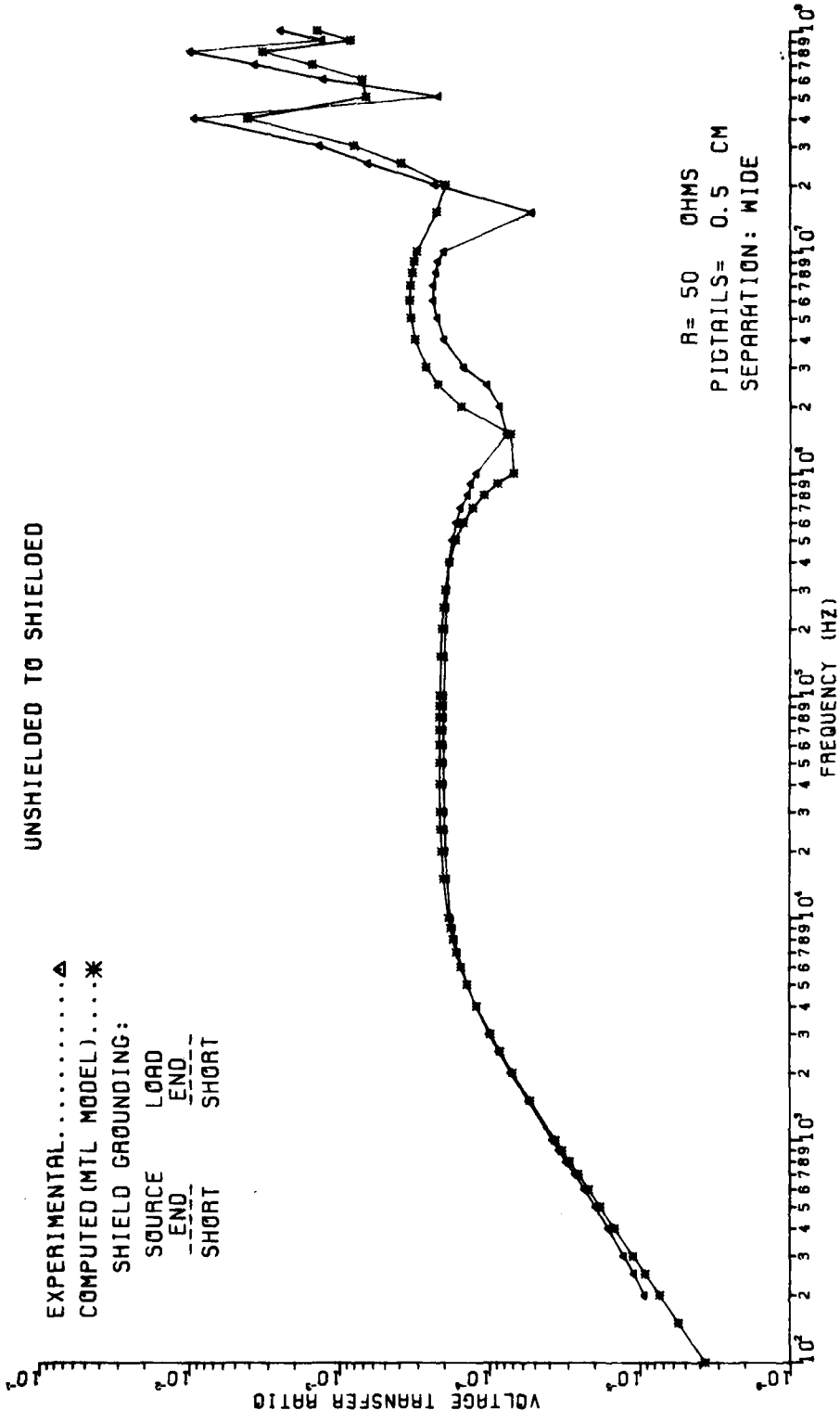
UNSHIELDED TO SHIELDED
EXPERIMENTAL.....Δ
COMPUTED(MTL MODEL)....*
SHIELD GROUNDING:
SOURCE LOAD
END END
SHORT SHORT
R= 50 OHMS
PIGTAILS= 0.5 CM
SEPARATION: WIDE
VOLTAGE TRANSFER RATIO
FREQUENCY (HZ)

Figure E-1.

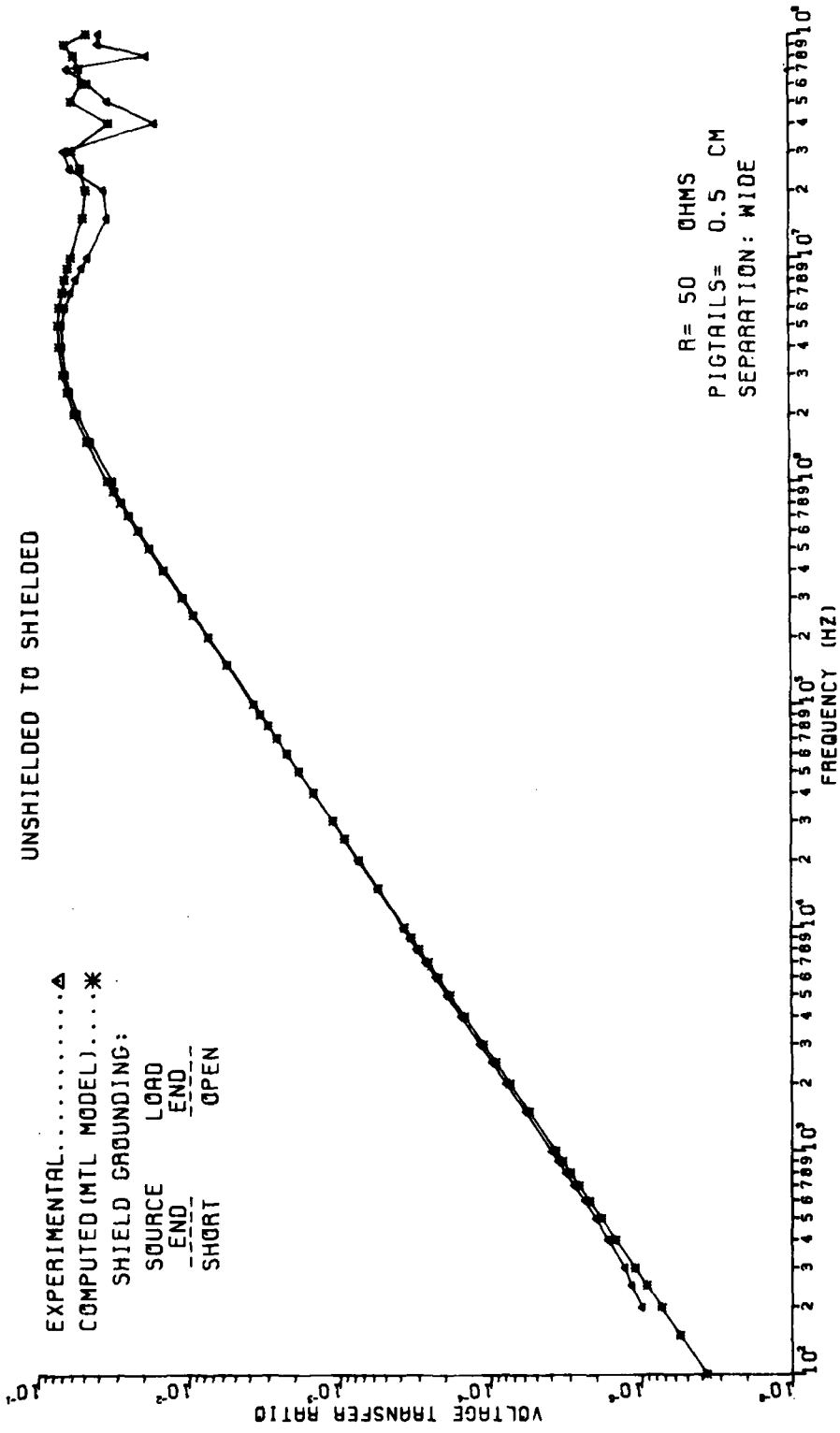
UNSHIELDED TO SHIELDED
EXPERIMENTAL.....Δ
COMPUTED(MTL MODEL)....*
SHIELD GROUNDING:
SOURCE LOAD
END END
SHORT OPEN
R= 50 OHMS
PIGTAILS= 0.5 CM
SEPARATION: WIDE
VOLTAGE TRANSFER RATIO
FREQUENCY (HZ)

Figure E-2.

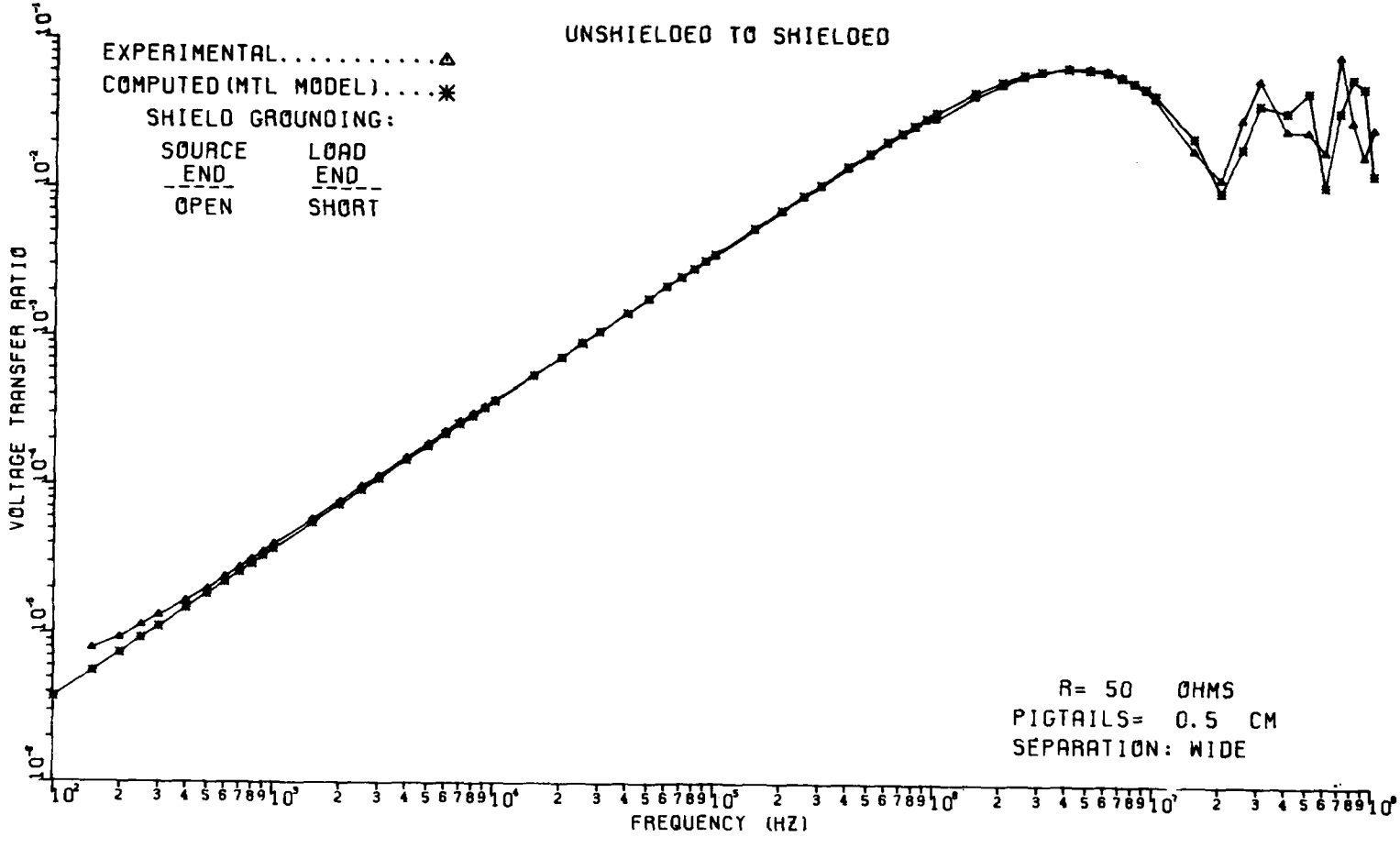
UNSHIELDED TO SHIELDED
EXPERIMENTAL.....△
COMPUTED (MTL MODEL)....✳
SHIELD GROUNDING:
SOURCE END
OPEN
LOAD END
SHORT
VOLTAGE TRANSFER RATIO
FREQUENCY (HZ)
R= 50 OHMS
PIGTAILS= 0.5 CM
SEPARATION: WIDE

Figure E-3.

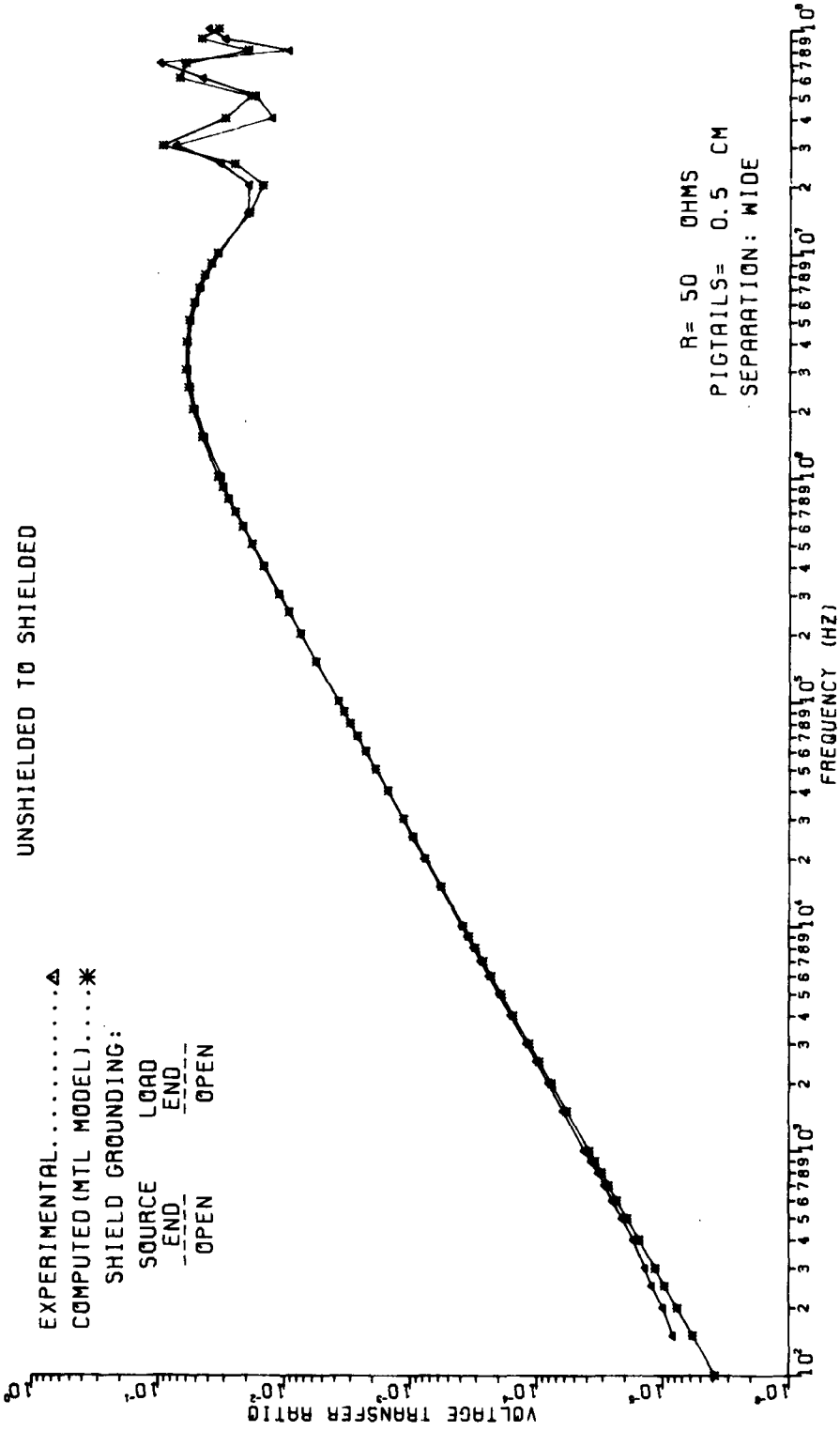
UNSHIELDED TO SHIELDED
EXPERIMENTAL.....Δ
COMPUTED(MTL MODEL)....*
SHIELD GROUNDING:
SOURCE END
OPEN
LOAD END
OPEN
R= 50 OHMS
PIGTAILS= 0.5 CM
SEPARATION: WIDE
VOLTAGE TRANSFER RATIO
FREQUENCY (HZ)

Figure E-4.

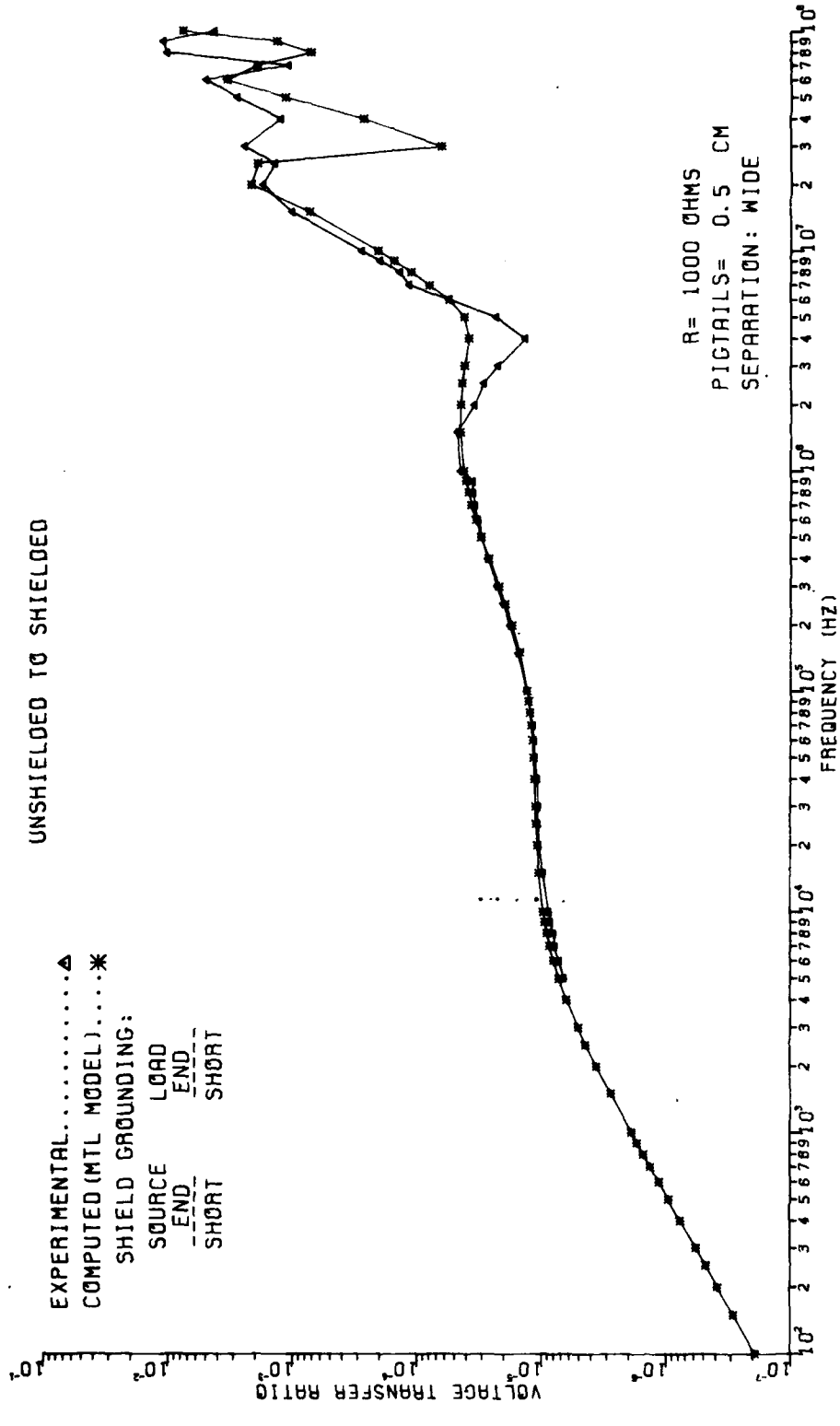
UNSHIELDED TO SHIELDED
EXPERIMENTAL.....Δ
COMPUTED(MTL MODEL).....*
SHIELD GROUNDING:
SOURCE END
LOAD END
SHORT
SHORT
R= 1000 OHMS
PIGTAILS= 0.5 CM
SEPARATION: WIDE
VOLTAGE TRANSFER RATIO
FREQUENCY (HZ)

Figure E-5.

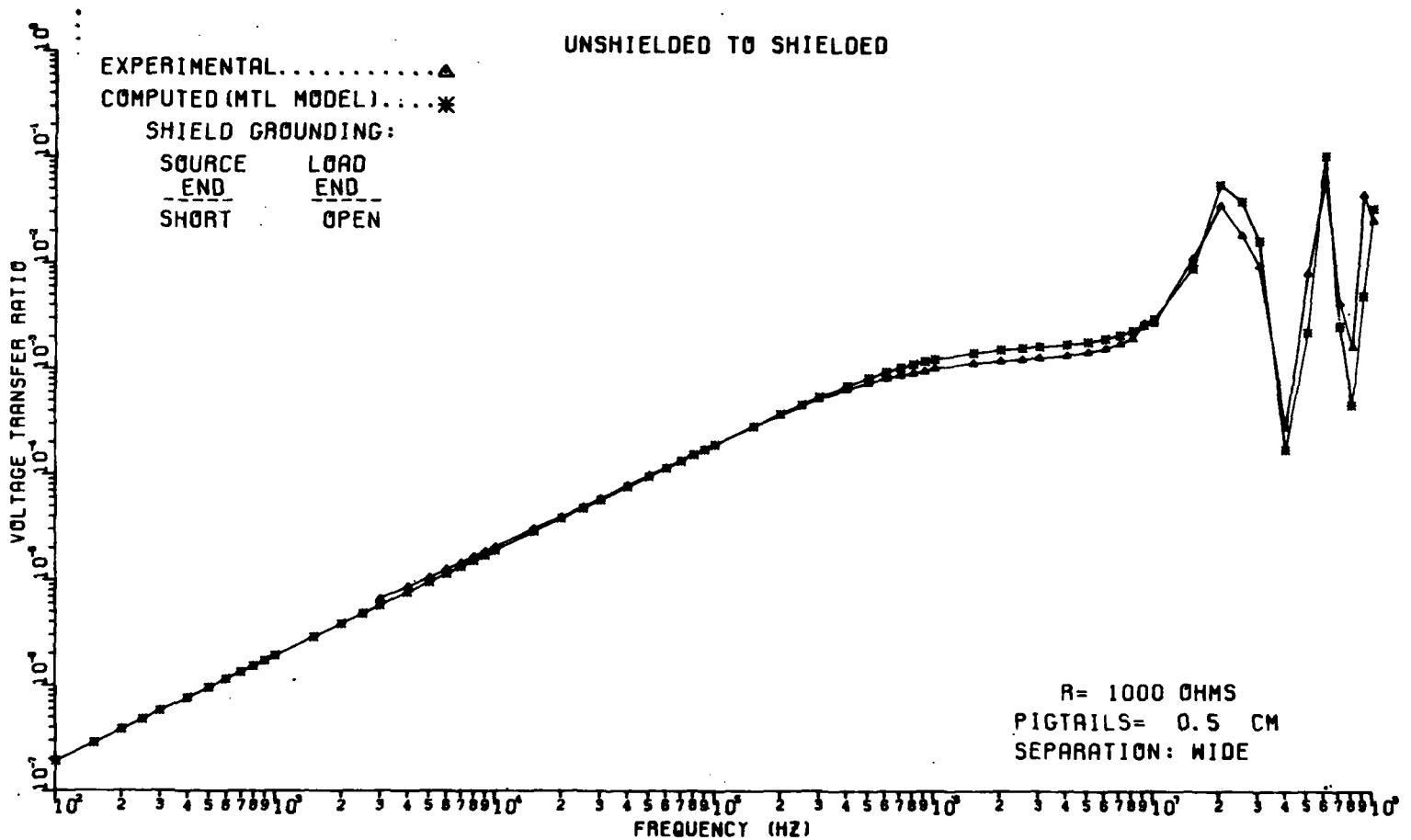
UNSHIELDED TO SHIELDED
EXPERIMENTAL.....
COMPUTED (MTL MODEL).....
SHIELD GROUNDING:
SOURCE END
LOAD END
SHORT
OPEN
R= 1000 OHMS
PIGTAILS= 0.5 CM
SEPARATION: WIDE
VOLTAGE TRANSFER RATIO
FREQUENCY (HZ)

Figure E-6.

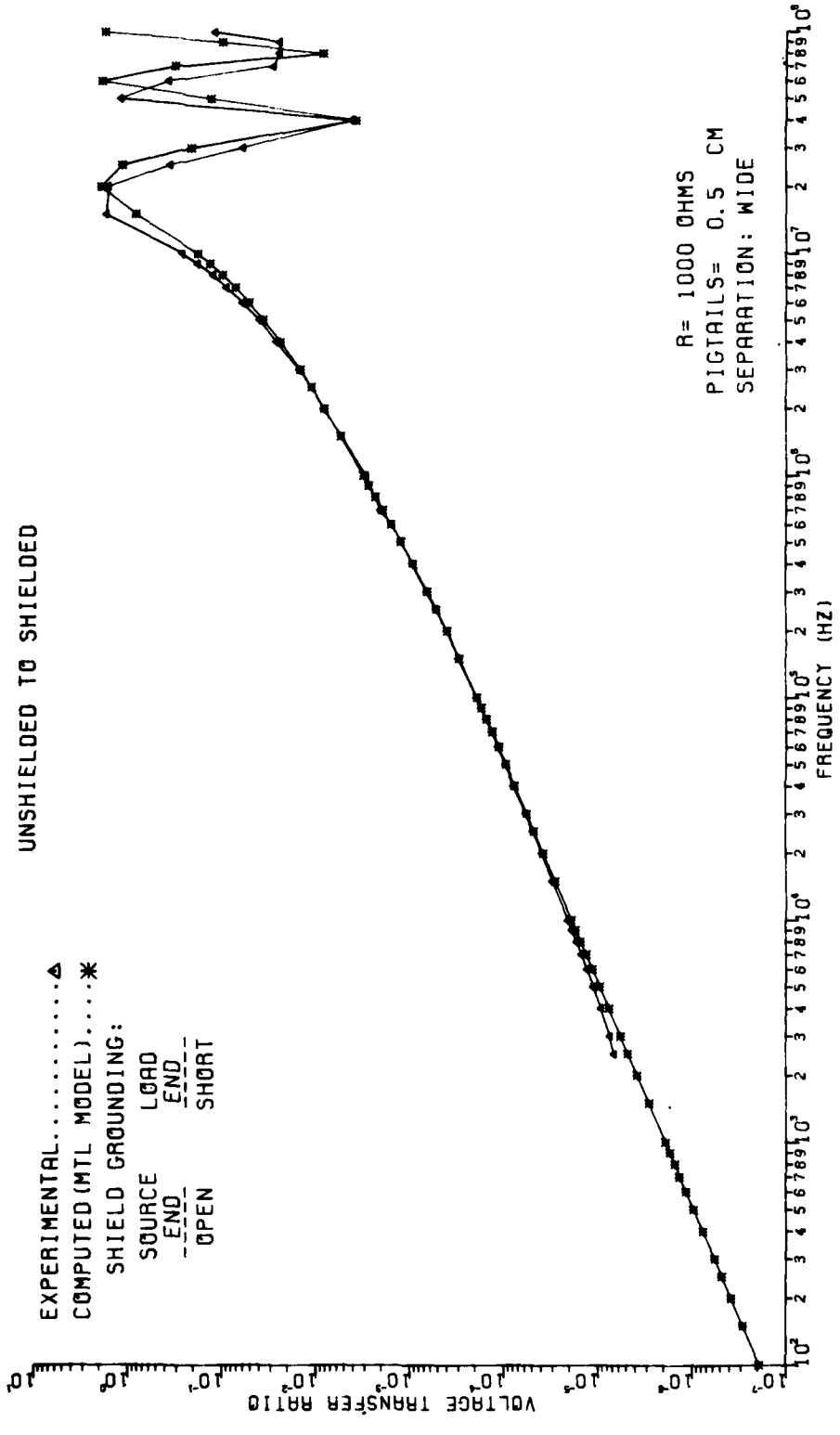
UNSHIELDED TO SHIELDED
EXPERIMENTAL.....Δ
COMPUTED(MTL MODEL)....*
SHIELD GROUNDING:
SOURCE END
LOAD END
OPEN
SHORT
R= 1000 OHMS
PIGTAILS= 0.5 CM
SEPARATION: WIDE
VOLTAGE TRANSFER RATIO
FREQUENCY (HZ)

Figure E-7.

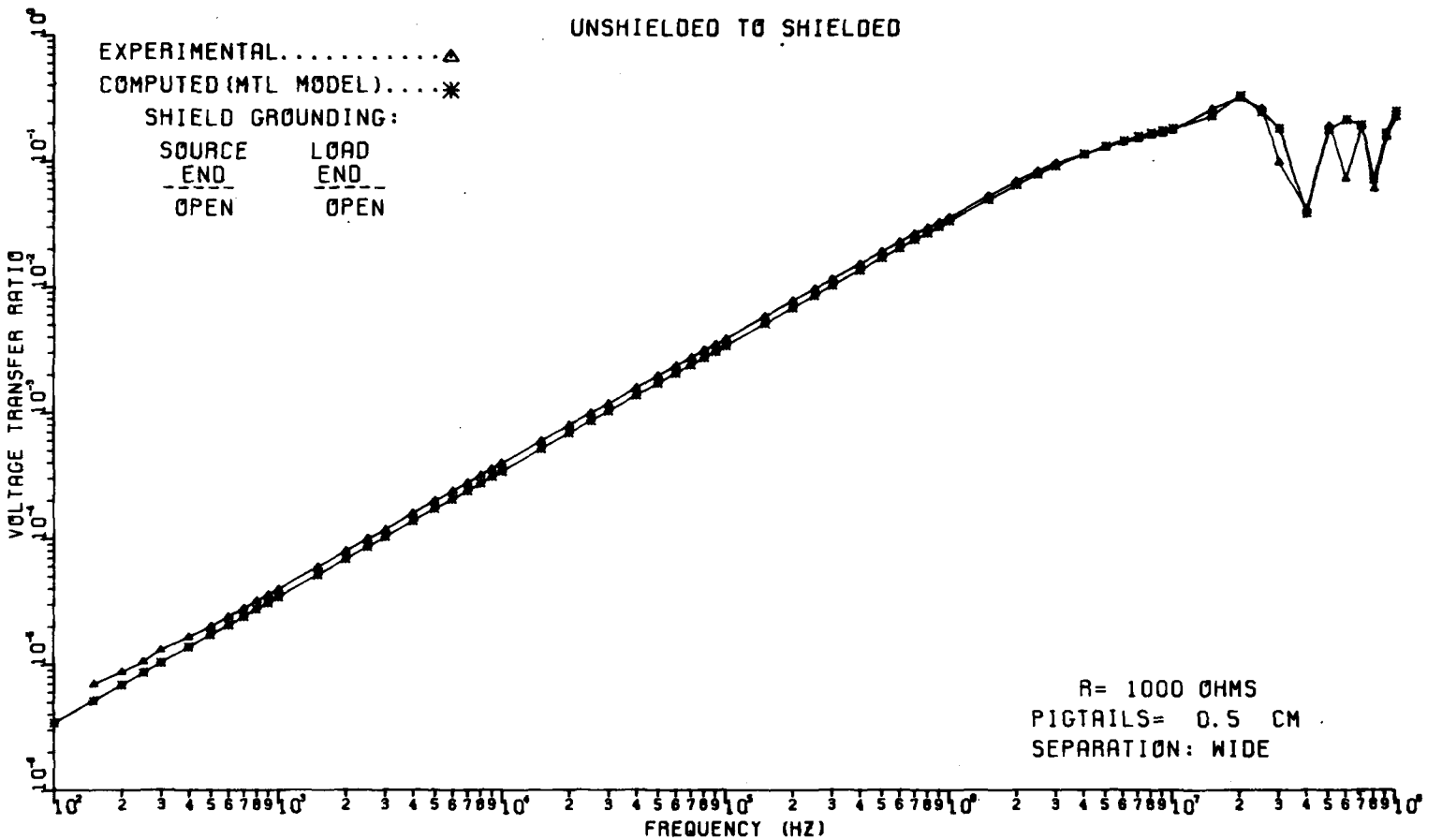
UNSHIELDED TO SHIELDED
EXPERIMENTAL.....
COMPUTED (MTL MODEL)....
SHIELD GROUNDING:
SOURCE END
LOAD END
OPEN
OPEN
VOLTAGE TRANSFER RATIO
FREQUENCY (HZ)
R= 1000 OHMS
PIGTAILS= 0.5 CM
SEPARATION: WIDE

Figure E-8.

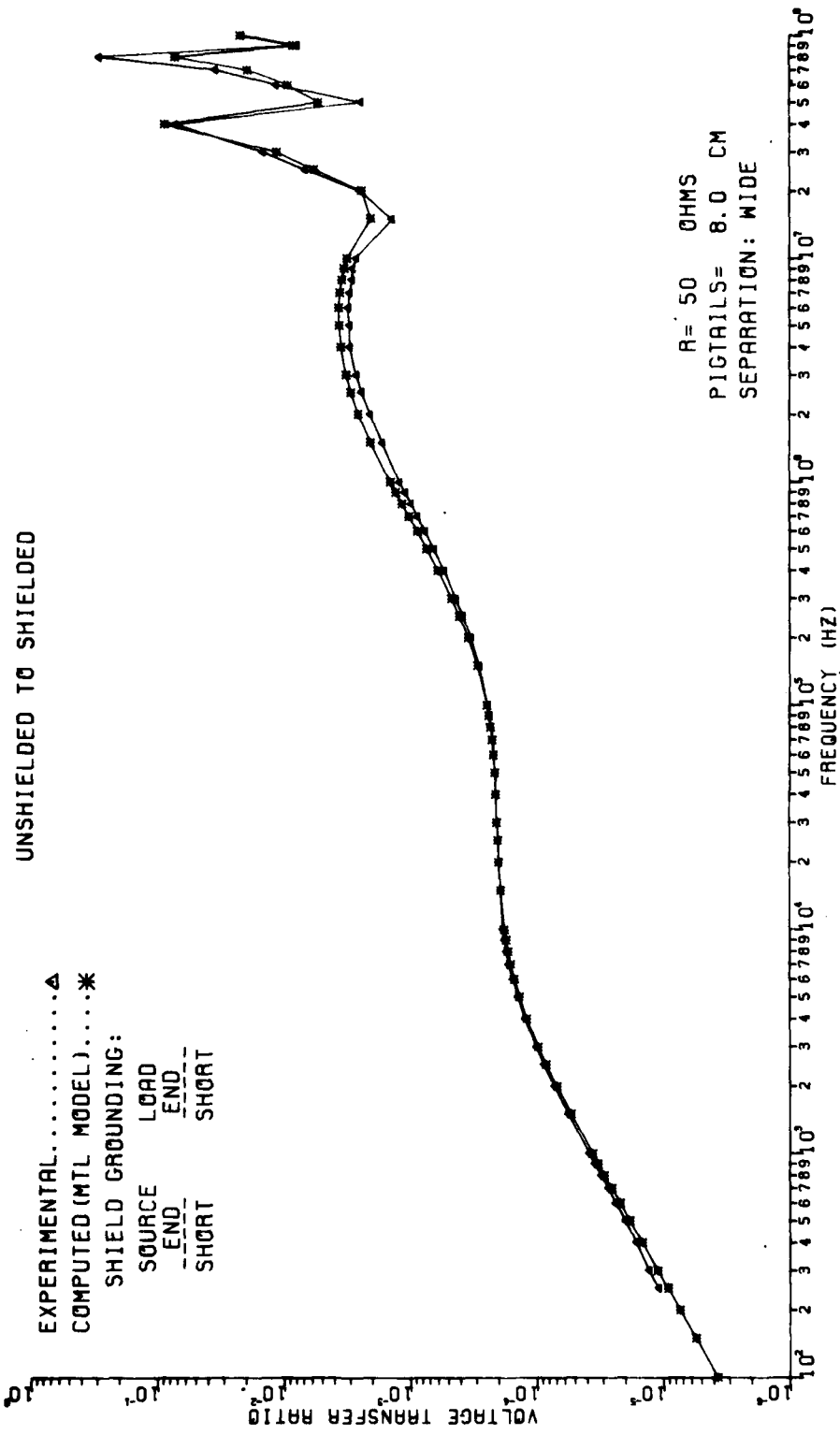
UNSHIELDED TO SHIELDED
EXPERIMENTAL.....Δ
COMPUTED(MTL MODEL)....*
SHIELD GROUNDING:
SOURCE LOAD
END END
SHORT SHORT
R= 50 OHMS
PIGTAILS= 8.0 CM
SEPARATION: WIDE
VOLTAGE TRANSFER RATIO
FREQUENCY (HZ)

Figure E-9.

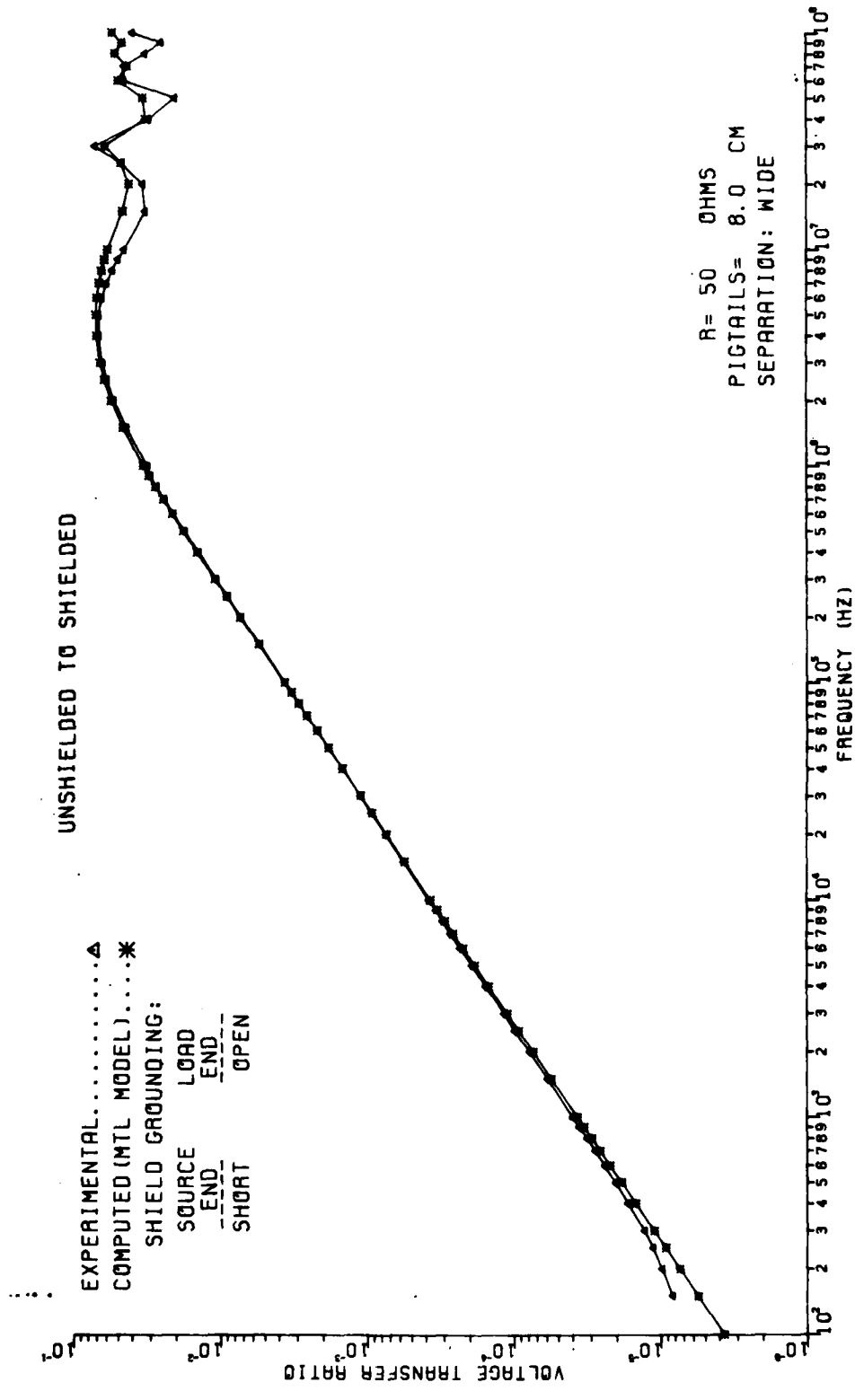
UNSHIELDED TO SHIELDED
EXPERIMENTAL.....Δ
COMPUTED(MTL MODEL)....*
SHIELD GROUNDING:
SOURCE LOAD
END END
SHORT OPEN
R= 50 OHMS
PIGTAILS= 8.0 CM
SEPARATION: WIDE
VOLTAGE TRANSFER RATIO
FREQUENCY (HZ)

Figure E-10.

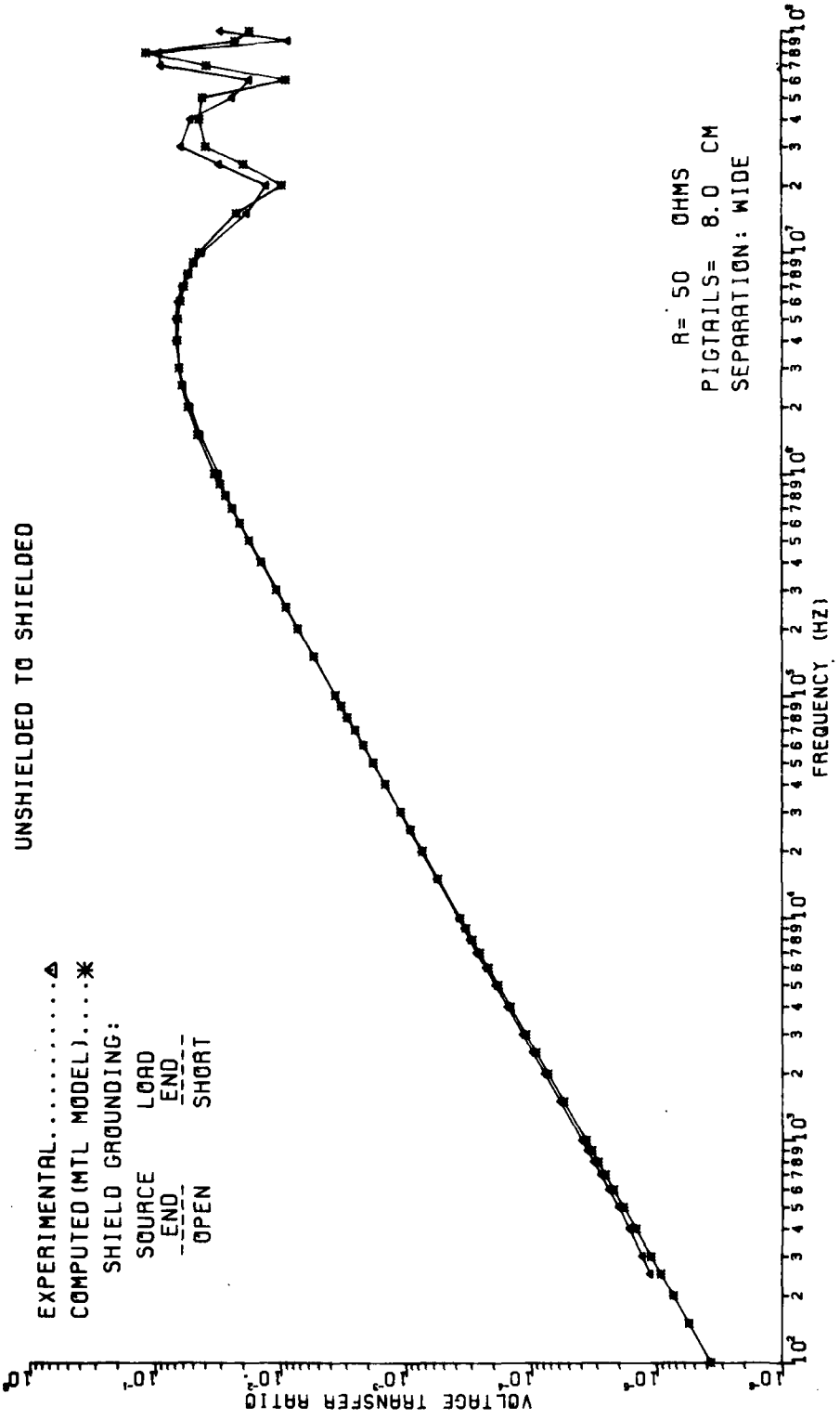
UNSHIELDED TO SHIELDED
EXPERIMENTAL.....Δ
COMPUTED(MTL MODEL).....*
SHIELD GROUNDING:
SOURCE LOAD
END END
OPEN SHORT
R= 50 OHMS
PIGTAILS= 8.0 CM
SEPARATION: WIDE
VOLTAGE TRANSFER RATIO
FREQUENCY (HZ)

Figure E-11.

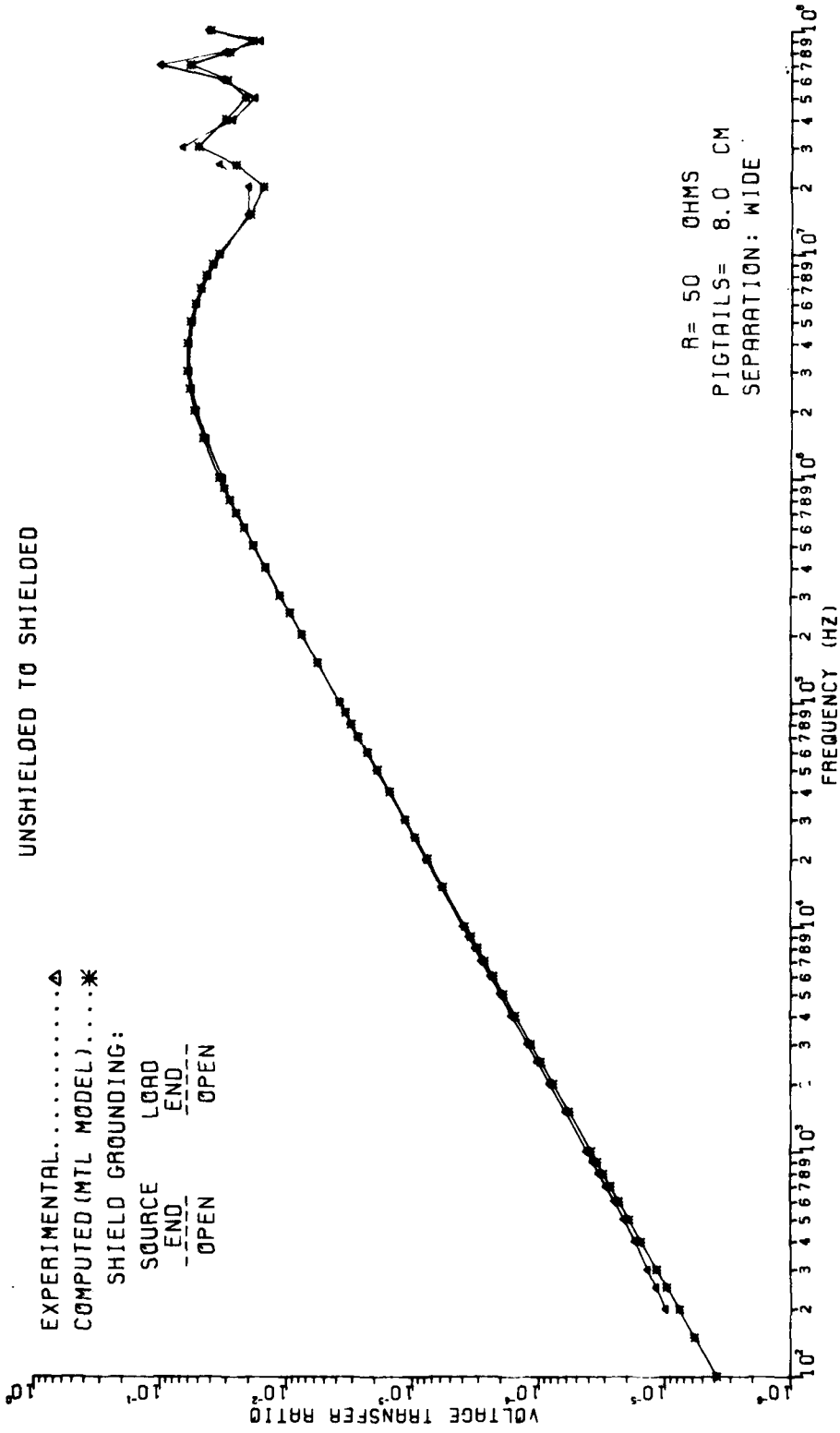
UNSHIELDED TO SHIELDED
EXPERIMENTAL.....Δ
COMPUTED(MTL MODEL)....*
SHIELD GROUNDING:
SOURCE LOAD
END END
OPEN OPEN
R= 50 OHMS
PIGTAILS= 8.0 CM
SEPARATION: WIDE
VOLTAGE TRANSFER RATIO
FREQUENCY (HZ)

Figure E-12.

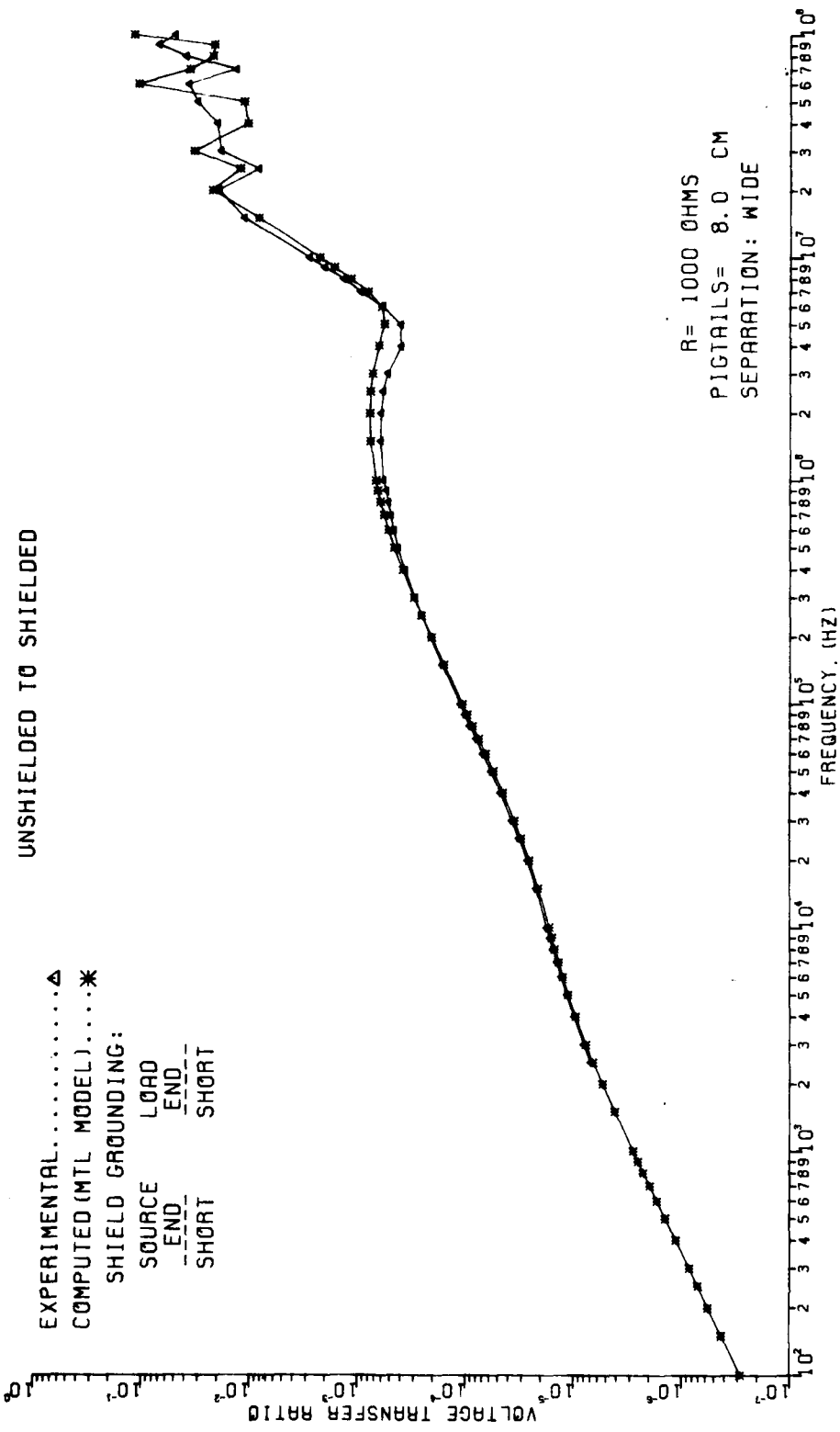
UNSHIELDED TO SHIELDED
EXPERIMENTAL.....Δ
COMPUTED(MTL MODEL)....*
SHIELD GROUNDING:
SOURCE LOAD
END END
SHORT SHORT
R= 1000 OHMS
PIGTAILS= 8.0 CM
SEPARATION: WIDE
VOLTAGE TRANSFER RATIO
FREQUENCY, (HZ)

Figure E-13.

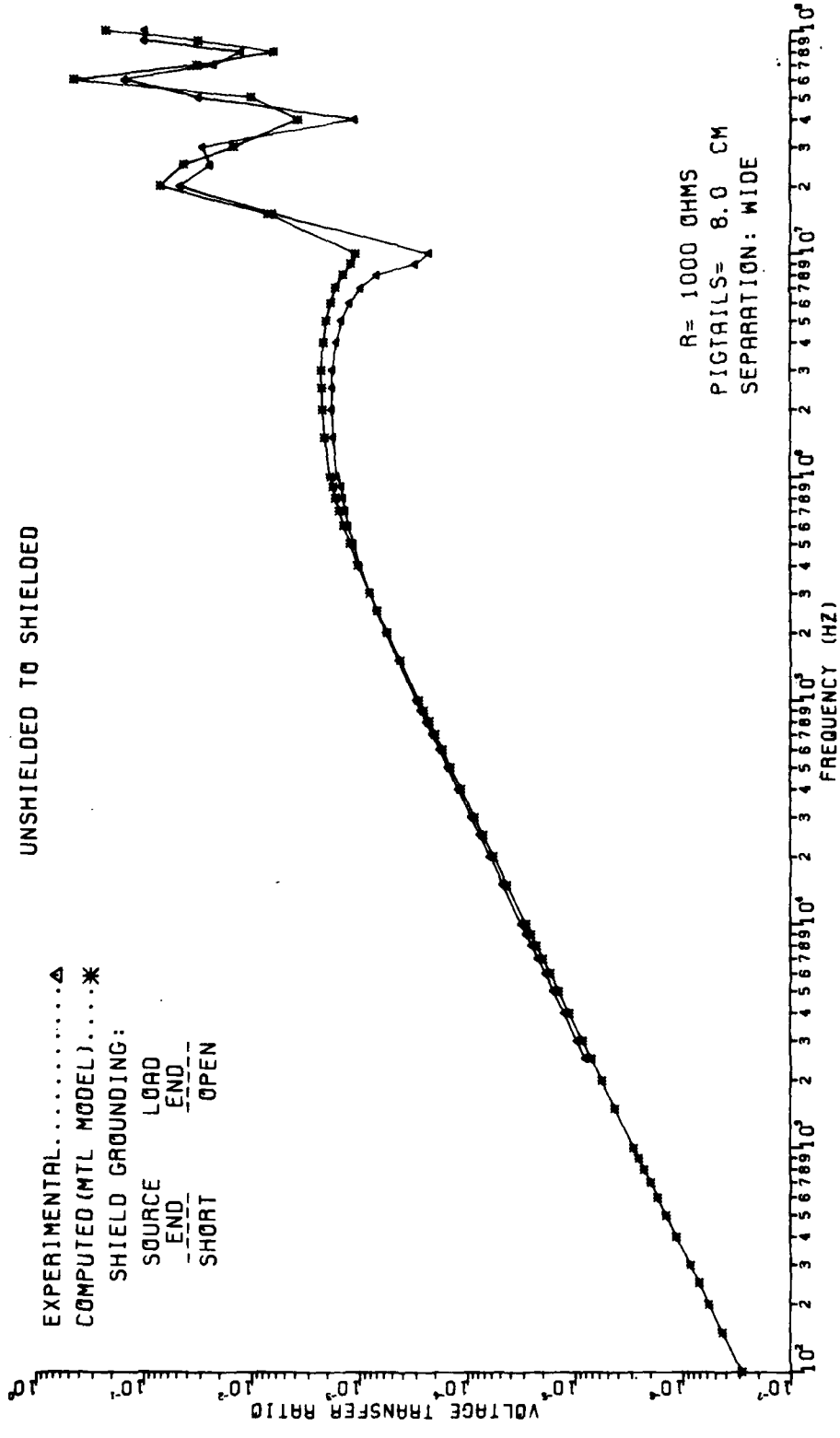
UNSHIELDED TO SHIELDED
EXPERIMENTAL.....Δ
COMPUTED(MTL MODEL)....*
SHIELD GROUNDING:
SOURCE LOAD
END END
SHORT OPEN
R= 1000 OHMS
PIGTAILS= 8.0 CM
SEPARATION: WIDE
VOLTAGE TRANSFER RATIO
FREQUENCY (HZ)

Figure E-14.

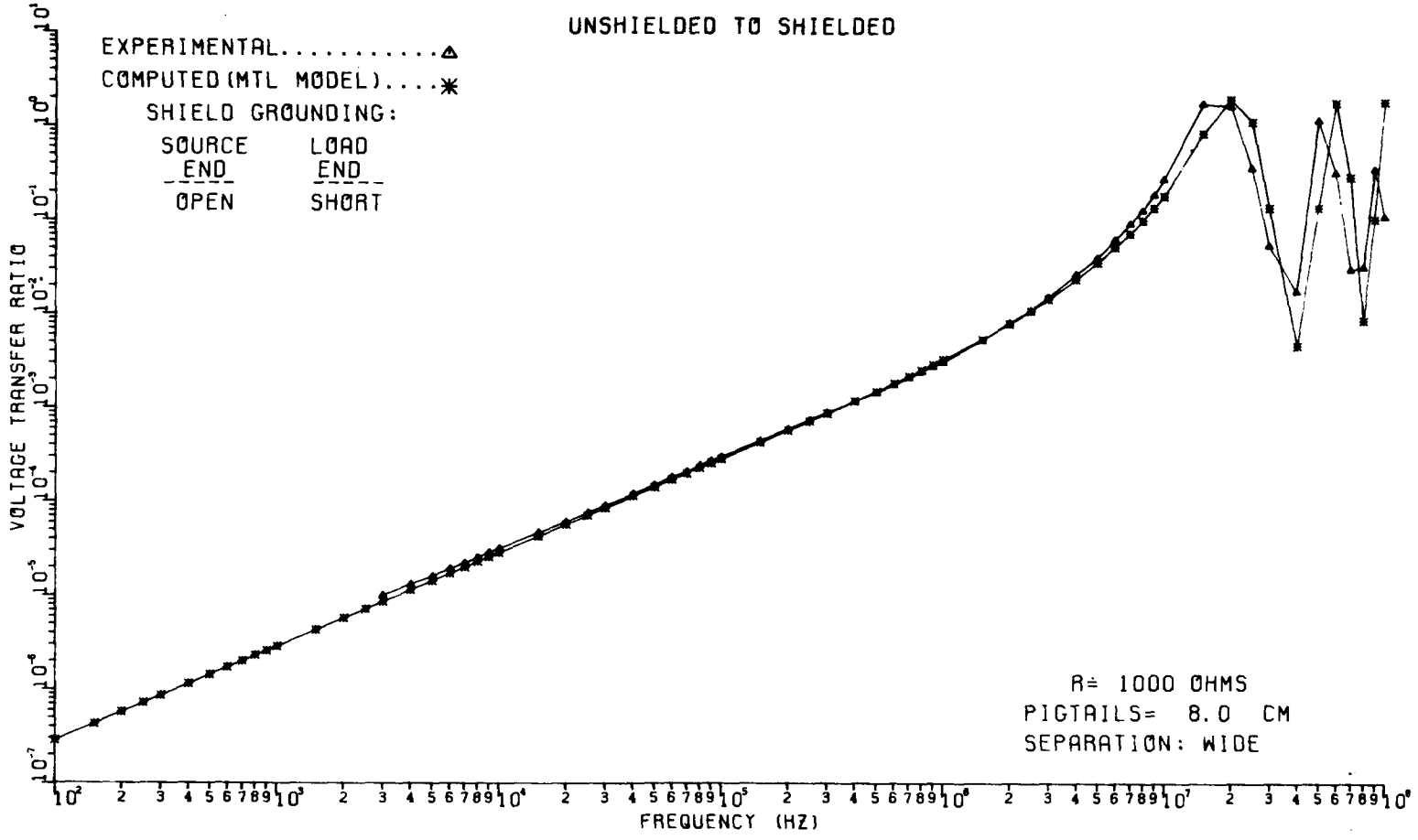
UNSHIELDED TO SHIELDED
EXPERIMENTAL.....△
COMPUTED(MTL MODEL)....✳
SHIELD GROUNDING:
SOURCE END
OPEN
LOAD END
SHORT
VOLTAGE TRANSFER RATIO
FREQUENCY (HZ)
R= 1000 OHMS
PIGTAILS= 8.0 CM
SEPARATION: WIDE

Figure E-15.

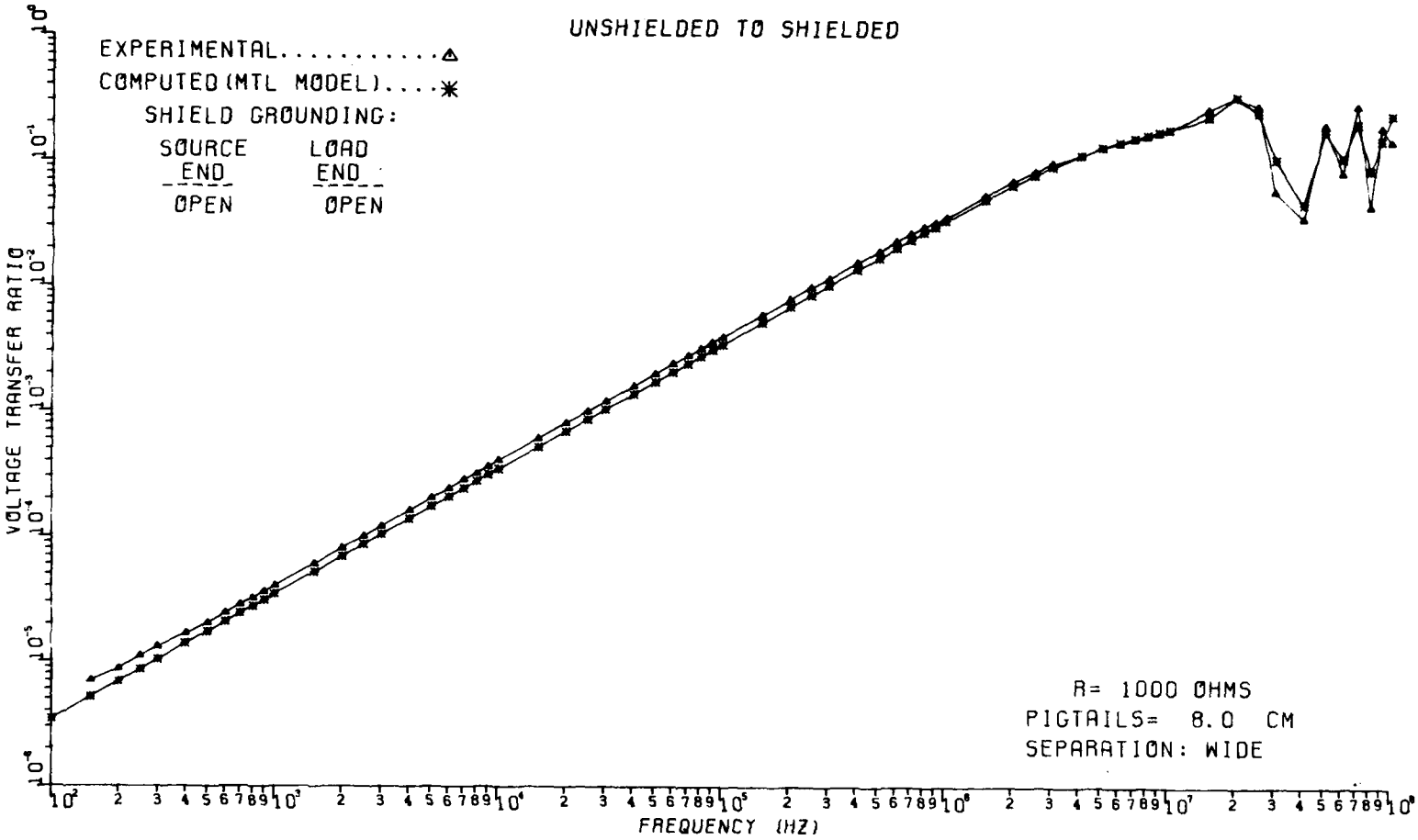
UNSHIELDED TO SHIELDED
EXPERIMENTAL.....△
COMPUTED(MTL MODEL)....✳
SHIELD GROUNDING:
SOURCE END
OPEN
LOAD END
OPEN
VOLTAGE TRANSFER RATIO
FREQUENCY (HZ)
R= 1000 OHMS
PIGTAILS= 8.0 CM
SEPARATION: WIDE

Figure E-16.

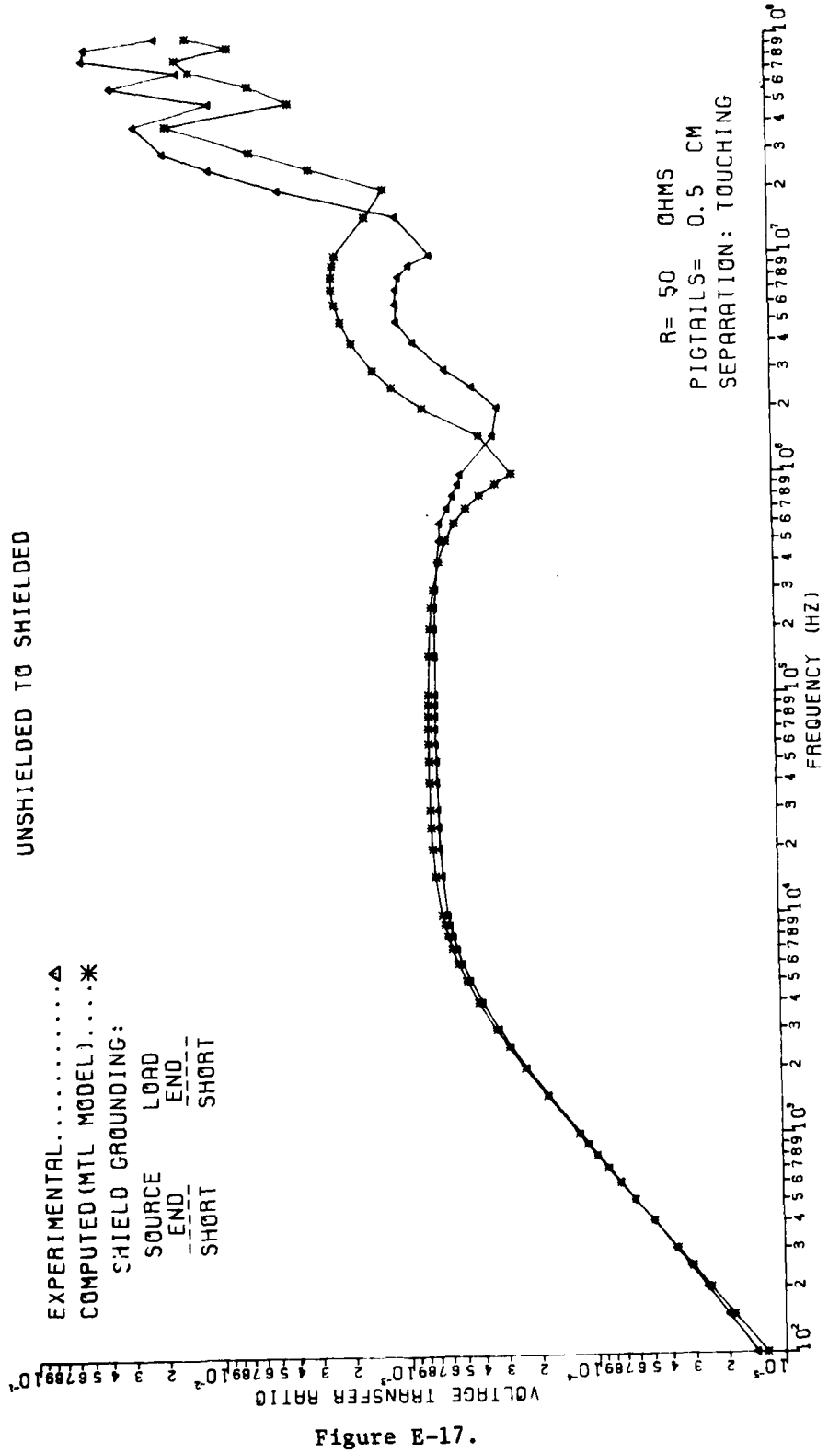
UNSHIELDED TO SHIELDED
EXPERIMENTAL.....Δ
COMPUTED(MTL MODEL)....*
SHIELD GROUNDING:
SOURCE END
LOAD END
SHORT
SHORT
R= 50 OHMS
PIGTAILS= 0.5 CM
SEPARATION: TOUCHING
VOLTAGE TRANSFER RATIO
FREQUENCY (HZ)

Figure E-17.

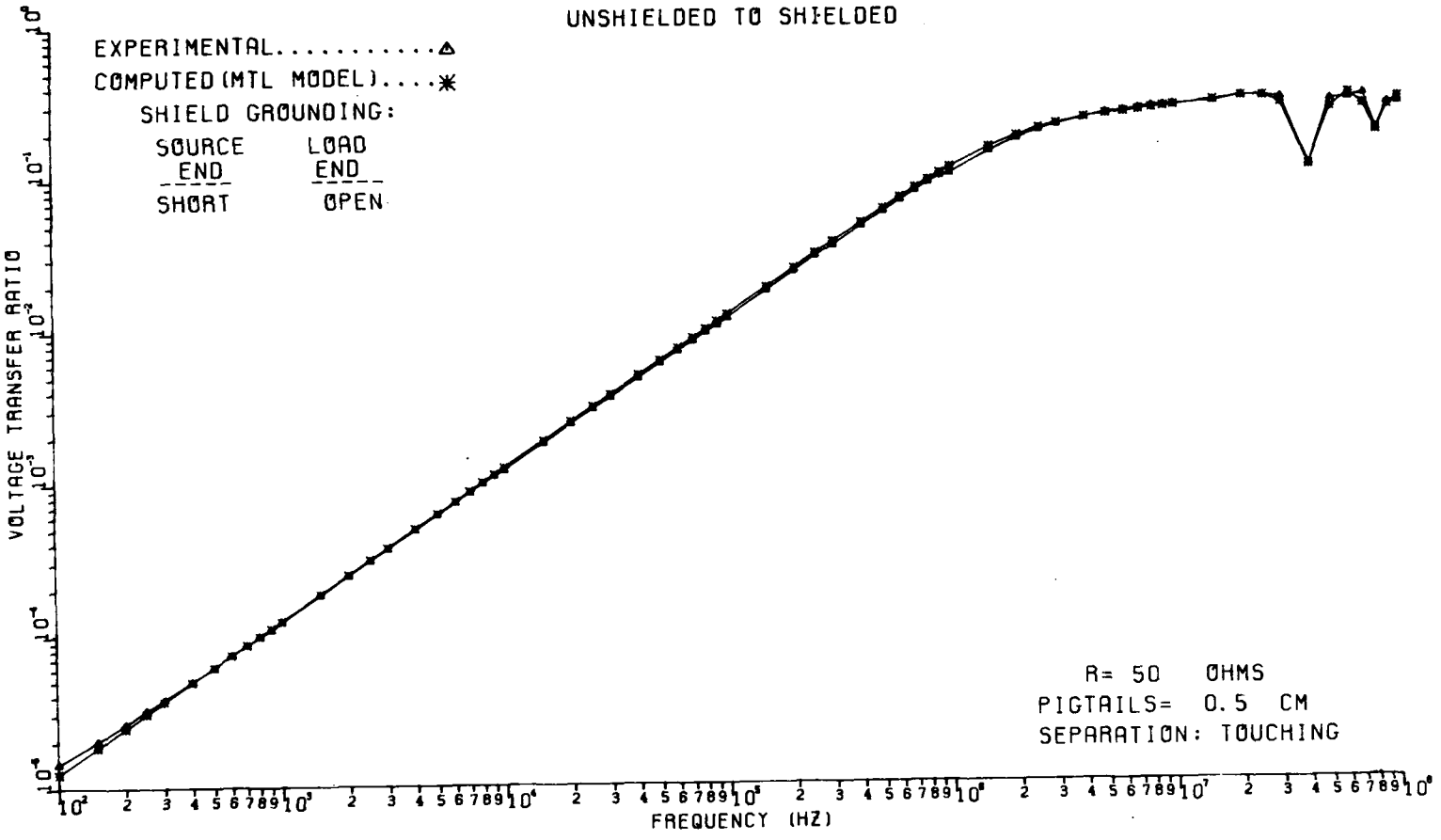
UNSHIELDED TO SHIELDED
EXPERIMENTAL.....Δ
COMPUTED (MTL MODEL)....*
SHIELD GROUNDING:
SOURCE END
SHORT
LOAD END
OPEN
VOLTAGE TRANSFER RATIO
FREQUENCY (HZ)
R= 50 OHMS
PIGTAILS= 0.5 CM
SEPARATION: TOUCHING

Figure E-18.

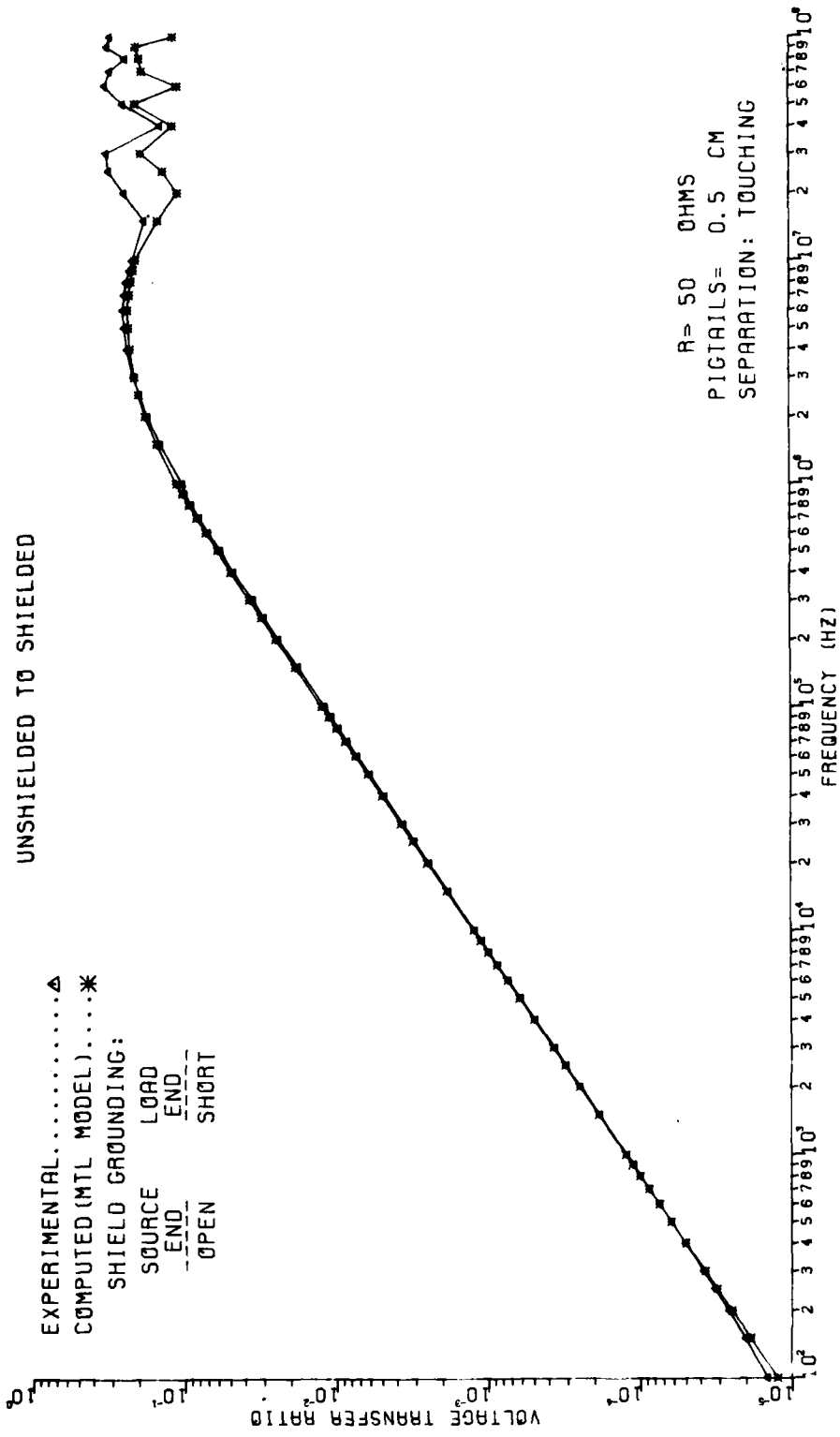
UNSHIELDED TO SHIELDED
EXPERIMENTAL.....Δ
COMPUTED(MTL MODEL)....*
SHIELD GROUNDING:
SOURCE LOAD
END END
OPEN SHORT
R= 50 OHMS
PIGTAILS= 0.5 CM
SEPARATION: TOUCHING
VOLTAGE TRANSFER RATIO
FREQUENCY (HZ)

Figure E-19.

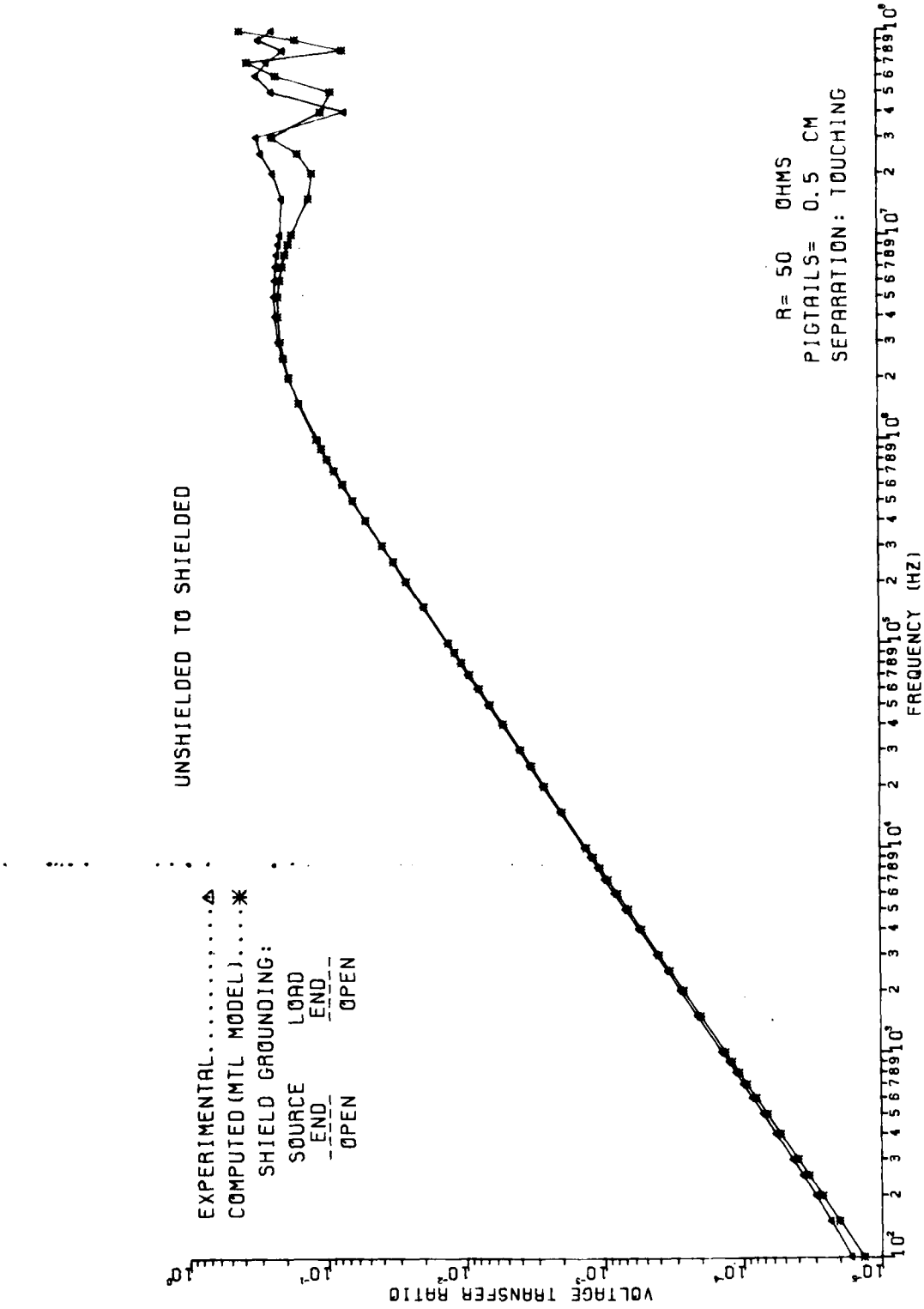
UNSHIELDED TO SHIELDED
EXPERIMENTAL.....Δ
COMPUTED(MTL MODEL)....*
SHIELD GROUNDING:
SOURCE LOAD
END END
OPEN OPEN
R= 50 OHMS
PIGTAILS= 0.5 CM
SEPARATION: TOUCHING
VOLTAGE TRANSFER RATIO
FREQUENCY (HZ)

Figure E-20.

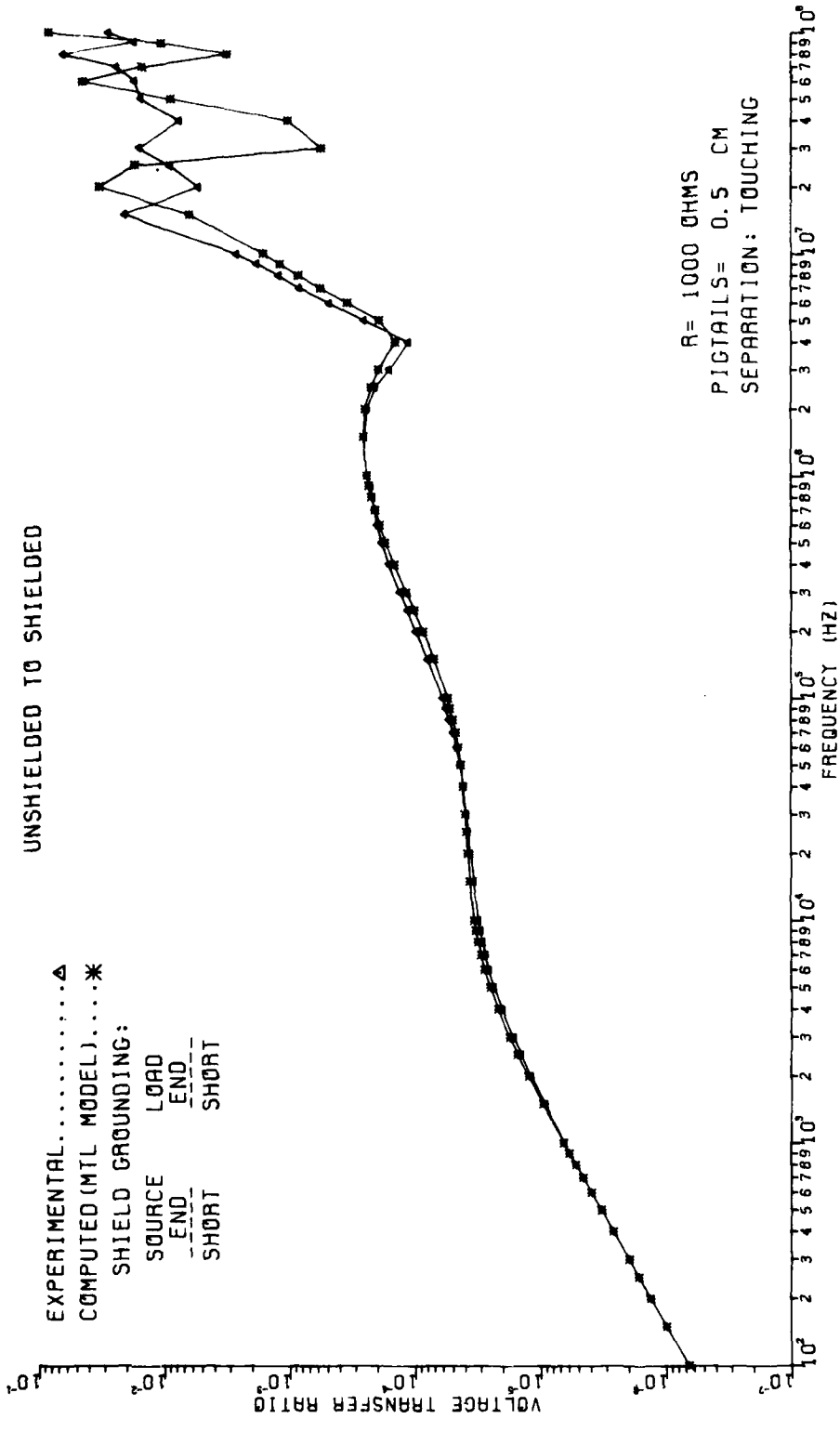
UNSHIELDED TO SHIELDED
EXPERIMENTAL.....Δ
COMPUTED(MTL MODEL)....*
SHIELD GROUNDING:
SOURCE LOAD
END END
SHORT SHORT
R= 1000 OHMS
PIGTAILS= 0.5 CM
SEPARATION: TOUCHING
VOLTAGE TRANSFER RATIO
FREQUENCY (HZ)

Figure E-21.

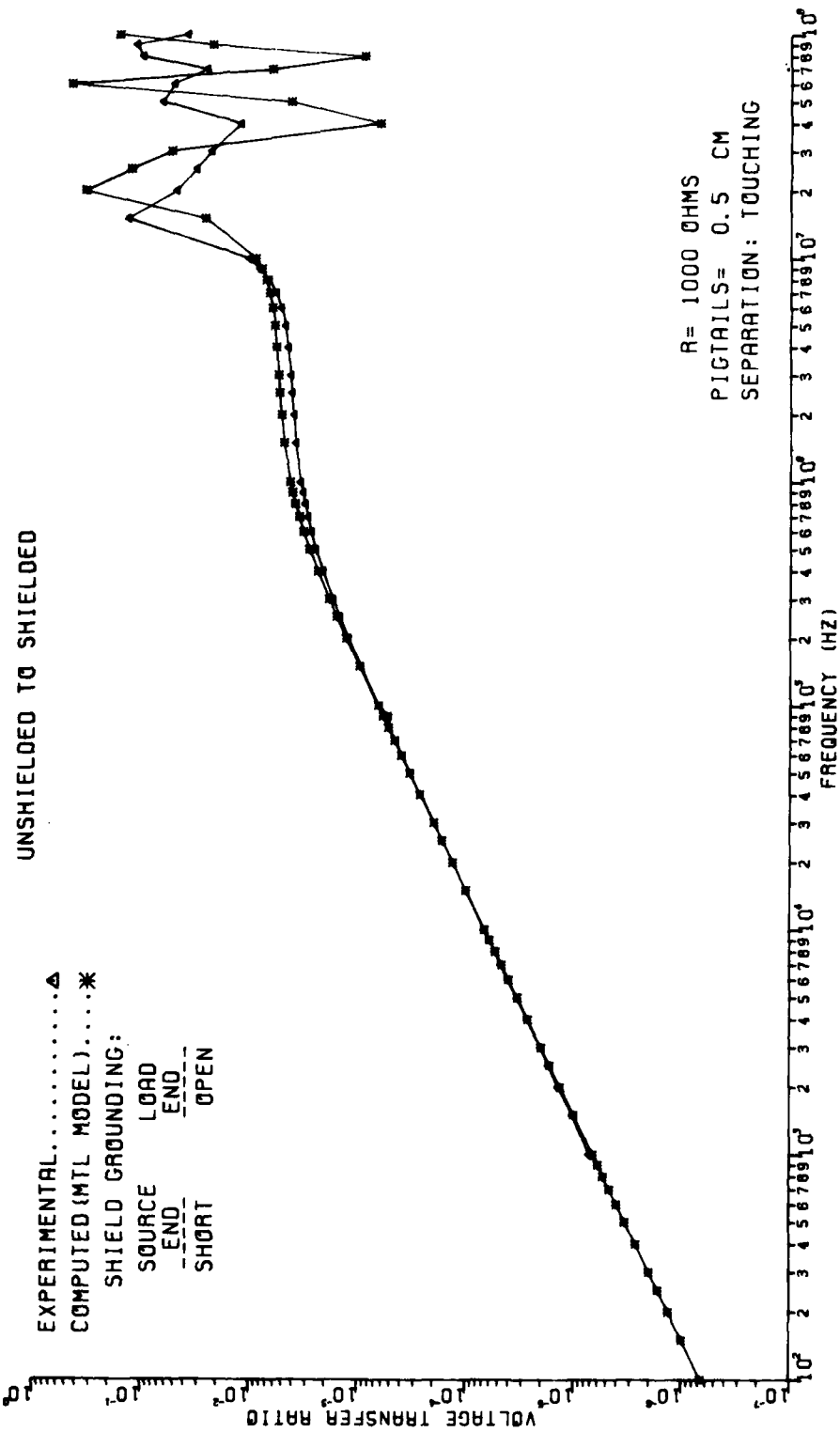
UNSHIELDED TO SHIELDED
EXPERIMENTAL.....Δ
COMPUTED(MTL MODEL)....*
SHIELD GROUNDING:
SOURCE LOAD
END END
SHORT OPEN
R= 1000 OHMS
PIGTAILS= 0.5 CM
SEPARATION: TOUCHING
VOLTAGE TRANSFER RATIO
FREQUENCY (HZ)

Figure E-22.

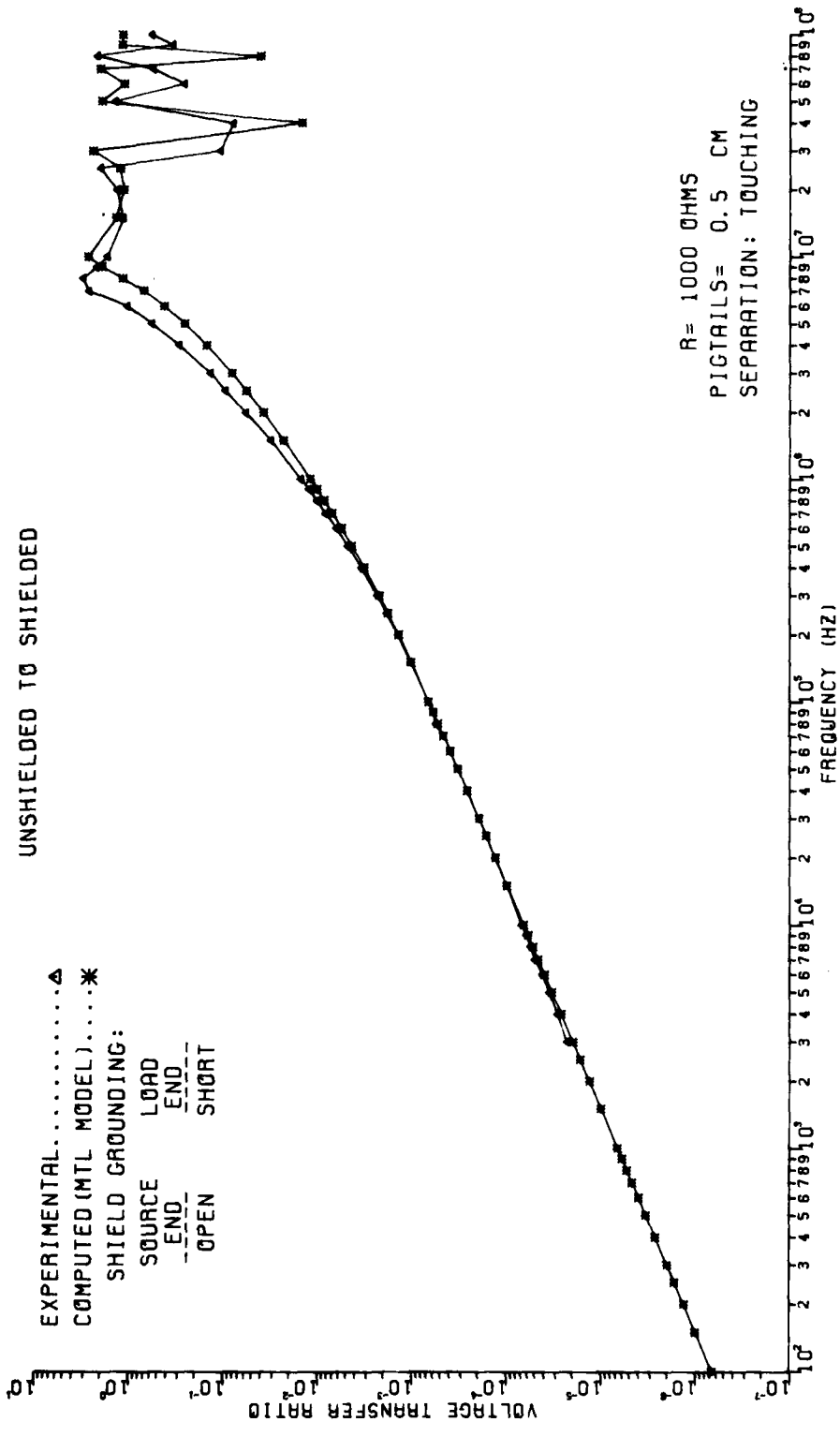
UNSHIELDED TO SHIELDED
EXPERIMENTAL.....Δ
COMPUTED(MTL MODEL)....*
SHIELD GROUNDING:
SOURCE LOAD
END END
OPEN SHORT
R= 1000 OHMS
PIGTAILS= 0.5 CM
SEPARATION: TOUCHING
VOLTAGE TRANSFER RATIO
FREQUENCY (HZ)

Figure E-23.

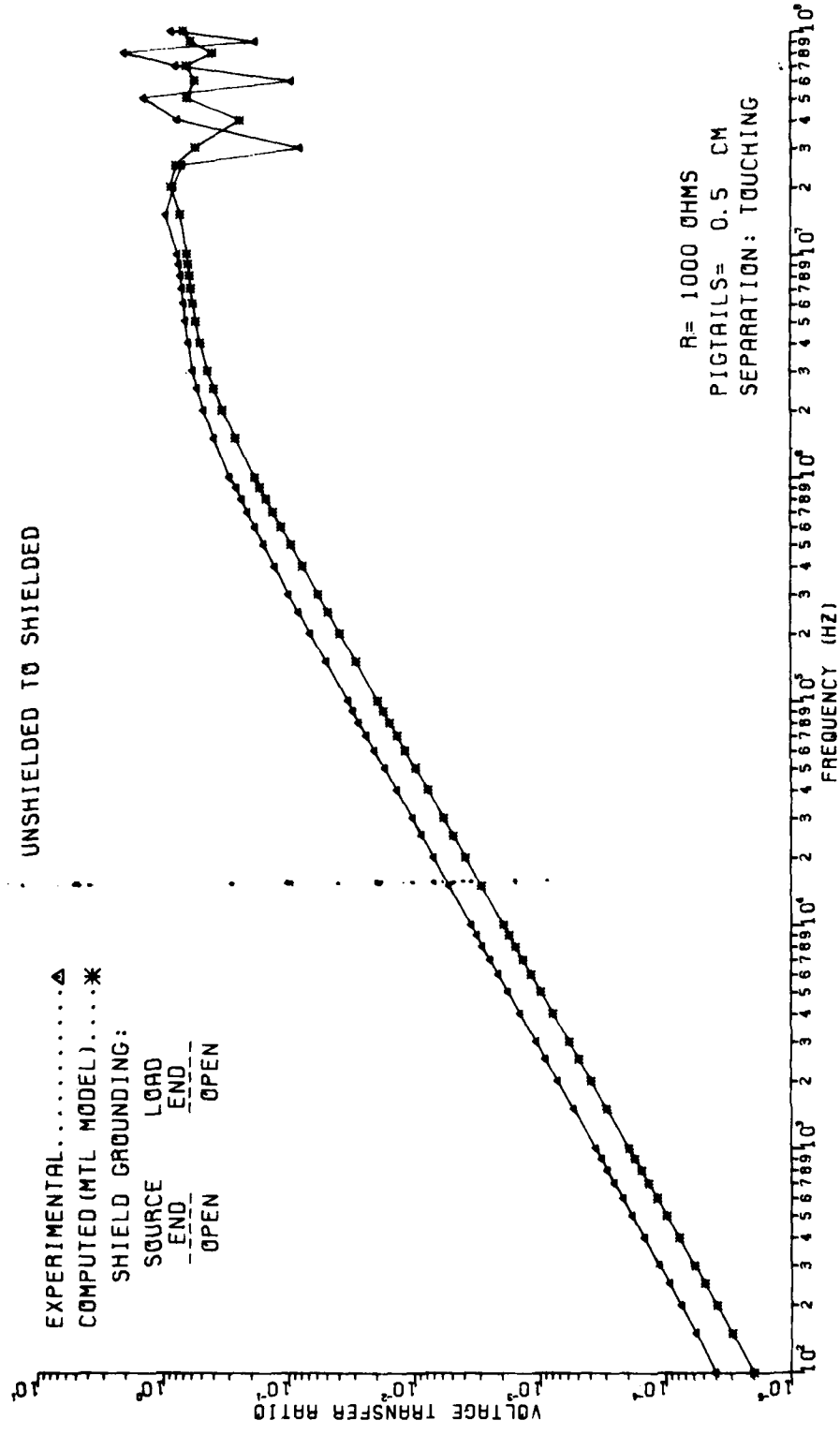
UNSHIELDED TO SHIELDED
EXPERIMENTAL.....Δ
COMPUTED(MTL MODEL)....*
SHIELD GROUNDING:
SOURCE END
OPEN
LOAD END
OPEN
R= 1000 OHMS
PIGTAILS= 0.5 CM
SEPARATION: TOUCHING
VOLTAGE TRANSFER RATIO
FREQUENCY (HZ)

Figure E-24.

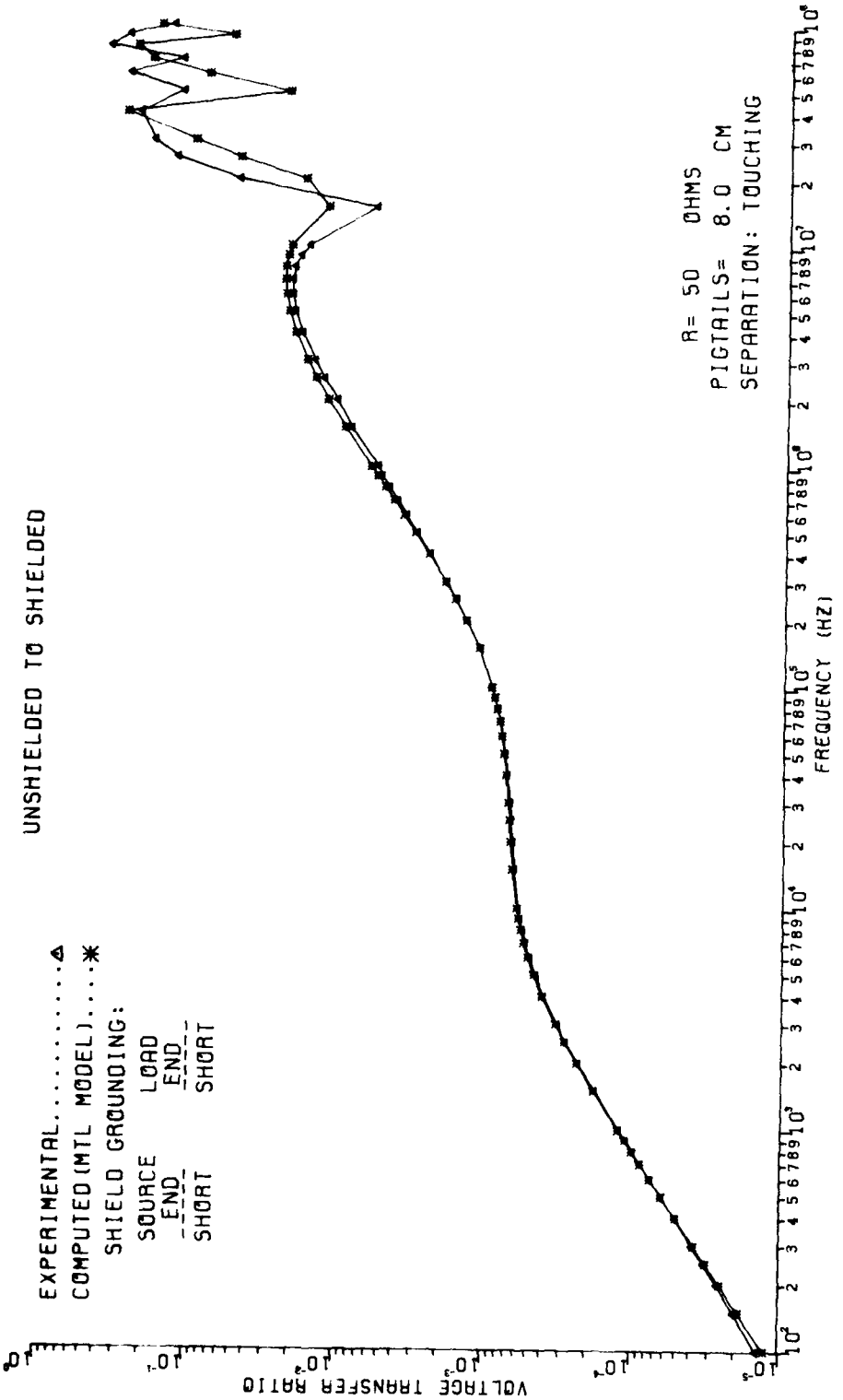
UNSHIELDED TØ SHIELDED
EXPERIMENTAL.....Δ
COMPUTED(MTL MODEL).....*
SHIELD GROUNDING:
SOURCE LØAD
END END
SHØRT SHØRT
R= 50 ØHMS
PIGTAILS= 8.0 CM
SEPARATION: TOUCHING
VOLTAGE TRANSFER RATIO
FREQUENCY (HZ)

Figure E-25.

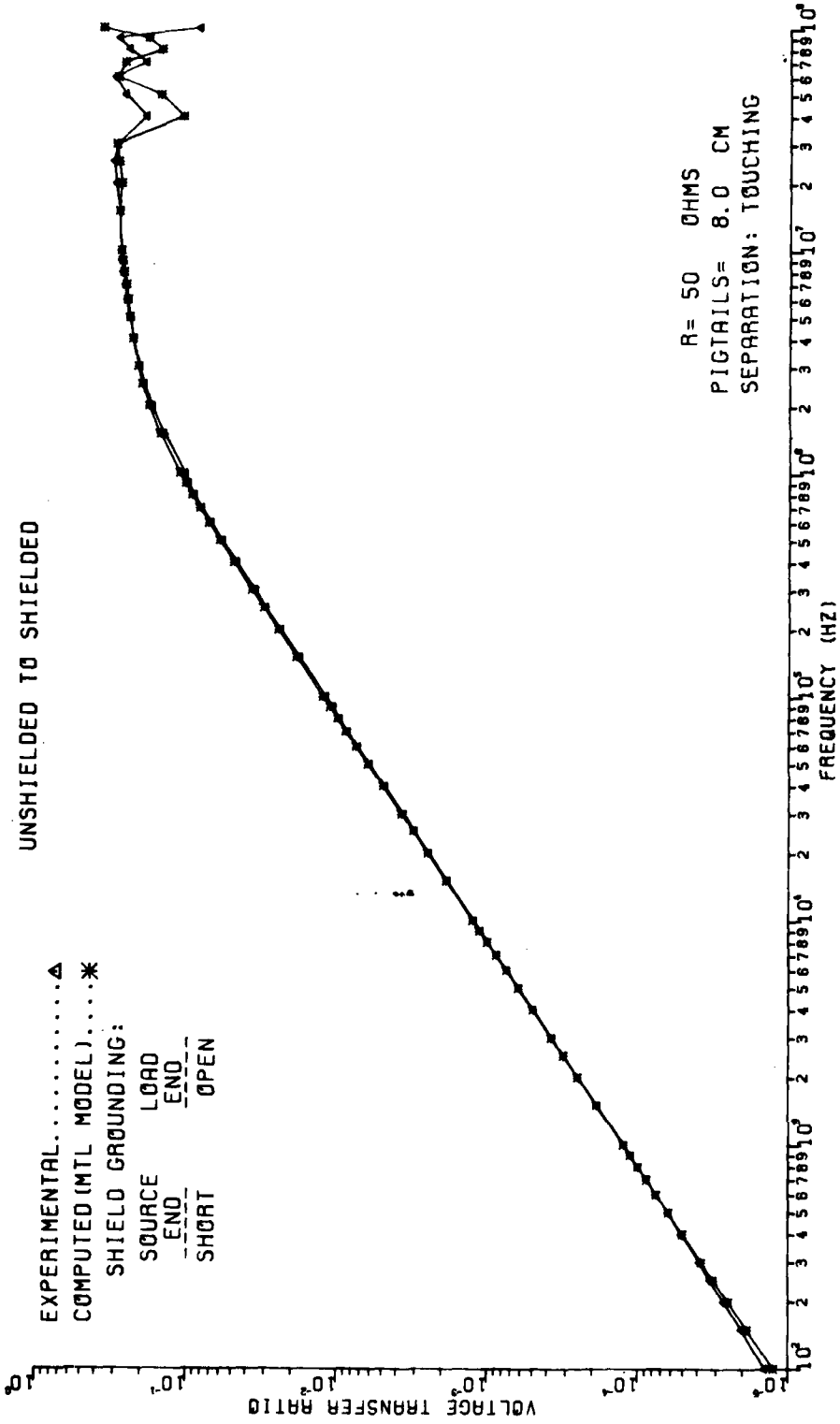
UNSHIELDED TO SHIELDED
EXPERIMENTAL.....Δ
COMPUTED(MTL MODEL).....*
SHIELD GROUNDING:
SOURCE LOAD
END END
SHORT OPEN
R= 50 OHMS
PIGTAILS= 8.0 CM
SEPARATION: TOUCHING
VOLTAGE TRANSFER RATIO
FREQUENCY (HZ)

Figure E-26.

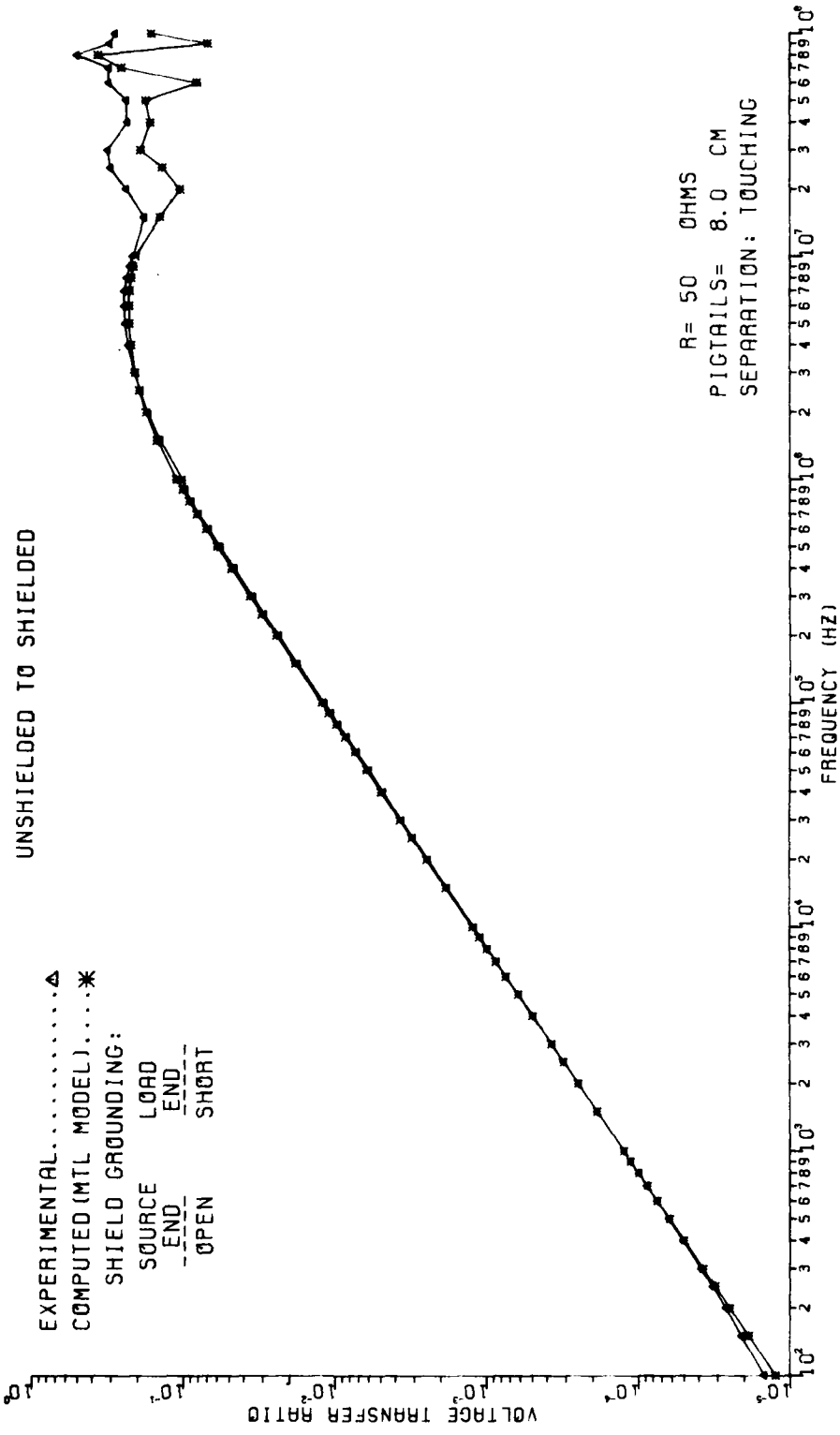
UNSHIELDED TO SHIELDED
EXPERIMENTAL.....Δ
COMPUTED(MTL MODEL).....*
SHIELD GROUNDING:
SOURCE END
LOAD END
OPEN
SHORT
R= 50 OHMS
PIGTAILS= 8.0 CM
SEPARATION: TOUCHING
VOLTAGE TRANSFER RATIO
FREQUENCY (HZ)

Figure E-27.

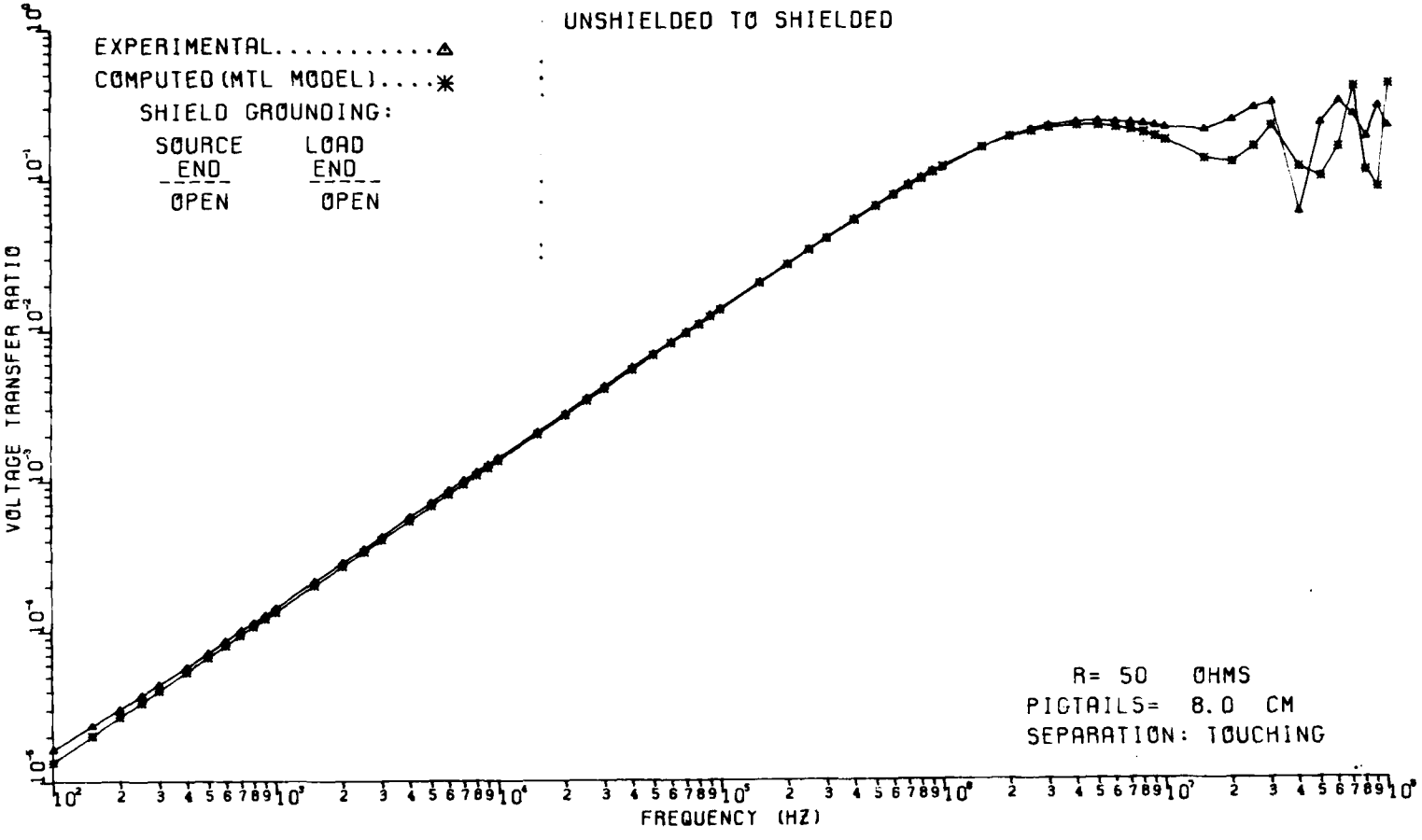
UNSHIELDED TO SHIELDED
EXPERIMENTAL.....△
COMPUTED (MTL MODEL)....✳
SHIELD GROUNDING:
SOURCE END
OPEN
LOAD END
OPEN
VOLTAGE TRANSFER RATIO
FREQUENCY (HZ)
R= 50 OHMS
PIGTAILS= 8.0 CM
SEPARATION: TOUCHING

Figure E-28.

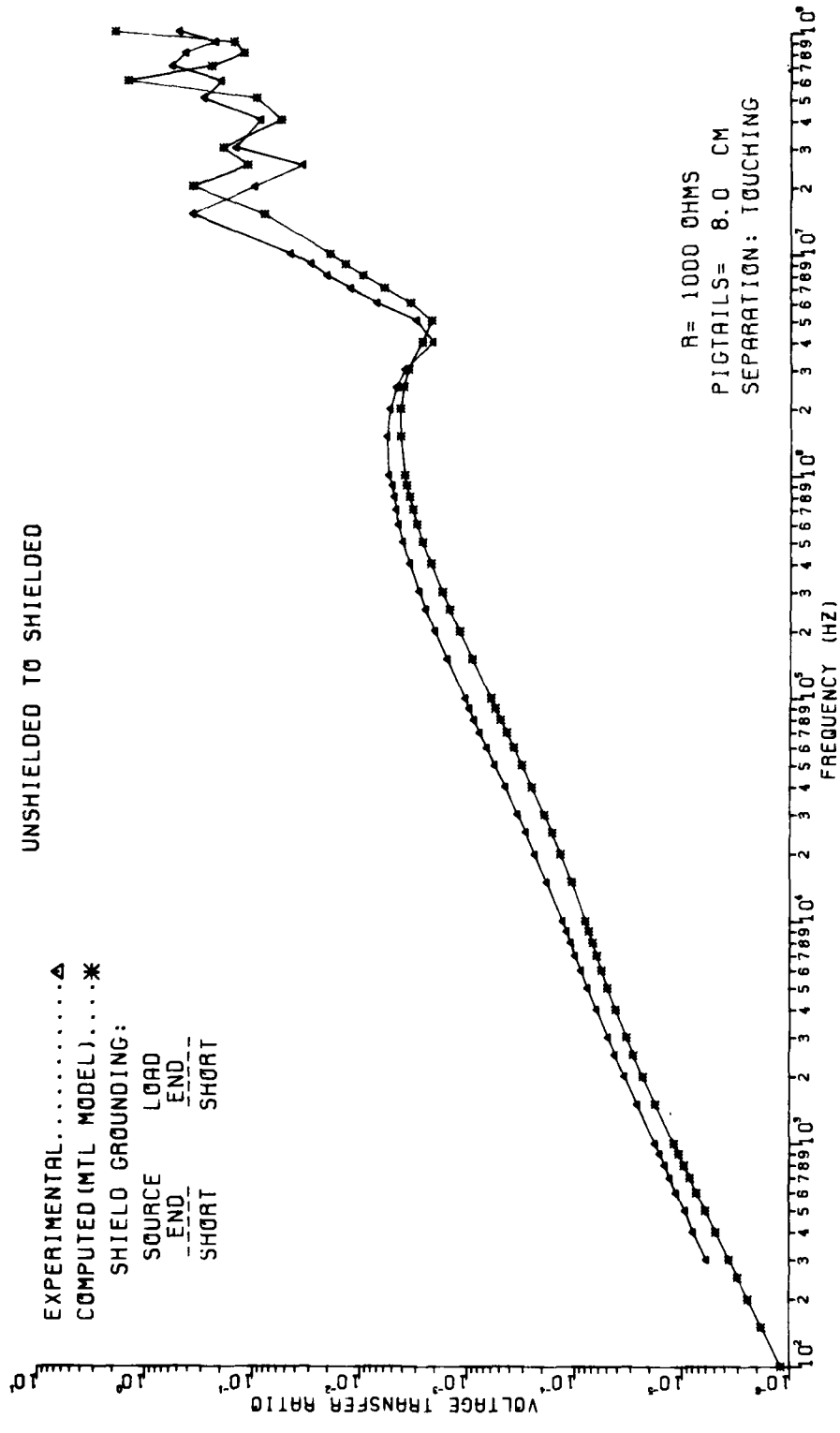
UNSHIELDED TØ SHIELDED
EXPERIMENTAL.....Δ
COMPUTED(MTL MODEL)....*
SHIELD GROUNDING:
SOURCE END
SHØRT
LØAD END
SHØRT
R= 1000 ØHMS
PIGTAILS= 8.0 CM
SEPARATIØN: TØUCHING
VOLTAGE TRANSFER RATIO
FREQUENCY (HZ)

Figure E-29.

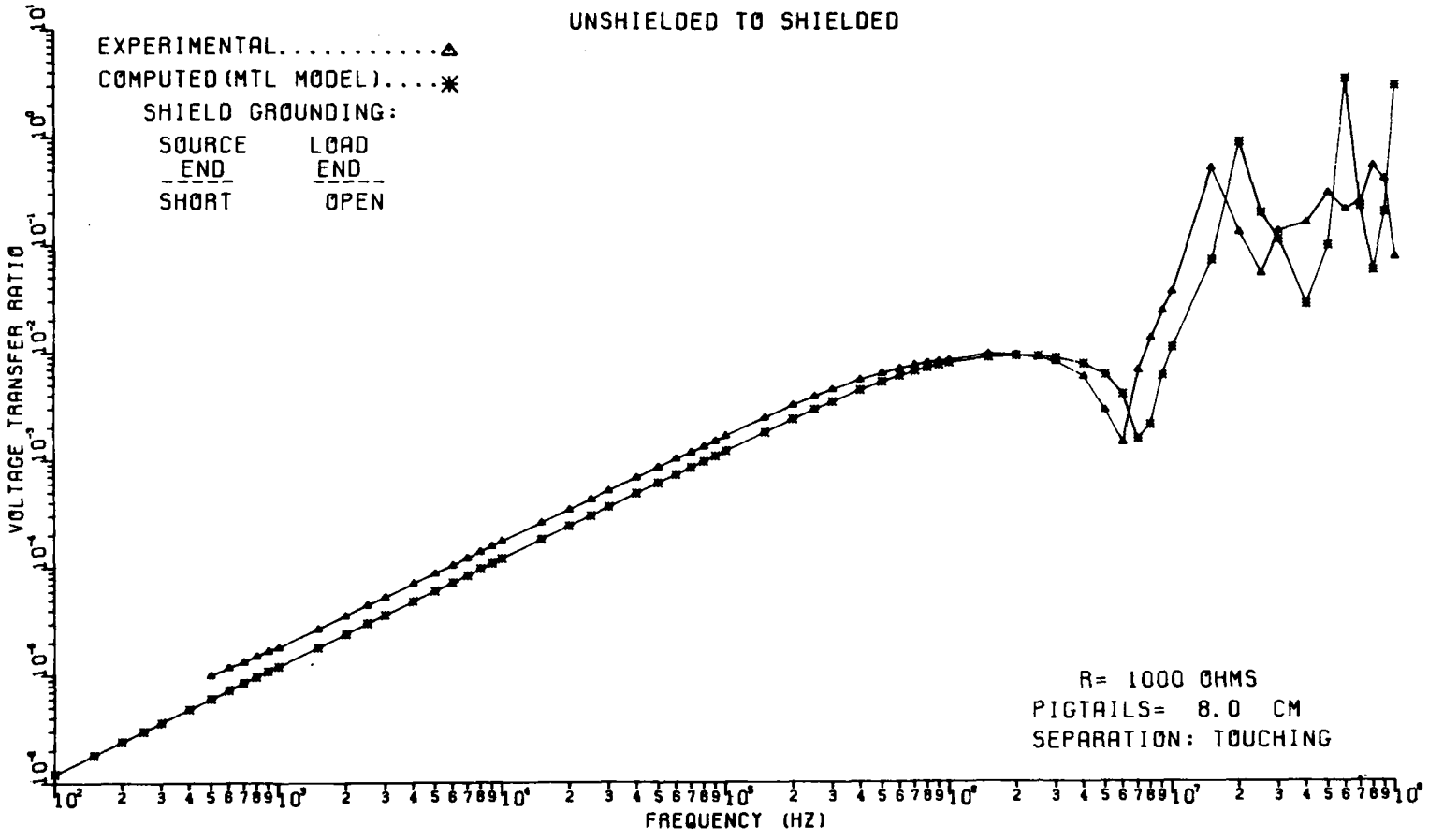
UNSHIELDED TO SHIELDED
EXPERIMENTAL.....△
COMPUTED(MTL MODEL)....✳
SHIELD GROUNDING:
SOURCE END
SHORT
LOAD END
OPEN
R= 1000 OHMS
PIGTAILS= 8.0 CM
SEPARATION: TOUCHING
VOLTAGE TRANSFER RATIO
FREQUENCY (HZ)

Figure E-30.

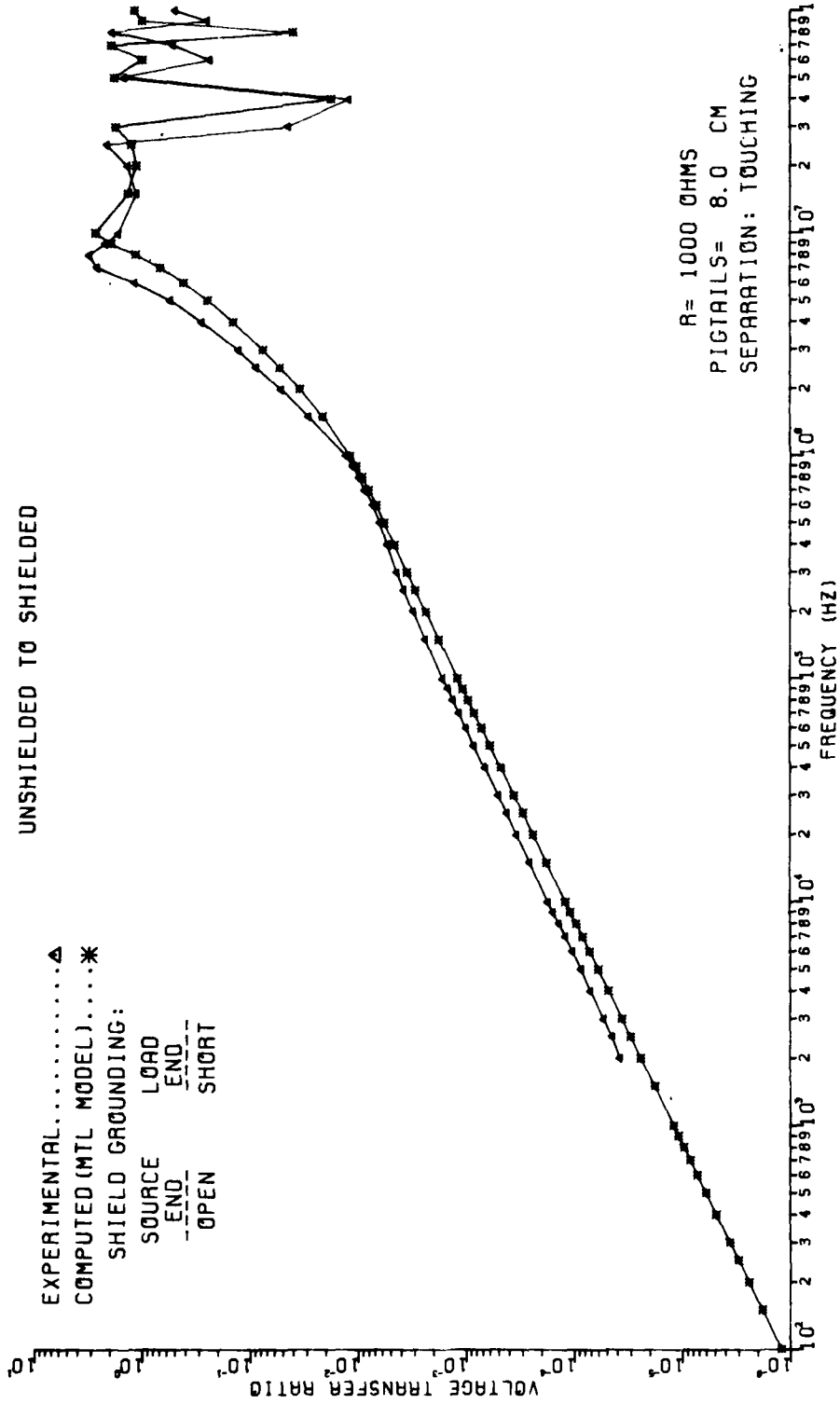
UNSHIELDED TO SHIELDED
EXPERIMENTAL.....Δ
COMPUTED(MTL MODEL)....*
SHIELD GROUNDING:
SOURCE LOAD
END END
OPEN SHORT
R= 1000 OHMS
PIGTAILS= 8.0 CM
SEPARATION: TOUCHING
VOLTAGE TRANSFER RATIO
FREQUENCY (HZ)

Figure E-31.

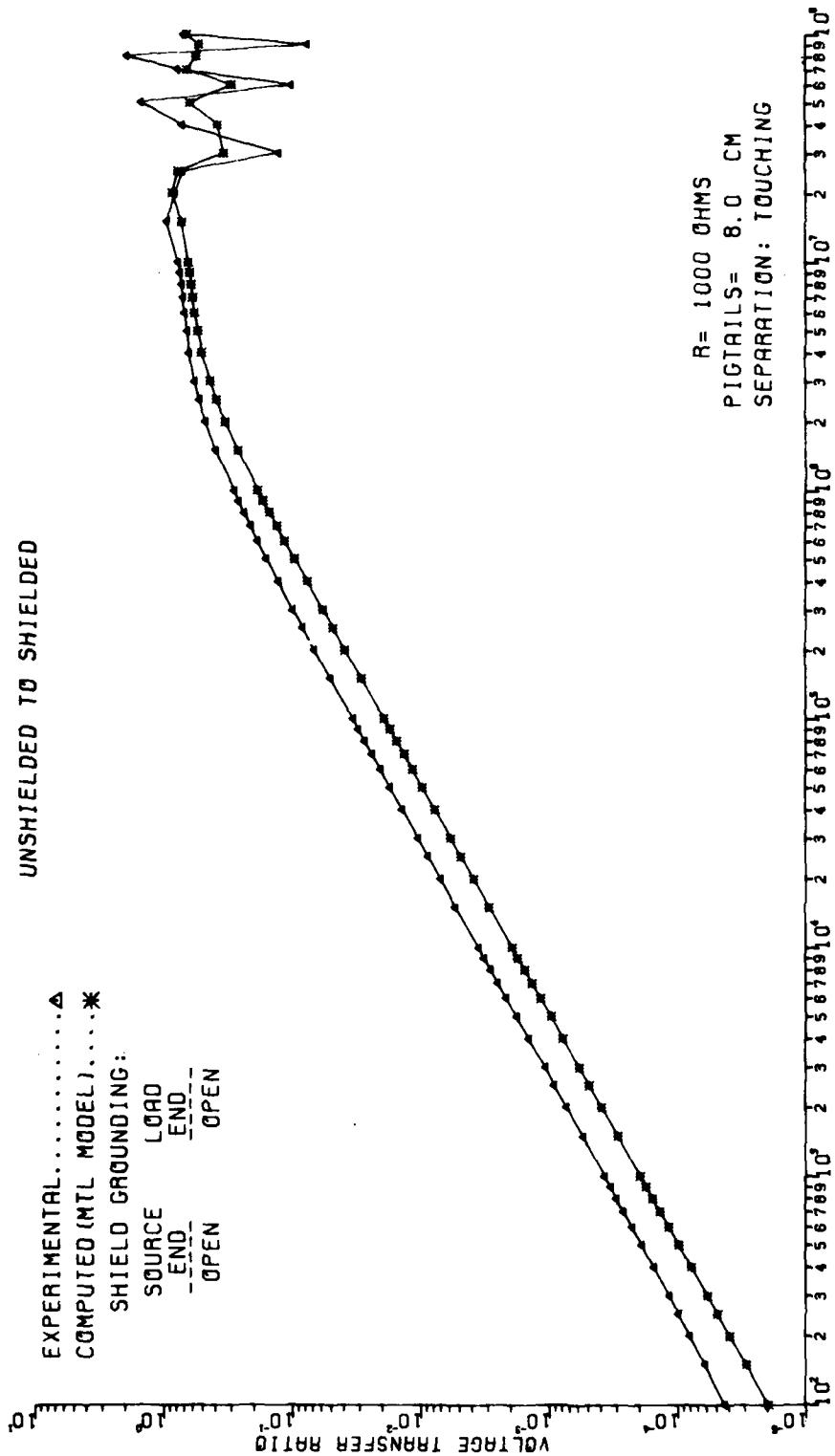
UNSHIELDED TO SHIELDED
EXPERIMENTAL.....Δ
COMPUTED(MTL MODEL)....*
SHIELD GROUNDING:
SOURCE END
LOAD END
OPEN
OPEN
R= 1000 OHMS
PIGTAILS= 8.0 CM
SEPARATION: TOUCHING
VOLTAGE TRANSFER RATIO
FREQUENCY (HZ)

Figure E-32.

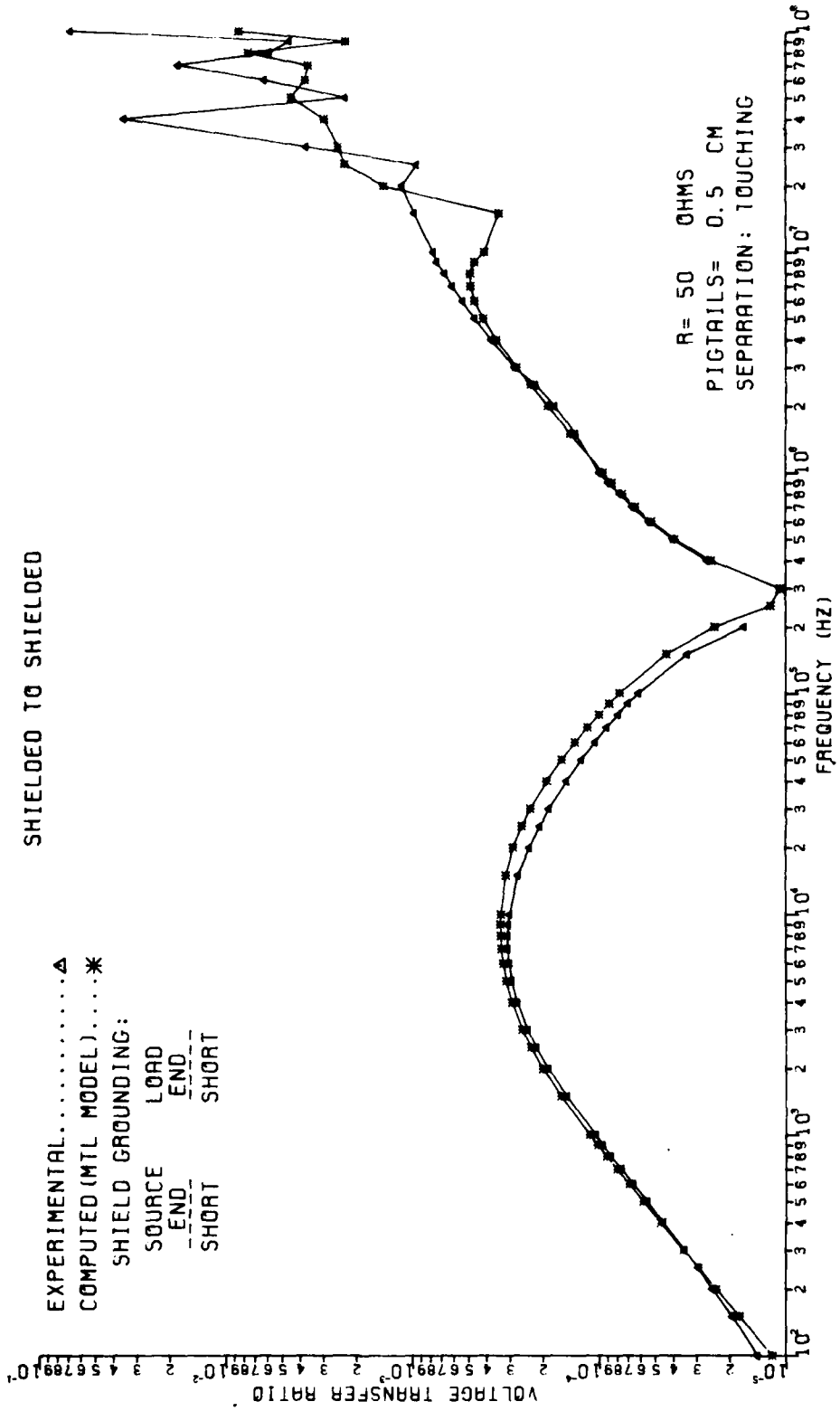
SHIELDED TO SHIELDED
EXPERIMENTAL.....Δ
COMPUTED(MTL MODEL).....*
SHIELD GROUNDING:
SOURCE LOAD
END END
SHORT SHORT
R= 50 OHMS
PIGTAILS= 0.5 CM
SEPARATION: TOUCHING
VOLTAGE TRANSFER RATIO
FREQUENCY (HZ)

Figure E-33.

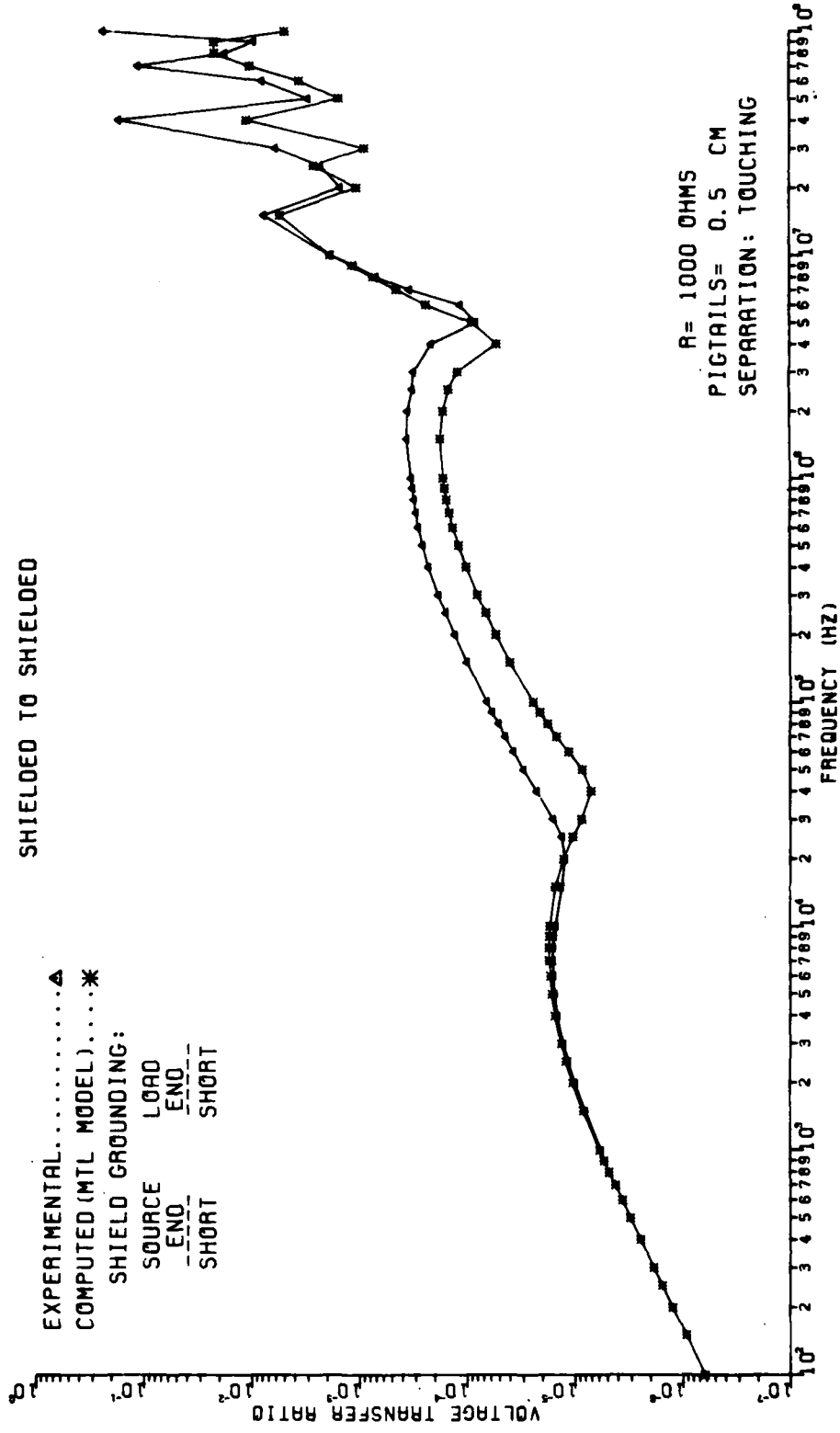
SHIELDED TO SHIELDED
EXPERIMENTAL.....▲
COMPUTED(MTL MODEL)....*
SHIELD GROUNDING:
SOURCE LOAD
END END
SHORT SHORT
R= 1000 OHMS
PIGTAILS= 0.5 CM
SEPARATION: TOUCHING
VOLTAGE TRANSFER RATIO
FREQUENCY (HZ)

Figure E-34.

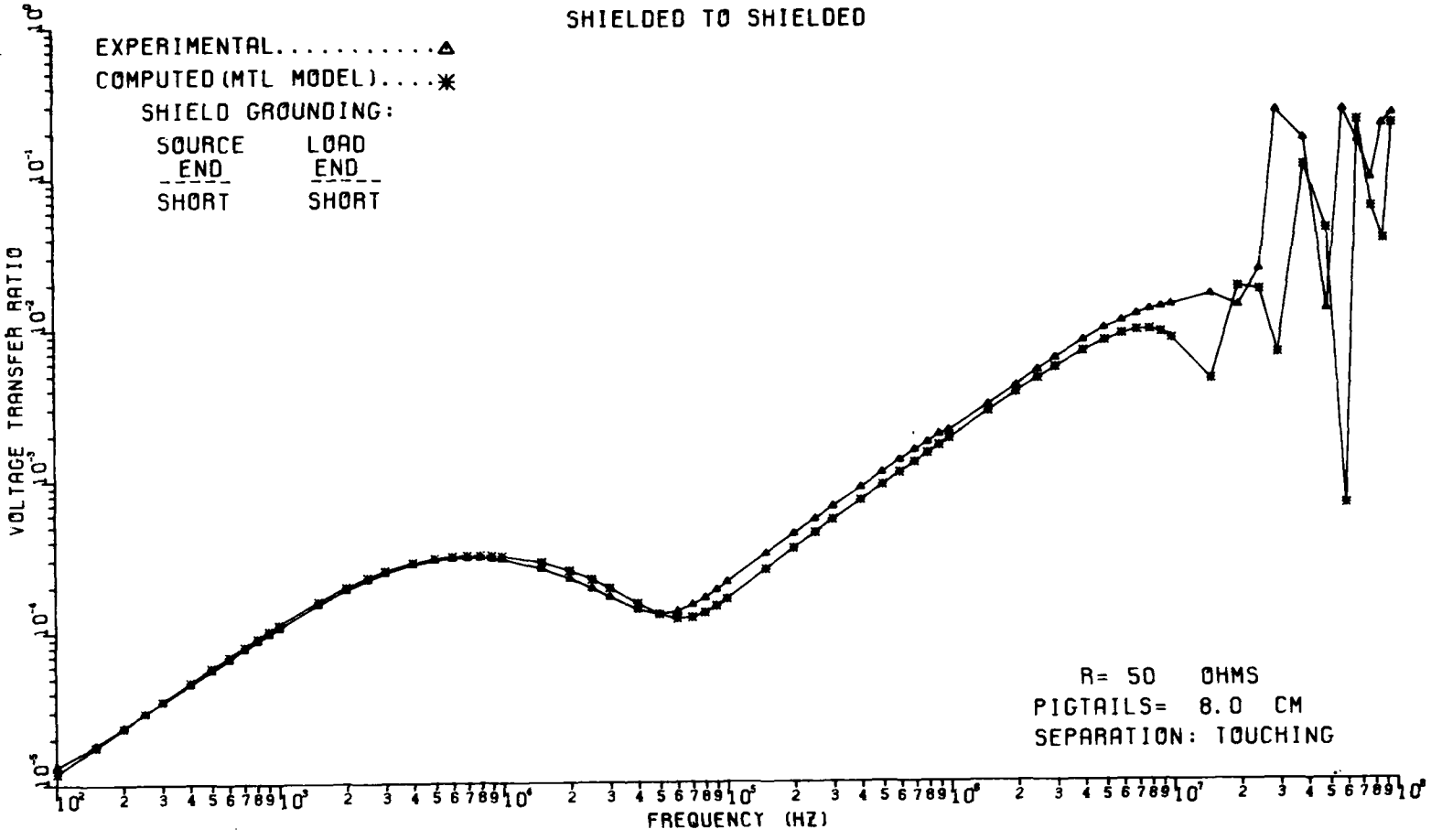
SHIELDED TO SHIELDED
EXPERIMENTAL.....Δ
COMPUTED(MTL MODEL)....*
SHIELD GROUNDING:
SOURCE END
SHORT
LOAD END
SHORT
VOLTAGE TRANSFER RATIO
FREQUENCY (HZ)
R= 50 OHMS
PIGTAILS= 8.0 CM
SEPARATION: TOUCHING

Figure E-35.

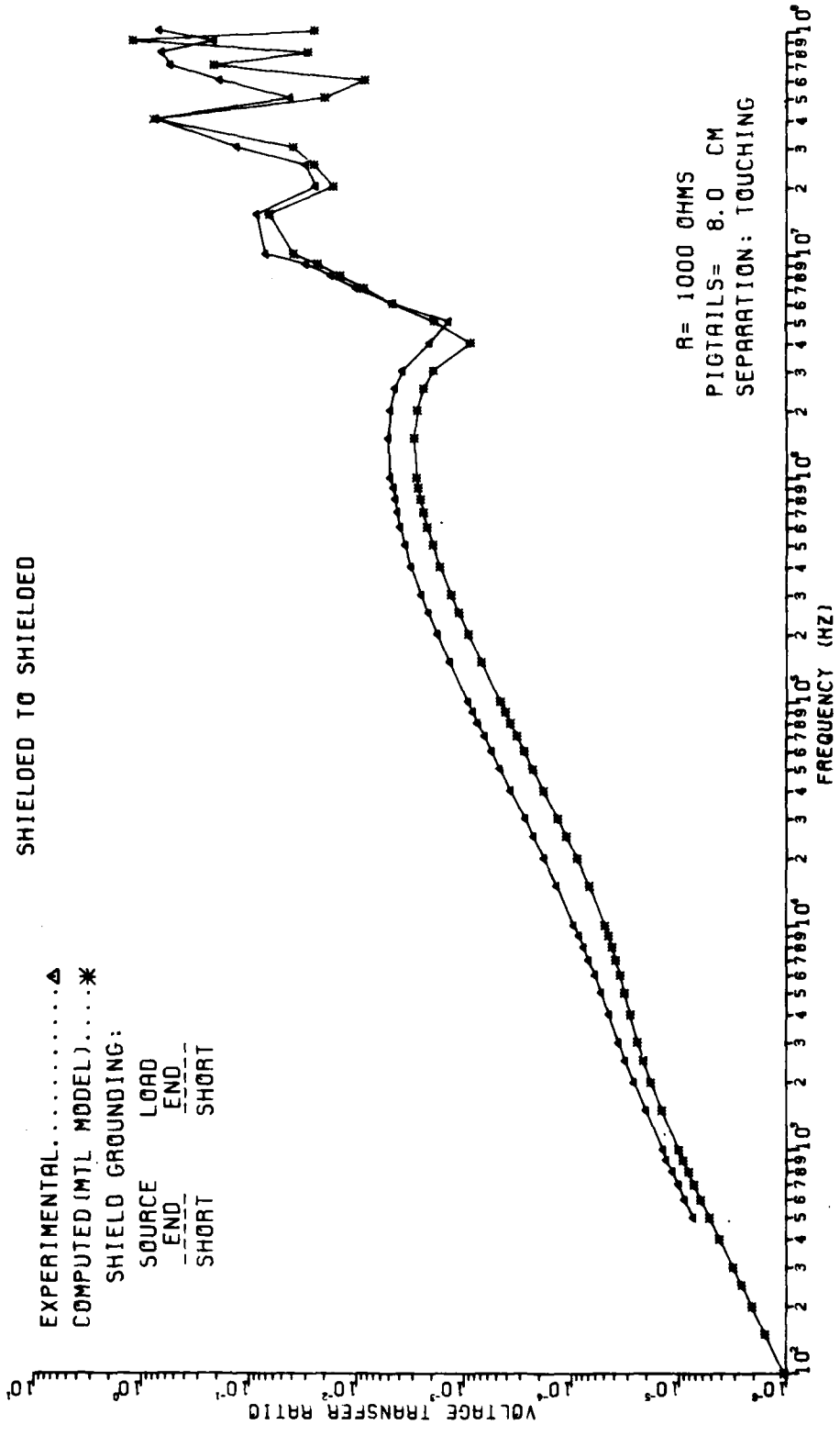
SHIELOED TO SHIELOED
EXPERIMENTAL.....Δ
COMPUTED(MTL MODEL).....*
SHIELD GROUNDING:
SOURCE END
LOAD END
SHORT
SHORT
R= 1000 OHMS
PIGTAILS= 8.0 CM
SEPARATION: TOUCHING
VOLTAGE TRANSFER RATIO
FREQUENCY (HZ)

Figure E-36.

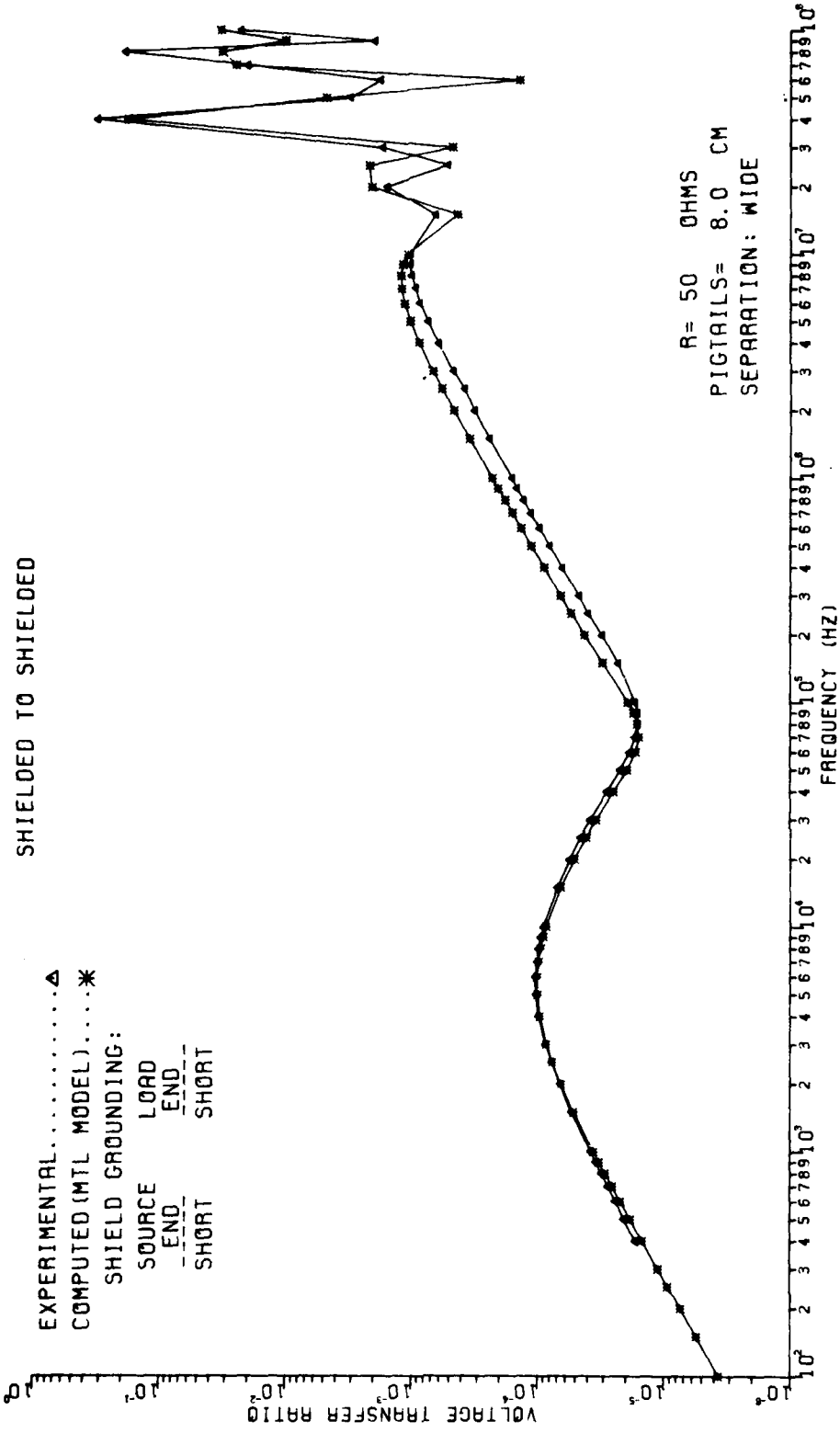
SHIELDED TO SHIELDED
EXPERIMENTAL.....Δ
COMPUTED(MTL MODEL)....*
SHIELD GROUNDING:
SOURCE LOAD
END END
SHORT SHORT
R= 50 OHMS
PIGTAILS= 8.0 CM
SEPARATION: WIDE
VOLTAGE TRANSFER RATIO
FREQUENCY (HZ)

Figure E-37.

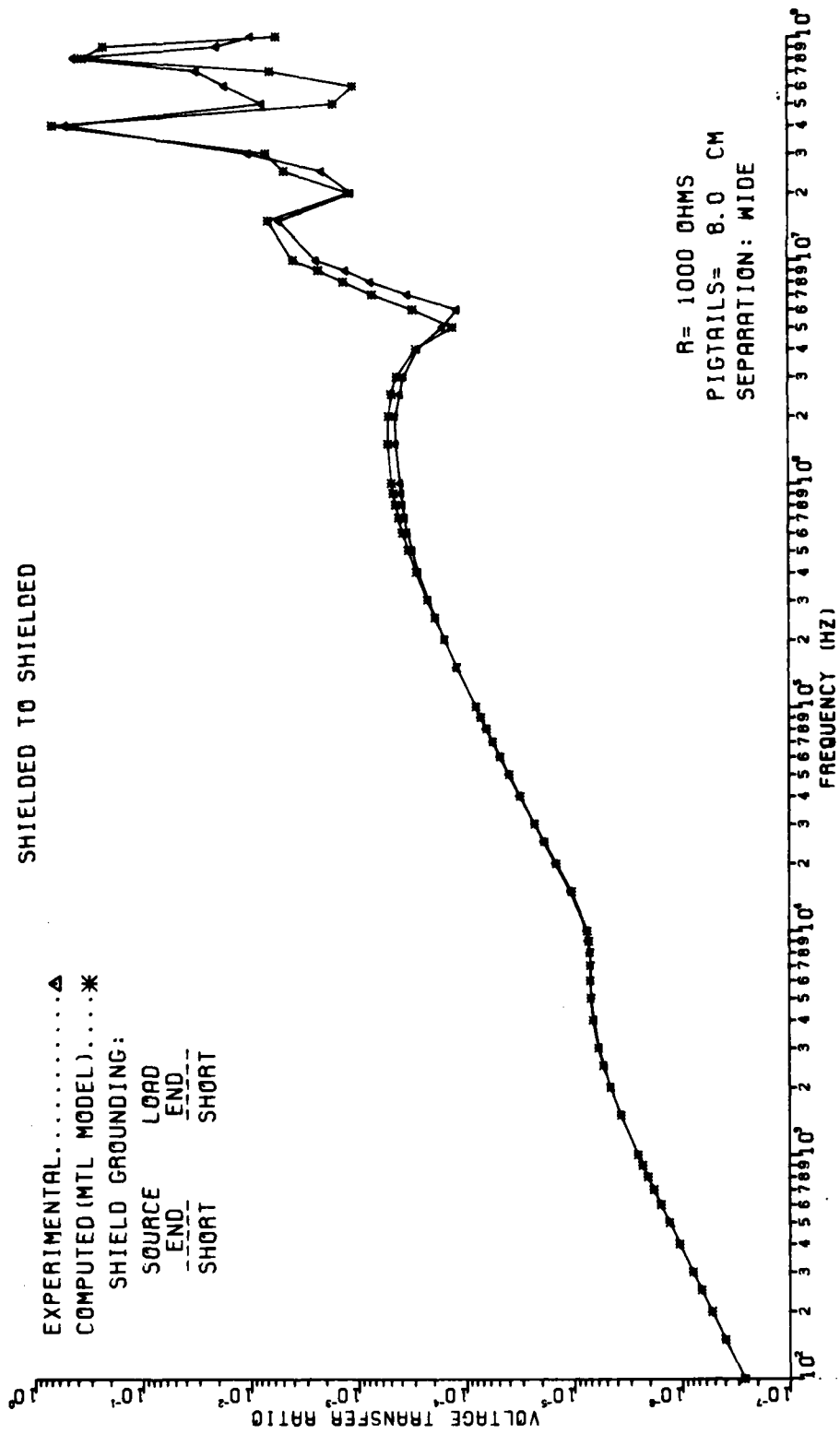
SHIELDED TO SHIELDED
EXPERIMENTAL.....Δ
COMPUTED(MTL MODEL)....*
SHIELD GROUNDING:
SOURCE LOAD
END END
SHORT SHORT
R= 1000 OHMS
PIGTAILS= 8.0 CM
SEPARATION: WIDE
VOLTAGE TRANSFER RATIO
FREQUENCY (HZ)

Figure E-38.

APPENDIX F

The purpose of this appendix is to show that the capacitive cross-sectional equivalent circuit shown in Fig. 13(a) is correct. Consider Fig. F-1(a) in which we have shown the per-unit-length mutual and self capacitances for the unshielded to shielded configuration. We wish to show that for solid shields, the per-unit-length capacitive elements shown with dashed lines, c_{GR} and c_{RR}, must be zero. We may write the following linear relationships between the per-unit-length conductor charges, q_G, q_R, q_S and the conductor voltages with respect to ground, V_G, V_R, V_S [7]:

$$q_G = c_{GG}V_G + c_{GR}(V_G - V_R) + c_{GS}(V_G - V_S) \tag{F-1a}$$

$$q_R = c_{GR}(V_R - V_G) + c_{RR}V_R + c_{RS}(V_R - V_S) \tag{F-1b}$$

$$q_S = c_{GS}(V_S - V_G) + c_{RS}(V_S - V_R) + c_{SS}V_S \tag{F-1c}$$

We wish to show that

$$c_{GR} = c_{RR} = 0 \tag{F-2}$$

Reciprocity can be used to show that mutual elements are the same, i.e., $c_{GR} = c_{RG}$, $c_{GS} = c_{SG}$, $c_{RS} = c_{SR}$ [7].

First consider equation (F-1b). If we set $q_R = 0$, this equation becomes

$$0 = c_{GR}(V_R - V_G) + c_{RR}V_R + c_{RS}(V_R - V_S) \tag{F-3}$$

However, if $q_R = 0$, then, according to Gauss' law, there can be no field within the shielded region so that $V_R = V_S$. Substituting this into (F-3) we obtain

$$0 = c_{GR}(V_R - V_G) + c_{RR}V_R \tag{F-4}$$

or

$$V_G = \frac{c_{GR} + c_{RR}}{c_{GR}} V_R \tag{F-5}$$

Substituting (F-5) into (F-1b) we obtain

$$q_R = c_{GR}V_R - c_{GR}\left(\frac{c_{GR} + c_{RR}}{c_{GR}}\right)V_R + c_{RR}V_R + c_{RS}V_R - c_{RS}V_S \tag{F-1b}$$

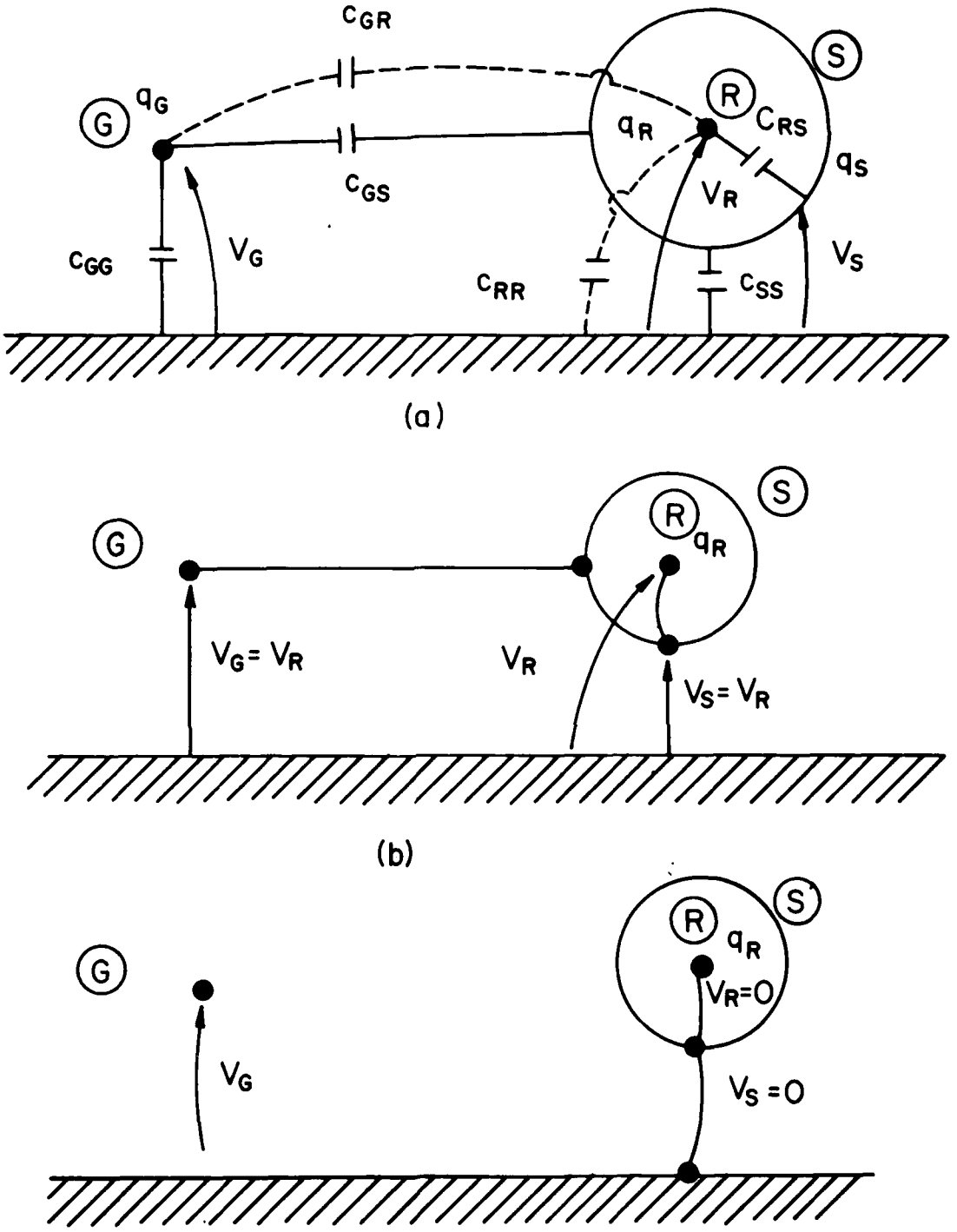
C_{GR}
G
q_G
S
R
C_{RS}
q_R
q_S
C_{GS}
V_R
C_{GG}
V_G
C_{RR}
C_{SS}
V_S
(a)
G
S
R
q_R
$V_G = V_R$
V_R
$V_S = V_R$
(b)
G
S
R
q_R
$V_R = 0$
V_G
$V_S = 0$
(c)

Figure F-1.

or

$$q_R = c_{RS}V_R - c_{RS}V_S \tag{F-1b}$$

This implies that $c_{GR} = c_{RR} = 0$ as was to be proven.

An alternate proof can be obtained in the following manner. From equation (F-1b) we may obtain

$$c_{RR} = \frac{q_R}{V_R}\Bigg|_{\substack{V_R = V_G \\ V_R = V_S}} \tag{F-6}$$

This configuration for determining c_{RR} is shown in Fig. F-1(b) where short circuits are used to impose the conditions $V_R = V_G = V_S$. Clearly $q_R = 0$ for if q_R were not zero then a field would exist within the shielded region (by Gauss' law) and $V_R \neq V_G$.

Also from equation (F-1b) we obtain

$$c_{GR} = \frac{q_R}{(V_R - V_G)}\Bigg|_{\substack{V_R = 0 \\ V_R = V_S}} \tag{F-7}$$

This configuration is also shown in Fig. F-1(c) where short circuits are used to impose the conditions $V_R = V_S = 0$. Equation (F-7) requires

$$c_{GR} = -\frac{q_R}{V_G}\Bigg|_{V_R = V_S = 0} \tag{F-8}$$

Again q_R must be zero otherwise V_S would not equal V_R.

Thus we have shown that, electrostatically, $c_{GR} = c_{RR} = 0$ for the unshielded to shielded (or shielded to unshielded) case and solid shields. This is a fairly obvious result. Similar conclusions can be obtained for the shielded to shielded case for solid shields.

APPENDIX G

Effect of Wire Insulation Dielectric on Pigtail Coupling

We found that the predictions of both the simple low-frequency model and the more complex multiconductor transmission line (MTL) model were quite good for "low impedance" loads, i.e., R = 50Ω.† For an electrically short line these models provided predictions within 1 dB - 3 dB. On the other hand, for "high impedance" loads, R = 1kΩ, the coupling predictions of both models were often less than the actual coupling when pigtail coupling was dominant for the TOUCHING separation. (See Figures C-2, C-10, C-15, C-16.) For R = 1kΩ and the WIDE separation, the coupling predictions seemed to be fairly accurate with predictions errors of typically only approximately 1 dB less than the actual coupling. (For example, see Fig. C-12.) The purpose of this appendix is to demonstrate that this is due to the fact that the presence of the wire dielectric insulation was ignored in computing the mutual capacitance, c_{GR}, which was used in the low-frequency model and MTL model.

First let us reconsider the low-frequency model for the unshielded to unshielded case shown in Fig. 3(a). The received voltage, V_{out}, across the load impedance, Z_{SR}, at the source end of the receptor circuit is, for a sufficiently small frequency, the sum of capacitive and inductive coupling contributions. These are given by (4-1):

$$V_{out}^{IND} = \frac{Z_{SR}}{Z_{SR} + Z_{LR}} (j\omega \ell_{GR} \mathcal{L}) I_G \qquad \text{(G-1a)}$$

$$V_{out}^{CAP} = \frac{Z_{SR} Z_{LR}}{Z_{SR} + Z_{LR}} (j\omega c_{GR} \mathcal{L}) V_G \qquad \text{(G-1b)}$$

where V_G and I_G are the voltage and current, respectively, of the generator line circuit and are given by

$$V_G = \frac{Z_{LG}}{Z_{SG} + Z_{LG}} V_S \qquad \text{(G-2a)}$$

$$I_G = \frac{V_S}{Z_{SG} + Z_{LG}} \qquad \text{(G-2b)}$$

The total voltage is approximately

†For the shielded to shielded case the predictions of the low-frequency model were somewhat poorer than the MTL model which was apparently due to neglecting the pigtail wires of the generator circuit.

$$V_{out} \doteq V_{out}^{IND} + V_{out}^{CAP} \qquad (G\text{-}3)$$

Note that errors in computing the per-unit-length mutual inductance, ℓ_{GR}, and mutual capacitance, c_{GR}, will be directly reflected in the appropriate coupling contribution. For example, if c_{GR} is in error by 6dB so is V_{out}^{CAP}. If $V_{out}^{CAP} >> V_{out}^{IND}$, then V_{out} will be in error by the error in c_{GR}. If $V_{out}^{IND} >> V_{out}^{CAP}$, then errors in computing c_{GR} are of no consequence in the V_{out} total prediction.

For shielded wires, the form of the pigtail coupling contribution is identical to (G-1) except that $\mathcal{L}$ in (G-1) is replaced for the shielded case by the pigtail length, $2\mathcal{L}_p$. Thus when coupling over the pigtail section dominates the coupling over the shielded section, errors in computing c_{GR} for the pigtail sections may incur errors. If the capacitive coupling portion of this pigtail coupling dominates the inductive coupling component and pigtail coupling is dominant, errors in computing c_{GR} will result in errors in the total prediction of the model. If inductive coupling dominates capacitive coupling over this pigtail section and pigtail coupling is dominant, errors in c_{GR} will result in virtually no errors in the total prediction model.

The per-unit-length mutual inductance, ℓ_{GR}, and mutual capacitance, c_{GR}, were computed in (4-3) and (4-8) by (1) assuming that the conductors are separated sufficiently so that the current and charge distribution around the cross-sectional periphery of each conductor are essentially constant around the periphery, and (2) neglecting the dielectric insulation of the wires. Assumption (1) is reasonably accurate for a ratio of wire separation to wire radius of 5 [7, 30, 31]. For the TOUCHING separation this ratio is approximately 4. However assumption (2), neglecting the wire insulation dielectric, will lead to c_{GR}, and the resulting capacitive coupling prediction, being in error (underprediction) by about 5dB - 6dB for the TOUCHING separation and only about 1.5dB for the WIDE separation. Clearly the dielectric insulation does not affect the per-unit-length mutual inductance, ℓ_{GR}, so that if the inductive coupling predominates (R = 50Ω), errors in c_{GR} resulting from neglecting the dielectric insulation have virtually no effect on the total coupling. However if capacitive coupling is predominant as is the case for R = 1kΩ, then neglecting the dielectric insulation will result in the total coupling prediction being less than it should be by about 6dB for the TOUCHING separation and

about 1.5 dB for the WIDE separation.

To support the above assertions that neglecting the wire dielectric insulation provides errors in c_{GR} of 5dB - 6dB for the TOUCHING separation and only 1.5dB for the WIDE separation we provide the following evidence. The case of two identical, dielectric insulated wires (without a ground plane) was investigated in [30,31]. (See also reference [7], Chapter V for a comprehensive discussion of this problem.) The mutual capacitance, c_m, for this seemingly simple case of two cylindrical conductors with cylindrical dielectric insulation cannot be computed in closed form, and a numerical approximation technique, the method of moments, was used to obtain c_m and include the effect of the insulation [7, 30, 31]. The dielectric insulation was assumed to have a relative permittivity of $\varepsilon_r = 3.0$ and the insulation thickness and wire radius were equal. This case roughly corresponds to the cases in this report in which the dielectric insulations had $\varepsilon_r \doteq 2.1$ (Teflon) to $\varepsilon_r \doteq 3.5$ (PVC) and the insulations were approximately equal to the wire radii. Although a ground plane is present in this report, the height of the two wires above the ground plane (1.5cm $\doteq \frac{5}{8}$ inch) seems to be sufficiently large (for the TOUCHING separations) for the ground plane to have a minor effect. For the case investigated in [30,31] it was found that the dielectric insulation for the wires touching caused the mutual capacitance, c_m, to increase a factor of 1.96 or 5.85dB. See page E-1 of reference [30]. Thus it is reasonable to assume a corresponding error for the similar cases in this report.

To provide further evidence, an approximation for the mutual capacitance between two identical, dielectric insulated wires both at the same height above a ground plane was developed in [7]. (See [7], Chapter V, pp. 112-122.) The result is

$$c_{GR} \doteq \frac{B}{A^2 - B^2} \tag{G-4}$$

where

$$A = \frac{1}{2\pi\varepsilon_v}\left\{\ell n\left(\frac{2h}{r_w + t}\right) + \frac{(r_w + t)}{\varepsilon_r}\,\ell n\left(\frac{r_w + t}{r_w}\right)\left[(\varepsilon_r - 1)\frac{(r_w + t)}{4h^2} + \frac{1}{(r_w + t)}\right]\right\} \tag{G-5}$$

where ε_r is the relative permittivity of the dielectrics, h is the height of the wires above ground, r_w is the wire radii, and t is the thickness of the insulations. This can be further approximated by

$$A \doteq \frac{1}{2\pi\varepsilon_v} \left\{ \ell n \left(\frac{2h}{r_w + t} \right) + \frac{1}{\varepsilon_r} \ell n \left(\frac{r_w + t}{r_w} \right) \right\} \qquad \text{(G-6)}$$

when $4h^2 >> (\varepsilon_r - 1)(r_w + t)^2$. Also

$$B = \frac{1}{2\pi\varepsilon_v} \left\{ \ell n \left(\frac{\sqrt{4h^2 + d^2}}{d} \right) + \ell n \left(\frac{r_w + t}{r_w} \right) \left[\frac{(\varepsilon_r - 1)(r_w + t)}{\varepsilon_r d \left(1 + \frac{d^2}{4h^2} \right)} \right] \right\} \qquad \text{(G-7)}$$

where d is the wire separation. For the unshielded to unshielded case (touching separation) the wires were #22 gauge, Teflon insulated so that

$$d = .23 \text{ cm}$$
$$h = 1.5 \text{ cm}$$
$$r_w = 25.3 \text{ mils}$$
$$t \doteq 20 \text{ mils}$$
$$\varepsilon_r \doteq 2.1$$

and we compute

$$c_{GR} = 29.63 \text{ pF/m}$$

With the dielectric removed (and d = .23 cm maintained) we compute

$$c_{GR} = 17.5 \text{ pF/m}$$

The ratio of c_{GR} with the dielectric to c_{GR} without the dielectric is 1.7 or 4.6dB. For a separation of d = 1.5 cm, we find that this ratio is only 1.2 or 1.6dB: a modest and negligible effect. Thus the capacitive coupling predictions for TOUCHING separation should be increased by a factor of at least 1.7 or 4.6dB.

The unshielded to unshielded cases for R = 50Ω and TOUCHING separation in Fig. C-1 and R = 1kΩ in Fig. C-2 are replotted in Fig. G-1 and Fig. G-2, respectively, where the capacitive coupling is increased by 4.6dB. Note that for R = 50Ω in Fig. G-1, since inductive coupling was predominant, the increase in capacitive coupling due to the dielectric has virtually no effect and the predictions were quite good in the first place. For R = 1kΩ in Fig. G-2, the capacitive coupling was predominant and in error by about 6dB. Increasing the capacitive coupling by 4.6dB to account for the dielectric yields a total pre-

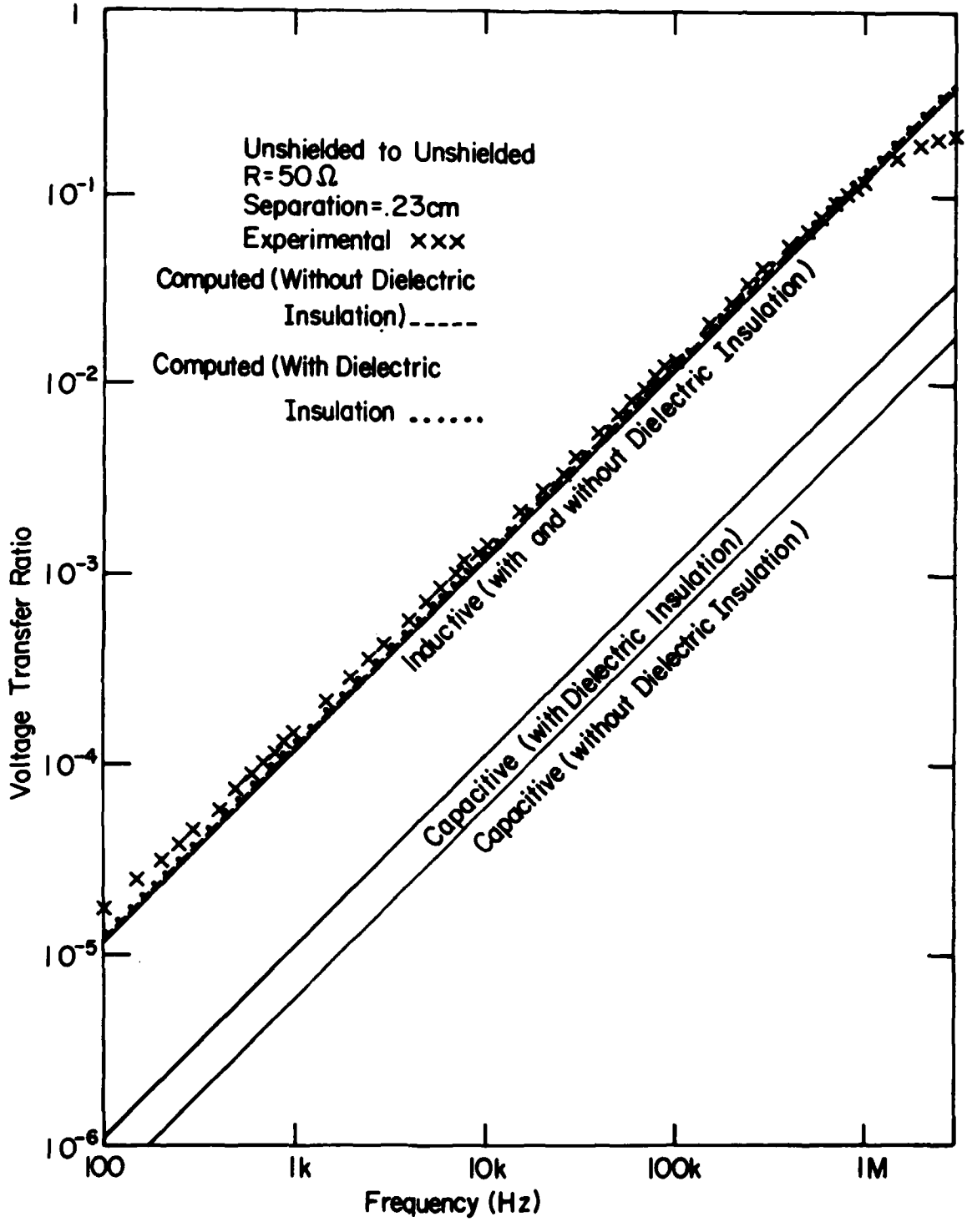

Fig. G-1. Effect of wire insulation dielectric on pigtail coupling (R = 50Ω).

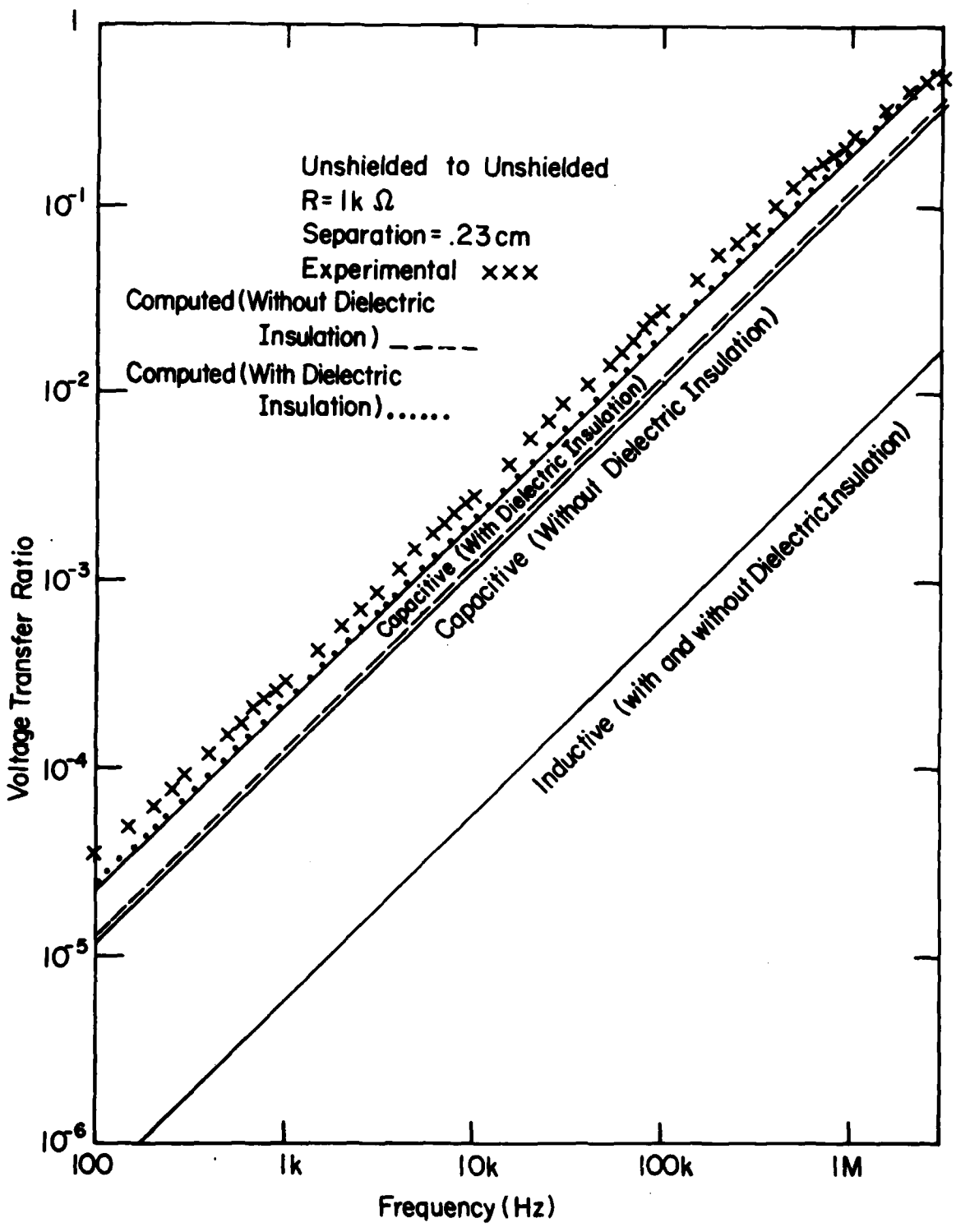

Fig. G-2. Effect of wire insulation dielectric on pigtail coupling (R = 1kΩ).

diction error of only about 1.5 dB which is quite reasonable. The corresponding results for the WIDE separation are shown in Fig. C-3 and Fig. C-4. Note that for R = 1kΩ in Fig. C-4, the predictions are quite good even though the insulation dielectric is not included in c_{GR} which tends to confirm these observations.

The results in (G-4) through (G-7) which indicated an increase in c_{GR} due to the dielectric on the order of a factor of 1.7 for the TOUCHING separation include the dielectric but essentially assume the wires are separated sufficiently so that the charge distribution around the conductor-dielectric and dielectric-free space peripheries are constant. Clearly for the TOUCHING case this is not satisified so that the increase of 1.7 is a lower bound. We would probably expect that results of two wires without the ground plane (ε_r = 3.0, r_w = t, touching) [30], which showed an increase of a factor of 1.96, to be an upper bound. Therefore it is clear that if one takes the effort to compute c_{GR} accurately and in the presence of the dielectric insulations, then prediction errors for R = 1kΩ would be quite similar to those for R = 50Ω: typically within 1 dB to 3 dB.

All other predictions, unshielded to shielded as well as shielded to shielded, for R = 1kΩ should also be increased by approximately 5 dB to 6 dB for the TOUCHING cases for frequencies where the pigtail coupling is predominant. For R = 50Ω, essentially no change in the predictions due to the dielectric need be included.

One final point should be noted. There are a few cases in which the predictions of the both models are consistently below the actual results for <u>all frequencies</u>. All of these occur for R = 1kΩ. See Fig. E-8, E-16, E-24, E-29, E-30, E-31, E-32, E-36 and E-38. For R = 1kΩ the pigtail coupling is clearly capacitive. In some of these situations the coupling over the pigtail sections and the coupling over the shielded section are on the same order (see Fig. C-10 and C-12) for the lower frequencies so that the error in computing c_{GR} due to the presence of dielectric insulation clearly explains this widespread, consistent prediction error. On the other hand, for the shield ungrounded (see Fig. E-24 and E-32) the coupling levels are some 20 dB above those for the shield double-end grounded or single-end grounded. For example, compare Fig. E-29, E-30, E-31 and E-32 in which R = 1kΩ, pigtail length is 8 cm and separation is TOUCHING. Clearly then if the pigtail coupling was not

dominant at these lower frequencies for at least one end of the shield grounded it is not dominant for the shield ungrounded since the coupling levels are higher by 20 dB. This prediction error is explainable by the observation that for the shield ungrounded, the coupling is essentially unaffected by the shield (it may be removed). In this case we essentially have two unshielded wires, and the shield, not being grounded at at least one end, does not serve to reduce the capacitive coupling over the shielded section to essentially zero. Therefore, even though pigtail coupling is not dominant at the lower frequencies, the dielectric insulation of the shielded wire over the shielded section has an effect similar to that occuring over the pigtail sections.

In the experimental and computed results, it was noted that an ungrounded shield had virtually no effect on the crosstalk; that is, the crosstalk for the unshielded to unshielded case and the unshielded to shielded case with the shield not grounded at either end differed by less than 1.5 dB when the line was electrically short. For low impedance loads, R = 50Ω, it is clear that this should be the case since inductive coupling predominates in the unshielded to unshielded case, and an ungrounded shield does not affect this. However, for high impedance loads, R = 1kΩ, capacitive coupling dominates in the unshielded to unshielded case and it is not clear than an ungrounded shield has virtually no effect. In this final section, we wish to illustrate why this occurs.

The equivalent circuit for the per-unit-length capacitances for the unshielded to shielded configuration with the shield ungrounded is shown in Fig. G-3(a). We can obtain the effective mutual capacitance between the generator and receptor wires, c_m, by using a Y-Δ transformation as shown in Fig. G-3(a). (See reference [22] pp. 249-252.) The Y consists of c_{GS}, c_{SS}, c_{RS} where c_{GS}, c_{SS}, c_{RS} are the per-unit-length capacitances between the generator wire and the shield, between the shield and the ground plane and between the shield and the receptor wire, respectively. We are interested in eliminating the shield node labeled as Ⓢ and obtaining c_m. The Y-Δ transformation yields

$$c_m = \frac{c_{GS}c_{RS}}{c_{RS} + c_{GS} + c_{SS}} \qquad \text{(G-8)}$$

For the touching separation we obtain

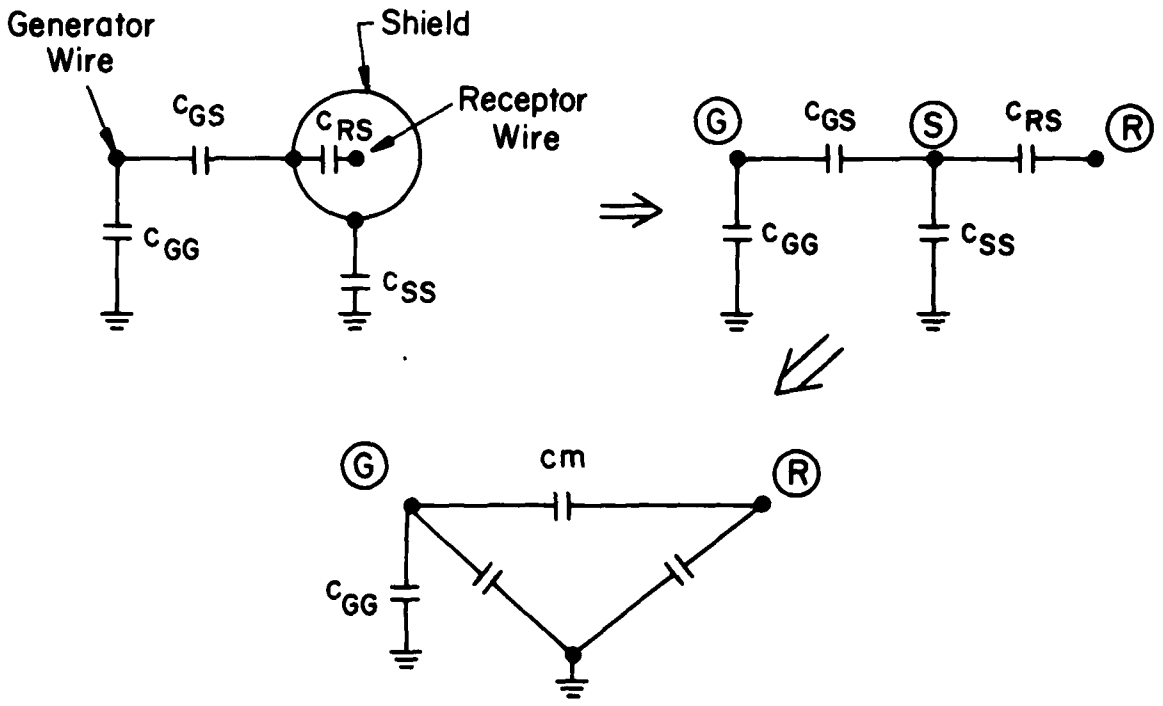

(a)
Unshielded to Shielded
Shield Ungrounded

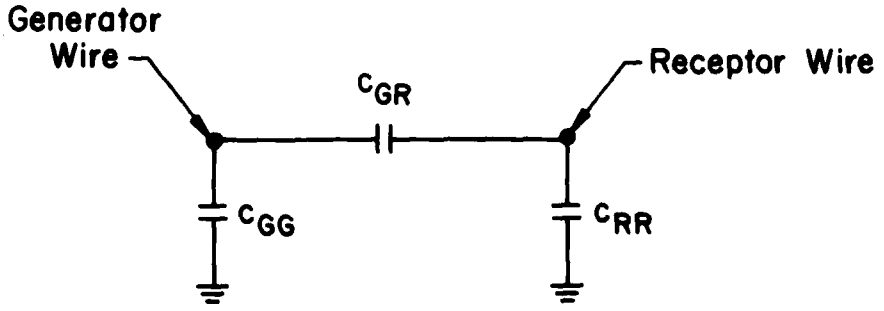

(b)
Unshielded to Unshielded

Figure G-3.

$$c_{RS} = \frac{2\pi\varepsilon_v\varepsilon_r}{\ell n(r_s/r_{wR})} \tag{G-9}$$

$$= 114.64 \text{ pF/m}$$

and

$$c_{GS} = \mu_v\varepsilon_v \frac{\ell_{GS}}{|\underset{\sim}{L}|} \tag{G-10}$$

$$= 21.1 \text{ pF/m}$$

$$c_{SS} = \mu_v\varepsilon_v \frac{\ell_{GG}}{|\underset{\sim}{L}|} - c_{GS} \tag{G-11}$$

$$= 12.27 \text{ pF/m}$$

where

$$|\underset{\sim}{L}| = \ell_{GG}\ell_{SS} - \ell_{GS}^2 \tag{G-12}$$

as explained in Section IV. (See equations (4-3) - (4-8).) Thus the effective mutual capacitance between the generator and receptor wires for the unshielded to shielded case with the shield ungrounded is obtained from (G-8) as

$$c_m = 16.34 \text{ pF/m} \tag{G-13}$$

For the unshielded to unshielded case and the touching separation shown in Fig. G-3(b), the mutual capacitance between the generator and receptor wires is computed to be

$$c_{GR} = \mu_v\varepsilon_v \frac{\ell_{GR}}{|\underset{\sim}{L}|} \tag{G-14}$$

$$= 10.23 \text{ pF/m}$$

where

$$|\underset{\sim}{L}| = \ell_{GR}\ell_{RR} - \ell_{GR}^2 \tag{G-15}$$

The ratio of these two mutual capacitances is

$$20 \log_{10} \left(\frac{c_m}{c_{GR}}\right) = 20 \log_{10} (1.6) \qquad \text{(G-16)}$$

$$= 4.07 \text{ dB}$$

which indicates a minor effect of the ungrounded shield. The insulation dielectric as well as the close proximity of the wires were neglected in computing the above capacitances. Thus the ratio in (G-16) is approximate and subject to the remarks at the beginning of this appendix.

Note in (G-8) that $c_{RS} >> c_{GS}$ and $c_{RS} >> c_{SS}$ so that c_m becomes approximately

$$c_m \tilde{=} c_{GS} \qquad \text{(G-17)}$$

Thus the effective mutual capacitance between the generator wire and the receptor wire in the unshielded to shielded case with the shield ungrounded is approximately the capacitance between the generator wire and the shield (a "fatter" wire than the receptor wire).

MISSION
of
Rome Air Development Center

RADC plans and executes research, development, test and selected acquisition programs in support of Command, Control Communications and Intelligence (C^3I) activities. Technical and engineering support within areas of technical competence is provided to ESD Program Offices (POs) and other ESD elements. The principal technical mission areas are communications, electromagnetic guidance and control, surveillance of ground and aerospace objects, intelligence data collection and handling, information system technology, ionospheric propagation, solid state sciences, microwave physics and electronic reliability, maintainability and compatibility.